CHARACTERIZING PLAG1 IN HUMAN HEMATOPOIETIC STEM CELLS

CHARACTERIZING THE ROLE OF THE TRANSCRIPTION FACTOR PLAG1 IN HUMAN HEMATOPOIETIC STEM AND PROGENITOR CELLS

BY AVA KEYVANI CHAHI, M.Sc., B.Sc.

A Thesis Submitted to the School of Graduate Studies in Partial Fulfilment of the Requirements for Degree Doctor of Philosophy

McMaster University DOCTOR OF PHILOSOPHY (2022) Hamilton, Ontario
(Biochemistry and Biomedical Sciences)

TITLE: Characterizing the role of the transcription factor PLAG1 in human hematopoietic stem and progenitor cells.
AUTHOR: Ava Keyvani Chahi, M.Sc., B.Sc. (McMaster University)
SUPERVISOR: Kristin Hope
NUMBER OF PAGES: 156

LAY ABSTRACT

Blood production (hematopoiesis) is a stem cell-driven regenerative system that can repair damaged blood systems and therefore offer lifesaving treatments for devastating malignancies and immune disorders. Realizing the full potential of hematopoietic stem cells (HSCs) is encumbered by our inability to maintain HSCs with long-term functionality in clinical settings. Enhanced fundamental insights into the properties that define human HSC identity and fates can thus inform the rational design and advancement of HSC-based therapies. We discovered a regulator, PLAG1, that is essential for the long-term blood production function of human HSCs. When elevated PLAG1 amplified the absolute number of human HSCs 15-fold and improved their maintenance and function in clinically-relevant culture and transplantation settings. Using genome-wide technologies paired with functional assays we elucidated that PLAG1 employs a multi-pronged strategy to rewire protein production rates as a means to enhance HSC preservation and function. Our findings highlight regulation of protein production as an untapped strategy that could be incorporated into clinical settings to improve patient outcomes.

ABSTRACT

Hematopoietic stem cell (HSC) dormancy is understood as supportive of HSC function and their long-term integrity. While regulation of stress responses incurred as a result of HSC activation is recognized as important in maintaining stem cell function, little is understood of the preventative machinery present in human HSCs that may serve to resist their activation and promote HSC self-renewal. We demonstrate that the transcription factor PLAG1 is essential for long-term HSC function and when overexpressed endows a 15.6-fold enhancement in the frequency of functional HSCs in stimulatory conditions. Genome-wide measures of chromatin occupancy and PLAG1-directed gene expression changes combined with functional measures reveal that PLAG1 dampens protein synthesis, restrains cell growth and division, and enhances survival, with the primitive cell advantages it imparts being attenuated by addition of the potent translation activator, c-MYC. We find PLAG1 capitalizes on multiple regulatory factors to ensure protective diminished protein synthesis including 4EBP1 and translation-targeting miR-127, and does so independently of stress response signaling. Overall, our study identifies PLAG1 as an enforcer of human HSC dormancy and self-renewal through its highly context-specific regulation of protein biosynthesis, and classifies PLAG1 among a rare set of *bona fide* regulators of mRNA translation in these cells. Our findings showcase the importance of regulated translation control underlying human HSC physiology, its dysregulation under activating demands, and the potential if its targeting for therapeutic benefit.

ACKNOWLEDGEMENTS

First and foremost, I wish to acknowledge my supervisor, Kristin. My words will never come close to honouring the impact Kristin has had in my life and training or conveying my gratitude to her. From the beginning I was inspired by the curiosity and ambition with which Kristin pursues science. Months into meeting Kristin, she said to me [about her research goals] "I don't want to half-a$$ this," which was enough to convince me this was a PhD worth pursuing. As a supervisor she has been so much more than an enthusiastic and driven scientist. Kristin has a knack for catering her training program to match each student's needs, which in my case involved lots of lengthy, inspirational, high-level, but sometimes totally off-topic conversations. I also needed a generous dose of encouragement and pep-talks, and somehow, wholly inexplicable to me, Kristin has an endless supply of optimism. Kristin leads with compassion, and her empathy and support ultimately afforded me the possibility to complete a PhD as a somewhat senior student with a full and sometimes complicated life. I am astutely aware that the backing and accommodation I received when I was unable to move with the lab was decisive in the positive course of the conclusion of my degree. And now, I am beyond overwhelmed by Kristin's enormous support to me and my growing family. I am deeply grateful for the bond we have formed and feel she will be a life-long ally for me, and only hope she knows I too will always be rooting for her success and happiness.

I have been fortunate to have amazing committee members who have contributed valuable scientific insight, helped to keep me focused, and on more than one occasion cut me some slack! I'm so grateful to have had the opportunity to see Brad in action at McMaster and retain him on my committee after his move to Manitoba. Truly, Brad exemplifies principles of integrity, excellence and compassion like no other. He has a heart of gold, and has been sincerely missed! Dr. Miller too has contributed invaluably; always leading with "I have no skin in the game" and yet asking engaging and interesting questions. I am also very thankful for his role in supporting my continued work at McMaster following the Hope lab relocation. What might have seemed a small gesture was really determinant in enabling me to complete my research goals and degree.

Though the moment has not yet come it must be stated how beyond excited and appreciative I am that Dr. Signer has agreed to participate in this examination. Dr. Signer is the leading contributor to the study of protein production and proteostasis in hematopoietic stem cells. His body of work, which has been impressively elegant and rigorous, has borne insights that have been integral to the interpretation and contextualization of our findings, and informing our research questions. Most people know that I'm not one to schmooze, but I'm genuinely feeling equal parts stoked and humbled for this opportunity.

I am deeply indebted to and appreciative of Muluken who initiated the research into PLAG1 and contributed important findings. MVP award goes to Minomi, the most compassionate and helpful sorting technician/ psychotherapist, but above that a dear friend. I must also thank Josh and Tony who have been supportive of my work without question or hesitation, and just for being an all-around laugh! I'm so grateful for the team we have become. I also want to acknowledge Dana, the sweetest undergrad, it was such a pleasure to work with her and so rewarding to see her flourishing. I'm also very thankful to our collaborators for all their contributions: Veronique, Sajid, Drs. Bader and De Carvalho for their support in computational analysis; Gabriela and Eric for their assistance with our miRNA and CUT&RUN experiments; and Lina and Dr. Lu for their efforts on our proteomics project.

Last but not least, I am so thankful for the support of my partner, Tom, who has been by my side through the nearly decade-long ups and [melt] downs of two graduate degrees. I sincerely doubt that I could have stayed the course without his support, patience and motivation. Finally, the time is coming that we can press the play button on adulthood. I want to acknowledge my parents who have made the greatest possible sacrifices in their own lives to make opportunities possible for their children. They have long ago lost track of what it is I even do but have been unwavering in their confidence in me (though I'm sure they too are ready for me to get a "real job"). And of course, I cannot forget my sister, Aram, who doesn't know which of a protein or a nucleus is larger but cheers me on anyways.

TABLE OF CONTENTS

LIST OF FIGURES AND TABLES

LIST OF ABBREVIATIONS

4EBP	Eukaryotic translation initiation factor 4E-binding protein
4EGI-1	Eukaryotic translation initiation factor 4E and 4G interaction inhibitor
5-FU	5-Fluorouracil
AF	AlexaFluor®
AGM	Aorta-Gonad-Mesonephros
AhR	Aryl Hydrocarbon Receptor
AML	Acute Myeloid Leukemia
Baso-E	basophilic erythroblast
BFP	Blue Fluorescent Protein
BFU-E	Burst Forming Unit-Erythroid
BM	Bone Marrow
BrdU	Bromodeoxyuridine
CB	[Umbilical] Cord Blood
CD	Cluster of Differentiation
CFU	Colony Forming Unit
CFU-C	Culture Colony Forming Unit
CFU-E	Colony Forming Unit-Erythroid
CFU-G	Colony Forming Unit-Granulocyte
CFU-GEMM	Colony Forming Unit-Granulocyte, Erythroid, Macrophage, Megakaryocyte
CFU-GM	Colony Forming Unit-Granulocyte, Macrophage
CFU-M	Colony Forming Unit-Macrophage
CFU-S	Spleen Colony Forming Unit
ChIP	Chromatin Immunoprecipitation
CLP	Common Lymphoid Progenitor
CML	Chronic Myelogenous Leukemia
CMP	Common Myeloid Progenitor
CMV	cytomegalovirus [promoter]
CUT&RUN	Cleavage Under Targets & Release Using Nuclease
CUT&TAG	Cleavage Under Targets and Tagmentation
DGE	Differential Gene Expression
DNA	Deoxyribonucleic acid
DSB	Double Stranded [DNA] Break
EF1	Valproic Acid
EGFP	Enhanced Green Fluorescent Protein
eIF4E	Eukaryotic translation initiation factor 4E
eIF4G	Eukaryotic translation initiation factor 4G
ELDA	Extreme Limiting Dilution Analysis

EM	Enrichment Map
ER	Endoplasmic Reticulum
FACS	Fluorescence Activated Cell Sorting
FBS	Fetal Bovine Serum
FC	Fold Change
FLT3	Fms-like tyrosine kinase receptor 3 ligand
FSC	Forward Scatter
GM-SCF	Granulocyte macrophage-colony stimulating factor
GMP	Granulocyte Monocyte Progenitor
GSEA	Gene Set Enrichment Analysis
GvHD	Graft versus Host Disease
GvL	Graft versus Leukemia
HbA	Hemoglobin Adult
HbF	Hemoglobin Fetal
HLA	Human Leukocyte Antigen
hsa	Homo Sapien
HSC	Hematopoetic Stem Cell
HSPC	Hematopoetic Stem and Progenitor Cell
HSPCT	Hematopoetic Stem and Progenitor Cell Transplantation
IGF2	Insulin-like Growth Factor 2
IL	Interleukin
IL6	Interleukin 6
IMDM	Iscove's Modified Dulbecco's Medium
ISR	Integrated Stress Response
IT	Intermediate
Lin	Lineage
LMPP	Lymphoid Primed Multipotent Progenitor
LSC	Leukemia Stem Cell
LT	Long-Term
LTC-IC	Long Term Culture Initiating Cell
MDS	Myelodysplastic Syndrome
MEP	Megakaryocyte-Erythrocyte Progenitor
miR	micro-RNA
MLP	Multi-Lymphoid Progenitor
MMP	Mitochondrial Membrane Potential
MNC	Mononucleated Cell
mPB	mobilized Peripheral Blood
MPP	Multipotent Progenitor
MSC	Mesenchymal Stem Cell
MSI2	Musashi-2

MW	Mann-Whitney
NHEJ	Nonhomologous End Joining
NK	Natural Killer
NOD	Nonobese Diabetic
NSG	Nonobese Diabetic, Severe Combined Immune Deficiency, IL-2R common gamma chain mutated
OE	Overexpressing or Overexpression
OMA	Omacetaxine mepesuccinate
OP-Puro	O-propargyl-puromycin
ORA	Overrepresentation analysis
OrthoE	orthochromatic erythroblast
PFA	Paraformaldehyde
PGK	Phosphoglycerate Kinase [promoter]
PLAG1	Pleomorphic Adenoma Gene 1
PolyE	polychromatophilic erythroblast
Pro-E	proerythroblast
qRT-PCR	Quantitative Real Time Polymerase Chain Reaction
RBC	Red Blood Cell
Retic	Reticulocyte
RNA	Ribonucleic acid
RNA-seq	RNA sequencing
ROS	Reactive Oxygen Species
RP	Ribosomal Protein
RPG	Ribosomal Protein-coding Gene
RPL	Ribosomal Protein Large (60S) subunit
RPS	Ribosomal Protein Small (40S) subunit
rRNA	ribosomal RNA
SCD	Sickle Cell Disease
SCF	Stem Cell Factor
SCID	Severe Combined Immune Deficiency
scRNA-seq	single cell RNA sequencing
SFEM	Serum Free Expansion Media
SFFV	spleen focus forming virus [promoter]
shRNA	short hairpin RNA
SR-1	Stem Regenin-1
SSC	Side Scatter
ST	Short-Term
TCA	Tricarboxylic Acid Cycle
TEPA	Tetraethylenepentamine
TF	Transcription Factor

TMRE	Tetramethylrhodamine ethyl ester
TNC	Total Nucleated Cell
tNGFR	truncated Nerve Growth Factor Receptor
Tpo	Thrombopoietin
UPR	Unfolded Protein Response
USF2	Upstream Stimulatory Factor
VPA	Valproic Acid
WB	Western Blot
Zn	Zinc

DECLARATION OF ACADEMIC ACHIEVEMENT

I contributed to the design and execution of the research presented herein, as well as performed analysis and interpretation of functional and computational data and writing of all the sections of this thesis. Dr. Kristin Hope directed and supervised the research projects, and aided in the interpretation of results and editing of this thesis. Muluken Belew performed experiments and contributed significantly to data collection. Joshua Xu and Stefan Rentas provided experimental support. Tony Chen and Sonam Bhatia assisted with bioinformatic analysis. Our collaborators Veronique Voisin, and Sajid Marhon, supervised by Dr. Gary Bader and Dr. Daniel De Carvalho, respectively, assisted with bioinformatic analysis. Our collaborators Gabriela Krivdova and Eric Lechman, supervised by Dr. John Dick assisted with experiments. Our collaborators Lina Liu and Dr. Yu Lu performed experiments.

CHAPTER 1

Introduction

1.0 Blood formation: a brief history

Hematopoiesis is the process by which trillions of erythroid, myeloid and lymphoid cells of the blood and immune system are replenished over an individual's life span[1]. Ontologically this begins in vertebrates from the mesodermal precursor cells, hemangioblasts, which gives rise both to the hematopoietic and endothelial tissues. Functionally erythro-myeloid restricted hematopoiesis is first evident in the 3-week-old fetal yolk sac. Definitive multilineage hematopoiesis later emerges in the aorta-gonad-mesonephros (**AGM**) and umbilical cord blood of both human and mouse embryos. Subsequently in the fetal liver expansion of the life-time supply of hematopoietic precursor cells occurs before they migrate to the fetal bone marrow (**BM**) by the second trimester where they remain to sustain hematopoiesis throughout adult life-time[2-4]. We now appreciate that life-long hematopoiesis is sustained by a common ancestral cell known as the hematopoietic stem cell (**HSC**) through their dual capacity for multipotent differentiation into all blood cell types and self-renewal, a specialized division that produces another HSC[5,6]. However, prior to empirical evidence in support of a common cell of origin for hematopoietic tissue the regenerative power of HSC was already being clinically leveraged[7].

The first ever hematopoietic cell transfusions were recorded in 1939 to transiently treat aplastic anemia[8]. In 1945 the nuclear fallout of World War II (**WWII**) provided the impetus to understand and treat the effects of radiation exposure. Scientific and clinical experiments in the wake of WWII ultimately gave rise to modern-day stem cell biology and regenerative medicine[5,6,9]. The BM was identified as a highly radiosensitive tissue and radioprotection in mice was conferred by lead-shielding of spleen and BM tissues[10,11]. Radioprotection could also be endowed through syngeneic BM transplantation[11-15] and it was later shown by tracking DNA marks that this was specifically due to proliferation and hematopoietic regeneration from donor cells[16]. The first allogeneic hematopoietic cell transplantations were reported in 1957 by Dr. E. Donnall Thomas[17], however at that stage this was still far from a curative approach as only 2/6 patients were engrafted with donor cells and all passed away by 100 days post-transplant. Hindsight would reveal that this experimental medicine was being attempted without sufficient understanding of mechanisms governing immunogenicity and its interplay in transplantation paradigms[7]. To this point, near synchronously Barnes *et al*. (1956,1957) demonstrated that mice with acute leukemia treated with radiation to eliminate the leukemic cells then transplanted with syngeneic BM died due to relapse. On the contrary, transplantation with allogeneic BM prevented disease relapse but led to mouse recipient mortality due to a condition the authors termed "wasting syndrome"[18,19], which we can now appreciate reflected an imbalance in the positive effect of graft versus leukemia (**GvL**) and negative effect of graft versus host disease (**GvHD**). Insights that followed thereafter into the role of major histocompatibility complex molecules (human leukocyte antigens (HLAs)) in self-tolerance[9] significantly enhanced the cure rate for AML by allogeneic transplantation to 50% in 1979; and in 1990 garnered a Nobel Prize to Dr. Thomas[7]. After sixty-five years of breakthroughs hematopoietic stem and progenitor cell (**HSPC**) transplantation (**HSPCT**) now represents an important therapy for the treatment of malignant and non-malignant diseases[20].

1.1 Evidence of Blood-forming Stem Cells

The notion of a common ancestral cell for multi-lymphoid, myeloid and erythroid hematopoiesis was debated since the early 1900's, but was largely based on conjecture until the devastation caused by nuclear weaponry provided the impetus to empirically identify and characterize a cell with radio-protective regenerative potentiall[21,22]. This void was first addressed by the seminal works of Canadian scientists Drs. Till and McCulloch beginning in the 1960's. The

post-war research provided key observations that gave credence to the notion of a long-term source of hematopoietic cells existing within the BM: 1) hematopoietic tissue is highly radiosensitive[10], 2) spleen shielding or BM transplantation can protect against radiation sickness[11-13] and 3) radio-protection conferred by BMT was attributed to proliferation and differentiation of donor hematopoietic cells[16]

However, it remained to be shown whether long-term hematopoiesis was derived from a single ancestral cell or multiple lineage-committed cells and elucidate their frequencies in the BM. Upon this foundation Drs. Till and McCulloch first designed a quantitative assay to determine the number of BM cells to confer radioprotection. Their study in 1960 demonstrated that 10^4-10^6 donor BM cells increasingly prevented radiation-induced mortality in mice, with little enhancement beyond the 10^6 cells dosage[23]. In 1961 they demonstrated the presentation of donor-derived hematopoietic nodules or colonies on host spleens 7-10 days post-transplantation, which could be titrated down to 1 in 10^4 donor BM cells and were referred to as spleen colony forming units (**CFU-S**)[24]. Based on chromosome markers it was determined that spleen colonies are derived from a single parental cell[25]. Moreover, cells of spleen colonies that are capable of continued proliferation were also capable of differentiation and some spleen colonies contain cells that could induce the formation of spleen colonies in secondarily transplanted mice[26], providing evidence for paradigms of hierarchical differentiation and long-term self-renewal. Morphologically some spleen colonies presented a mixture of cell lineages (erythrocytes, megakaryocytes, granulocytes and monocytes) and some produced lymphoid cells, providing the first key evidence for the notion of a singular multipotent stem cell that could give rise to all hematopoietic cell types[27,28]. The CFU-S assay was taken as the first modelling tool for HSC as it captured cells capable of proliferation, multipotency, and self-renewal[5,6].

However, early on it was shown that CFU-S could be separated based on differing capacities for self-renewal[29], spleen colonies were vastly variable in lineage composition[27,28], and that differentiation potentials of these cells could vary further depending on the hematopoietic niche (BM vs. Spleen) [6]. This indicated that the identity of each CFU-S was highly heterogeneous and likely indicated that each were generated from unique cell types unresolved at the time[6,30]. Moreover, the Iscove lab would later demonstrated that day 7 CFU-S are transient, specifically that spleen colonies apparent 12-14 days post-transplant are derived independently as opposed to being the progeny of 7-10 day CFU-S and were more primitive and self-renewing[31]. Together these findings set a precedence for the existence of intermediate progenitors, underscored remaining limitations in functional identification and isolation of bona fide HSC, and overall emphasized the need for more advanced methods for both retrospective and prospective characterization of HSC and the transitionary states that give rise to mature blood[6].

1.2 Prospective isolation of Murine HSC and Modelling Murine Hematopoiesis

Improved models to operationally define HSCs and model hematopoiesis returned to the functional definition of an HSC: a cell capable of long-term multilineage BM population. Using X/Y-chromosome discrimination male-to-female BM chimerism assays elucidated that engraftment kinetics involved both an early phase of radioprotection that prevents lethal aplasia and a distinct late phase of BM population, furthering the paradigm of transitory hierarchical states[32,33]. By similar methods, Jones *et al*. (1998) fractionated murine BM cells based on density and demonstrated that day 8 and day 12 CFU-S potential almost exclusively existed in higher density rapidly and intermediately sedimenting cells and that these were the cells that provided short-term radioprotection. Enduring (60 day) BM reconstitution was restricted to slowly

sedimenting BM fractions and provided little early radioprotection; and supported the conclusion that *bona fide* HSCs may be as few as 0.25% of the day 12 CFU-S cells[33].

Advances in congenic mouse strains[34], monoclonal antibodies and fluorescence activated cell sorting (FACS)[35,36], paved the way to effectively purify and operationally identify these rare and morphologically indistinct HSC from BM[37], and serve as foundational methodologies still used by hematopoietic researchers today[6,38]. In particular, the generation of mice congenic for alleles of the ubiquitous blood-surface antigen Cd45 and allele-specific (Cd45.1 vs Cd45.2) antibodies allowed for host-donor discrimination in transplant models[34]. Surface antigen-based prospective isolation of murine hematopoietic cell types was pioneered by the group of Irving Weissman and a series of findings they reported would show that mature blood cell types expressed unique surface antigens[6]. One of their pivotal discoveries was that B-cell precursors lacked expression of the mature B-cell surface marker, B220, prompting the hypothesis that mature lineage markers may be absent on primitive cells. Indeed, by performing negative selection of known lineage markers (B220, Gr-1, Mac-1, CD4 and CD8= Lin^-) they were able to enrich for multipotent BM reconstituting cells[39,40]. By way of antibody libraries the prospective separation of mouse HSC was progressively enriched through the identification of positive Sca-1 and cKit/Cd117 expression ($Lin^-Sca\text{-}1^+cKit^+$= LSK)[36]. The most sustained repopulating capacity could be further be demarcated in LSK cells that were $Cd34^-$ [41] or $Cd150^+Cd48^-$ ("SLAM")[42,43] enabling purification of murine LT-HSC to approximately 1 in a few[38] (**Figure 1**).

When monitored for sufficient length of time clonal BM engraftment kinetics revealed that within the multipotent cell fraction there are very early transitionary states between the most potent long-term vs. intermediate and short-term self-renewing HSCs. In particular, the earliest multilineage grafts peak at approximately 2-3 weeks post-transplant with exhaustion apparent by 4-6 weeks and the next wave of transient engraftment peaks at 4-8 weeks exhausting by 16 weeks. Another population of intermediate HSCs can form grafts for up to 6-8 months, and only the most long-term HSCs persist beyond 8 months and in serial transplantations. These transitionary states have been further demarcated by surface expression of Cd49b where 49b low cells possess the most long-term potential[44]. While these studies in mouse established a foundation and platform for the complementary assessment of human HSCs and hematopoiesis, this research was encumbered in the early days as species immunogenicity precluded the operational validation of human HSCs by mouse xenotransplantation[1,38].

1.3 Prospective isolation of Human HSC and Modelling Human hematopoiesis

First inspired by the CFU-S assays of Till and McCulloch early studies of primitive multipotent human hematopoietic cells leveraged *in vitro* colony formation (**CFU-C**) assays. CFU-Cs could be replenished over extended time courses *in vitro*, therefore the precursor cells that gave rise them were termed long-term culture initiating cells (**LTC-IC**). Like the murine CFU-S it was clear that LTC-IC were a heterogeneous cell population with varying differentiation and renewal capacities[1].

Tides turned for the study of human hematopoiesis with the development of immune-deficient mouse strains that enabled Dr. John Dick's group to pioneer human to mouse hematopoietic xenotransplantation models. They first demonstrated that intravenous injection of human BM in severe combined immune-deficient (Scid) mice lacking B and T cells could extended (> 4 months) myeloid and lymphoid engraftment[45]. To further impair the innate immune system of Scid mice they were backcrossed onto the nonobese diabetic (NOD-Scid) mouse strain[46], and to dually combat remaining NK cells in the NOD-Scid mice and their predisposition to thymic

lymphomas, the IL-2R common gamma chain was mutated (NSG)[47,48], altogether yielding a strain that permitted significantly enhanced human engraftment[1]. Xenotransplant-permissive animal models continue to advance, for example through genetic humanization of growth factors as has been achieved in the NSG-3GS mice which express human IL3, GM-CSF, Steel factor) or mice homozygous for hypomorphic W14 Kit allele both of which appear to enhance output of all human lineages[38]. However, to date much of our understanding of human hematopoiesis is derived from xenotransplantation in NSG strains.

As in the mouse system HSCs have been prospectively isolated via surface antigen expression, although deriving notably distinct signatures as compared to their mouse counterparts[2]. First CD34 expression on less than 5% of blood cells was identified to enrich for hematopoietic stem and progenitor cells (HSPCs)[49,50] and this to date remains an important benchmark of stem cell content in clinical transplantation samples[51,52]. Next CD90 (Thy1)$^+$ cells were shown to mark the most multipotent fraction of CD34$^+$ cells[53]. Negative selection of surface antigens CD45RA and CD38 gained upon differentiation further enriched the HSC fraction[54-56] (**Figure 2A**). As is the case in the murine system, multipotent human HSC can be further segregated for long-term (**LT**) (repopulate in xenotransplantation for ~30 weeks with serial engraftment capacity) or short-term (**ST**) (4-20 weeks) renewal capacity based on CD90[53] and integrin 6a (CD49f)[57] expression (**Figure 2B**).

1.4 Lineage specification in mouse and human hematopoiesis

HSCs at the apex of hematopoiesis give rise to two major blood lineages: lymphoid (T, B and NK cells) responsible for adaptive and innate immunity and more rapidly replenishing myeloid (granulocytes, monocytes, erythrocytes and megakaryocytes) (**Figure 1, 2A**). Prospective sorting (of bulk populations) and flow cytometric measures of mature cell output based on surface antigen expression produced the earliest models summarizing the relationships between stem cells, immature progenitors and terminal mature cells[1,5,6,58].

Starting from murine studies, the identification of multipotent progenitor (**MPP**) populations that gave rise to all blood cell types but extinguish quickly demonstrated that self-renewal is diminished in progenitor states prior to lineage commitment[59,60]. Next, the discovery of distinct populations of committed myeloid progenitors (**CMP**)[61,62] and committed lymphoid progenitors (**CLP**)[63] suggested that starting from the separation of myeloid and lymphoid lineages discrete bifurcation events occurred (to produce oligo-, bi-, uni-potent progenitors) until a single mature cell type was the dominant output. However, this classical model of a step-wise hematopoietic output is over simplified in many ways.

Early evidence *in vitro* indicated that lymphoid potential was often coupled with some degree of myeloid potential, therefore lymphoid-restriction is more likely a continuous process rather than demarcated by discrete populations[64]. To this point, from murine BM a progenitor was isolated with transient lympho-myeloid repopulation potential that was lymphoid-biased and depleted of erythroid/megakaryocyte potential, which was termed a lymphoid-primed multipotent progenitor (**LMPP**)[65-67] (**Figure 1, left**). Similarly other groups found that HSCs can give rise to multiple functionally distinct groups of MPP with multilineage potential but clear lineage biases[68-70] (**Figure 1, right**). Retaining some level of myeloid potential is a proposed adaptive feature to ensure in the event of stress or trauma, and applicably in the context of transplantation, rapidly depleting myeloid cells can be replenished[69,70].

Correspondingly, from the human system an early progenitor population (CD34$^+$CD38$^-$ CD90$^{-/lo}$CD45RA$^+$) was identified with lymphoid (B, T, NK) potential that could also give rise to

some myeloid cell types, but not erythroid/megakaryocyte cells, which was termed a multi-lymphoid progenitor (**MLP**)[71,72]. Transcriptomic profiles of sorted hematopoietic progenitor populations also supported the paradigm that early hematopoiesis and lymphoid specification progressed on a gradual continuum, based on the observation of many shared features across cell types with distinct fate potentials[73]. While myeloid fate decisions appeared to more closely follow the classical model of bifurcated lineage specification downstream of the CMP[62] (where in humans $CD135^{+}CD45RA^{-}$ CMPs have become fully myeloid-restricted and give rise to $CD135^{-}CD45RA^{-}$ megakaryocyte-erythroid progenitors (**MEPs**) or $CD135^{+}CD45RA^{+}$ granulocyte-monocyte progenitors (**GMPs**)[72], Notta *et al*. (2016) more recently showed using clonal repopulation assays that in fact unipotent cells can derive directly from HSCs[74]. Specifically, they demonstrated a developmental shift where fetal tissue contains oligopotent progenitors while adult tissue is mainly composed of multipotent and unipotent cells, and erythroid or megakaryocyte cells can derive directly from multipotent HSCs, suggesting a closer developmental path from HSC to erythroid and megakaryocyte lineages[74]. Advances in single cell RNA-sequencing (**scRNA-seq**) has enabled mapping of snapshots of transcriptional states that exist in hematopoietic subsets and provides granular support of the view that "differentiation" is a continuous process without clear transcriptional boundaries, that even unipotent progenitors exist on a spectrum of developmental stages[75,76]. In sum we now have a burgeoning appreciation that the path of hematopoietic differentiation is a highly complex gradient of priming and cellular decisions in response to intrinsic and extrinsic signals; and in hand with this complexity comes uncertainty, as defining cell fate decisions from cell potentials remains challenging (see section **1.5 Hematopoiesis in High Definition: Combining State and Fate Mapping** for further discussion). Moreover, the enhanced insights into step-wise changes in differentiation potential and biases in marker-defined hematopoietic subpopulation is an important tool in screening and profiling fundamental cellular and molecular biology in enriched cell types.

1.5 Hematopoiesis in High Definition: Combining State and Fate Mapping[77]

The past decade has seen a significant shift in our understanding of the hematopoietic system. What was once believed to be a rigid hierarchical structure with uniform cell populations residing at discrete tiers of a multilineage to unilineage hierarchy is now appreciated to be a much more complex and heterogeneous system. The hematopoietic stem cell (HSC) compartment for instance has been shown to contain both highly dormant and proliferative subsets and encompasses stem cells with a range of differentiation potentials[58,68,78]. Whether these HSC clones with distinct fate biases differ or are related transcriptionally and how they might transit from one type to another remain open questions. All told, the emerging realization of the highly nuanced nature of hematopoiesis challenges efforts that hope to capitalize on a mechanistic understanding of fate decision-making in the blood system to advance cell-based therapies or chart the origins of disease. To address this, novel tools are emerging that allow an unparalleled understanding of both the molecular nature of individual cells in a tissue as well as their ontological relationship to other types[79,80]. In particular, two studies published recently in Science and Cell Stem Cell unite lineage tracing and scRNA-seq to make possible simultaneous measurements of clonal history and cell identity in hematopoiesis[81,82].

Lineage tracing approaches involve heritably marking an ancestral cell in order to track and identify the more mature cell types it derives. Historically these strategies have been limited by a low diversity of tags (dyes or fluorescent markers). Advances in DNA barcoding now enable high-throughput clonal tracking, however the established "fate maps" remain limited in resolution

due to the existing requirement that endpoint measurements adhere to "known" cell types[83]. Conversely, unbiased single-cell molecular profiling has enabled the construction of granular theoretical tissue hierarchies without prior knowledge of cell types. By interrogating gene expression from many cells across all stages of differentiation scRNA-seq has been used to predict differentiation trajectories and generate high resolution "state maps". Inherent to this approach is the need to catalogue many co-existing clonally diverse populations, and while attempts have been made to reconcile individual ontologies from these transcriptomes the accuracy of the inferred lineage reconstruction is unknown[84].

In two recent complementary studies, Weinreb *et al*. (2020)[81] and Pei *et al*. (2020)[82] developed new genetic labeling strategies that result in expressed barcodes which are simultaneously detected with global transcriptional information in scRNA-seq workflows. In doing so their efforts represent some of the first attempts to synthesize fate and state maps as a means to bridge the existing gaps in the hematopoietic atlas. First, Weinreb and colleagues introduced LARRY (lineage and RNA recovery), a protocol involving lentiviral delivery of GFP 3'UTR-encoded DNA barcodes into mouse hematopoietic stem and progenitor cells (HSPC) *ex vivo*. Cells were allowed to undergo an initial round of division to expand clonal sisters which were then sampled for scRNA-seq immediately and sequentially at multiple time points from either in vitro culture or *in vivo* after transplantation. By overlaying differentiation paths of clonally related sister cells onto the scRNA-seq state maps the authors defined clear transcriptional boundaries that encompass unipotent progenitors while bi and oligopotent progenitors existed in a structured continuum of gene expression. Comparison of in vitro and in vivo trajectories demonstrated that despite transcriptomic lineage priming, fate determination can be significantly swayed by environmental cues. Weinreb and colleagues demonstrated that while transcriptional state correlates with fate outcome, it is accurate in predicting cellular decision-making only ~50-60% of the time, suggesting that other "hidden" non-transcriptional variables contribute to fate. While powerful, the authors pointed out that LARRY requires that the system under query is amenable to ex vivo manipulation and serial sampling, and impinges on the assumption that early division sister cells are highly similar.

In contrast Pei *et al*. described a complementary method to track clonal progression and single-cell transcriptomes of HSC without *in vitro* manipulation and in their native environment. Here they developed the *PolyLoxExpress* allele which is composed of a cassette of 9 arrayed DNA blocks interspersed by loxP sites that is positioned in the 3'UTR of a transgenic reporter. In the presence of a pulse of Cre, in this case induced by tamoxifen in Tie2 expressing cells, random rearrangements occur in the array resulting in a diversity of DNA barcodes. The authors took advantage of the knowledge that Tie2 marks developing HSCs to induce endogenous barcodes in utero. They found that this approach was highly successful in tagging the majority of adult HSCs before their migration into the BM. By combining clonal relationships and scRNA-seq of the resultant adult hematopoietic populations Pei and colleagues were able to functionally define adult HSC as either multilineage, myeloid-erythroid restricted or differentiation inactive (in their words "childless") in their fate potentials as well as to show that like-fated HSCs generate like-fated HSCs. While whole transcriptome clustering did not readily elucidate fate determination, the authors were able to apply knowledge of fate outcomes to uncover specific transcriptional signatures that distinguished the differentially fated HSC. Intriguingly they also demonstrate that when assessed at a single-cell level, fate potential under physiological conditions is not strongly associated with transcriptional profiles of canonical short- or long-term HSC that have been defined by their capacity to sustain hematopoietic engraftment after transplantation. Furthermore,

by dissecting at a single-cell level the cell cycling states of HSC with varying fate potentials Pei and team provided evidence that dormant HSCs *in vivo* are both differentiation-active and inactive, informing on how these presupposed reserve cells might function when awakened[68].

The complementary approaches applied in each of these studies provide exciting opportunities for future research. In particular, the nature of *ex vivo* labeling and sister cell tracing employed by Weinreb *et al*. positions it as an ideal approach for detailed study of human hematopoietic cells that cannot be interrogated *in situ*. The application of this strategy could uncover state determinants that define *bona fide* functional HSCs, enhance HSPC output, or govern trajectories toward clinically relevant mature cell types in culture and after transplantation. On the other hand, the tool developed by Pei and colleagues could prove valuable to interrogate native and clonally driven, non-physiological hematopoiesis such as that which occurs in response to mutations that seed hematopoietic disease, aging, or injury, the latter of which has already been attempted using a CRISPR-based approach by Bowling *et al*. (2020)[85]. Lastly, rapid advances in genome-wide single-cell technologies (e.g., proteomics and epigenetics) all but ensure new and potentially more predictive dimensions in state maps which will contribute to establishing an unprecedented molecular understanding of the blueprints that specify developmental, regenerative, and pathogenic cellular ontologies in the hematopoietic system.

1.6 HSCs in the Clinic

HSPCT has been in clinical practice for >60 years and is the leading cell-based therapy[20]. While once reserved to the highest-risk cancer patients, HSPCT is now a treatment for a number of malignant and non-malignant disorders, including blood replenishment post-irradiation, congenital and acquired autoimmune or blood disorders[86-91] and has been used to treat more than a million patients to date[20]. HSPCs can be of either autologous (self) or allogeneic (donor) sources. Allogeneic HSPCs sources can further be grouped as coming from adult donor mobilized peripheral blood (**mPB**) or BM or from umbilical cord blood (**CB**)[20] (**Table 1**). As of 2012 ~58% of transplantations were still of an autologous source, and only 5-6% of transplants were performed for the treatment of non-malignant diseases indicating that there is significant room for the range of clinical indications to continue to grow[92]. Self-tolerance is a major advantage of autologous HSPCT, however even with extensive HSC purification, residual pre- or frank malignant stem cells contaminate autologous BM or peripheral blood risking relapse[20,93] and highlighting a key clinical gap that allogeneic HSPCT could fill with further advancements. A major barrier in allogeneic HSPCT is procuring sufficiently HLA-matched donations[92]. Greater than 30% of patients will not find an HLA matched donor and this challenge is drastically increased in racially diverse individuals. Poor HLA matches can put transplant recipients at risk of life-threatening acute and/or chronic GvHD, which occurs when donated HSPC give rise to immune cells that recognize the recipient's body as foreign[92,94-97]. To this point, immunologically superior CB presents as an appealing alternative source for allo-HSPCs[94,96,98].

The first CB HSPCT was performed in 1989 to treat a pediatric patient with Fanconi's anemia[99]. CB HSPCs can be easily and non-invasively harvested and CB banking has been underway both privately and publicly since 1993[100], making it relatively easy to procure. Additionally, as it is immunologically naïve CB is more permissive to HLA-mismatching and possesses significantly reduced risk of GvHD relative to adult-sourced HSPCs while simultaneously its mild allo-reactivity has been shown to support a positive immunotherapeutic graft-vs-leukemia effect[96]. While CB is a highly enriched source of $CD34^+$ and long-term reconstituting cells compared to adult HSPC sources[101,102] the donations are inherently small,

limiting the absolute number of HSPC available per donation[92]. Transplanting insufficient numbers of HSCs can lead to delayed hematopoietic recovery, long-term graft failure and ultimately increase patient morbidity and/or mortality[103,104]. Therefore, a major pre-clinical objective has been to amplify HSPCs with enhanced functional properties to improve transplant outcomes [51,105,106]. These objectives aim to dually expand committed cells to initiate rapid myeloid repopulation in an immune-ablated patient while also expanding and/or maintaining long-term repopulation competent cells. In many ways these objectives have been at odds with one another such that established culture conditions activate stem cells to promote their division and differentiation but do so at the expense of their long-term self-renewal.

Using autologous peripheral blood HSPCs it was initially demonstrated that their *ex vivo* expansion in cytokine-supplemented media could accelerate neutrophil repopulation in clinical transplantation. Applying the same principles to cord blood expansion Shpall *et al*. (2002) showed that while it is feasible to expand allo-CB HSPCs they were not imparted with the same rapid advantage[107]. Directly comparing the series of advances to follow is challenged by the fact each trial employed different protocols, namely the use of dual cord blood units from different donors, vs. a single manipulated unit, vs. a single unit divided as a manipulated and an unmanipulated fraction. Adding the Notch1 ligand DLK1 to the cytokine-supplemented media Delaney *et al*. (2010) presented the first example of ex vivo expanded HSPCs accelerating time to neutrophil recovery in clinical setting, however this procedure required a lengthy culture (16-21 days) and at 3 months follow up the majority of patients showed dominance of the unmanipulated CB unit[108,109]. Attempting to further recapitulate their native environment 14-day mesenchymal stem cell (MSC) co-culture systems were developed to expand CB HSPCs[110] for double unit transplantation. While time to myeloid engraftment was significantly improved the unmanipulated unit dominated and was the only source of hematopoiesis in all patients by 1 year follow up[111]. These approaches made use of double cord blood units and depletion of the manipulated grafts are strongly presumed to be the result of allo-T cells from the unmanipulated unit against the expanded unit, where T-cell depletion would have occurred in myeloid-stimulatory culture[112]. Clinical trials of CB HSPCs expanded for 21 days with the copper chelator tetraethylenepentamine (**TEPA**, StemEx®) similarly showed accelerated hematopoietic recovery however as the manipulated and unmanipulated fractions were derived from a single unit the long-term maintenance of the expanded graft is unknown[113]. On the other hand, when assessed in phase I/II clinical trial NiCord®, a cord blood product expanded for 21 days in the presence of nicotinamide and co-infused with the unit's T-cell fraction, was able to shorten the time to hematopoietic recovery, sustain long-term engraftment in most patients, and be used as a stand-alone product[114,115]. Many other approaches have been attempted with varying success, and most of which have not yet been tested in clinical trials. These include the addition of Prostaglandin e2[116], altering the extracellular matrix for example using zwitterionic hydrogel[117,118], and epigenetic and metabolic rewiring with valproic acid (**VPA**)[119-122]. Two of the most notable examples to date are CB HSPC expansion via small molecules StemRegenin-1 (**SR-1**) or UM171 explained more below.

Screening a library of 100,000 molecules, SR-1 was identified for its ability to increase $CD34^+$ cells cultured in cytokine-supplemented media by inhibiting the transcription factor (**TF**) Aryl hydrocarbon Receptor (**AhR**)[105]. SR-1 supplementation resulted in unparalleled 330-fold expansion of $CD34^+$ cells over 15 days, far exceeding other approaches at the time, and in some cases yielding more than the maximum transplantable cell dose[52]. When tested in limiting dilution series xenotransplantation SR-1 increased HSC frequencies relative to base cultured cells 15-fold and 17-fold relative to uncultured cells[105]. When tested in double CB phase I/II clinical trial

transplantation the SR-1 manipulated graft was dominant in 11/17 patients, despite lower CD3 T cell doses from those units. Moreover, in these 11 patients the time to neutrophil and platelet recovery was significantly faster and engraftment was sustained at the 1 year follow up time point[52].

UM171 was also identified by screening a library of 5280 compounds which yielded 7 hits, of which only 2 acted in an AhR-independent manner. Further chemical optimization of the more potent of the two compounds yielded UM171 with capacity for $CD34^+$ expansion. UM171 must be constantly present in the culture media but following 12 days of culture was able to expand $CD34^+$ to similar levels as SR-1 and outcompeted SR-1 at expanding phenotypic LT-HSCs. When tested in limiting dilution series xenotransplantation UM171 expanded functional LT-HSCs 15-fold relative to base culture and displayed a non-significant 6-fold elevation in LT-HSC frequencies relative to SR-1 supplemented cultures. Interestingly the combination of SR-1 and UM171 did not synergistically provide added advantage over either treatment alone[51]. The follow up phase I/II clinical trial results recently published showed that patients that received a single 7-day UM171-manipulated CB unit experienced rapid neutrophil and platelet recovery, no patients had graft failure after 1 year, and all appeared to experience less severe GvHD[123]. However, the mechanisms of action downstream of UM171 remain elusive.

While significant gains in advancing the clinical utility of CB HSPCs have been made, lengthy expansion regimens required by these interventions pose as a manufacturing barrier and risk replicative damage, differentiation, exhaustion or contamination[51,105,114]. For some expansion modalities transient repopulation by manipulated HSPCs and the requirement of a second unmanipulated CB unit[52,109,111,113] points to persisting limitations in our ability to recapitulate HSC physiology *in vitro*[124,125]. Moreover, we do not fully understand the biology underlying those most potent CB expanding agents. These gaps and limitations in promoting self-renewal and preservation of long-term HSC under various regenerative demands more broadly pose as barriers to the advancement of multiple clinical applications in the areas of *ex vivo* tissue engineering and gene therapy. Enhanced fundamental insights into the properties that define long-term identity and fate-choices in human HSCs can thus inform the rational design and advancement of HSC-based regenerative therapies.

1.7 HSC Quiescence: Protection from replicative a metabolic stress

In the fetal liver, where HSC expansion occurs, nearly all HSC are actively cycling and self-renewing[126] however shortly after birth (in mouse 3 weeks and in human 1-3 years) adult BM HSCs exist principally in a quiescent state[126-128]. The developmental shift in proliferative capacities is also mirrored when comparing cultured human CB to BM HSPCs wherein CB cells exhibit a higher capacity for replication in the same timeframe of culture[129]. Each cellular division cycle introduces the risk of damage by DNA breaks, mutations, telomerase shortening or damage from excess reactive oxygen species (**ROS**). As such, quiescence is believed to protect HSC from replicative and metabolic stress, which contributes to their aging and exhaustion, thereby preserving the long-term integrity of the HSC pool[130,131].

Two main methods have been used to measure divisional history in murine HSCs, incorporation of the thymine analogue BrdU or conditional expression of histone H2B-GFP fusion protein where cells are pulsed to label DNA with BrdU or H2B-GFP and in a subsequent chase period the labels will be partitioned into daughter cells through cell division. The decay kinetics are therefore a readout of the number of divisions that occur over a defined time interval, such that label-retention marks cells that are not actively dividing[132]. Estimates from BrdU incorporation

experiments indicate that at any given time approximately 8-10% of multipotent mouse HSPCs are asynchronously transiting cell cycle and divide approximately once in 30-50 days[133]. Using enhanced purification strategies these estimates were refined to show ~5% of LT-HSC vs. 18-19% of ST-HSC or MPP incorporated BrdU immediately following a 1-hour pulse, and that there is a progressive increase the proportion of actively cycling cells as progenitor sub-populations became more lineage-committed, which roughly correlates to the size and blood production needs of that population[134]. This was also consistent with the understanding of HSC as slow dividing and progenitors as fast dividing as inferred by their sensitivity to the cell cycle-targeting cytotoxin 5-fluorouracil (**5-FU**)[135], which was also historically used to enrich HSC from murine BM[136]. The symmetric (self-renewal) vs. asymmetric (differentiation) nature of divisions is also correlated with expression changes in specific cell cycle genes. For example LT-HSC differentiation into ST-HSC is associated with elevated cyclin D1, while commitment to MPP is associated with reductions in cyclin dependent kinase inhibitors (p16, p18, p27, p57) and increases in cyclin G2 & B1[134].

Using the histone H2B-GFP fusion protein to track cell divisions it was further shown that among the HSC population there is a small fraction that are more dormant and retain their label for 120 (22%), 213 (18%) or 380 (few) days, whereas all progenitor cells experience label decay by 100 days[68,137]. Moreover, *in vivo* HSCs return to quiescence following almost every division, whereas *ex vivo* they do not[68]. It is predicted that this dormant subfraction of HSC was not captured by BrdU tracking experiments because it is mildly cytotoxic leading to HSC activation[132,138]. Thus within the "LT-HSC" fraction cells are heterogeneous with regards to their quiescence and dormancy with two types of subpopulations having been proposed: a homeostatic or "activated" subset (~70%) that divides every 30-50 days and contributes to daily blood production needs and a "dormant" subset (~30%) that has very low level activation of the replication machinery, restricted metabolic status and undergoes division every ~150 days. It is the latter subpopulation that has been proposed as the likely reservoir that supports hematopoiesis in the case of injury[132].

While similar measurements *in situ* in the human context are not possible, evidence supporting that, like in the murine system, human LT-HSC are also more deeply quiescent than their immediately downstream progeny has recently been presented. Assessing LT vs. ST human HSCs in culture Laurenti *et al* (2016) show that the time to first division (i.e the decision to exit G0) is longer in LT-HSC, and as more cycles are accumulated the time to quiescence exit also decreases. Looking at gene expression changes a notable difference in LT- and ST-HSCs was the expression of cell cycle genes, in particular CDK6[139]. However, many CDK6-expressing ST-HSCs did not co-express its complex partners Cyclin D1 and D3, thus CDK6 expression is proposed as a priming event rather than an indicator of actively engaged cell cycle progression[139]. Additionally, modelling suggests human HSCs divide once per 40 weeks[140], and when compared to mouse, cat[141] and non-human primates[142], suggests a conserved number of HSC divisions over the lifespan of different mammalian species. This also highlights a key difference in the relative contribution of HSC vs. progenitors to daily blood production in mouse and human, and thus potentially the species-specific molecular determinants of these properties[2]. A key example of this is the differential use of p53-mediated DNA damage pathways in mouse and human HSCs. Double stranded break (**DSB**) repair can occur by two complementary methods, either homologous recombination which is restricted to cycling cells as it makes use of a sister chromatid as a repair template, or nonhomologous end joining (**NHEJ**) which is more error-prone but can occur in non-replicating cells. Upon irradiation-induced DSB, quiescent mouse HSCs will favour p53-mediated signaling to promote survival, slow cycling, and repair DNA damage by NHEJ, ultimately

predisposing them to genomic instability[143] . In contrast, human HSCs are more likely to delay DNA repair and undergo apoptosis in response to irradiation-induced DNA damage[144]. These different mechanisms likely reflect the differing tolerance for accumulating DNA damage in cells with significantly different lifespans[1,2].

HSC must balance their metabolic program to adapt to changes in energy demands as they switch between dormant/quiescent or active/cycle-primed and cycling states. HSCs maintain low mitochondrial membrane potential (**MMP**)[145], therefore it has been believed that HSC rely on glycolysis for ATP production while restricting ROS accumulation[146]. While there is debate on whether this is primarily directed by cell-extrinsic signals from a hypoxic niche or cell-intrinsic mechanisms[145,147], the focus here will mainly be on intrinsic signaling. Transcriptionally activated HSCs express elevated signatures of tricarboxylic acid cycle (**TCA**) and other anabolic processes in what appears to be a gradual gain in metabolic activity preceding cell division[148]. To this point, using 5-FU to induce HSC cycling Umemoto *et al*. (2018) show that murine HSCs experience heightened MMP and a requisite influx of calcium prior to engaging cell division. Moreover, using a calcium channel blocker they show that decreased calcium levels can prolong cell division resulting in a favouring of renewal over differentiation[149], interestingly highlighting the intersection between metabolism, cycling and cell fate. Consistent with the notion of a heterogeneous LT-HSC population Liang *et al*. (2020) show that 75% of the murine HSC population exhibits high MMP (activated/primed) while 25% have low MMP (dormant), but that this is notably not marked by a shift in glycolysis[150]. MMP-high HSCs in fact are still reliant on high levels of glycolysis to feed the TCA cycle and similarly to previous reports[151], they show that MMP -low and -high HSCs have comparable mitochondrial mass. Their findings attribute low-MMP to a key distinction between lysosome-mediated mitochondria turnover in these populations, suggesting that in MMP-low HSCs the mitochondria appear less mature and associated with "sluggish" or less active lysosomes[150]. In contrast, recent evidence from human LT-HSCs subjected to culture-induced activation indicates high levels of lysosome activity, driven by its transcription activator TFEB, are required to maintain their quiescence. In this context lysosomes appear responsible for trafficking surface receptors, such as transferrin receptor 1 (TfR1) to limit their activation and preserve metabolic stillness[152]. The same study also showed that, like in their murine counterparts[148], when human LT-HSC transition between quiescent and active states MYC and its cell cycle, metabolism and protein production targets are elevated[152], and that MYC counteracts TFEB by repressing the expression of lysosome components.

It has repeatedly been demonstrated by transplantation assays that the most potent cells capable of long-term engraftment reside in the quiescent (G0) or dormant state[68,127,153,154], and that loss of this potency is seen when HSC exit quiescence and enter G1[134]. Similarly, fractionating the mouse and human HSC compartment based on MMP using tetramethylrhodamine, ethyl ester (**TMRE**) dye can enrich for cells with the greatest serial transplantation potential[150,155], and metabolic disruption in murine HSC leading to quiescence exit, such as the loss of Lkb1[156], Meis or Hif-1a[157] impairs hematopoietic repopulation. Both mobilization of human HSC and their *ex vivo* culture stimulate the cells into cell cycle[68] and as such, a standing prediction is that re-establishing the quiescent or dormant state in these donor cells could have important implications for improving clinical transplantation outcomes[134,158]. Indeed, murine HSC in hibernation cultures that support a more dormant *in vivo*-like molecular identity maintain their transplantation and renewal capacities, features readily lost by HSC in cytokine-rich activating cultures[159]. Additionally, restraining lysosome activity and calcium levels to promote a low metabolic status improves sustained murine HSC engraftment[150,160]. Lastly, while there are only a few examples,

we see from studies of human HSCs that establishing quiescent or dormant features improves their numerical maintenance and endurance in xenotransplantation. For example, ectopic expression of TFEB or a constitutively nuclear variant amplified the number of serially engrafting human HSC by enhancing lysosome-mediated quiescence, however this appears at the expense of robust graft sizes, suggesting this could be at the expense of effective progenitor and blood repopulation[152]. Overexpression of INKA1 (and to a lesser extent pharmacological inhibition of its target PAK4) enforced quiescence in cultured CB HSPCs to amplify the frequency of long-term engrafting HSCs while enforcing an initial latency phase in early stage of xenotransplantation[161]. Xie *et al*. (2019) also found upon differentiation or culture-activation human HSPCs experience lipostatic stress, and that genetic or pharmacological inhibition of the endoplasmic reticulum (**ER**)-associated ceramide biosynthesis enzyme DEGS1 in CB HSPCs endows lipostasis reminiscent of dormant (i.e. uncultured) cells to increase LT-HSC frequency on a per-cell basis in culture. They further showed that this approach could additively improve LT-HSC frequencies imparted by dual SR1 and UM171 treatment, although at the expense of culture-expanded committed progenitors[162].

1.8 HSC Protein Synthesis and Proteostasis

As discussed above, HSCs must dynamically regulate cellular metabolism to balance dormancy and activation decisions to ensure daily and life-long hematopoiesis. Protein production rates are in many contexts co-regulated with cellular metabolism, and when activate can also fuel cellular growth and division[163,164]. Indeed, in their native BM environment murine HSCs, like several other types of stem cells, require tightly-controlled low levels of protein synthesis[165,166]. Reduced protein synthesis in heterozygous *Rpl24* mutant HSCs impaired *in vivo* regeneration and conversely translation activation by *Pten* deletion led to HSC depletion[165]. Similar to their developmentally-linked enhancement in proliferative capacities, translation rates are elevated in fetal compared to adult murine HSCs, but interestingly fetal HSCs are still just as sensitive to impaired ribosome biogenesis[166]. Regulation of HSC translation rates is also partly uncoupled from their quiescence status, such that translation is lower in dividing HSCs than dividing progenitors[165]. Similarly, translation rates are lower in quiescent HSCs than equally quiescent fractions of leukemia stem cells (LSCs)[167]. This importantly points to the role of regulated protein production as supportive of HSC physiology in ways that transcend its influence over cellular proliferation[165]. To this point, San Jose *et al*. (2020) elegantly demonstrated firstly using ubiquitin proteosome reporters and unfolded protein labels that murine HSCs maintain higher proteome quality than progenitor cells. Secondly, using a number of genetic models, they showed that in functionally defective HSC with activated translation (*Pten* deleted) there was an accumulation of ubiquitinated and unfolded proteins and that hematopoietic function and protein integrity could both be restored by inhibiting translation (*Rpl24* mutated)[168]. The researchers also demonstrated that high proteome quality is critical to the maintenance of HSC function independent of translation rates by using a mouse model with mutations in alanyl-tRNA synthetase to increase amino acid misincorporation but not translation rates[168]. Additionally, restraining ER stress/unfolded protein response (**UPR**) by Developmental pluripotency-associated 5 (Dppa5) overexpression in murine HSCs exposed to extended culture significantly enhanced their LT repopulation activity[169]. Van Galen *et al*. (2014) also show that relative to progenitors human HSCs are highly sensitive to activation of endoplasmic reticulum UPR and their survival and repopulation capacity after ER insult can be improved by ectopic expression of the protein chaperone ERDJ4[170]. Importantly however the most potent stem fractions of both cord blood and leukemia also employ stress-induced delay in translation initiation and attenuation of global translation via the Integrated Stress Response (**ISR**)

as a protective mechanism to achieve an appropriate pro-survival balance in response to mild-to-moderate "homeostatic-level" stressors, such as culture, transplantation or amino acid deprivation[171]. Therefore, highly regulated translation rates serve as one means by which HSCs not only promote their dormancy but also ensure with exquisite control their proteostatic integrity to evade attrition or death due to proteotoxicity.

Transcriptional profiles from both mouse and human HSCs point to a robust activation of protein production machinery associated with HSC activation[148,152,172], as has also been shown for other stem cell types[173]. In response to stimulatory conditions the activation of stress effectors in murine HSC serves to rebalance proteostasis by favouring diminished translation rates[172,174]. Kruta *et al*. (2021) recently demonstrated in murine hematopoietic cells that HSCs selectively experience a rapid and significant hyperactivation of translation when placed *in ex vivo* culture[172]. The associated cytosolic protein stress stimulates the nuclear localization of the Hsf1 TF where it promotes gene expression programs to restore proteostasis and promote survival; and enforcing this mechanism via Hsf1 agonists in cultured murine HSCs improved their hematopoietic repopulation in serial transplantation[172]. Another example is enhancement of both human and mouse hematopoietic *in vivo* repopulation following a brief *ex vivo* treatment with Angiogenin (RNase5), which from detailed murine investigation was shown to enact opposing translation control in stem vs. progenitor cells. In progenitor cells Angiogenin is localized in the nucleus to promote the expression of ribosomal RNA (**rRNA**), but in stem cells it moves to stress granules in the cytoplasm where it promotes suppressed global translation while preferentially driving the translation of ISR genes[174]. While translation control in human HSCs and its utility as a means to preserve the human HSC pool for regenerative medicine remains largely underexplored, the association of ribosomopathies with a number of phenotypically diverse human blood disorders[175-177], including the activation of protein biosynthesis in high-risk MDS and frank leukemia[167] showcases the conserved and critical importance of nuanced control of protein production in the developing and adult human hematopoietic system. Moreover, while these studies have significantly informed on the multifactorial contributions to HSC dormancy and fate, they also raise a number of key questions: under activating conditions what are the dynamics of translation in human HSCs vs mature hematopoietic cell types?; can translation modulation be supportive of human HSCs?; can translation regulation be decoupled from stress response? and what factor(s) control translation in human HSCs?

1.9 Searching for Regulators of Human HSC Renewal: MSI2 and PLAG1

As noted above there are key differences in murine and human HSC including lifespan, cycling kinetics, telomere length and DNA repair mechanisms. It is therefore reasonable to conclude there could exist species-specific molecular determinants of HSC cellular properties[2]. This is made more evident by the fact that many key mutations underlying human disease states do not confer the same disease phenotypes in mice[38] (**Table 2**). The murine model has been an indispensable system to garner cellular and molecular insights into hematopoiesis, particularly for measures *in situ*, under homeostasis or throughout development and insights here have in many cases been found paralleled in human counterpart cells. However, it is also important to note that molecular regulators of HSCs, including those that can act as self-renewal agonists or seed leukemic transformation are defined as such specifically in the human context. A notable example of such discrepancy is HoxB4, which when overexpressed in murine HSCs expands stem cells 1000-fold[178], but when ectopically expressed in $CD34^+$ CB only produced a 2-4x expansion of human HSC[179,180].

Our research team demonstrated that, consistent with mouse studies[181], the RNA-binding protein Musashi-2 (**MSI2**) is essential for human CB HSC self-renewal, and supraphysiological levels of MSI2 is capable of amplifying HSPCs with long-term BM reconstitution potential by inhibiting AhR, similar to SR-1[182]. Dysregulated MSI2 levels have also been associated with aberrant hematopoiesis[183-193], thus it was conjectured that identifying upstream MSI2 regulators may inform on critical mechanisms that maintain HSPC homeostasis and seed the discovery of novel factors involved in human hematopoiesis. To this point Belew *et al*. (2018) designed a reporter-based promoter activation screen in the K562 cell line derived from BM of a patient with Chronic Myelogenous Leukemia (**CML**) in search of TFs capable of trans-activating the MSI2 promoter[194]. Two TFs, Upstream Stimulatory Factor (USF) 2 and Pleomorphic Adenoma Gene (PLAG)1, were individually capable of modestly activating the MSI2 promoter and endogenous MSI2 expression in K562 cells, and when dually overexpressed, they cooperated to significantly elevate MSI2 expression 2.5-fold higher than either factor alone. USF2 expression is ubiquitous in the hematopoietic hierarchy and was previously shown as putatively important in maintaining HSC fate through regulation of HOXB4 gene expression[195,196]. On the other hand, PLAG1, expression is highly enriched in the primitive HSC compartment.

PLAG1 is a member of the PLAG family of zinc (Zn)-finger TFs that also includes PLAG-like 1 (PLAGL1) and PLAG-like 2 (PLAGL2). The *PLAG1* gene was discovered by studying recurrent chromosome rearrangements associated with pleomorphic adenomas of salivary gland[197]. Reciprocal translocation events between *PLAG1* and *CTNNB1* (encodes β-catenin), *LIFR* (encodes leukemia inhibitory factor receptor), *CHCHD7* (encodes: Coiled-Coil-Helix-Coiled-Coil-Helix Domain Containing 7*)* and *SII/TCEA* (encodes transcription elongation factor SII) results in "promoter swapping" between the relatively low level expressed and developmentally-regulated PLAG1 and these more constitutively and highly expressed gene products leading to significantly elevated levels of PLAG1[198-200]. The PLAG1 gene encodes 3 protein variants. Full-length PLAG1 (PLAG1-A) encodes 7 N-terminal Zn-fingers and a C-terminal serine-rich transactivation domain. The Zn-fingers recognize a bipartite G-rich consensus motif consisting of the core GRGGC that is recognized by Zn finger 6 and 7, and separated by 8-6 nucleotides a RGGK G-cluster is recognized by Zn finger 3. Alternative splicing forms an 82-nt N-truncated variant called PLAG1-B and alternative translation initiation at Met-100 encodes the shortest PLAG1 variant (PLAG1-S)[197,201]. In the primitive human hematopoietic compartment PLAG1 is predominantly expressed as PLAG1-B and PLAG1-S variants[194].

Comparing microarray-based gene expression profiles from PLAG1-elevated pleomorphic adenomas to normal salivary gland tissue and HEK293 cells immediately following induction of ectopic PLAG1, Voz *et al*. (2004) show that several PLAG1 targets are growth factors, including insulin-like growth factor 2 (IGF2), cytokine-like factor 1 (CLF-1) and bone-derived growth factor 1 (BPGF-1)[202]. IGF2 expression is correlated with PLAG1 and activated by PLAG1 in several cell contexts, including PLAG1-transformed murine pleomorphic adenoma[203,204], human pleomorphic adenomas[202,205], HEK293 cells[202], human hepatoblastomas[206] and PLAG1-transformed NIH-3T3 fibroblast cells[207]. Moreover, fibroblasts deficient for the IGF2 (and IGF1) receptor, IGF-1R, could not be transformed by ectopic PLAG1[207], therefore the prevailing view is that PLAG1 impinges on dysregulation of IGF2-induction of IGF-1R and downstream mitogenic MAPK signaling and anti-apoptotic PI3K-AKT signaling to promote tumorigenesis[208]. It is also presumed that Igf2 is an important effector contributing to fetal growth restriction in constitutive Plag1 knockout mice[209], and in PLAG1-mutated cases of Russell-Silver syndrome, a human fetal growth disorder[210]. In addition to IGF2 upregulation noted in murine and human cell systems, transformation of murine

salivary glands by Plag1 overexpression was associated with elevated expression of the imprinted long non-coding RNA from the same loci as Igf2, H19, and elevated expression of another imprinted loci Dlk1/Gtl2 (DLK1/MEG3 in human)[203]. PLAG1 also activated expression of the imprinted cyclin dependent kinase inhibitor 1C (CDKN1C /p57) in human salivary tumors, which given its function as a cell cycle inhibitor is somewhat incongruent with PLAG1's role as an oncogene[202]. These targets are notable in the study of hematopoiesis as in the murine system CDKN1C (p57) is an essential regulator of HSC quiescence and renewal[211,212], Igf2 signaling is regulated via a feedback loop whereby miRNA (miR)-674 encoded from H19 inhibits Igf1R-PI3K-AKT signaling and multiple miRs encoded from the Gtl2 locus likewise inhibit PI3K-AKT signaling to promote fetal HSC quiescence[213,214]. In general, very little is known of the role of PLAG1 in healthy or adult tissues, possibly in part because past experiments relied on relatively insensitive approaches to determine PLAG1 expression in adult tissues and it has been assumed to be either not present or present at functionally insignificant levels in these settings[197,201]. Our findings that PLAG1 can cooperatively activate MSI2 expression and more refined expression profiling showing that PLAG1 levels are detectable and enriched in the primitive hematopoietic context provide the impetus to investigate its role in this context.

Summary of Intent

1. Functional characterization of the role of PLAG1 in human HSPCs.
2. Profile the PLAG1-directed molecular circuitry via genome-wide approaches in human HSPCs.
3. Functional validation of the molecular mechanisms downstream of PLAG1 in human HSPCs.

Table 1: Summary of sources of HSPC for transplantation, advantages and disadvantages

Source	**Autologous**	**Allogeneic**	
	Patients own stem cells	**Adult Donor Bone Marrow or Peripheral Blood**	**Umbilical Cord Blood**
Advantages	* Self-tolerance	* Larger donation	* Higher tolerance for HLA mismatch * Anti-cancer immunotherapy
Disadvantages	* Trace contamination by mutated cells	* Invasive * Challenging to find HLA-matched donor * Complications due to poor match (GvHD)	* Small donation sizes and paucity of stem cells

Table 2: Genes associated with human diseases with discordant phenotypes in mouse models.

Gene Mutation	Human Disease	Mouse Phenotype	References
FANCA	Fanconi anemia	Normal	Cheng et al. 2000 [215] Bakker et al. 2013 [216]
DKC1 and **TERC**	Dyskeratosis congenita, gene affects telomers	Later onset BM failure, Mouse telomers are long	Walne and Dokal 2009 [217]
MPL	Congenital megakaryocytic thrombocytopenia, thrombocytopenia and early BM failure	Thrombocytopenia without BM failure, but HSC defects evident in secondary transplants	Alexander et al. 1996 [218] Kimura et al. 1998 [219] King et al. 2005 [220]
RPS19	Diamond-Blackfan anemia	Mild RBC reduction	McGowan et al. 2008 [221] Devlin et al. 2010 [222]
ELANE	Severe Congenital Neutropenia	None	Grenda et al. 2002 [223]
HAX1	Severe Congenital Neutropenia	None	Peckl-Schmid et al. 2010 [224]
BTK	Severe Combined Immune Deficiency (B cell)	None	Conley et al. 2000 [225]
BLNK	Severe Combined Immune Deficiency (B cell)	Mild reduction in B cells	Conley et al. 2000 [225]

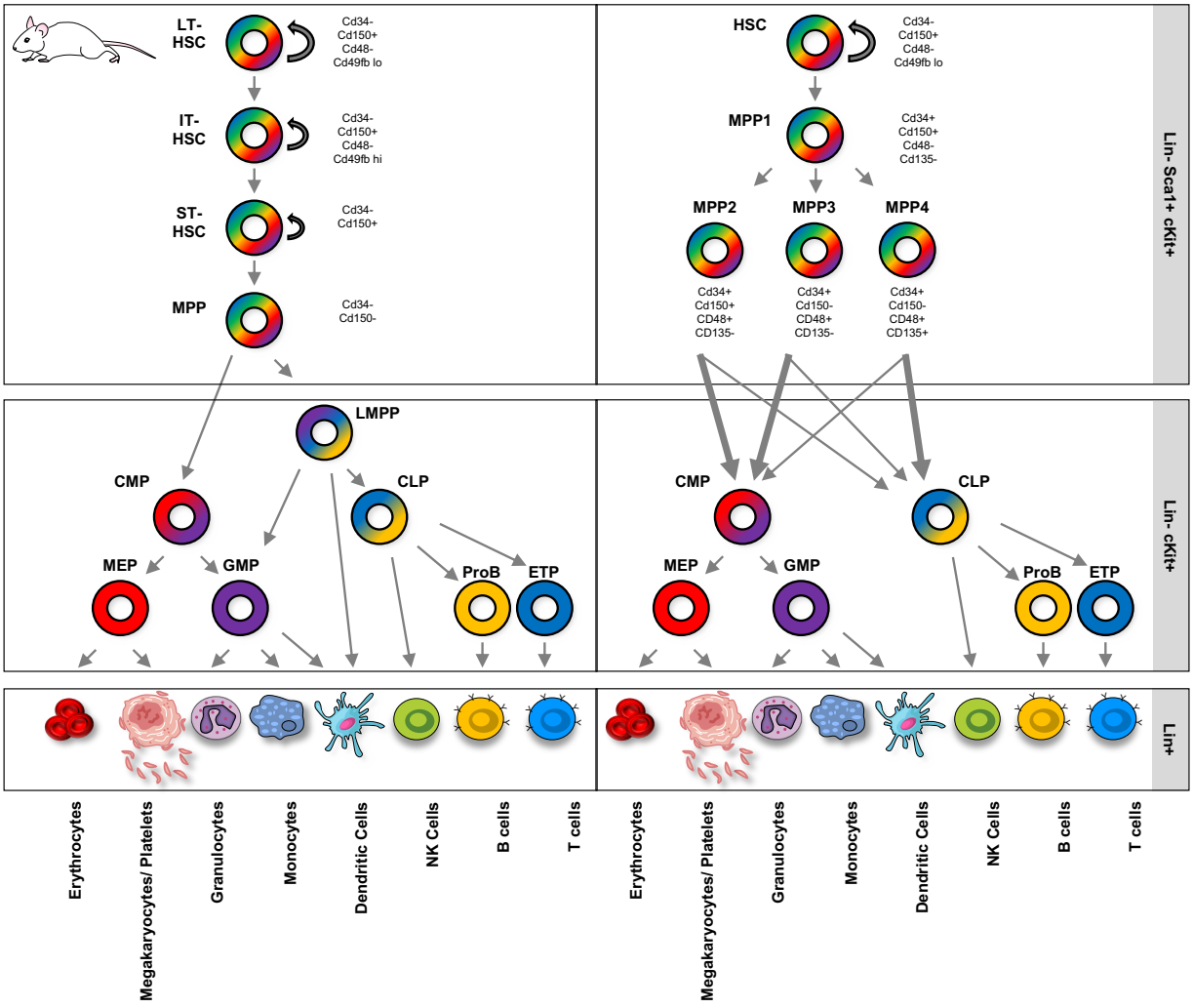
LT-HSC
Cd34-
Cd150+
Cd48-
Cd49fb lo
IT-HSC
Cd34-
Cd150+
Cd48-
Cd49fb hi
ST-HSC
Cd34-
Cd150+
MPP
Cd34-
Cd150-
HSC
Cd34-
Cd150+
Cd48-
Cd49fb lo
MPP1
Cd34+
Cd150+
Cd48-
Cd135-
MPP2
Cd34+
Cd150+
CD48+
CD135-
MPP3
Cd34+
Cd150-
CD48+
CD135-
MPP4
Cd34+
Cd150-
CD48+
CD135+
Lin- Sca1+ cKit+
LMPP
CMP
CLP
MEP
GMP
ProB
ETP
Lin- cKit+
Lin+
Erythrocytes
Megakaryocytes/ Platelets
Granulocytes
Monocytes
Dendritic Cells
NK Cells
B cells
T cells

Figure 1: Mouse hematopoietic hierarchy. Two models of the murine hematopoietic hierarchy with HSCs at the apex and terminally differentiated blood cells at the bottom. These are simplified step-wise depictions of complex relationships between heterogeneous stem and progenitor cell populations leading to lineage restriction. Surface markers are listed for the multipotent cell types.

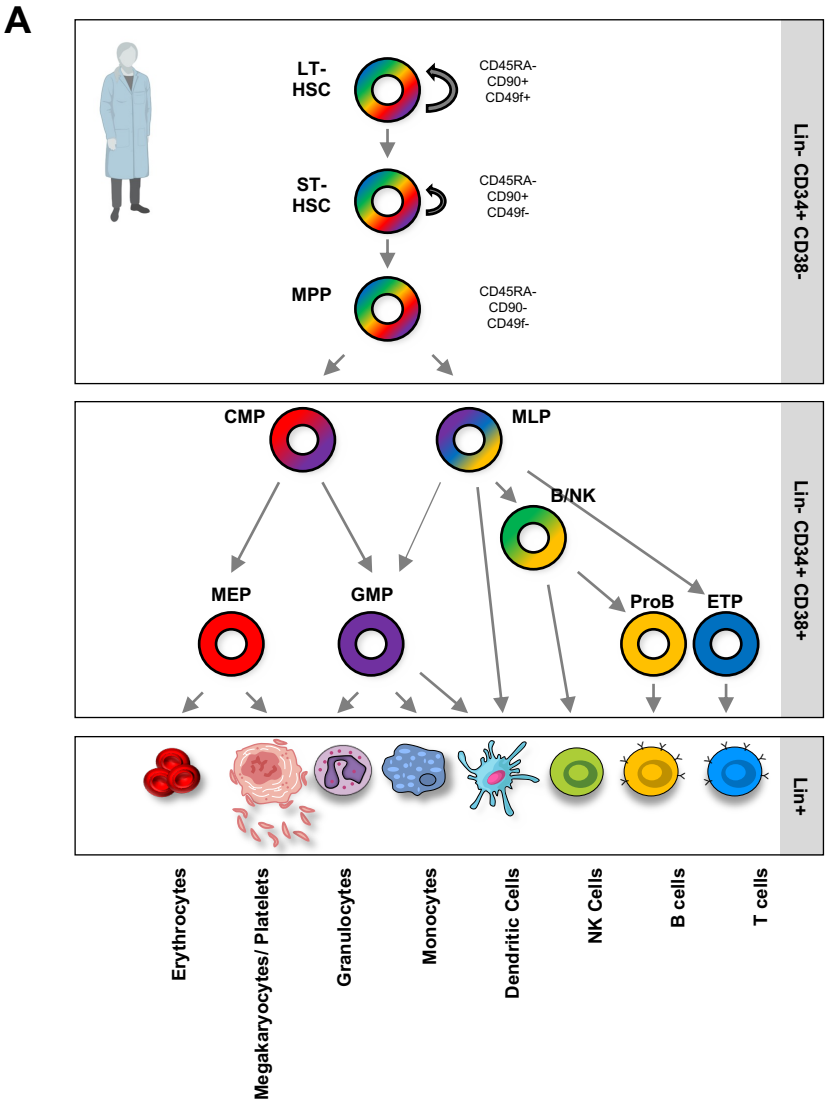
A
LT-HSC
CD45RA-
CD90+
CD49f+
ST-HSC
CD45RA-
CD90+
CD49f-
MPP
CD45RA-
CD90-
CD49f-
Lin- CD34+ CD38-
CMP
MLP
B/NK
MEP
GMP
ProB
ETP
Lin- CD34+ CD38+
Lin+
Erythrocytes
Megakaryocytes/ Platelets
Granulocytes
Monocytes
Dendritic Cells
NK Cells
B cells
T cells

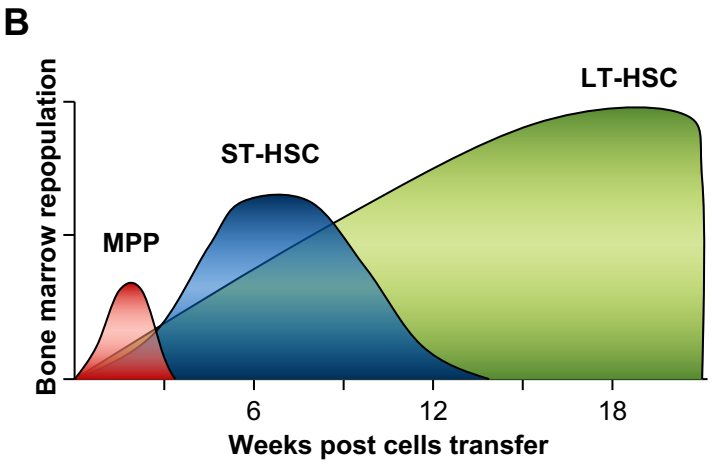
B
LT-HSC
ST-HSC
MPP
Bone marrow repopulation
6
12
18
Weeks post cells transfer

Figure 2: Human hematopoietic hierarchy. (A) Step-wise model of relationships between heterogeneous stem and progenitor cell populations leading to lineage restriction, with HSCs at the apex and terminally differentiated blood cells at the bottom, in human hematopoiesis. **(B)** Schematic of waves of hematopoietic repopulation indicating the cell of origin for each phase.

CHAPTER 2

Materials and Methods

Vectors

Previously used shRNA against the PLAG1 coding sequence (1shPLAG1) or Luciferase[194] had been designed using RNAi Central Design Tool as described in Hope *et al*. (2010)[181] and were cloned downstream of CMV in a miRE30 scaffold[226] in pZIP-CMV-ZsGreen lentiviral expression vector via EcoRI and XhoI for use *in vitro*. For use *in vivo* the same 1shPLAG1 was cloned downstream of U6 via AgeI and EcoRI in PLKO.1-TRC (Addgene Plasmid 10878[227]) in which Puro was replaced with GFP (PLKO.1-TRC-GFP) and compared to shRNA against scramble sequence. A second PLAG1 shRNA targeting the 3'UTR (2shPLAG1) was designed by the Broad Institute GPP Web Portal (https://portals.broadinstitute.org/gpp/public/gene/search) and cloned downstream of U6 via AgeI and EcoRI in PLKO.1-TRC-GFP. Human PLAG1-A, B and S and firefly Luciferase control were previously cloned into pSMALB downstream of the SFFV promoter and bidirectionally to minimal CMV driving BFP expression[194]. Human c-MYC and truncated-NGFR control were expressed in MA1 downstream of hPGK promoter and bidirectionally to minimal CMV driving GFP expression as previously described in Rentas *et al*. (2016)[182]. The microRNA-127 sequence was purchased from Abmgood in the pLenti-GIII-EF1a vector and ZsGreen was cloned downstream of the microRNA sequence or control empty vector via XbaI. The inhibitory sponge against miR-127-5p consisted of eight consecutive bulged 26-mer target sequences separated by 4-mers which was purchased from ThermoFisher Scientific and cloned downstream of SFFV and GFP with XbaI and EcoRI as described previously in Gentner *et al*. (2009)[228] and Lechman *et al*. (2012)[229]. Refer also to **Table 3.**

Cord blood CD34$^+$ cell isolation, lentiviral transduction and *ex vivo* culture

Lin$^-$ cord blood cells were isolated by density gradient centrifugation with Ficoll-Paque and magnetically enriched with EasySep Human Progenitor Cell Enrichment Kit according to the manufacturer's protocols and viably frozen in FBS-10% DMSO. Lin$^-$CD34$^+$ cells were isolated by fluorescence-activated cell sorting (FACS) and cultured in StemSpan Serum Free Expansion Medium supplemented with 20ng/mL Thrombopoietin and Interleukin 6 and 100ng/mL Stem Cell Factor and Flt3 ligand (SFEM-TSF6) at 37^{o}C 5% CO_2 for 6-12 hours prior to lentiviral introduction at multiplicity of infection of 50-100 lentiviral particles per cell. Following a 72 hours transduction period when transgene expression is maximal, transduction-marker-positive cells were isolated by FACS. For cultures treated with 1uM AKTi[230] or 50nM rapamycin[231], inhibitors were purchased from MedChemExpress, dissolved in DMSO as 500x stocks, and added to cultures following FACS-isolation of BFP$^+$ transduced cells. Refer also to **Tables 4-6**.

Erythroid differentiation culture

As described above Lin-CD34+ cells were FACS isolated and cultured for 4 days in SFEM-TSF6. For the following stages media conditions are described in Figure X and cells were cultured in 24-well plates in 1 mL medium. When changing media at the end of each stage, cells were pelleted down and resuspended in the media of the next stage. Cell number seeded at the beginning of stage I, II, and III are: 10^5, $2*10^5$, and $3x10^5$/well. At day 2 or 3 of stage I, II, and III, 500μL fresh media was added and cell density was maintained below $2x10^6$/mL.

Clonogenic progenitor assays

Clonogenic progenitor cell (colony forming unit, CFU) assays were done in complete semi-solid methylcellulose medium (ColonyGEL™ 1102) with FACS-purified transduced cells. 300 cells/mL were mixed with ColonyGEL™ 1102 using a blunt end needle and syringe and plated in technical

duplicate per biological replicate in 35 mm tissue culture dishes and incubated at 37°C 5% CO_2. Manual colony enumeration and scoring as BFU-E, CFU-G, CFU-M, CFU-GM or CFU-GEMM was performed 10-14 days after plating. For secondary clonogenic assays, single primary CFU-GEMMs were plucked and dissociated by vortexing in IMDM, resuspended in 1mL ColonyGEL™ 1102 and plated in single wells of a 24-well plate. Primary CFU-GEMMs were imaged with a Q-Colour3 digital camera mounted to an Olympus IX5 microscope with a 40X objective lens. Image-Pro imaging software was used to acquire images and subsequent image processing was performed with ImageJ software. Refer also to **Tables 4-6**.

Cell line culture and lentiviral production

To generate lentivirus LentiX cells cultured in DMEM with 10% FBS and 1mM sodium pyruvate at 37°C 5% CO_2 were transiently transfected with Lipofectamine 2000 (ThermoFisher) following manufacturer's protocol with pMD2.G and psPAX2 packaging plasmids (Addgene) to create VSV-G pseudotyped lentiviral particles. Lentivirus was harvested 72-hours post-transfection by ultracentrifugation (25,000g, 2-hours, 4°C) and resuspended in StemSpan Serum Free Expansion Medium. Lentiviral preparations were titrated on HeLa cultured in DMEM with 10% FBS at 37°C 5% CO_2.

K562 cells were cultured in IMDM with 10% FBS at 37°C 5% CO_2.

Refer also to **Tables 4-6**.

Mouse Xenotransplantation

All mouse work was carried out in compliance with the ethical regulations approved by the animal research ethics board (AREB), McMaster University, in pathogen-free facility. Six to twelve-week-old, age- and sex-matched *NSG* mice (Jackson Laboratories) were sub-lethally irradiated (315 cGy) 1 day prior to intra-femoral injection of CB HSPC.

Mice were euthanized by cervical dislocation 10-20 weeks post-transplant. Injected right femur was separated from other hind limb bones (left femur, tibiae, iliac crests; "bone marrow (BM)") and mononucleated cells (MNCs) were isolated by crushing in IMDM-2% FBS and passage through 40uM cell strainer. Splenocytes were harvested by passage through 40uM cell strainer[182]**.** Red blood cells in samples were lysed with ammonium chloride buffer prior to flow cytometric analysis or secondary xenotransplantation. Refer also to **Tables 4-6**.

Extreme Limiting Dilution Analysis

Following xenotransplantation positive engraftment was considered >0.5% human chimerism including both myeloid ($CD45^+BFP^+CD33^+$) and lymphoid ($CD45^+BFP^+CD19^+$) lineages in either the injected femur and/or BM 14 weeks post-primary transplant and 10 weeks post-secondary transplant. HSC frequencies were calculated using ELDA software[232]. For secondary recipient input cells, bone marrow and injected femur of engrafted primary mice that received equivalent total PLAG1-S overexpression or control $CD34^+$ dosages were pooled and transplanted into secondary recipients. The total BFP+ cells within primary mouse marrow was estimated based on TNC counts obtained from NSG femurs, tibias and pelvis and proportional accounting from Colvin *et al*. [233,234] to derive the fold change of HSC expansion in vivo. (HSC frequency from secondary transplant x total BFP+ cells in primary mice= Total HSC at primary transplant endpoint; HSC frequency from primary transplant x total CD34+BFP+ cells transplanted= Total HSC at primary input; Total HSC at primary transplant endpoint/ Total HSC at primary input = HSC fold change in vivo).

Flow Cytometry

Immunophenotyping: Fresh or cultured CB cells were blocked with human IgG (200ug/ml), and mouse-derived grafts were blocked with mouse Fc and human IgG before staining in PEF (PBS, 2% FBS, 1mM EDTA) with antibodies against human CD45, CD33, CD15, CD14, CD19, CD71, CD235a (GlyA), CD41a, and/or CD34.

Apoptosis: Annexin V and 7-AAD co-staining was done in Annexin Binding Buffer.

Intracellular staining: Cells were fixed and permeabilized with BD Cytofix/Cytoperm plus 1x Halt Protease/Phosphatase inhibitor cocktail as per manufacturer's instructions. Fixed/permeabilized cells were blocked with human IgG and 10% donkey serum for 10 minutes at 4°C. Primary antibodies were diluted in blocking buffer and incubated with cells for 45 minutes at 4°C, washed with PBS and secondary antibodies were added for 45 minutes at 4°C and washed with PBS prior to analysis.

Cell cycle: Cells were fixed and permeabilized with BD Cytofix/Cytoperm and stained with Ki67 and Hoechst 33342 (10ug/ml).

Protein synthesis measurements: Cells were incubated with 50uM O-propargyl-puromycin (OP-Puro) for 1 hour prior to fixation/permeabilization. Click-iT® cycloaddition reaction was performed using Click-iT® Plus OP-Puro kit following manufacturer's protocol.

Refer to **Table 4** for details of reagents and antibodies.

Flow cytometry data acquisitions were done on BD LSR II using FACS Diva software or Beckman Coulter Cytoflex LX using CytExpert software. Data analysis was done on FlowJo software. FACS was done with Beckman Coulter MoFlow XDP using Summit software or BD Aria II using FACS Diva software. Refer also to **Tables 5 and 6**.

Immunofluorescence Microscopy

Immunofluorescence microscopy of MSI2 or cytoplasmic CYP1B1 proteins was done following methods in Rentas *et al*. (2016)[182]. Cell staining buffers were made in PBS. Cells were fixed in 2% paraformaldehyde for 10 minutes, washed and cytospun on to glass slides. Cells were then permeabilized (0.2% Triton X-100) for 20 minutes, blocked (0.1% saponin, 10% donkey serum) for 30 minutes and stained with anti-MSI2 or anti-CYP1B1 antibodies for 1 hour at room temperature. Primary antibody was washed twice by dunking in PBS chamber and secondary antibody staining was performed in 10% donkey serum with Alexafluor-647 donkey anti-rabbit antibody for 45 minutes and washed twice with PBS prior to mounting a coverslip with Prolong™ Gold Antifade containing DAPI. Several images (100-1000 cells total) were captured per slide at 20X magnification using an Operetta HCS Reader with epifluorescence illumination and standard filter sets. Columbus image analysis software was used to automatically identify cytoplasm boundaries and quantify cell area in square micrometer units. Refer also to **Tables 4-6**.

Chromatin Immunoprecipitation (ChIP)

For ChIP-seq, $1x10^8$ cells K562 cells co-overexpressing Flag-PLAG1-S and USF2 were cross-linked in 1% PFA and excess PFA was washed with glycine, cells were lysed in RIPA buffer containing protease inhibitors and nuclei were subjected to probe sonication. Two percent of each sample was used for Input sequencing. Twenty µg anti-Flag (Sigma, F1804) and Protein G dynabeads were used for IP. The precipitated complex was washed in low and high salt buffer and chromatin was eluted in TE buffer at 65°C before reverse cross-linking with Proteinase K (NEB, P8107S). Sequencing libraries were prepared using NEBNext® Ultra™ II DNA Library Prep Kit

for Illumina® (NEB, E7645S) and sequencing as 50 bps single ended reads was performed on Illumina HiSeq 1500 at a depth of 55 million reads per input and 42.5 million reads per IP.

ChIP-seq analysis:

The sequencing reads were quality controlled using fastQC, and the adaptors were removed using cutadapt software using the illumina universal primer sequence AGATCGGAAGAGCACACGTCTGAACTCCAGTCAC. The reads were aligned to human genome assembly GRCh38 using hisat2 aligner (version hisat2-2.0.4)[235], and duplicates were removed using samtools[236]. Fingerprint plots were generated using deepTools[237] to check efficiency of the ChIP experiments. Samtools merge was used to merge the input files to create a master background files, and MACS2[238] was used to called peaks from the individual ChIP replicates using the merged input files. The following peak calling parameters were used:

macs2 callpeak -t ChIP_file1.bam -c Input_merged.bam -f BAM -g hs –n ChIP_file1_peaks -B -s 50 --bw 150 -q 0.01 --outdir

Since the IP efficiency was lower for USF2 the peaks were called using the following less stringent parameters:

macs2 callpeak –t USF2_ChIP_file1.bam -c Input_merged.bam -f BAM -g hs -n ChIP_file1_peaks -B -s 50 --bw 150 -q 0.05 –m 2 50 --outdir

Bedtools intersect[239] was used to identify peaks common to the two replicates and were used for all downstream analysis. Peak files were annotated using HOMER[240] annotatepeaks.pl script using hg38 as the background. HOMER's mergepeaks function was used to identify Flag-PLAG and USF2 co-bound targets within 100bps, 200bps, 500bps, and a 1000bps from each other. findMotifsGenome.pl was used for motif analysis with the following parameters -size 200 –mask. The R-packages ChIPSeeker[241], and clusterProfiler[242] were used to perform peak distribution and pathway analysis. Significance of any enriched pathways and GO processes was addressed by setting pvalue Cutoff to 0.05, and by adjusting the p-values using Benjamini & Hochberg method that is built into the clusterProfiler package.

For ChIP-seq peak overlap with $CD34^+$ epigenetic marks data was downloaded from: https://egg2.wustl.edu/roadmap/data/byFileType/peaks/consolidated/narrowPeak/ (epigen ome ID: E050 #678C69 BLD.MOB.CD34.PC.F) and lifted over to hg38 before comparing with FLAG-PLAG1-S ChIP data using bedtools intersect -u. Epigenetic marks used were as follows: H3K4me3: Active promoter, H3K4me1: Enhancer, H3K27Ac: Enhancer, H3K9me3: Repressive promoter, H3K27me3: Repressive promoter. Figures are binary peak comparisons, eg, Does a FLAG-PLAG1-S peak overlap with H3K4me1? Yes or No; it does not account for the strength of binding. Each bar represents the intersection highlighted below with filled circles and connecting lines. The numbers on top of each bar represent the number of intersecting sites. FLAG-PLAG1-SChIP was used as the baseline for all comparisons. The box-plots below show various aspects of each intersection eg. peak scores (#scores), RNA-seq log FC (log2FC) or distance to TSS (dist_to_TSS) of all sites present in that intersection.

CUT&RUN

Lin^-CD34^+ cells were sorted 72 hours post-transduction to obtain 6-7x10^5 BFP^+ cells per biological replicate and subsequently 2x10^5 cells were used per antibody condition in CUT&RUN assay. Cells were washed in PBS and CUT&RUN assay was performed as previously described Skene *et al*. (2018)[243]. Protein A-Micrococcal nuclease (pA-MNase) fusion protein was kindly provided by Dr. Steven Henikoff. Briefly, cells were washed twice with a wash buffer and activated

BioMag®Plus Concanavalin A Beads were added dropwise while vortexing the samples. Wash buffer was removed by separating the samples on a magnet and antibody buffer containing 0.0125% digitonin and mouse anti-FLAG M2 or mouse IgG were added to the cell nuclei-beads mixture. Samples were incubated on a rotator overnight at 4°C, followed by incubation with rabbit anti-mouse secondary antibody for 1 hour at room temperature. Addition and activation of pA-Mnase and isolation of soluble DNA was performed as previously described[243]. DNA was extracted with the MinElute PCR Purification kit and DNA libraries were prepared with ThruPLEX® DNA-Seq and DNA Unique Dual Index Kits according to manufacturer's instructions. The number of PCR cycles for each library preparation was determined based on the Ct values from qPCR using Power SYBR Green PCR Master Mix. For each sample, 1 ul of DNA, 5 ul of PCR Master Mix, 10uM (0.4 ul) of each forward and reverse primer, and 3.2 uL of water were combined and qPCR was performed according to manufacturer's instruction. Library purification and size selection was performed with AMPure XP beads. Subsequently, libraries were sequenced on Novaseq6000 using 50bp paired-end reads to achieve sequencing depth of approximately 40M reads/samples. Refer also to **Tables 4 and 5**.

CUT&RUN analysis

CUT&RUN sequencing was trimmed using fastp v.0.19.5[244] and aligned to GRCh38 and S. cerevisiae yeast genome (sacCer3) for the spike-in normalization using bowtie2 v.2.3.5[245] with the same alignment setting as described previously[243]. Bam files were sorted and indexed based on the genomic coordinates using samtools v.1.9[236]. Bam files of the replicates were pooled, and peaks were called from the pooled replicates by MACS2 v.2.2.5[246] based on FLAG vs IgG with the spike-in control normalization and q-value cutoff <0.05. Peaks that overlap with the Encode black list have been removed. Peaks were annotated with the genomic features to find the overlap with promoter, intron, exon, intergenic, 5'UTR or 3'UTR loci. Promoters were defined as 2Kb upstream to 500bp downstream of the TSS. Motif analysis was performed using HOMER v.4.8[240], where normalized enrichment score for each motif is the fold change of the target percentage to the background percentage. If the target percentage is less than 5, 1 was added to the target and the background percentages before calculating the fold change to attenuate the FC of motifs with low target percentages. Bigwig files for the whole genome track signal have been created for the replicates and for the pooled replicates using the bamCoverage command from the deepTools package v.3.5.0[237] based on the spike-in control normalization. Heatmpas for the called peaks were plotted from bigwig files of the replicates using computeMatrix and the plotHeatmap commands in the deepTools package.

RNA isolation, library preparation and sequencing

Total RNA was isolated from FACS purified transduced BFP^+ Lin^-CD34^+ using TRIzol-LS following manufacturer's protocol, and then further purified using Rneasy Micro columns and quantified by QuBit. Quality of total RNA was assessed with BioAnalyzer Nano and all samples had a RIN above 8. 250 ng of total RNA was used for library preparation. Library preparation was done with the KAPA mRNAseq stranded kit. Ligation was made with 9 nM final concentration of Illumina index and 10 PCR cycles was required to amplify cDNA libraries. Libraries were quantified by QuBit and BioAnalyzer. All libraries were diluted to 10 nM and normalized by qPCR using the KAPA library quantification kit. Libraries were pooled to equimolar concentration. Sequencing was performed with the Illumina Hiseq2000 using the Hiseq Reagent Kit v3 (200

cycles, paired-end) using 1.7 nM of the pooled library. Samples were sequenced at 25-45 million paired-end depth. Refer also to **Tables 4 and 5**.

RNA sequencing Analysis

For the read alignments, sequences were trimmed for sequencing adapters and low quality 3' bases using Trimmomatic v.0.35 and aligned to the reference human genome version GRCh38 (gene annotation from Gencode version 24) using STAR v.2.5.1b. DESeq2 v.1.6.2 was then used to identify differentially expressed genes between the 2 groups with base Mean (mean of count values) of 8.552 used to eliminate low count genes. RNA library preparation, sequencing, alignment and differential expression (DE) analysis was done at Institute for Research in Immunology and Cancer's (IRIC) Genomics Platform (Montreal, Canada).

DMAP population comparisons

GSE24759 data were background corrected using Robust Multi-Array Average (RMA), quantile normalized using the expresso() function of the affy Bioconductor package (affy_1.38.1 , R 3.0.1), batch corrected using the ComBat() function of the sva package (sva_3.6.0) and scaled using the standard score. Bar graphs were created by calculating for significantly differentially expressed genes the number of scaled data that were above (>0) or below (<0) the mean for each population. Empirical p values were derived from the percentage of times the observed value (set of up or downregulated genes) was better represented in that population than random values tested for 1000 permutations.

Pathway analysis and Enrichment mapping

Pre-ranked GSEA was performed using GSEA software and rank formula (-log10(p-value) * sign(log2FC). Overrepresentation analysis in unranked gene lists was performed using g:Profiler[247]. The gene sets used for GSEA and g:Profiler were obtained from MsigDB-c2 and c3, NCI, IOB, Netpath, HumanCyc, Reactome, Panther and the Gene Ontology (GO) MP and BP databases, updated December 11 2020 (http://baderlab.org/GeneSets). Enrichment maps and cluster labels were generated using Cytoscape software (v.3.8.2) and EnrichmentMap (v3.0 and 3.3.1) and AutoAnnotate (v1.3.4) apps (FDR<0.1 and p value <0.05, unless otherwise indicated). Statistically significant overlaps between signature gene sets (PLAG1-S bound or miR-127 target genes) were performed using the EnrichmentMap app in Cytoscape and tested for Mann Whitney U p<0.05 and hypergeometric p<0.05. Refer also to **Table 7**.

RNA isolation, cDNA synthesis and Quantitative Real Time PCR (qRT-PCR)

Total RNA was isolated using Trizol-LS reagent following manufacturer's protocol. cDNA synthesis was done using qScript cDNA Synthesis Kit following manufacturer's protocol. qPCR for PLAG1 was done as in Belew *et al*. (2018) using Roche UPL primer probe set (**Table 3**) and PerfeCTa qPCR Supermix (**Table 4**). Fold change in transcript level was calculated according to the $2^{-\Delta\Delta Ct}$ method.

For miRNA qPCR cDNA synthesis from Trizol-isolated RNA was performed with qScript® microRNA cDNA Synthesis Kit with microRNA-specific and oligo dT adapter primers designed as described by manufacturer (**Table 4**). SensiFast SYBR Lo-ROX qPCR master mix was used with cDNA from 20ng total RNA per reaction, universal miRNA reverse primer compatible with

qScript® microRNA cDNA Synthesis oligo dT adapter, and miRNA-specific primers (**Table 3**). Measurements taken on QuantStudio 3 Real-Time PCR System (**Table 5**).

Western blots

K562 or HeLA cells pellets were resuspended in RIPA lysis buffer supplemented with cOmplete EDTA-free protease inhibitor cocktail (**Table 4**). Whole protein extracts were collected from supernatant following 10 minutes >12000g centrifugation at 4°C to pellet cell debris. Lysate in 1x NuPAGE LDS sample loading buffer was resolved on 10% Bis-Tris PAGE then transferred onto immobilon-P PVDF membrane (EMD Millipore) by wet transfer. Membrane was blocked for 1hr using 5% BSA/TBST. Primary antibody was diluted 1/1000 and incubated with membrane overnight at 4°C with rotation. Following 3 10 minute TBST washes IRDye secondary antibodies diluted 1/10-20,000 in TBST was incubated for 1hour at room temperature with rotation. Following 3 10 minute TBST washes membranes were imaged on LI-COR Odyssey imaging station. (**Tables 4 and 5**)

Myc ChIP-seq analysis

Publicly available CODEX Myc ChIP-Seq data generated in HPC7 cell line to find the targets and determine how many of these are in the ribosome biogenesis pathway repressed by PLAG1 overexpression. The ChIP-Seq data BED file were downloaded from ArrayExpress (accession number: E-MTAB-3954). The BED file contains the chromosomal positions of the binding peaks. Genes nearby the peaks were retrieved using GREAT (Stanford, http://bejerano.stanford.edu/great/public/html/) using a 5kb rule (peaks up to 5kb upstream and 1kb downstream the TSS). The mouse mm9 is the reference genome used for the ChIP-Seq reads alignment. Human orthologs to these genes were retrieved using BioMart – Ensembl (http://www.ensembl.org/biomart/) with gene symbols as key values. 1747 regions (peaks) were contained in the BED file. 1511 human genes were retrieved using the 5kb rule.

Cytoscape and iRegulon app (v1.3) was used to validate the CODEX MYC targets and to visualize the size of the overlap between the CODEX ChIP-Seq targets and the iRegulon prediction. We used the 5kb rule Myc targets list filtered by PLAG overexpression at a p-value cutoff of 0.05 which consists of 153 genes as input list for iRegulon. iRegulon was run using default parameters. 104 genes out of these 153 genes also present in a ChIP-Seq track coming from MYC ChIP-seq on human K562 produced by the Snyder lab and available in the iRegulon database (https://www.encodeproject.org/targets/MYC-human/).

Table 3: Oligonucleotide Sequences

Name	Accession	Application	Sequence
1shPLAG1	NM_001114635.2	knockdown	TGCAGTTAAACCTCTACAACA
2shPLAG1	NM_001114635.2	knockdown	ATGAGGCAGACTCGCTTATTT
shLuciferase	M15077.1	knockdown	CGATATGGGCTGAATACAAAT
shScramble	NA	knockdown	CCTAAGGTTAAGTCGCCCTCG
hsa-microRNA 127	NR_029696.1	overexpression	TGTGATCACTGTCTCCAGCCTGCTGAAG CTCAGAGGGCTCTGATTCAGAAAGATCA TCGGATCCGTCTGAGCTTGGCTGGTCGGAAGTCTCATCATC
microRNA-127-5p-TB	NR_029696.1	inhibition	[ATCAGAGCCCTCGATCTGAGCTTCAGCGAT]8
Reverse complement primer miR127-5p	NR_029696.1	miR cDNA synthesis	ATCAGAGCCCTCTGAGCTTCAG
Reverse complement primer SNORD48	NR_002745.1	miR cDNA synthesis	GGTCAGAGCGCTGCGGTGATGGCATCAGCGACACACTCAGAGTTACCTGGGGTCATCATCACT
Oligo dT Adaptor	NA	miR cDNA synthesis	AAAAAAAAAAAAAAAAAAAATGTCTCGCCTACCACACCCTTACCGCCATTCAGGTCTATGC
Universal miRNA reverse primer	NA	miR qPCR	GCATAGACCTGAATGGCGGTA
miR127-5p primer	NR_029696.1	miR qPCR	CTGAAGCTCAGAGGGCTCTGAT
SNORD48 primer	NR_002745.1	miR qPCR	AGTGATGATGACCCCAGGTAACTCTGAGTGTGTCGCTGATGCCATCACCGCAGCGCTCTGACC
UPL70-hu-PLAG1-Fwd	NM_002655.2	qPCR	gtccagcccgaaatatgaga
UPL70-hu-PLAG1-Rev	NM_002655.2	qPCR	cagcaccaagaggcaacc

Table 4: Reagents

Reagent	Working Concentration	Supplier	Catalogue #
Ficoll-Paque	15mL per 35mL 1:2 cord blood:PBS	GE Healthcare	17-5442-03
EasySep Human Progenitor Cell Enrichment Kit	100uL antibody, 200uL magnetic beads per 50-100million MNC in 2mL	StemCell Technologies	19356
StemSpan Serum Free Expansion Medium	1X	Stem Cell Technologies	9650
recombinant human Thrombopoietin (TPO)	20ng/mL	Peprotech	AF-300-18-50UG
recombinant human Stem Cell Factor (SCF)	100ng/mL	R&D Systems	255-SC-050
recombinant human Flt3 ligand (FLT3-L)	100ng/mL	R&D Systems	308-FKN-100
recombinant human Interleukin 6 (IL-6)	20ng/mL	Peprotech	AF-200-06
AKT inhibitor VIII (AKTi-1/2)	1uM	Cedarlane/MedChemExpress	HY-10355
Rapamycin	50nM	Cedarlane/MedChemExpress	HY-10219
ColonyGEL™ 1102	1X	Reachbio	1102
Sterile, Blunt-End Needles, 16 Gauge with Luer Lock	NA	StemCell Technologies	28110
IMDM with L-Glutamine and HEPES	1X	Wisent Bioproducts	319-105-CL
FBS	2-90% as indicated	Wisent Bioproducts	098-150
ammonium chloride solution	1X	StemCell Technologies	7850
Purified Rat Anti-Mouse CD16/CD32 (Mouse BD Fc Block™)	1ug/1million cells (2uL/100uL)	BD Biosciences	553142
human IgG	20-200ug/<1million cells/100uL	Sigma	I4506-10MG
Mouse anti-CD45-FITC (HI30)	0.5-1uL/<1million cells/ 100uL	BD Biosciences	555482
Mouse anti-CD45-Pacific Blue (HI30)	0.5-1uL/<1million cells/ 100uL	ThermoFisher	MHCD4528
Mouse anti-CD33-PE (P67.6)	0.5-1uL/<1million cells/ 100uL	BD Biosciences	340679

Mouse anti-CD33-BV605 (P67.6)	0.5-1uL/<1million cells/ 100uL	BD Biosciences	744352
Mouse anti-CD15-APC (HI98)	0.5-1uL/<1million cells/ 100uL	BD Biosciences	551376
Mouse anti-CD15-BV786 (HI98)	0.5-1uL/<1million cells/ 100uL	BD Biosciences	741013
Mouse anti-CD14-PE-Cy7 (MϕP9)	0.5-1uL/<1million cells/ 100uL	BD Biosciences	663195
Mouse anti-CD14-APC-Cy7 (MϕP9)	0.5-1uL/<1million cells/ 100uL	BD Biosciences	663195
Mouse anti-CD19-APC (HIB19)	0.5-1uL/<1million cells/ 100uL	BD Biosciences	555415
Mouse anti-CD19-AlexaFluor700 (HIB19)	0.5-1uL/<1million cells/ 100uL	BD Biosciences	557921
Mouse anti-CD71-PE (M-A712)	0.5-1uL/<1million cells/ 100uL	BD Biosciences	555537
Mouse anti-CD235a (GlyA)-PE-Cy7 (HIR2)	0.5-1uL/<1million cells/ 100uL	BD Biosciences	563666
Mouse anti-CD41a-BV711 (HIP8)	0.5-1uL/<1million cells/ 100uL	BD Biosciences	740778
Mouse anti-CD34-APC (581)	0.5-1uL/<1million cells/ 100uL	BD Biosciences	555824
Rabbit anti-phospho-AktS473 (736E11)	1/50uL	Cell Signaling Technologies	3787
Rabbit anti-pan-Akt (C67E7)	1/50uL	Cell Signaling Technologies	4691
Rabbit anti-phospho-mTORS2448 (D9C2)	1/50uL	Cell Signaling Technologies	2971
Mouse anti-mTOR (L27D4)	1/50uL	Cell Signaling Technologies	4517
Rabbit anti-phospho-RPS6Ser240/244 (D6F8 XP)	1/50uL	Cell Signaling Technologies	5364
phospho-4E-BP1Thr37/46 (236B4)	1/50uL	Cell Signaling Technologies	2855
Rabbit anti-Myc (9E11)	1/50uL	Abcam	ab56
Anti-c-Myc (phospho S62) antibody [33A12E10]	1/50uL	Abcam	ab78318
Recombinant Anti-c-Myc (phospho T58) antibody [EPR17923]	1/50uL	Abcam	ab185655
Human/Mouse/Rat GSK-3 beta Antibody	1/50uL	R&D Systems	MAB2506-SP

Human Phospho-GSK-3 beta (S9) Antibody	1/50uL	R&D Systems	MAB25062-SP
Mouse anti-EIF2S1	1/50uL	Abcam	ab5369
Mouse anti-Ki67-PE-Cy7 (B56)	1/50uL	BD Biosciences	561283
Rabbit anti-MSI2	1/50uL	Abcam	ab76148
Mouse anti-FLAG (M2)	0.01 mg/mL, 1/100uL	Sigma	F1804
mouse IgG	0.01 mg/mL	Thermo Fisher	10400C
Alexafluor-488 conjugated secondary donkey anti-rabbit or anti-mouse IgG (H+L)	1/2500uL	Invitrogen	A32790, A32766
Alexafluor-647 conjugated secondary donkey anti-rabbit or anti-mouse IgG (H+L)	1/2500uL	Invitrogen	A32795, A32787
Alexafluor-546 conjugated secondary donkey anti-rabbit or anti-mouse IgG (H+L)	1/2500uL		A10040, A10036
BD Cytofix/Cytoperm	1X	BD Biosciences	554714
100x Halt Protease/Phosphatase inhibitor cocktail	1X	ThermoFisher Scientific	78440
Click-iT® Plus O-propargyl-puromycin (OPPuro) kit	NA	ThermoFisher	C10456, C10458
Rabbit anti-CYP1B1 (EPR14972)	1/50uL	Abcam	ab185954
Lenti-X™ 293T	NA	Cedarlane/Takara	632180
HeLa	NA	ATCC	CCL-2
K-562	NA	ATCC	CCL-243
Normal Donkey Serum	10%	Jackson Immuno research laboratories	017-000-121
ProLong™ Gold Antifade Mountant with DAPI	1X	Invitrogen	P36931
Dynabeads® Protein G for Immunoprecipitation		Thermo Fisher	10003D
Proteinase K		NEB	P8107S

NEBNext® Ultra™ II DNA Library Prep Kit for Illumina®		NEB	E7645S
BioMag®Plus Concanavalin A	10uL/ CUT&RUN reaction	Bangs Laboratories	BP531
Spermidine. BioUltra. for molecular biology. ≥99.5% (GC)	0.05mM	Sigma	124-20-9
Digitonin, High Purity	0.0125%	Calbiochem™ , EMD Millipore™	300410250MG
Rabbit anti-mouse secondary antibody, for CUT&RUN	1mg/mL	Thermo Fisher	31188
MinElute PCR Purification kit	NA	Qiagen	28004
ThruPLEX® DNA-Seq Kit	NA	Takara	R400675
DNA Unique Dual Index Kit	NA	Takara	R400666
Power SYBR Green PCR Master Mix	1X	ThermoFisher	4367659
AMPure XP beads	NA	Beckman	A63880
TRIzol-LS	1X	ThermoFisher Scientific	10296028
RNeasy Micro columns	NA	Qiagen	74004
KAPA mRNAseq stranded kit	NA	KAPA	KK8420
KAPA library quantification kit	NA	KAPA	KK4973
qScript® microRNA cDNA Synthesis Kit	1X	QuantaBio	95107
qScript™ cDNA SuperMix	1x	VWR, QuantaBio	CA101414-104
SensiFast SYBR Lo-ROX	1X	FroggaBio	BIO-94005
PerfeCTa® qPCR SuperMix, Low ROX™	1x	VWR, QuantaBio	CA101414-134
Annexin V Alexafluor-350	1/50uL	Invitrogen	A23202
Annexin V Alexafluor-647 conjugate	1/50uL	Invitrogen	A23204
7-AAD	1/100uL	BioLegend	559925

Annexin Binding Buffer	1X	BioLegend	422201
RIPA lysis buffer	50mM Tris HCl pH 8, 150 mM NaCl, 1% NP-40, 0.5% sodium Deoxycholate, 0.1% SDS, 2mM EDTA	NA	NA
COmplete™ , Mini, EDTA-free Protease Inhibitor Cocktail	1x	Sigma	4693159001
NuPAGE® LDS Sample Buffer (4X)	1x	Fisher Scientific	NP0007
Wet Transfer Buffer	25mM Tris, 250mM Glycine and 15% methanol buffer	NA	NA
TBST	50 mM Tris, 150 mM NaCl, pH 7.6, 0.05% Tween-20	NA	NA
IRDye 680 Goat Anti-Rabbit	1/20,000-1/10,000	LI-COR Biosciences	cat# 926-32221
IRDye 800CW Goat anti-Mouse	1/20,000-1/10,000	LI-COR Biosciences	cat# 926-32210

Table 5: Equipment

Instrument	**Supplier**
Q-Colour3 Digital Camera	Olympus
Olympus IX5 Microscope	Olympus
Operetta HCS Reader	Perkin Elmer
BD LSR II	BD Biosciences
Cytoflex LX	Beckman Coulter
MoFlow XDP	Beckman Coulter
BD Aria II	BD Biosciences
Novaseq6000	Illumina
Illumina Hiseq2000	Illumina
Illumina HiSeq 1500	Illumina
BioAnalyzer Nano	Agilent
QuantStudio 3 Real-Time PCR System	ThermoFisher Scientific, A28136
LI-COR Odyssey imaging station	LI-COR Biosciences

Table 6: Software

Software	Supplier/Citation
Image-Pro imaging	Media Cybernetics
ImageJ	Rasband, W.S., U. S. National Institutes of Health, Bethesda, Maryland, USA, (1997-2018); https://imagej.nih.gov/ij/
Columbus image analysis software	Perkin Elmer
Extreme Limiting Dilution Analysis	Hu,Y. & Smyth, G.K., Journal of Immunological Methods 347, 70-78, (2009); http://bioinf.wehi.edu.au/software/elda/
FACSDiva v6	BD Biosciences
CytExpert	Beckman Coulter
MoFlo Summit	Beckman Coulter
FlowJo v9 and v10	Tree Star
Prism	GraphPad
Microsoft Excel for Mac v 16.53	Microsoft
GSEA v4.1.0	http://software.broadinstitute.org/gsea/index.jsp
Cytoscape v3.8.2	https://cytoscape.org/download.html
g:Profiler	Raudvere U, Kolberg L, Kuzmin I, et al. g:Profiler: a web server for functional enrichment analysis and conversions of gene lists (2019 update). *Nucleic Acids Res*. 2019;47(W1):W191-W198; https://biit.cs.ut.ee/gprofiler/gost
R v3.6.0	https://www.R-project.org
R Studio v1.2.1335	https://www.rstudio.com/products/rstudio/download/
HOMER v4.8	http://homer.ucsd.edu/homer/

CHAPTER 3

Functional characterization of the role of PLAG1 in human HSPCs

3.1 PLAG1 is enriched in and essential to human HSC.

We previously showed that when ectopically co-expressed, either short isoform of PLAG1 (-S and -B) (**Figure 3A**) and the USF2 TFs can co-operatively transactivate the pro-self-renewal gene MSI2[194]. However, while USF2 expression is relatively stable across the human hematopoietic hierarchy (**Figure 3B,C**), PLAG1 is specifically elevated in the HSC-enriched sub-fractions from human CB[74,194,248,249] and murine BM[250], and in human BM profiled by single-cell-sequencing (**Figure 3B-F**)[251]; altogether suggesting that PLAG1 may have important heretofore unexplored functions in the most primitive hematopoietic cells.

To evaluate this CB-derived Lin^-CD34^+ HSPCs expressing PLAG1-targeting shRNAs (**Figure 3H**) were assessed relative to control for *in vitro* CFU potential, short-term renewal in serum-free cytokine-supplemented suspension culture, and long-term *in vivo* repopulation capacities (**Figure 4A**). PLAG1-depleted HSPCs generated fewer colonies, due mainly to reduced erythroid (BFU-E) and primitive granulocyte-erythroid-megakaryocyte-monocyte (CFU-GEMM) colonies (**Figure 4B**). This was mirrored in suspension culture where 1shPLAG1 significantly reduced total nucleated cell (TNC) and $CD34^+$ outputs over 7 days (**Figure 4C, D**). Six weeks following NSG mouse xenotransplantation, when engraftment is largely contributed by progenitors, there was a modest but non-significant reduction in the representation of 1shPLAG1-expressing GFP^+ cells (**Figure 4E**). However, sixteen weeks following transplant when the graft is sustained by *bona fide* HSCs engraftment by 1shPLAG1-expressing cells was significantly impaired 11-14-fold (**Figure 4F**). Patterns in reduced CFU output and impaired of long-term BM reconstitution were replicated by a second independent shRNA targeting the PLAG1 3'UTR (**Figure 4G, H**), however the more modest impairment may be attributed to a lower knockdown efficiency (**Figure 3H**).

3.2 PLAG1-S is a positive regulator of human HSPC fitness.

Although PLAG1 was identified as a putatively important regulatory factor in hematopoiesis because of its role upstream of MSI2, expression mining revealed intriguing differences in the profiles of PLAG1 and MSI2 signifying that PLAG1 may have MSI2-independent functions and its role in human HSC physiology may transcend the PLAG1/USF2-MSI2 regulatory axis. First, in the homeostatic human hierarchy PLAG1 expression is highly restricted to the non-cycling HSC compartment, whereas MSI2 is strongly expressed in both non-cycling and cycling HSC and $CD34^+$ progenitors (**Figure 5A**)[252]. Secondly, upon 5-fluoruracil (5-FU) stress-induction of mouse HSC cycling, Msi2 is elevated while Plag1 is repressed (**Figure 5B**)[149]. Most importantly and unexpectedly, overexpression of PLAG1-S without USF2 in Lin^-CD34^+ cells is insufficient to enhance MSI2 protein expression (**Figure 5C**). Moreover, PLAG1 levels are reduced in human HSPC when activated by transplantation (**Figure 5D**)[139] or culture stimulation (**Figure 5E-G**)[152,162,253]. Therefore, to explore the potential for an independent function of PLAG1 in modulating human HSPC fate decisions in these contexts we assayed Lin^-CD34^+ CB cells *in vitro* and *in vivo* upon gain of PLAG1 (**Figure 6A**).

Individual overexpression of each of the three PLAG1 isoforms (**Figure 3A**)[194,197,201] increased CFU output, driven primarily by BFU-Es (**Figure 6B**). Importantly, and consistent with the absence of elevated MSI2 expression (**Figure 5C**), the composition of primary CFUs generated by overexpression of PLAG1 proteins differs from that of MSI2 overexpression, which were elevated in CFU-M and CFU-GEMM[182]. The shorter PLAG1 isoforms (-S and -B) significantly enhanced GEMM replating efficiency and promoted $CD34^+$ cell expansion in myeloid-supporting culture over 7 days, with a peak advantage at day 4, whereas full-length PLAG1-A was less

effective at supporting HSPC renewal in these settings (**Figure 6C-F**). In PLAG1-S overexpressing (PLAG1-S^{OE}) cultures enhanced CD34 maintenance occurs concurrently with limiting the frequency of committed CD33^{+} cells (**Figure 6G**). Altogether, these findings point to the short isoforms of PLAG1 as important positive regulators of human HSPC, and contextualize our past observation that these isoforms are preferentially expressed in the HSC-enriched compartment of human CB[194].

Given the strong and comparable *in vitro* phenotypes between PLAG1-S and PLAG1-B and only a 17 amino acid difference, we prioritized the shortest form, PLAG1-S, for assessment in competitive repopulation assays (**Figure 6A**). Following a 4 or 6-week repopulation period in NSG mice, PLAG1-S^{OE} and control short-term progenitors are similarly competitive at contributing to BM engraftment, however in the injected femur, where homing was not required, the absolute size of the PLAG1-S^{OE} grafts were significantly larger than control (**Figure 7A**), suggesting some enhancement of progenitor production *ex vivo*. After 16 weeks, the proportion and intensity of the BFP transduction marker relative to input levels was significantly enhanced in the BM of PLAG1-S^{OE} recipients compared to control (**Figure 7B,C**). Given that BFP intensity from this bidirectional promoter vector configuration provides a surrogate measure for transgene expression[170,254], this indicates that co-transplanted cells overexpressing PLAG1-S to higher levels outcompete those expressing lower levels. Importantly, the enhanced fitness of PLAG1-S^{OE} HSCs was neither associated with splenomegaly (**Figure 7D**), nor elevation of the CD34^{+} HSPC compartment; and PLAG1-S^{OE} grafts displayed balanced erythroid, myeloid and lymphoid multilineage output based on expression of CD71, CD235a (GlyA), CD41a, CD33, CD14, CD15, and CD19 (**Figure 7E**), indicating that ectopic PLAG1-S does not provoke aberrant differentiation or pre-malignant phenotypes.

As we see *Plag1* levels are diminished in murine HSCs treated with cycle-inducing 5-FU and in various contexts of human HSC activation we next tested whether constitutive overexpression of PLAG1-S in CB HSCs could impact their fitness following *in vivo* 5-FU insult. Transduced Lin^{-}CD34^{+} cells were xenotransplanted into irradiated NSG and after 4 weeks mice were injected with 150mg/kg 5-FU intraperitoneally (**Figure 8A)**. The results are equivocal as statistical significance is not met, however overall, we find in all hematopoietic niches tested that after 16 weeks PLAG1-S^{OE} cells have improved competitive engraftment capacity compared to control (**Figure 8B, C**). Compared to our experiment where mice are not subject to 5-FU insult PLAG1-S^{OE} cells outcompete their controls 1.5-fold and 2.9-fold more in the injected femur and spleen respectively, suggesting that elevated PLAG1-S levels may have enhanced the HSC preservation *in vivo* when subjected to this additional challenge.

3.3 PLAG1-S overexpression promotes self-renewal of long-term human HSC.

The *in vitro* and *in vivo* profiling of PLAG1-S overexpressing CB HSPC highlights a putative ability for ectopic PLAG1-S to preserve the stemness and/or promote the self-renewal of functional long-term HSC in settings where they are known to be severely compromised. To quantitively evaluate this, we performed gold standard primary xenotransplantation in limiting dilution series, of the culture-derived progeny of Lin^{-}CD34^{+} CB cells immediately post-induction of ectopic PLAG1-S to determine *ex vivo* HSC frequencies (**Figure 9A**). Fourteen weeks following primary xenotransplantation, across the same input cell dosages, only 33% of mice transplanted with control cells, compared to 66% of mice transplanted with PLAG1-S^{OE} cells met multilineage BM engraftment criteria (**Figure 9B, D**). Extreme limiting dilution analysis (ELDA)[232] was used to determined that the frequency of HSC in Lin^{-}CD34^{+} cells overexpressing PLAG1-S was 1 in

every 715, compared to 1 in 11,156 for controls, representing a 15.6-fold enhancement of HSC frequency immediately following induction of ectopic PLAG1-S (**Figure 9C, D**). A similar analysis of splenic grafts revealed 75-fold enhancement in primitive cells capable of repopulating this environment (**Figure 9E-G**), however the overall size of splenic grafts were 4-8 fold smaller than in the bone marrow niches. Notably, HSC renewal achieved by ectopic MSI2 does not occur at this early timepoint post-transduction[182], highlighting a unique functional capacity of PLAG1-S which is enacted via MSI2-independent means.

Serial transplantation of primary grafts in limiting dilution was next performed to calculate HSC expansion *in vivo* under homeostatic conditions (**Figure 10A**). At endpoint, netting 24 weeks *in vivo*, we first confirmed enduring balanced multilineage differentiation by PLAG1-S^{OE} HSC using CD33 marker of myeloid and CD19 marker of lymphoid outputs (**Figure 10B**). Secondary recipients of PLAG1-S^{OE} cells exhibited heightened engraftment attributed to 4.8-fold higher HSC frequencies in primary grafts relative to control primary grafts (**Figure 10C, D**). Having determined the frequency of BFP+ HSC present in the faction of primary bone marrow transplanted into secondary mice we next back-calculated the total BFP^{+} HSCs in primary donor mice using femur and hind limb counts and proportional accounting from empirically validated total marrow counts for NSG mice[233] (**Figure 10E, Column 11**). Similarly, using HSC frequencies determined from the primary LDA the total BFP^{+} HSC initially transplanted into the donor mice was calculated (**Figure 10E, Column 12**) and the fold change (#HSCs into secondary mice/ #HSCs into primary mice) allowed us to determined self-renewal that occurred *in vivo*. Upon this detailed accounting we find that enhanced engraftment in secondary recipients is not the result of enhanced continued renewal *in vivo* (**Figure 10E, Column 13**) and is primarily attributed to the initial *ex vivo* promotion of the HSC compartment. These results, which are consistent with the aforementioned observation that the CD34^{+} compartment of PLAG1-S^{OE} grafts is not enlarged, quantitively demonstrate that PLAG1-S overexpression does not impart excessive HSC self-renewal characteristic of clonal hematopoiesis or pre-malignancy; and that the potent promotion of HSCs in a stimulatory setting is not associated with detrimental exhaustion of the long-term HSC compartment.

To test for the effect of PLAG1-S on HSC renewal over longer periods *in vitro,* as has been reported for MSI2[182], cells cultured for 7 additional days were subjected to limiting dilution xenotransplantation (**Figure 11A**). Relative to immediately post-induction of ectopic PLAG1-S, the number of functional HSCs continue to increase 1.6-fold and sustain 4.3-fold higher frequencies relative to control (**Figure 11B-E**). Thus, the potent stem cell advantage endowed by PLAG1-S, though sustained in culture, can be maximally achieved shortly after PLAG1-S induction, underscoring PLAG1-S as an early-actor in promoting HSC function to improve hematopoietic repopulation.

3.4 Summary.

Herein we present 4 key findings:

1. PLAG1 expression is enriched in the most dormant human HSC compartments and appears decreased in its expression upon HSC activation.
2. PLAG1 is an essential regulator of long-term human hematopoietic repopulation.
3. Elevated expression of the short PLAG1 isoform (PLAG1-S) can improve human HSC fitness long-term and under stimulatory conditions; and amplify the number of functional HSCs 15-fold.

And

4. The functional advantage imparted by PLAG1-S is phenotypically distinct from gains observed upon MSI2 overexpression.

Our findings also underscore a key question: What are the molecular targets of PLAG1-S that enable its positive regulation of human HSCs?

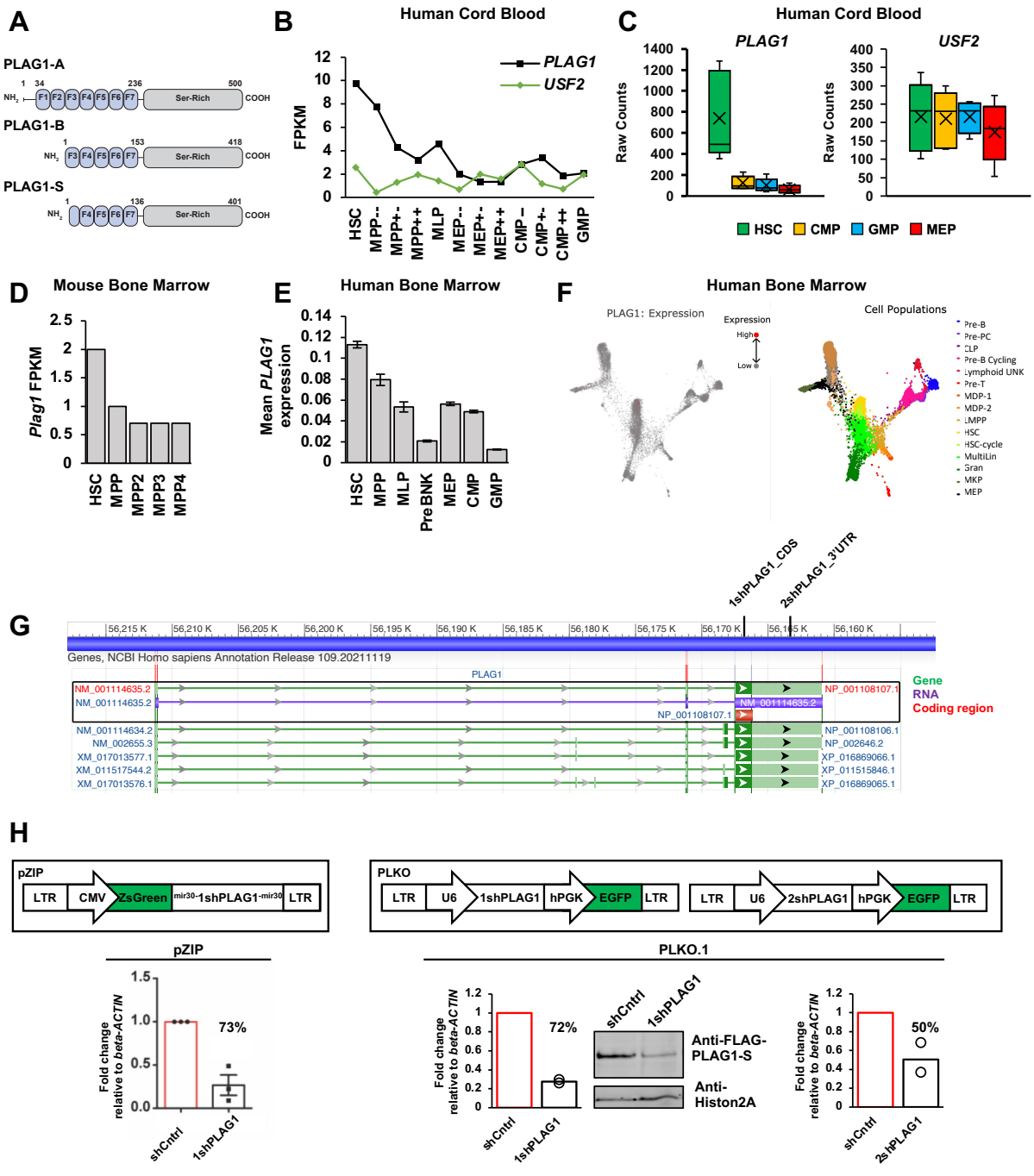
A
PLAG1-A
PLAG1-B
PLAG1-S
Ser-Rich
B
Human Cord Blood
PLAG1
USF2
FPKM
C
Human Cord Blood
PLAG1
USF2
Raw Counts
HSC
CMP
GMP
MEP
D
Mouse Bone Marrow
Plag1 FPKM
E
Human Bone Marrow
Mean PLAG1 expression
F
Human Bone Marrow
PLAG1: Expression
Cell Populations
G
1shPLAG1_CDS
2shPLAG1_3'UTR
Genes, NCBI Homo sapiens Annotation Release 109.20211119
PLAG1
Gene
RNA
Coding region
H
pZIP
PLKO
pZIP
PLKO.1
Fold change relative to beta-ACTIN
73%
72%
50%
shCntrl
1shPLAG1
2shPLAG1
Anti-FLAG-PLAG1-S
Anti-Histon2A

Figure 3: PLAG1 is enriched in human HSCs. (A) Schematic of three PLAG1 isoforms A, B and S from top to bottom. Alternative splicing of the full-length PLAG1-A produces the 82 amino acid N-terminal truncated product, PLAG1-B, and alternative translation start at Met 99 encodes PLAG1-S, the shortest isoform. **(B,C)** PLAG1 and USF2 transcript expression from RNA-seq of in fractionated human cord blood[74,249]. Box plot is of exclusive median, whiskers show variability outside upper and lower quartile, and X marks the mean. **(D)** Plag1 transcript expression from fractionated murine bone marrow[250]. **(E,F)** Mean PLAG1 transcript expression from single cell RNA-seq of human bone marrow[251,252]. **(G)** PLAG1 gene structure and location of shRNAs targeting PLAG1. **(H)** Schematics of lentivectors used for PLAG1 knockdown and knockdown validation by qPCR in wild type HeLa cells and western blot with anti-FLAG antibody targeted against overexpressed FLAG-PLAG1-S in HeLa cells.

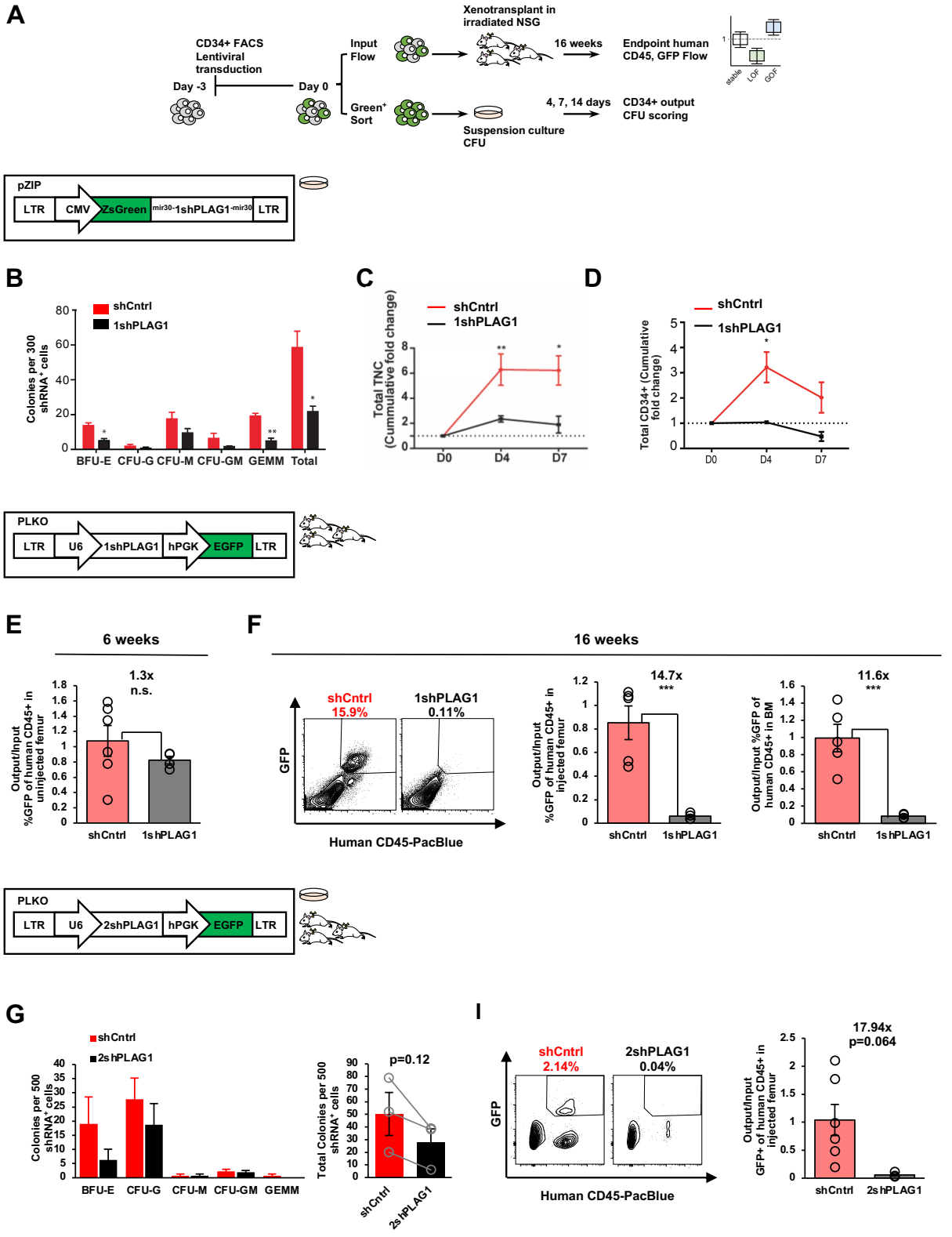
A
CD34+ FACS
Lentiviral
transduction
Day -3
Day 0
Input
Flow
Green+
Sort
Xenotransplant in
irradiated NSG
16 weeks
Endpoint human
CD45, GFP Flow
4, 7, 14 days
CD34+ output
CFU scoring
Suspension culture
CFU
stable
LOF
GOF
pZIP
LTR
CMV
ZsGreen
mir30-1shPLAG1-mir30
LTR
B
shCntrl
1shPLAG1
Colonies per 300
shRNA+ cells
BFU-E
CFU-G
CFU-M
CFU-GM
GEMM
Total
C
shCntrl
1shPLAG1
Total TNC
(Cummulative fold change)
D0
D4
D7
D
shCntrl
1shPLAG1
Total CD34+ (Cumulative
fold change)
D0
D4
D7
PLKO
LTR
U6
1shPLAG1
hPGK
EGFP
LTR
E
6 weeks
1.3x
n.s.
Output/Input
%GFP of human CD45+ in
uninjected femur
shCntrl
1shPLAG1
F
16 weeks
shCntrl
15.9%
1shPLAG1
0.11%
GFP
Human CD45-PacBlue
14.7x
***
Output/Input
%GFP of human CD45+ in
injected femur
shCntrl
1shPLAG1
11.6x
***
Output/Input %GFP of
human CD45+ in BM
shCntrl
1shPLAG1
PLKO
LTR
U6
2shPLAG1
hPGK
EGFP
LTR
G
shCntrl
2shPLAG1
Colonies per 500
shRNA+ cells
BFU-E
CFU-G
CFU-M
CFU-GM
GEMM
p=0.12
Total Colonies per 500
shRNA+ cells
shCntrl
2shPLAG1
I
shCntrl
2.14%
2shPLAG1
0.04%
GFP
Human CD45-PacBlue
17.94x
p=0.064
Output/Input
GFP+ of human CD45+ in
injected femur
shCntrl
2shPLAG1

Figure 4: PLAG1 is essential in human HSCs. (A) Schematic of Lin$^-$CD34$^+$ CB HSPC *in vitro* and *in vivo* functional assay timelines and lentivectors used for PLAG1 knockdown. **(B)** Primary CFU output by Lin$^-$CD34$^+$ HSPCs expressing shLuciferase control or 1shPLAG1 hairpins. **(C)** Cumulative *in vitro* total nucleated cell (TNC) fold change of cultured of Lin$^-$CD34$^+$ HSPC expressing shLuciferase control or 1shPLAG1hairpins. **(D)** Cumulative *in vitro* CD34$^+$ cell fold change of cultured of Lin$^-$CD34$^+$ HSPCs expressing shLuciferase control or 1shPLAG1hairpins. **(E)** GFP$^+$ engraftment in the uninjected femur of primary NSG mice 6 weeks after xenotransplantation of Lin$^-$CD34$^+$ cells expressing either shScramble control (n=6) or 1shPLAG1 (n=4) hairpins normalized to input % GFP$^+$ levels. **(F)** Representative flow plot and GFP$^+$ engraftment in the injected femur and uninjected bone marrow of primary NSG mice 16 weeks after xenotransplantation of Lin$^-$CD34$^+$ cells expressing either shScramble control (n=6) or 1shPLAG1 (n=4) hairpins normalized to input % GFP$^+$ levels. **(G)** Primary CFU output by Lin$^-$CD34$^+$ HSPC expressing shScramble control or 2shPLAG1 hairpins. **(H)** GFP$^+$ engraftment in the injected femur of primary NSG mice 16 weeks after xenotransplantation of Lin-CD34+ cells expressing either the shScramble control (n=6) or 2shPLAG1 (n=3) hairpins normalized to input % GFP$^+$ levels.

Data is presented as average +/- SEM unless otherwise indicated. Each point represents one mouse or an individual CB unit. *** $p<0.005$, ** $p<0.01$, * $p<0.05$.

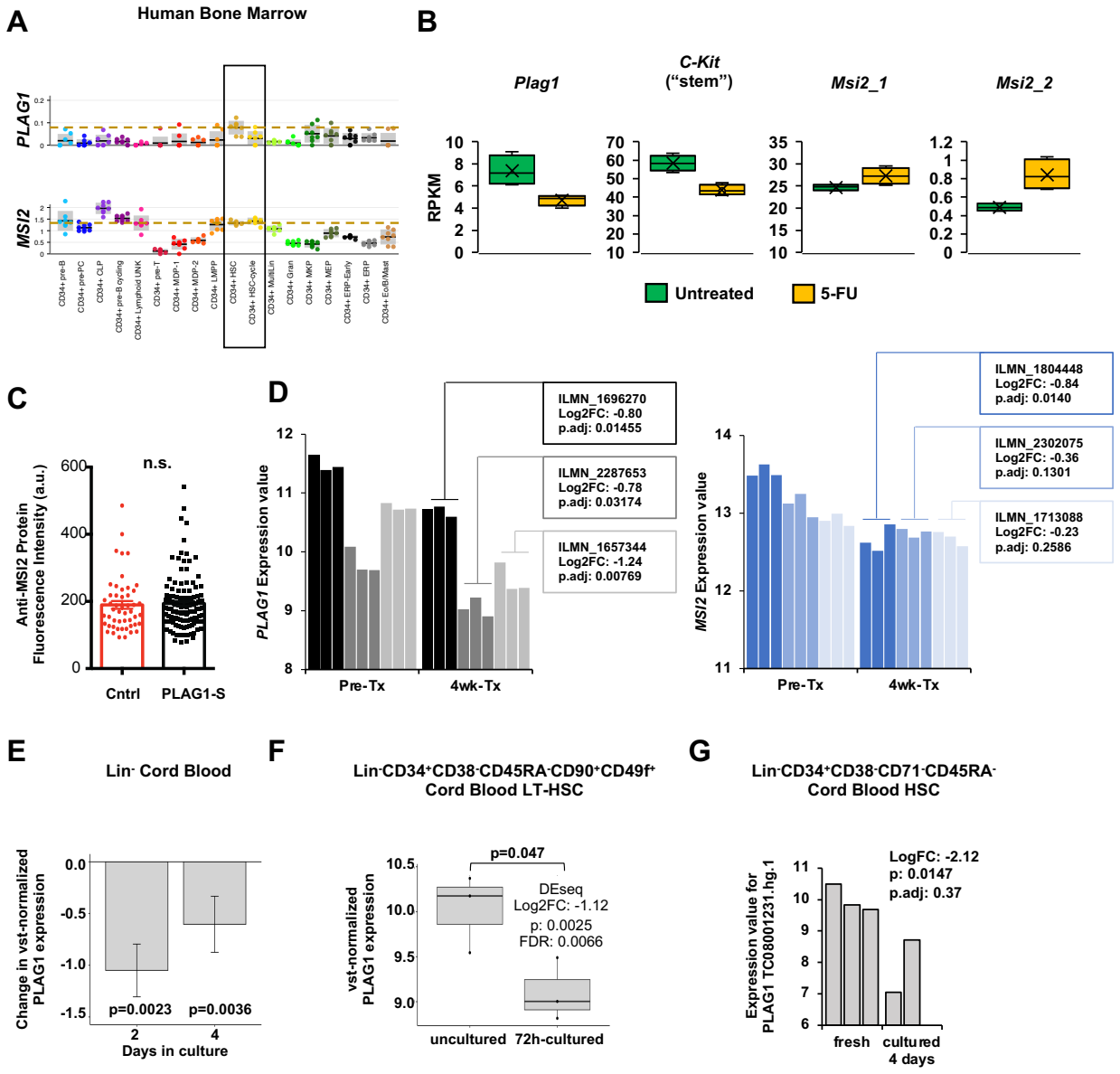
A
Human Bone Marrow
PLAG1
MSI2
B
Plag1
C-Kit ("stem")
Msi2_1
Msi2_2
RPKM
Untreated
5-FU
C
Anti-MSI2 Protein Fluorescence Intensity (a.u.)
n.s.
Cntrl
PLAG1-S
D
PLAG1 Expression value
ILMN_1696270
Log2FC: -0.80
p.adj: 0.01455
ILMN_2287653
Log2FC: -0.78
p.adj: 0.03174
ILMN_1657344
Log2FC: -1.24
p.adj: 0.00769
Pre-Tx
4wk-Tx
MSI2 Expression value
ILMN_1804448
Log2FC: -0.84
p.adj: 0.0140
ILMN_2302075
Log2FC: -0.36
p.adj: 0.1301
ILMN_1713088
Log2FC: -0.23
p.adj: 0.2586
E
Lin- Cord Blood
Change in vst-normalized PLAG1 expression
p=0.0023
p=0.0036
Days in culture
F
Lin-CD34+CD38-CD45RA-CD90+CD49f+ Cord Blood LT-HSC
vst-normalized PLAG1 expression
p=0.047
DEseq
Log2FC: -1.12
p: 0.0025
FDR: 0.0066
uncultured
72h-cultured
G
Lin-CD34+CD38-CD71-CD45RA- Cord Blood HSC
Expression value for PLAG1 TC08001231.hg.1
LogFC: -2.12
p: 0.0147
p.adj: 0.37
fresh
cultured 4 days

Figure 5: PLAG1 is enriched in dormant human HSCs and anti-correlated with MSI2. (A) PLAG1 and MSI2 transcript expression in human bone marrow cell populations determined by single cell RNA-seq[252]. **(B)** Changes in transcript expression of Plag1, Msi2, and stem-marker c-Kit in murine $Lin^-Cd150^+Cd48^-Eprc^+$ HSCs after treatment with 5-FU[149]. **(C)** MSI2 protein expression measured by immunofluorescence microscopy in PLAG1-S overexpressing Lin^-CD34^+ cells. Each point is a single cell. **(D)** PLAG1 and MSI2 expression in long-term CB HSCs prior to and 4 weeks following xenotransplantation in conditioned NSG mice[139] **(E)** Change in variance-stabilizing transformed (vst) PLAG1 transcript expression in Lin^- cord blood cells cultured for 2 or 4 days showing the p value from one-tailed Student's t-test[162] and **(F)** in 72 hour-cultured long-term CB HSCs showing the p value from one-tailed Student's t-test and differential expression from DEseq analysis[152]. **(G)** PLAG1 expression in long-term CB HSCs co-cultured with stromal cells for 4 days[253].

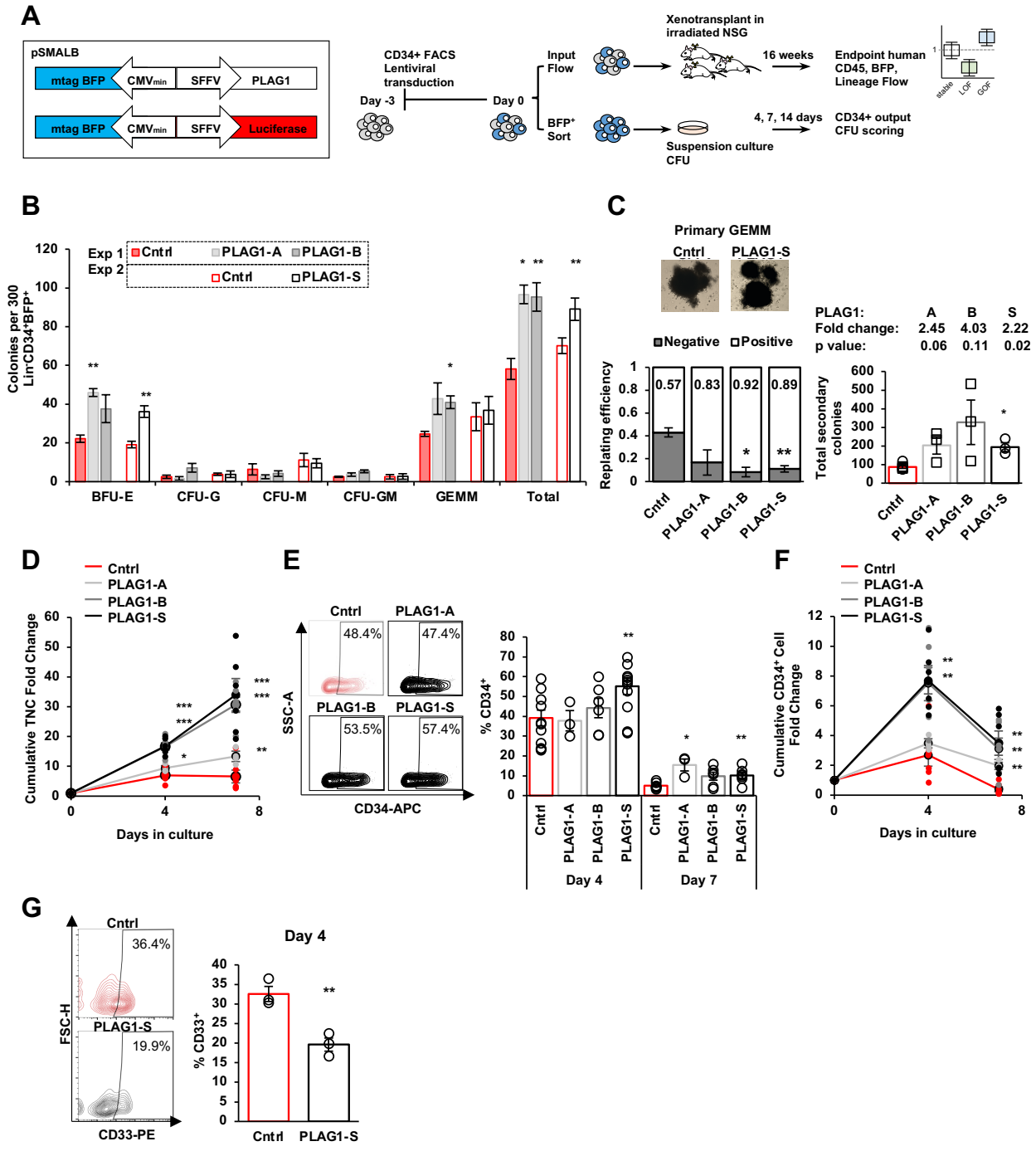
A
pSMALB
mtag BFP
CMVmin
SFFV
PLAG1
Luciferase
CD34+ FACS
Lentiviral
transduction
Day -3
Day 0
Input
Flow
BFP+
Sort
Xenotransplant in
irradiated NSG
16 weeks
Endpoint human
CD45, BFP,
Lineage Flow
4, 7, 14 days
CD34+ output
CFU scoring
Suspension culture
CFU
B
Exp 1
Exp 2
Cntrl
PLAG1-A
PLAG1-B
PLAG1-S
Colonies per 300
Lin-CD34+BFP+
BFU-E
CFU-G
CFU-M
CFU-GM
GEMM
Total
C
Primary GEMM
Cntrl
PLAG1-S
Negative
Positive
Replating efficiency
0.57
0.83
0.92
0.89
PLAG1:
Fold change:
p value:
A
B
S
2.45
4.03
2.22
0.06
0.11
0.02
Total secondary
colonies
D
Cntrl
PLAG1-A
PLAG1-B
PLAG1-S
Cumulative TNC Fold Change
Days in culture
E
48.4%
47.4%
53.5%
57.4%
SSC-A
CD34-APC
% CD34+
Day 4
Day 7
F
Cumulative CD34+ Cell
Fold Change
Days in culture
G
36.4%
19.9%
FSC-H
CD33-PE
% CD33+

Figure 6: PLAG1-S is a positive regulator of human HSPC fitness. (A) Schematic of Lin^-CD34^+ CB HSPC *in vitro* and *in vivo* functional assay timelines and lentivectors used for overexpression of PLAG1 protein isoforms. **(B)** Primary CFU output by $BFP^+Lin^-CD34^+$ cells overexpressing PLAG1-A, B or S or Luciferase control (n=3). **(C)** Secondary CFU replating efficiency (for each condition 12 GEMMs from three distinct CB units were replated into new wells. Negative indicates no secondary colonies were derived from the primary GEMM, Positive indicates at least one secondary colony was derived from the primary GEMM) and the total number of secondary colonies on positive plates with images of representative primary GEMM colonies used. **(D)** Cumulative *in vitro* total nucleated cell (TNC) fold change of cultured of Lin^-CD34^+ cells overexpressing PLAG1-A (n=3), B, or S or Luciferase control (n=6). **(E)** Representative flow plots and frequency of CD34 positivity in PLAG1-A (n=3), B, or S or Luciferase control (n=6) overexpressing cultures after 4 and 7 days *ex vivo*. **(F)** Cumulative *in vitro* $CD34^+$ cell fold change of cultured of Lin^-CD34^+ cells overexpressing PLAG1-A (n=3), B, or S or Luciferase control (n=6). **(G)** Representative flow plots and overall CD33 frequency in PLAG1-S^{OE} Lin^-CD34^+ HSPC after 4 days of *ex vivo* culture (n=3).

Data is presented as average +/- SEM unless otherwise indicated. Each point represents one mouse or an individual CB unit. *** $p<0.005$, ** $p<0.01$, * $p<0.05$.

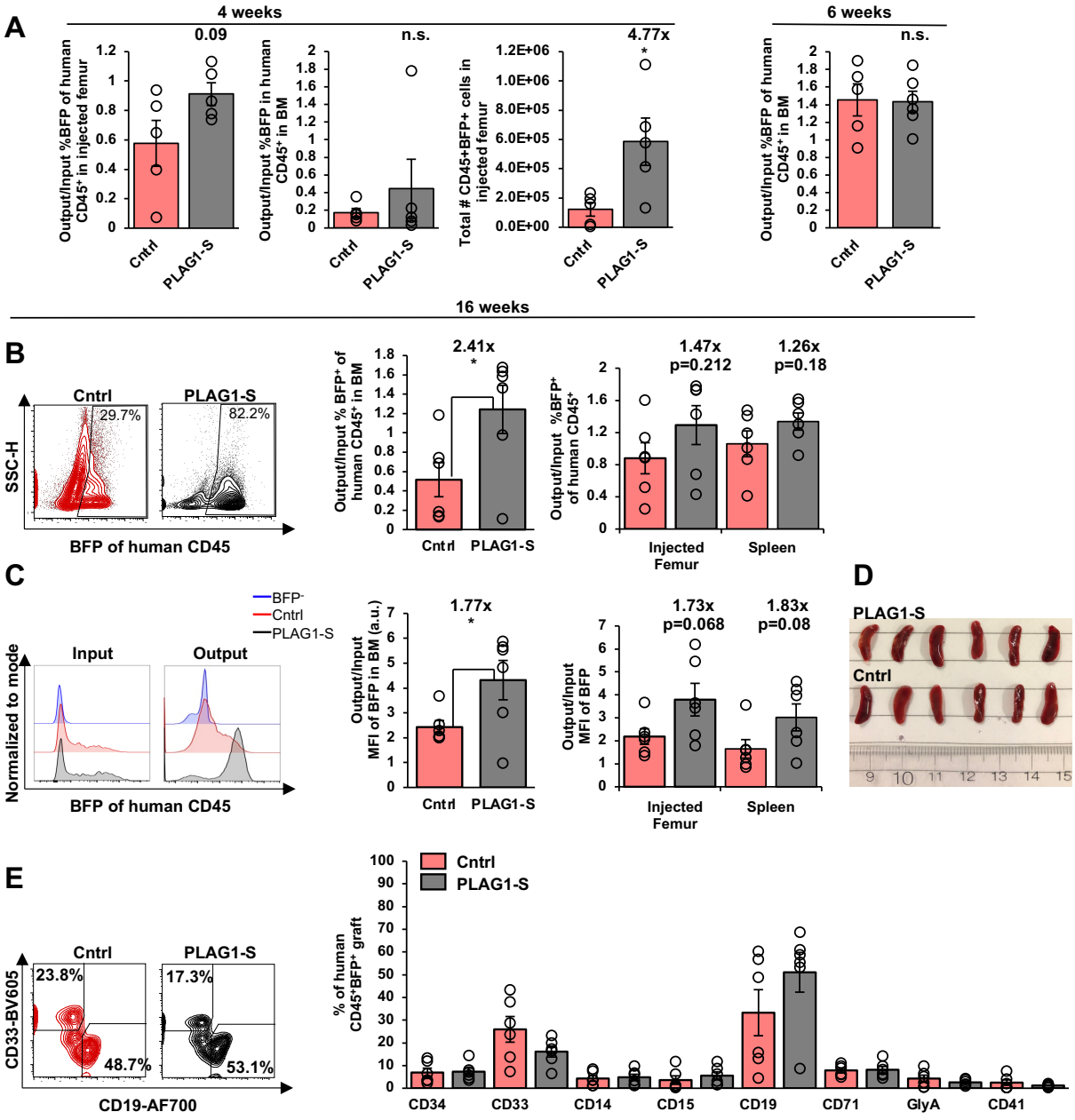

		IF			BM			SPLN		
Description	Population	SFFV	PLAG1-S	ttest	SFFV	PLAG1-S	ttest	SFFV	PLAG1-S	ttest
myeloid progenitor	CD34+CD33+	2.64666667	1.92	0.48317952	2.9555	0.904	0.38212366	1.52166667	0.78183333	0.39683664
myeloid	CD34-CD33+	19.665	18.7633333	0.90012655	10.6116667	9	0.78052341	15.6033333	7.985	0.23054272
mature myeloid	CD14+CD15+	2.92166667	3.42166667	0.80360119	1.925	2.33333333	0.72175935	0.535	0.50666667	0.92198351
erythroid progenitor	CD34+CD71+	3.10333333	2.82666667	0.83832144	3.94166667	2.085	0.21839534	0.48666667	0.52166667	0.92941277
erythroid	CD34-CD71+	5.43	8.05833333	0.29432677	21.37	13.9083333	0.32743087	9.03833333	15.5466667	0.29935514
erythroid	CD71+GlyA-	6.88166667	7.01666667	0.96589521	4.53	5.07166667	0.73018272	8.52833333	14.1466667	0.33545632
mature erythroid	CD71+GlyA+	0.5815	1.96666667	0.13166875	1.75	1.96	0.82291554	0.267	0.45	0.46629227
mature erythroid	CD71-GlyA+	0.675	0.92333333	0.53077148	2.52333333	0.625	0.05746416	3.04	0.91166667	0.19468379
megakaryocyte progenitor	CD34+CD41a+	0.75766667	0.35816667	0.40474993	3.60666667	2.53666667	0.45204829	0.68516667	0.51933333	0.75298788
megakaryocyte	CD34-CD41a+	1.23	1.05166667	0.81507414	4.49166667	4.91666667	0.79591084	10.0333333	4.00666667	0.23297737
lymphoid progenitor	CD34+CD19+	2.38	4.31666667	**0.03502068**	2.1705	1.32983333	0.48556219	0.74166667	0.86833333	0.58673367
lymphoid	CD34-CD19+	51.8	56.9333333	0.60064332	3.59166667	10.5333333	0.51849573	37.255	63.99	0.12617649
	CD34+	6.07333333	9.13	0.12044687	6.92166667	7.29833333	0.88246723	3.99333333	2.315	0.22266065
	CD33+	19.985	18.7833333	0.86719172	25.9383333	16.13	0.14109105	26.3333333	11.9266667	0.20621459
	CD14+	5.255	5.78166667	0.86283077	4.29666667	4.83166667	0.77554999	2.52833333	2.35	0.87038001
	CD15+	4.09166667	8.07333333	0.17409095	3.59333333	5.55333333	0.45486655	2.17833333	1.81666667	0.68919971
	CD71+	7.46316667	8.98333333	0.60234642	7.86	8.145	0.87336857	8.79533333	14.5966667	0.3089233
	GlyA+	1.2565	2.89	0.14978575	4.27333333	2.585	0.31218016	3.307	1.36166667	0.27221961
	CD41a+	1.5205	1.203	0.71577533	2.48716667	1.22066667	0.32530581	7.78533333	3.04133333	0.20527466
	CD19+	48	55.5166667	0.46948249	33.2766667	51.065	0.213226	29.79	56.0366667	0.10905259

Figure 7: PLAG1-S is a positive regulator of human HSC fitness. (A) BFP^+ engraftment in the injected femur and uninjected bone marrow of primary NSG mice 4 or 6 weeks after xenotransplantation of Lin^-CD34^+ cells overexpressing PLAG1-S or Cntrl normalized to input % BFP^+ levels (n=5). **(B)** Representative flow plots and quantification relative to input proportions of BFP representation in $CD45^+$ human grafts in bone marrow, injected femur and spleen of primary NSG mice 16 weeks after receiving Lin^-CD34^+ cells overexpressing either PLAG1-S or Luciferase control (n=6). **(C)** Representative flow plots of input and output BFP fluorescence intensity and quantification of output/input BFP median fluorescence intensity in bone marrow, injected femur and spleen of primary NSG mice 16 weeks after receiving Lin^-CD34^+ cells overexpressing either PLAG1-S or Luciferase control (n=6). **(D)** Spleens from primary NSG mice xenotransplanted with either PLAG1-S^{OE} or control Lin^-CD34^+ cells. **(E)** Representative flow plots of lineage markers in endpoint primary NSG grafts and endpoint frequencies of lineage markers in PLAG1-S^{OE} or control grafts in primary NSG mice.

Data is presented as average +/- SEM unless otherwise indicated. Each point represents one mouse or an individual CB unit. *** $p<0.005$, ** $p<0.01$, * $p<0.05$.

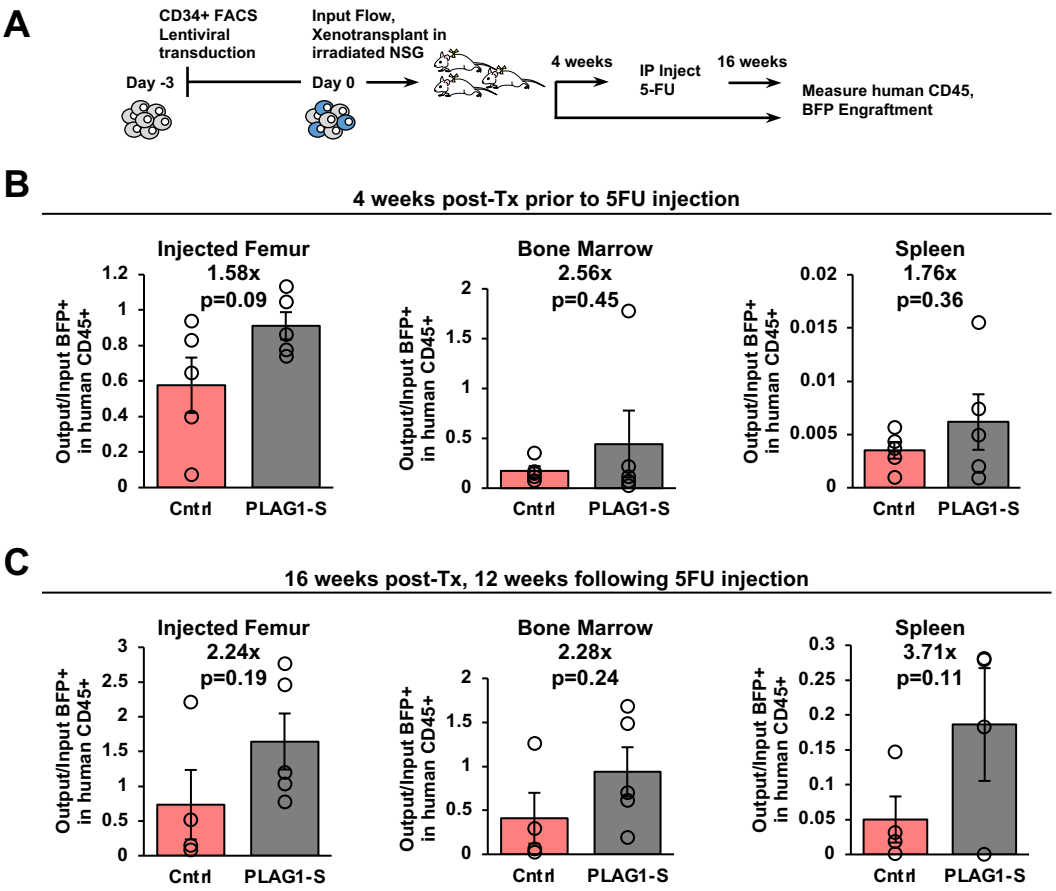
A
CD34+ FACS
Lentiviral
transduction
Day -3
Input Flow,
Xenotransplant in
irradiated NSG
Day 0
4 weeks
IP Inject
5-FU
16 weeks
Measure human CD45,
BFP Engraftment
B
4 weeks post-Tx prior to 5FU injection
Injected Femur
1.58x
p=0.09
Bone Marrow
2.56x
p=0.45
Spleen
1.76x
p=0.36
Output/Input BFP+
in human CD45+
Cntrl
PLAG1-S
C
16 weeks post-Tx, 12 weeks following 5FU injection
Injected Femur
2.24x
p=0.19
Bone Marrow
2.28x
p=0.24
Spleen
3.71x
p=0.11

Figure 8: PLAG1-S is a positive regulator of human HSC fitness after *in vivo* injury. (A) Schematic of $Lin^{-}CD34^{+}$ CB HSPC transduction, xenotransplantation, 5-FU insult and assessment timepoints. **(B)** BFP^{+} engraftment in the injected femur, uninjected bone marrow and spleen of primary NSG mice 4 weeks after xenotransplantation of $Lin^{-}CD34^{+}$ cells overexpressing PLAG1-S or Cntrl normalized to input % BFP^{+} levels (n=5). **(C)** BFP^{+} engraftment in the injected femur, uninjected bone marrow and spleen of primary NSG mice 12 weeks after 5-FU injection and 16 weeks after xenotransplantation of $Lin^{-}CD34^{+}$ cells overexpressing PLAG1-S or Cntrl normalized to input % BFP^{+} levels (n=5).

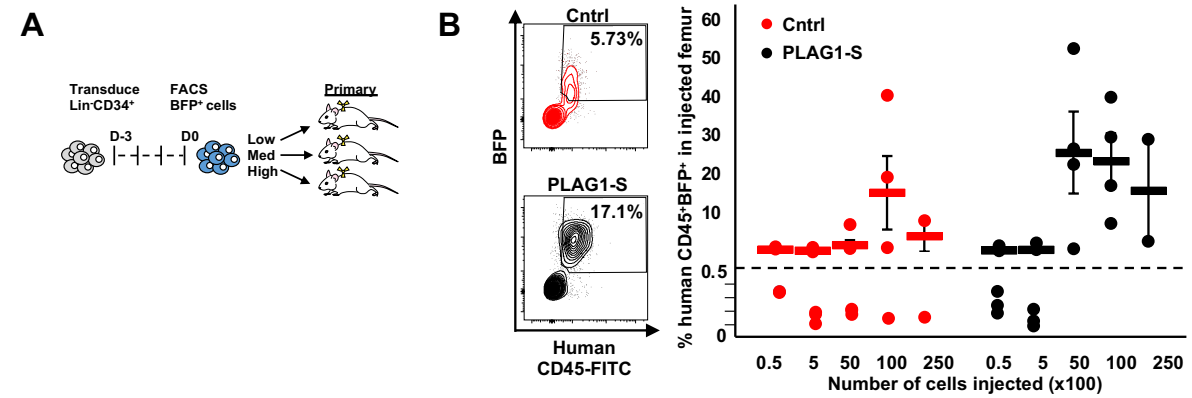

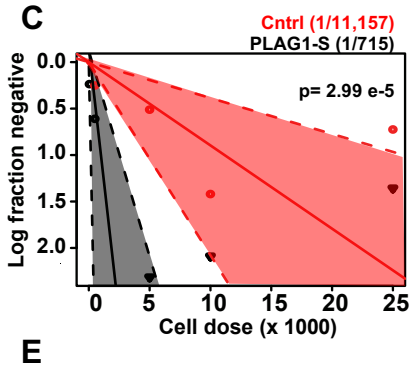

D

Vector	Total BFP+ cells	BFP+ cell dose/mouse	Number of mice transplanted	Number of mice with multilineage engraftment	BFP+ HSC frequency (0.95 confidence interval)	Number of BFP+ HSC
Cntrl	117750	25000	2	1	Lower: 1/28570	10.55
		10000	4	3	**Estimate: 1/11157**	
		5000	5	2	Upper: 1/4811	
		500	5	1		
		50	5	0		
PLAG1-S	117750	25000	2	2	Lower: 1/2225	164.69
		10000	4	4	**Estimate: 1/715**	
		5000	5	5	Upper: 1/230	
		500	5	2		
		50	5	1		

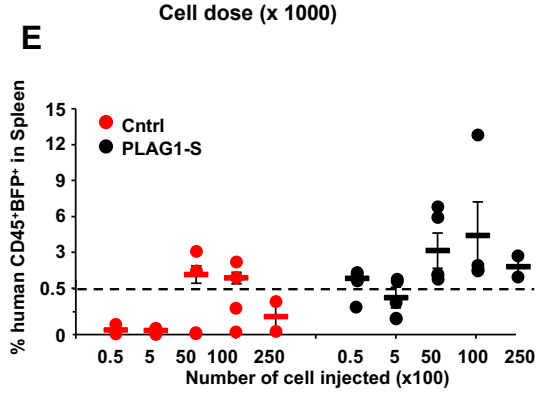

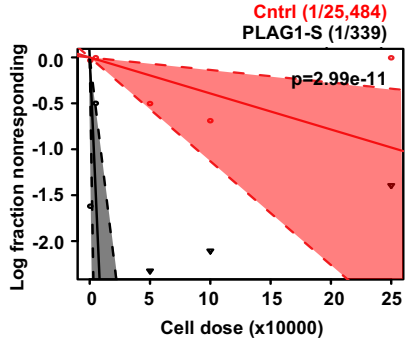

G

Vector	Total BFP+ cells	BFP+ cell dose/mouse	Number of mice transplanted	Number of mice with multilineage engraftment	BFP+ HSC frequency (0.95 confidence interval)	Number of BFP+ HSC
Cntrl	117750	25000	2	0	Lower: 1/73416	4.62
		10000	4	2	**Estimate: 1/25484**	
		5000	5	2	Upper: 1/8846	
		500	5	0		
		50	5	0		
PLAG1-S	117750	25000	2	2	Lower: 1/911	347.35
		10000	4	4	**Estimate: 1/339**	
		5000	5	5	Upper: 1/126	
		500	5	2		
		50	5	4		

Figure 9: PLAG1-S overexpression promotes self-renewal of human HSCs *ex vivo*. (A) Schematic of primary xenotransplantation in limiting dilution format. **(B)** Representative flow plots of $CD45^+BFP^+$ engraftment of primary recipient mice in injected femur. Percent $CD45^+BFP^+$ engraftment in injected femur of primary recipient mice across multiple cell input doses. Dashed line indicates cut off for calling engraftment, which was >0.5% human chimerism including both myeloid ($CD45^+BFP^+CD33^+$) and lymphoid ($CD45^+BFP^+CD19^+$) lineages. **(C,D)** Quantification of HSC frequency by ELDA[232] of injected femur of primary recipient mice. Shaded area under the curve represents 95% confidence interval of HSC frequency. **(E)** Percent engraftment in spleen of primary recipient mice across multiple cell input doses. Dashed line indicates cut off for calling engraftment, which was >0.5% human chimerism including both myeloid ($CD45^+BFP^+CD33^+$) and lymphoid ($CD45^+BFP^+CD19^+$) lineages. **(F,G)** Quantification of HSC frequency by ELDA[232] of splenic engraftment in primary recipient mice. Shaded area under the curve represents 95% confidence interval of HSC frequency.

Data is presented as average +/- SEM unless otherwise indicated. Each point represents one mouse. *** $p<0.005$, ** $p<0.01$, * $p<0.05$.

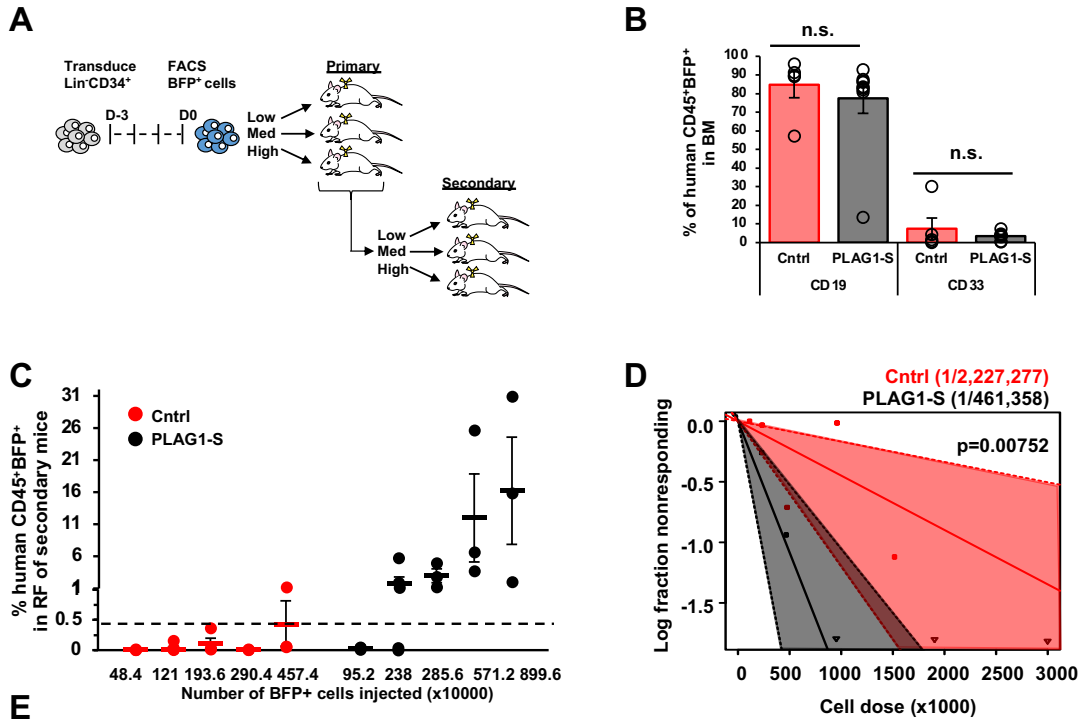

E

Vector	Total BM from 6 mice	Total BM pooled from 6 donor primary mice	% BFP+	Total BFP+ BM pooled from 6 donor primary mice	BFP+ cell dose	Number of secondary mice transplanted	Number of secondary mice with multilineage engraftment	BFP+ HSC frequency (0.95 confidence interval)	Number of BFP+ HSC transplanted into secondary mice	Total BFP+ HSC in 6 donor primary mice	# BFP+ HSC transplanted into 6 donor primary mice	Total BFP+ HSC Fold Change *in vivo*
Cntrl	810,000,000	91,800,000	12.1	11,107,800	4573800	3	2	Lower: 1/5952539	4.98	44.00	5.87	7.50
					2904000	3	0	**Estimate: 1/2227277**				
					1936000	4	2	Upper: 1/833386				
					1210000	5	0					
					484000	4	0					
PLAG1-S	810,000,000	87,800,000	23.8	20,896,400	8996400	3	3	Lower: 1/947791	45.29	417.85	91.60	4.56
					5712000	3	3	**Estimate: 1/461358**				
					2856000	3	3	Upper: 1/224577				
					2380000	5	3					
					952000	4	1					

Figure 10: PLAG1-S overexpression promotes self-renewal of long-term human HSCs *ex vivo* without exhaustion. A) Schematic of secondary xenotransplantation in limiting dilution format. **(B)** Frequency of lineage reconstitution in $CD45^{+}BFP^{+}$ grafts in injected femur of secondary recipient mice that received either PLAG1-S^{OE} primary bone marrow (n=9) or $Luciferase^{OE}$ control (n=5). **(C)** Percent $CD45^{+}BFP^{+}$ engraftment in injected femur of secondary recipient mice across multiple cell input doses. Dashed line indicates cut off for calling engraftment, which was the same as for primary mice. **(D,E)** Quantification of HSC frequency by ELDA[232] of injected femur or uninjected bone marrow of secondary recipient mice and of *in vivo* expansion. Shaded area under the curve represents 95% confidence interval of HSC frequency. Total BFP^{+} cells within whole-body BM of primary mice was extrapolated based on femur and hind limb counts and proportional accounting from Colvin et al. (2004)[182,233], and *in vivo* expansion is measured as the fold difference of total BFP^{+} HSC in donor mice relative to total day 0 HSCs initially transplanted into the 6 donor mice.

Data is presented as average +/- SEM unless otherwise indicated. Each point represents one mouse. *** $p<0.005$, ** $p<0.01$, * $p<0.05$.

A

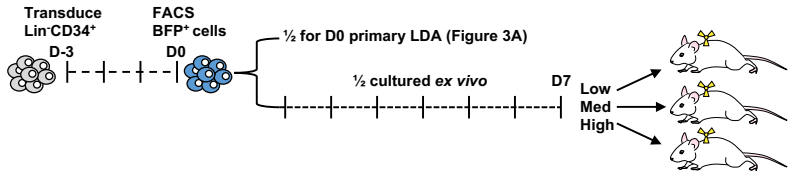

B

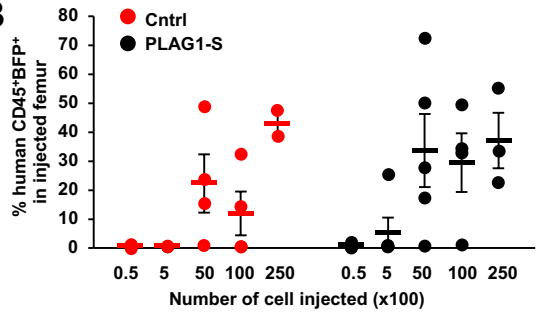

C

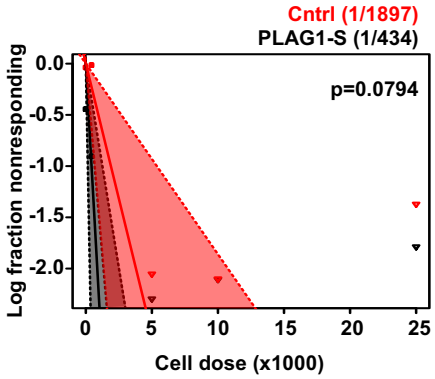

D

Vector	D0 BFP+ cell dose/mouse	Number of mice transplanted	Number of mice with multilineage engraftment	BFP+ HSC frequency (0.95 confidence interval)
Cntrl	25000	2	2	Lower: 1/5376
	10000	4	4	**Estimate: 1/1897**
	5000	4	4	Upper: 1/670
	500	3	0	
	50	5	0	
PLAG1-S	25000	3	3	Lower: 1/1255
	10000	4	4	**Estimate: 1/434**
	5000	5	5	Upper: 1/150
	500	5	3	
	50	3	1	

E

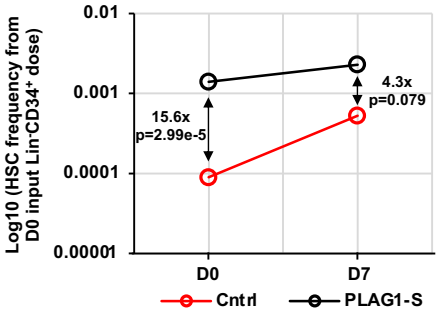

Figure 11: PLAG1-S overexpression promotes self-renewal of long-term human HSCs rapidly in culture. **(A)** Schematic of xenotransplantation of transduced $Lin^{-}CD34^{+}$ cells that were cultured 7 days *ex vivo*. **(B)** Percent engraftment in injected femur of primary mice that received multiple cell input doses of $Lin^{-}CD34^{+}$ cells overexpressing PLAG1-S or Luciferase control that were cultured *ex vivo* for 7 days. **(C,D)** Quantification of HSC frequency by ELDA for PLAG1-S^{OE} and $Luciferase^{OE}$ control $Lin^{-}CD34^{+}$ cells that were cultured 7 days *ex vivo* prior to xenotransplantation. Shaded area under the curve represents 95% confidence interval of HSC frequency. **(E)** Summary of HSC frequencies and expansion of PLAG1-S^{OE} and control $Lin^{-}CD34^{+}$ cells on day 0 and day 7 *of ex vivo* culture.

Data is presented as average +/- SEM unless otherwise indicated. Each point represents one mouse. *** $p<0.005$, ** $p<0.01$, * $p<0.05$.

CHAPTER 4

PLAG1-directed molecular circuitry in human HSPCs

4.1 PLAG1-S enforces a pro-HSC transcriptional state: Integrated analysis of genomic binding and transcriptional outcomes imparted by ectopic PLAG1-S.

To uncover the molecular targets underpinning the positive regulation of HSC by PLAG1-S we next aimed to profile global genomic binding and transcriptional changes imparted by ectopic PLAG1-S. We first performed CHIP-Seq on overexpressed FLAG-PLAG1-S in the CML-derived K562 cell line (**Figure 12A**). The chromatin was sheared to <500 bp fragments (**Figure 12B**), the efficiency of pull-down was validated by ChIP-western blot (**Figure 12C**) and subsequently by ChIP-seq fingerprint plot analysis (**Figure 12D**)[237]. ChIP-seq peak calling revealed PLAG1 occupied a total of 21,469 sites (**Figure 12D**). Consistent with its role as a transcription factor PLAG1 was preferentially associated with promoter regions (**Figure 12E**) and *de novo* motif discovery on sites bound by PLAG1 revealed not only the G-rich core consensus binding motif recognized by PLAG family members[199,255] but also identified an E-box containing consensus sequence bound with an equivalent frequency (**Figure 12G**). Notably this E-Box motif is shared by the PLAG1-S co-factor USF2, which was simultaneously overexpressed in these cells, suggesting possible reorganization of PLAG1 binding preference by the high presence of this cofactor. Comparison to $CD34^+$ epigenetic marks showed a high degree of overlap between PLAG1 binding sites in K562 cells and accessible regions of DNA in $CD34^+$ cells, including H3K4me3 (active promoter), H3K4me1 (enhancer), and H3K27Ac (enhancer) (**Figure 12H**). However, we reasoned the context-specific PLAG1 genome targets could be very different in $CD34^+$ cells, including possible PLAG1-S-enforced changes in the $CD34^+$ cell epigenetic landscape, compared to K562 cells. Thus, we next tested FLAG-PLAG1-S genomic binding Cleavage Under Targets and Release Using Nuclease (CUT&RUN) in Lin^-CD34^+ cells.

CUT&RUN is a technique developed in 2017 by Skene & Henikoff[256] that, analogously to chromatin immunoprecipitation (ChIP)-seq, enables global measurement of DNA loci bound by a DNA-binding protein. However, unlike ChIP-seq, CUT&RUN can recover high resolution DNA-binding profiles from very low, as few as 1000, input cells[243], allowing for its application in CB Lin^-CD34^+ cells. CUT&RUN performed specifically in Lin^-CD34^+ cells overexpressing FLAG-PLAG1-S identified 9788 reproducible genomic binding sites[243,256] (**Figure 13A, B**). Consistent with our ChIP-seq in K562 cells[194] and its known role as a TF, PLAG1-S sites are principally located in promoter regions (58.4%) (**Figure 13C**). *De novo* motif discovery revealed that PLAG1-S is predominantly (35%) bound to G-rich core consensus sequences expected for PLAG family members. To a lesser extent PLAG1-S is also bound to non-canonical motifs, including those commonly associated with other zinc-finger, GATA or RUNX TFs (**Figure 13D**), however we did not note an association to E-box motifs, suggesting as predicted that this motif is indeed either K562- or USF2-coOE- context dependent, where we are already aware PLAG1-S can have different molecular targets (i.e. MSI2). Comparison of genes bound by PLAG1-S in K562 and Lin^-CD34^+ cells revealed that while 78% of genes bound in Lin^-CD34^+ cells regardless of genomic loci were also occupied in K562, this intersection was reduced to only 60.8% when assessing promoter-bound genes specifically (**Figure 13E**, Fishers exact hypergeometric p=0.0). One possible explanation for the significant difference in promoter bound genes could point back to co-occupancy with USF2 in K562, which was >70% within promoter regions[194]. Moreover, despite a significant representation of $CD34^+$-occupied genes in the K562 data set, these 4521 genes represented only 39% of genes detected in K562 cells (**Figure 13E**), thus CUT&RUN in Lin^-CD34^+ cells provides a significant improvement in the resolution and specificity of the context-dependent PLAG1-S regulon, off which to search for putative direct targets.

To assess gene expression outcomes associated with PLAG1-S genomic binding events we next performed pairwise RNA-seq analysis. As with our CUT&RUN analysis, measurements of transcriptional changes were taken immediately following induction of ectopic PLAG1-S in an attempt to capture direct or immediate targets. Ectopic PLAG1-S significantly (p.adj<0.05) altered the expression of 543 genes. Consistent with its understood function as a transcription activator, 60% of the 291 upregulated genes are proximally bound by PLAG1-S, while 30% of downregulated genes are also directly bound (**Figure 13F**). Surprisingly, for activated genes PLAG1 binding is in fact underrepresented in the promoters and overrepresented in intronic regions, whereas genes repressed are mainly occupied by PLAG1 in their promoter regions (**Figure 13G**). While the overall magnitude of downregulation of gene expression is much lower than activation (**Figure 13F**), this data, similarly to other recent publications[257], suggests an underappreciated role for PLAG1-S in negative regulation of gene expression.

Moreover, we find that in agreement with our hypothesis that PLAG1-S influences HSC function via MSI2-independent mechanisms, that despite binding to both the MSI2 promoter and intron (**Figure 14A**), MSI2 transcript levels were unchanged (logFC: -0.1467, p.adj: 0.818) by ectopic PLAG1-S (**Figure 14B**). Additional support for our hypothesis is seen in the anticorrelation among the most highly differentially expressed genes in either PLAG1-S or MSI2 overexpressing CB HSPCs (**Figure 14C**). Altogether supporting the view that the activation of MSI2 gene expression by PLAG1-S is context and co-factor dependent

RNA-seq of HSPCs directly following up- or down- modulation of PLAG1 levels corroborates the respective immunophenotypic and functional outcomes both through the expression of stem-associated surface markers (CD34, CD90, EPCR) (**Figure 15A**) and by global alignment to transcriptional states of 20 human hematopoietic cell subpopulations[248], which show positive associations to primitive and erythroid ($CD34^{dim}CD133^{+}$, $CD34^{+}CD38^{-}$, $CD34^{+}CD71^{+}GlyA^{-}$ and $CD34^{-}CD71^{lo}GlyA^{+}$) signatures and negative associations to myeloid signatures correlated with high PLAG1 levels *in vitro* (**Figure 15B**). Moreover, among the top 15 differentially expressed genes in PLAG1-S^{OE} HSPCs we noted a significant elevation of hemoglobin subunit gamma 2 (*HBG2*), which is required for the formation of fetal hemoglobin (**Figure 15C**). Activation of fetal hemoglobin is an actively pursued treatment for beta-thalassemia and sickle cell disease[258,259], as such these transcriptional profiles and the elevation of BFU-E by PLAG1-S^{OE} HSPCs provided the impetus to further investigate the role of PLAG1-S in human erythropoiesis and its promotion of fetal hemoglobin. Expanded $Lin^{-}CD34^{+}$ HSPCs overexpressing either PLAG1-S or control were subject to a three-step *in vitro* erythroid differentiation culture and estimates of the frequencies of BFU-E, CFU-E/ProE, BasoE/PolyE, OrthoE/Retic cells in culture were made using CD34, CD71 and GlyA surface expression (**Figure 16A,B**); and HBF protein was measured by intracellular flow cytometry (IFC). Following 4 days in HSPC expansion media we find an elevated frequency of $CD34^{+}CD71^{+}$ (BFU-E) progenitors, in accordance with the results of our primary CFU assay. Over the course of culture, we find PLAG1-S^{OE} cells maintain higher levels of primitive BFU-E cells into the first stage of differentiation, and that throughout differentiation culture the output kinetics vary slightly, but that this does not impair their capacity to differentiate into more mature cell types (BasoE/PolyE, OrthoE/Retic) (**Figure 17A-C**). In HSPC-expansion conditions but not differentiated cultures we find a higher proportion of PLAG1-S^{OE} HSPCs expressing HbF (**Figure 18A, B**). However, in HbF-positive cells the relative protein levels are comparable for PLAG1-S^{OE} and control (**Figure 18C**).

Next, we performed Gene Set Enrichment Analysis (GSEA) and mapping (FDR<0.1) to explore the coordinated molecular circuits downstream of PLAG1-S. We noted that coordinated

pathway-level changes are dominated by negative enrichments (**Figure 19A**), furthering the support that PLAG1-S may also negatively regulate gene expression programs. A large, interconnected set of pathways reaffirms repression of genes required for mature myeloid cell functions (**Figure 19A**). The top-most negatively enriched gene sets, including peptide chain elongation, SRP-dependent co-translational protein targeting to the membrane, and cytoplasmic ribosomal proteins (**Figure 19B**), coalesce in the largest cluster of altered signatures and denotes a synchronized attenuation of mRNA translation machinery in PLAG1-S^{OE} HSPC (**Figure 19A**). These negative enrichments are driven largely by reduced expression of genes encoding ribosomal proteins (RPs) in PLAG1-S^{OE} HSPCs. When we examined all 80 human RP coding genes we observed that their expression is collectively reduced by an average of 9.7% (median 10.4%) +/- 5.7% standard deviation. Looking to the 25 RP genes with the most reproducibly significant change in their expression (DEseq $p<0.05$) the average reduction in expression is 15.7 +/- 1.8% (**Figure 19C**), demonstrating a general dampening of RP gene expression. Notably, when compared to GSEA of MSI2^{OE} HSPCs we find repression of translation machinery to be a unique feature of PLAG1-S^{OE} HSPCs (**Figure 20A, B**), further affirming an independent and mechanistically distinct function of PLAG1-S in enforcing human HSC physiology. We additionally find these signatures partly discordantly regulated in PLAG1^{KD} HSPCs (**Figure 21A, B**), specifically noting an overlap of discordant regulation of RP genes seen among the leading edges of both datasets (**Figure 21C**), suggesting these components of protein production machinery could be under direct control of PLAG1 in the context of human HSPCs.

To further assess the possibility of direct regulation of the protein production machinery by PLAG1-S we performed two over-representation analyses on the repertoire of genes detected by CUT&RUN as bound by PLAG1-S in HSPCs. Firstly, post-analysis in Cytoscape using either Mann-Whitney U test (**Figure 22A, orange edges**) or hypergeometric test (data not shown) indicates a significant overlap between the genes directly bound by PLAG1-S and genes belonging to the cluster of protein synthesis gene sets. This was also true when assessing only promoter-bound genes (data not shown). Additionally, over-representation analysis using gProfiler shows that 41 out of the 46 gene sets belonging to this cluster are significantly over-represented among PLAG1-S-bound genes (**Figure 22B**). Altogether this speaks to an unexpected ability of PLAG1-S to directly intersect with the regulation of protein synthesis machinery to regulate fate decisions in human HSPC.

Lastly, we noted an enrichment of DNA-regulating processes among PLAG1-S-bound targets (**Figure 22C**), and specifically among targets with significantly ($p.adj<0.05$) activated expression (**Figure 22D, Table 7**). These alterations may have the potential to influence the genomic landscape in PLAG1-S^{OE} HSPCs, possibly explaining context-specific differences in gene regulation and possibly contributing either additively or synergistically to the molecular mechanisms imparting the gain in HSC function. These are key questions whose answers could significantly inform our understanding of the role of PLAG1-S in HSC physiology and have yet to be explored.

4.2 PLAG1-S dampens protein synthesis and promotes dormancy in stimulated human HSPCs.

The state of attenuated translation machinery in PLAG1-S^{OE} HSPCs is intriguing given that tightly controlled protein synthesis is a hallmark of stem cell biology[165,260-263]. While others have demonstrated that culturing human HSPCs, like their murine counterparts, promotes exit from dormancy, loss of quiescence, and differentiation[134,139,153,162], little is known of their translation

dynamics within immediate and prolonged timeframes, and in comparison to more committed cells[172]. To gain these insights and contextualize the HSPC-specific PLAG1-S regulon we measured O-propargyl-puromycin (OP-Puro) incorporation in CB cells upon culture-induced stimulation[165,264,265] (**Figure 23A**). As early as 4-hours after being placed in culture $Lin^{-}CD34^{+}$ cells activate protein synthesis, and these levels progressively increase peaking at 9.5-fold after 48-hours. Subsequently translation rates drastically decline between 48 and 72-hours and plateau between 3-10 days, but do not return to base-line levels (**Figure 23B, C**). In contrast, more mature $Lin^{-}CD34^{-}$ cells experience only a modest elevation of translation after 24-hours that is diminished by 48-hours (**Figure 23D**), indicating that human HSPCs selectively undergo an immediate but transient pro-translation response when placed into culture. Evaluating PLAG1-S^{OE} HSPCs we observed that transcriptional reprogramming of protein biosynthetic processes indeed supports a 13% reduction in global translation rates in $Lin^{-}CD34^{+}$ cells *ex vivo* (**Figure 24A, B**). This appears selective to primitive hematopoietic cells as comparably handled K562 and $Lin^{-}CD34^{-}$ cells overexpressing PLAG1-S display unchanged and heighted translation levels, respectively (**Figure 24C, D**).

Protein biosynthesis and ribosome biogenesis are major drivers of cellular anabolism, which is generally correlated with cellular enlargement and division[163,164,266-269], both of which can predict HSC exhaustion[153,270]. To this point we noticed that the forward scatter (FSC-H) profile, which relatively approximates cell diameter, of cultured untransduced $CD34^{+}$ cells trended with protein synthesis rates with a significant enlargement observed at 48h in culture coincident with the peak in their translation rates. Notably this *in vitro* activation of mRNA translation and cellular enlargement of CB HSPCs appears to precede when their first cellular division is expected[139] (**Figure 23C**). We also observed that the steady increase in translation between 6-48 hours is paralleled by a steady gain in side scatter intensity (SSC-A), which does not resolve with translation and cell diameter at 72 hours (**Figure 23E**). This result interestingly suggests that the translation response could be associated with irreversible change(s) in certain unknown cellular properties. SSC-A is a crude measure of the diverse composition cellular components; therefore, it is unclear exactly what this change represents. Some hypotheses include the priming of differentiation, as differentiated monocytes and granulocytes contain a higher density of cellular granules and components that refract laser light or activation of stress-induced granules involved in translation inhibition, protein folding or lysosomal/authophagial processes involved in restoring proteostasis.

Likewise, we find that depressed translation in PLAG1-S^{OE} HSPCs is associated with restraint in size, as measured by microscopy and flow cytometry (**Figure 25A,B**). GSEA did not uncover consensus control over cell cycle progression by PLAG1-S, however Hoechst/Ki-67 staining indicated that PLAG1-S^{OE} HSPCs are also restrained in cell cycle progression (**Figure 25C**), paralleling the correlation between PLAG1 expression and dormant HSCs (**Figure 5A-G**). While this may likely be secondary to translation regulation, we also noticed that expression of CDKN1C, an essential regulator of murine HSC quiescence and renewal[211,212], appears directly activated 2.5-fold by PLAG1-S in HSPCs, possibly contributing to the cell cycle profile of these cells.

Overall, there is an emerging picture of a dormant cell state endowed by PLAG1-S^{OE} and, although the gene expression profiles do not suggest transcriptional control cellular metabolism/mitochondrial respiration, this process is often co-regulated with protein production[164] and is a key feature of HSC dormancy[132,147]. As such we tested PLAG1-S^{OE} and control HSPCs harvested after 4 days of culture using the Seahorse XF Cell Mito Stress Test (Agilent). PLAG1-

S^{OE} cells display lower basal respiration rates and higher spare respiratory capacity (**Figure 25D,E**), typical of primitive hematopoietic cell types[271].

In vitro survival, which could contribute to amplifying a stem cell pool experiencing infrequent and/or slow division dynamics, is enhanced in PLAG1-S^{OE} cells, as measured by Annexin V (**Figure 26A**). Given that translation dynamics are highly interconnected with stress signaling that can dictate survival decisions, we profiled stress effectors in PLAG1-S^{OE} HSPCs. Firstly, pro-apoptotic p53 targets, which can be induced by imbalances in ribosome components, are not activated within the PLAG1-S^{OE} transcriptome (**Figure 26B,C**)[272,273]. CB HSPCs retain low levels of EIF2 subunits to maintain low translation rates while preferentially driving the translation of the ISR effector ATF4[171], a mechanism also supportive of muscle stem cell regeneration[262]. We find however that PLAG1-S^{OE} HSPCs do not display differential regulation of EIF2 subunits nor ATF4 target transcripts[171,274] (**Figure 26D**), suggesting that this pathway is not significantly at play in PLAG1-S^{OE} HSPC. Lastly, CB HSPC are selectively sensitive to stress associated with misfolded proteins[170] and low translation rates in murine HSCs is a mechanism that protects their proteome integrity[168]. To this point, we indeed see that reduced translation in PLAG1-S^{OE} HSPCs is associated with depressed expression of UPR signatures (**Figure 26E**). Altogether this suggests that dampened translation rates imparted by PLAG1-S is protective and forestalls stress responses.

In sum, we show that human HSPC selectively experience an immediate and transient pro-translation response when exposed to stimulatory conditions; and through transcriptional programming PLAG1-S limits translation in human HSPC to mitigate the impact of culture-induced protein stress and HSC activation. This manifests as PLAG1-S-induced reductions in differentiation, cell enlargement, division, mitochondrial metabolism, and death in human HSPC, altogether significantly enhancing HSC fitness and output *in vivo*.

4.3 Summary.

Herein we present 5 key findings:

1. PLAG1-S has context-dependent molecular targets.
2. CB HSPCs selectively experience an immediate and transient pro-translation response when exposed to *ex vivo* culture conditions used commonly for HSC-based therapies.
3. PLAG1-S directly binds and coordinates expression of protein production machinery in human HSPCs.
4. Translation regulation in PLAG1-S^{OE} HSPCs appears uncoupled or to pre-empt intracellular stress signaling

And

5. In enforcing this mechanism, PLAG1-S endows an *in situ*-like rate of protein production and simultaneously restrains growth, mitochondrial metabolism, proliferation, differentiation and death to ultimately enhance human HSC preservation and function in stimulatory culture and transplantation settings.

Our findings provide the impetus to explore the molecular players involved in promoting dampened translation and HSC dormancy downstream of PLAG1-S and the utility of translation inhibition in clinical regenerative strategies.

Table 7: A selection of DNA-regulating genes bound and upregulated by PLAG1-S in human HSPCs with putative connections of hematopoietic regulation.

Upregulated Gene	Description
PRDM11	DNA binding protein Methyltransferase activity Dispensable for healthy murine HSPCs[275] Loss of PRDM11 promotes MYC-driven lymphomagenesis[276]
DNMT3B	Genome-wide *de novo* methylation Repressed expression associated with leukemic progression and prognosis (contrast to DNMT3A expression)[277-279]
HDAC7	Histone deacetylation at lysine residues on the N-terminal of the core histones (H2A, H2B, H3 and H4). Primes for epigenetic repression. Required for murine B lymphocyte specification.[280] Repressed expression associated with lymphoid cancer progression and prognosis.[281,282]
RARA	DNA-binding, Retinoic Acid (RA) Receptor that forms heterodimers with retinoid X receptors to regulate RA response elements in DNA. When ligand (e.g. ATRA)-stimulated heterodimers recruit co-activators. When ligand is absent heterodimers recruit co-repressors (e.g. HDACs) Not essential for murine hematopoiesis but whole RAR system plays significant roles in hematopoietic homeostasis. Multiple gene fusions in acute promyelocytic leukemia with poor prognosis because less responsive to ATRA.[283]
ZNF521	Zinc Finger Transcription Factor, proto-oncogene Essential for murine HSC renewal and repopulation. Activation promotes murine HSPC expansion in vitro.[284] Highly expressed in human AMLs with MLL translocations. Repression impairs murine and human MLL-AML *in vitro* and *in vivo*.[284,285] Cooperates with co-overexpressed MLL-AF9 to promote CB HSPC expansion *in vitro*.[286]
SMAD6	DNA-binding, Inhibitory Smads (I-Smads), Smad6 and Smad7 (Smad6/7), are involved in feedback inhibition of the BMP signaling pathway Inhibits CB erythropoiesis.[287] Transcriptional network in fetal hematopoiesis.[288]
APOBEC 3C-G	DNA deaminase (C > U). May influence intracellular response to gene editing to improve engraftment, at the cost of pre-cancerous genome instability. [289-291]
KLF1	Essential transcriptional regulator of erythropoiesis Regulator of BCL11A, transcriptional switch for fetal-to-adult hemoglobin[292]
GATA1/2	Essential transcriptional regulators of erythropoiesis[292]

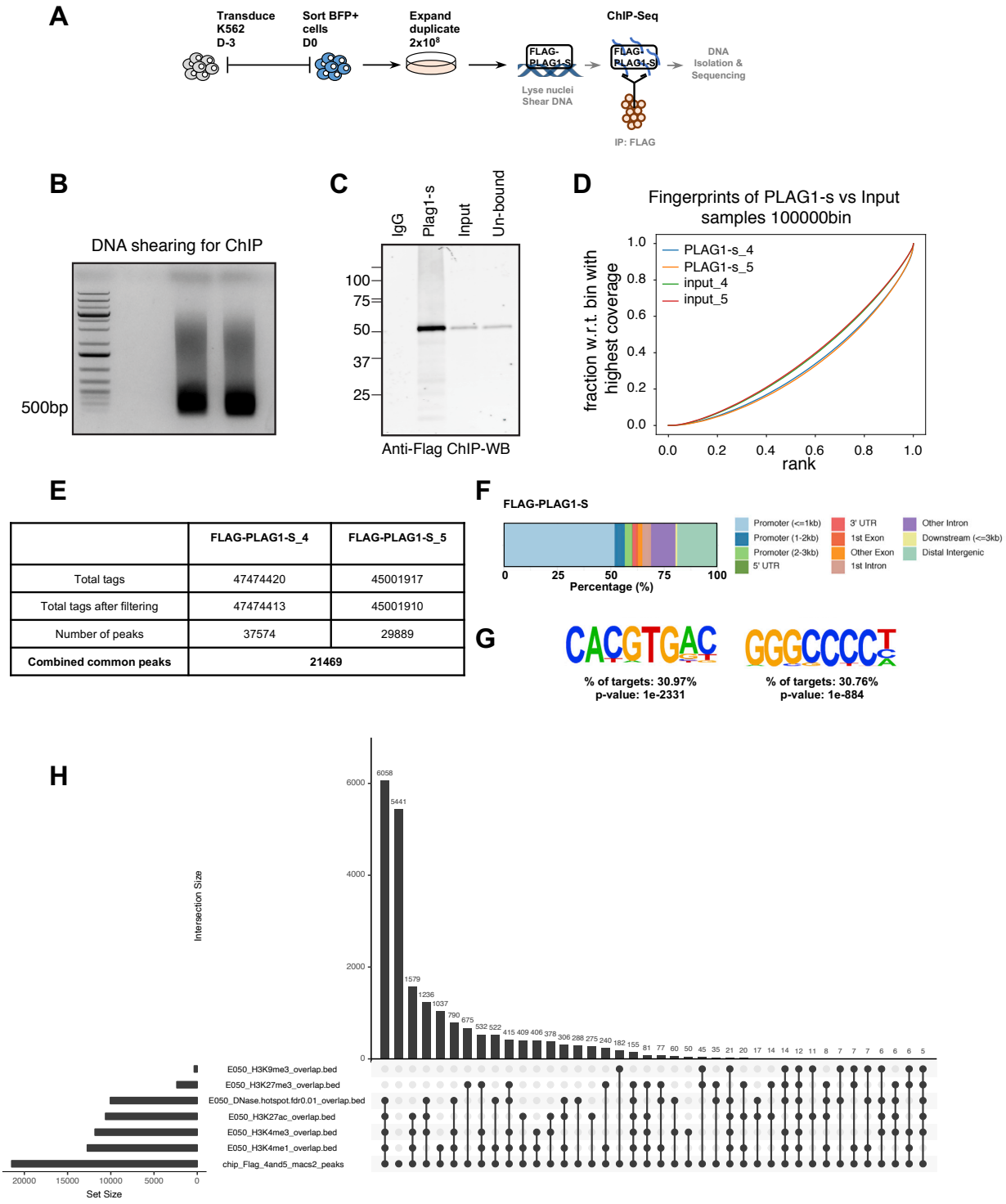

	FLAG-PLAG1-S_4	FLAG-PLAG1-S_5
Total tags	47474420	45001917
Total tags after filtering	47474413	45001910
Number of peaks	37574	29889
Combined common peaks	**21469**	

Figure 12: FLAG-PLAG1-S Chromatin Immunoprecipitation Sequencing in K562 cells. (A) Schematic of FLAG-PLAG1-S ChIP-seq performed in K562 cells. **(B)** Shearing profiles of the chromatin that was immunoprecipitated for ChIP-seq experiments. **(C)** ChIP-western blot profiles to assess the efficiency of antigen pull down prior to sequencing by anti-FLAG antibody. **(D)** Fingerprint plots showing the sequencing read coverage distribution across 100,000 randomly selected genomic bins for inputs as well as FLAG-PLAG1-S ChIP. **(E)** Summary of peak calling for individual replicates of K562 overexpressing FLAG-PLAG1-S (clones #4 and #5). Peaks that were common to the two replicates (combined common peaks) were used for all downstream analysis. **(F)** Peak distribution profiles of all combined common PLAG1-S ChIP peaks. **(G)** *De novo* motif discovery analysis of the PLAG1-S ChIP peaks. Top two most significantly enriched motifs identified by HOMER are shown. **(H)** Overlap between PLAG1-S ChIP-seq peaks from K562 and publicly available Epigenetic marks (H3K4me3: Active promoter, H3K4me1: Enhancer, H3K27Ac: Enhancer, H3K9me3: Repressive promoter, H3K27me3: Repressive promoter) from $CD34^{+}$ cells showing binary peak comparisons. Each bar represents the intersection highlighted below with filled circles and connecting lines. The numbers on top of each bar represent the number of intersecting sites. FLAG-PLAG1-SChIP was used as the baseline.

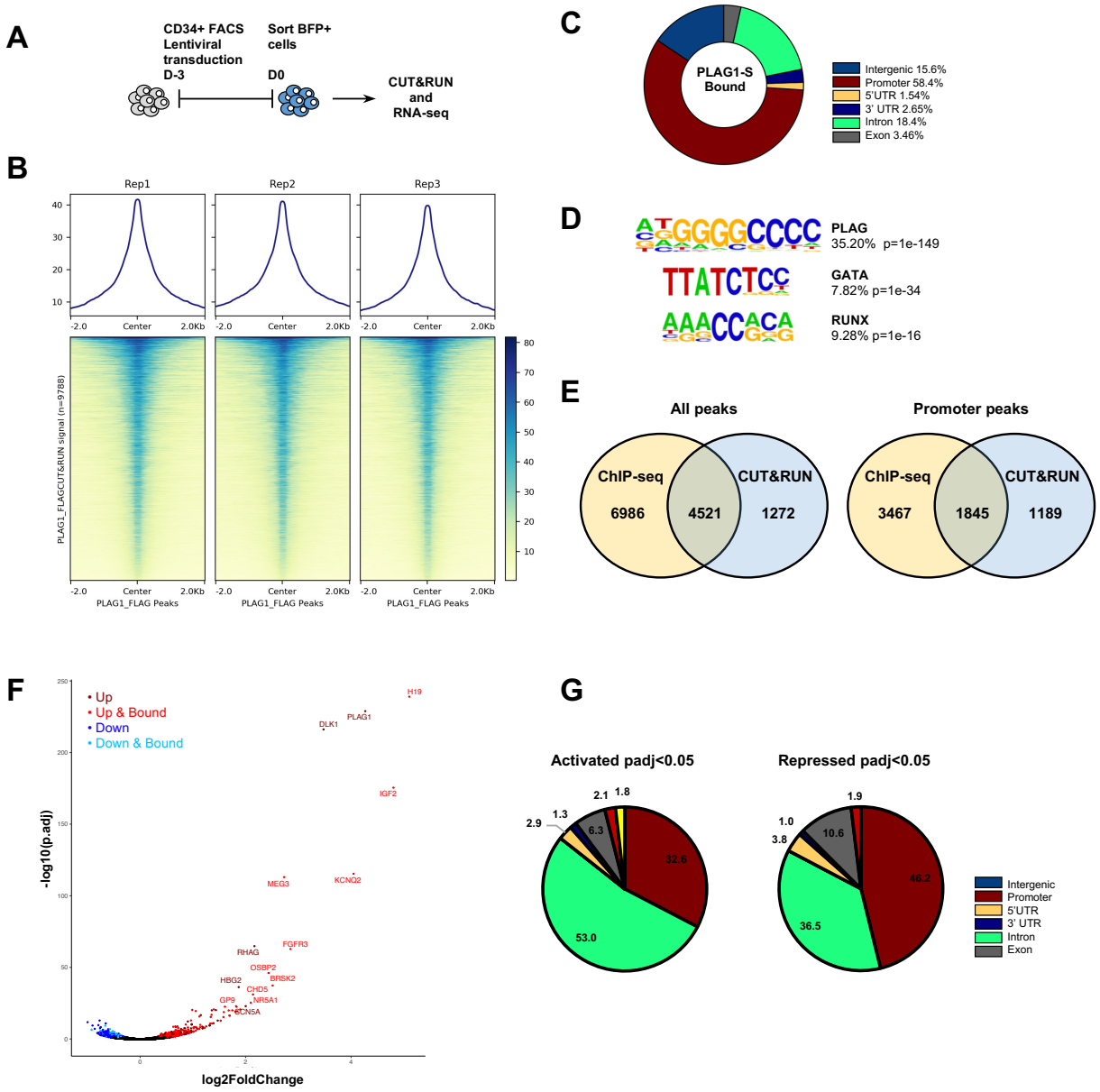
A
CD34+ FACS
Lentiviral
transduction
D-3
Sort BFP+
cells
D0
CUT&RUN
and
RNA-seq
B
Rep1
Rep2
Rep3
PLAG1_FLAGCUT&RUN signal (n=9788)
PLAG1_FLAG Peaks
C
PLAG1-S
Bound
Intergenic 15.6%
Promoter 58.4%
5'UTR 1.54%
3' UTR 2.65%
Intron 18.4%
Exon 3.46%
D
PLAG
35.20% p=1e-149
GATA
7.82% p=1e-34
RUNX
9.28% p=1e-16
E
All peaks
ChIP-seq
6986
4521
CUT&RUN
1272
Promoter peaks
ChIP-seq
3467
1845
CUT&RUN
1189
F
• Up
• Up & Bound
• Down
• Down & Bound
-log10(p.adj)
log2FoldChange
H19
PLAG1
DLK1
IGF2
MEG3
KCNQ2
FGFR3
RHAG
OSBP2
HBG2
BRSK2
CHD5
GP9
NR5A1
KCNA5
G
Activated padj<0.05
Repressed padj<0.05
Intergenic
Promoter
5'UTR
3' UTR
Intron
Exon

Figure 13: FLAG-PLAG1-S CUT&RUN and RNA-seq in human Lin$^-$CD34$^+$ HSPCs. (A) Schematic of FLAG-PLAG1-S CUT&RUN performed in CB Lin$^-$CD34$^+$ cells. **(B)** Heatmap of PLAG1-S binding sites identified by CUT&RUN. **(C)** Loci annotations and distribution of PLAG1-S binding sites in the Lin$^-$CD34$^+$ genome identified by CUT&RUN. **(D)** Enriched motifs among PLAG1-S genomic binding sites determined by HOMER indicating the % of PLAG1-S targets bound to the consensus and p-value of the enrichment relative to genome-wide background occurrence of the consensus. **(E)** Comparison of gene coverage between PLAG1-S ChIP seq done in K562 and PLAG1-S CUT&RUN done in CD34$^+$ cells. **(F)** Volcano plot of differential gene expression in PLAG1-S overexpressing Lin$^-$CD34$^+$ cells. Red- or blue-coloured genes are significantly changed by adjusted p value$<$ 0.05 and shaded dark or light based on PLAG1-S binding status. **(G)** Loci annotations and distribution of PLAG1-S binding sites on differentially expressed genes in the Lin$^-$CD34$^+$

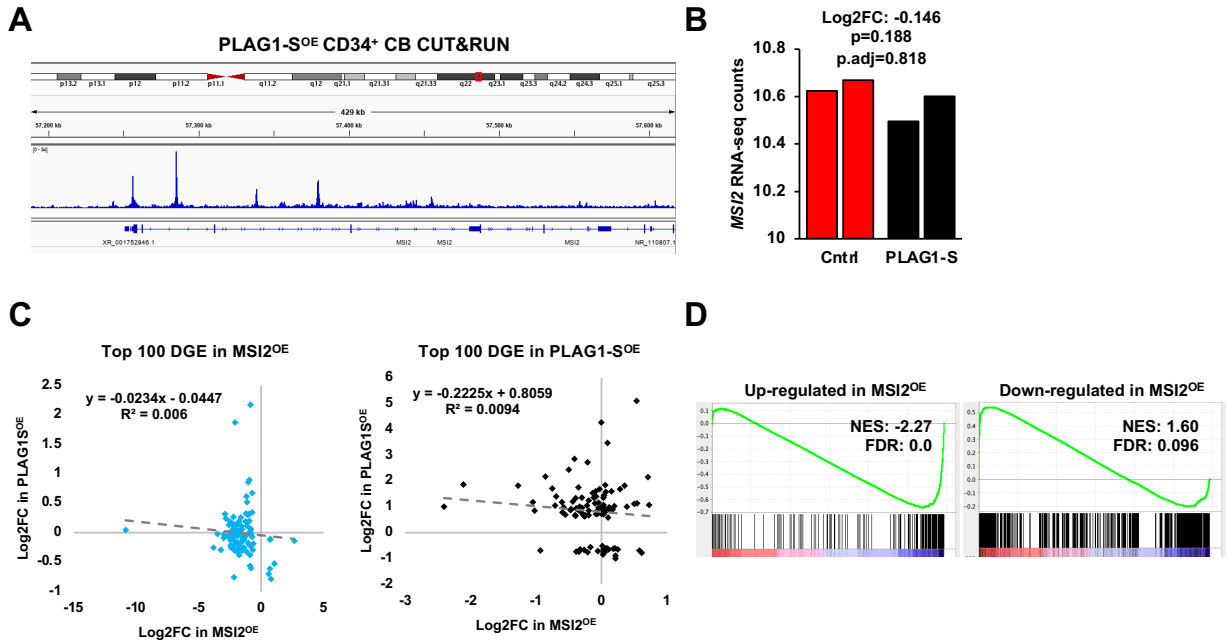
A
PLAG1-S^{OE} CD34^{+} CB CUT&RUN
B
Log2FC: -0.146
p=0.188
p.adj=0.818
MSI2 RNA-seq counts
Cntrl
PLAG1-S
C
Top 100 DGE in MSI2^{OE}
y = -0.0234x - 0.0447
R² = 0.006
Log2FC in PLAG1S^{OE}
Log2FC in MSI2^{OE}
Top 100 DGE in PLAG1-S^{OE}
y = -0.2225x + 0.8059
R² = 0.0094
Log2FC in PLAG1S^{OE}
Log2FC in MSI2^{OE}
D
Up-regulated in MSI2^{OE}
NES: -2.27
FDR: 0.0
Down-regulated in MSI2^{OE}
NES: 1.60
FDR: 0.096

Figure 14: PLAG1-S overexpression in Lin$^-$CD34$^+$ cells bypasses MSI2 pro-stem programs. **(A)** PLAG1-S is genomically bound to MSI2 in Lin$^-$CD34$^+$ cells. **(B)** Ectopic PLAG1-S does not alone activate MSI2 transcript expression in Lin$^-$CD34$^+$ HSPCs. **(C,D)** There is no correlation between differential gene expression in PLAG1-S^{OE} and MSI2^{OE} CB.

A

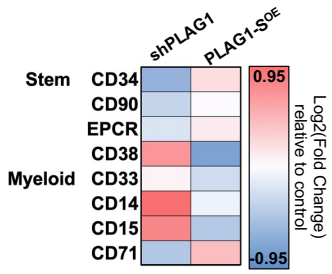

B

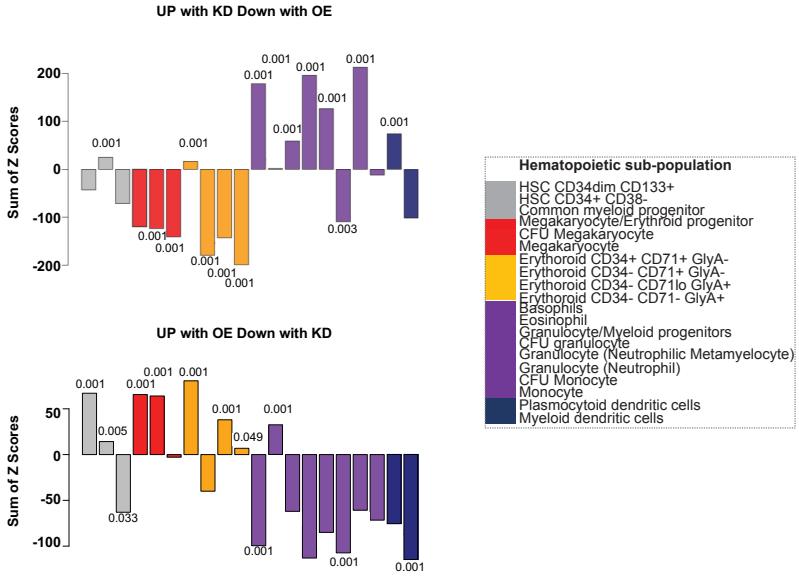

C

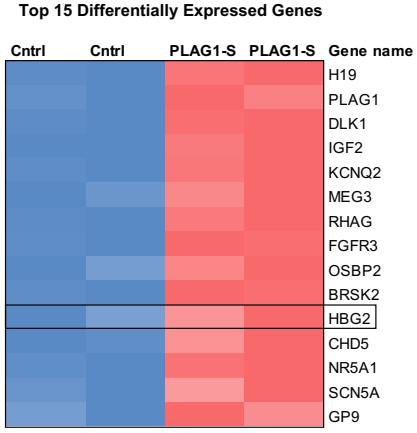

D

	Gene	CUT&RUN peaks	ChIP-seq Peaks	Log2FC	adj p-value
Fetal and Adult Hemoglobin	**HBA1-Hemoglobin alpha 1**	Promoter	N/A	1.00	7.91 e-06
	HBA2-Hemoglobin alpha 2	NA	Promoter	0.74	0.002
Fetal Hemoglobin	**HBG1-Hemoglobin gamma 1**	NA	NA	0.25	0.5096
	HBG2-Hemoglobin gamma 2	NA	Promoter Intergenic	1.87	5.84 e-37
Embryonic Hemoglobin	**HBZ-Hemoglobin zeta**	NA	Promoter Intron TTS	1.18	2.22 e-09
	HBE1-Hemoglobin epsilon 1	NA	N/A	0.70	0.00049
Core Erythroid Transcription Factors	**GATA1**	Intergenic Intergenic Promoter Intron Intron	Intergenic	0.57	0.0004
	KLF1	Intron	Exon Promoter Promoter	0.67	4.83 e-07
	TAL1	Promoter	Promoter Exon	0.14	0.906

Figure 15: PLAG1-S enforces stem and erythroid signatures in human HSPCs. (A) Heatmap of Log2 expression fold change for common stem and progenitor markers in PLAG1-SOE and shPLAG1 HSPCs relative to their respective controls. **(B)** PLAG1-S overexpression and shPLAG1 transcriptomic alignment to DMAP signatures of hematopoietic compartments[248]. Numbers above or below the bars indicate the empirical p value determined based on the percentage of times for which the observed value (set of up- or down-regulated genes) was as large or larger in that population than random values (equal number of randomly selected genes) based on 1,000 trials. **(C)** Top differentially expressed genes in PLAG1-S^{OE} $Lin^{-}CD34^{+}$ cells includes activation of *HBG2*. **(D)** Regulation of erythroid and hemoglobin genes by PLAG1-S in $Lin^{-}CD34^{+}$ cells.

A

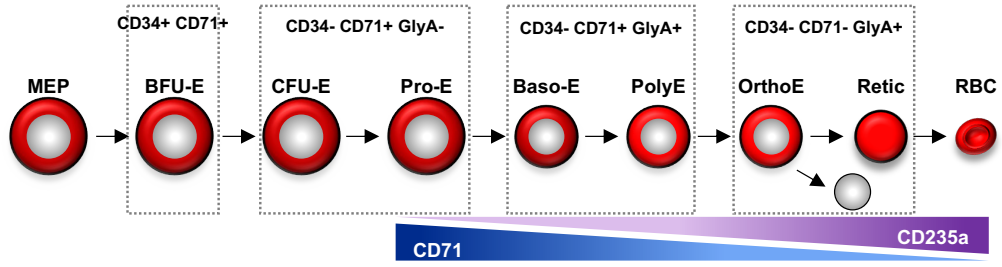

B

1 2 3 4	5 6 7 8 9	10 11 12 13	14 15 16 17 18 19 20 21 22
<HSPC Expansion> (4 days) • StemSpan SFEM medium • 1X cytokine mix (TPO, Flt-3 ligand, SCF, IL-6)	**<Differentiation I>** (5 days) • IMDM • 15% FBS • 2mM glutamine • 1% BSA • holo human transferrin: 500 μg/mL • rh insulin: 10 μg/mL • Dexamethasone: 1 μM • β-estradiol: 1 μM • IL-3: 5 ng/mL • SCF 100 ng/mL • Epo 6U	**<Differentiation II>** (4 days) • IMDM • 15% FBS • 2mM glutamine • 1% BSA • holo human transferrin: 500 μg/mL • rh insulin: 10 μg/mL • SCF 50 ng/mL • Epo 6U	**<Differentiation III>** (8 days) • IMDM • 15% FBS • 2mM glutamine • 1% BSA • holo human transferrin: 500 μg/mL • rh insulin: 10 μg/mL • Epo 2U ★ Fibronectin plates

Figure 16: Human Erythropoiesis. (A) Schematic of late stages of erythroid specification with key markers used for experimentation indicated above populations[293]. **(B)** Summary of culture system used to model erythroid differentiation in vitro[294].

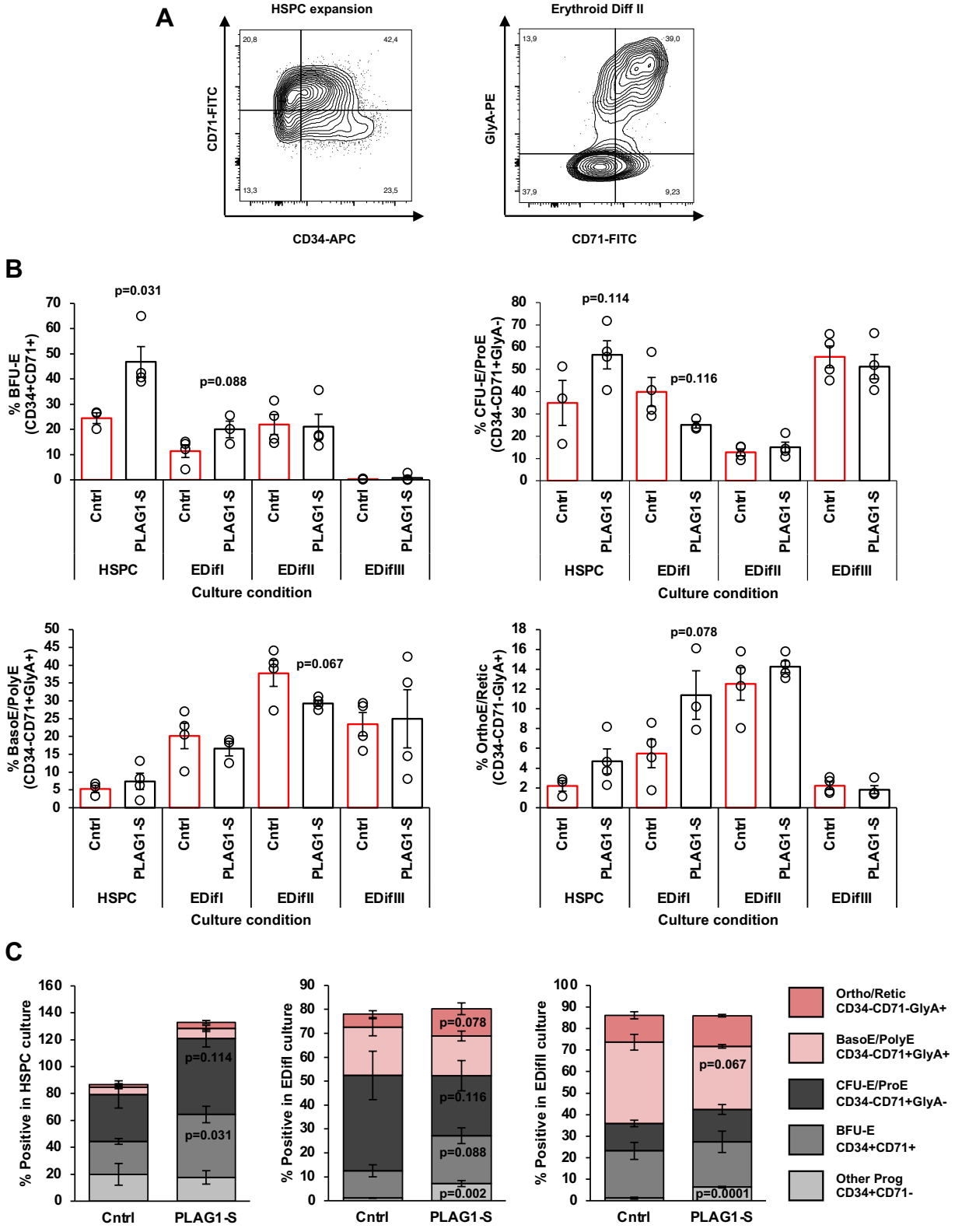
A
HSPC expansion
Erythroid Diff II
CD71-FITC
CD34-APC
GlyA-PE
CD71-FITC
B
% BFU-E (CD34+CD71+)
% CFU-E/ProE (CD34-CD71+GlyA-)
% BasoE/PolyE (CD34-CD71+GlyA+)
% OrthoE/Retic (CD34-CD71-GlyA+)
p=0.031
p=0.088
p=0.114
p=0.116
p=0.067
p=0.078
Cntrl
PLAG1-S
HSPC
EDifI
EDifII
EDifIII
Culture condition
C
% Positive in HSPC culture
% Positive in EDifI culture
% Positive in EDifII culture
Ortho/Retic CD34-CD71-GlyA+
BasoE/PolyE CD34-CD71+GlyA+
CFU-E/ProE CD34-CD71+GlyA-
BFU-E CD34+CD71+
Other Prog CD34+CD71-

Figure 17: PLAG1-S enforces primitiveness in erythroid-driving culture without differentiation block. (A) Representative flow plots for monitoring stem and erythroid markers in culture. **(B,C)** Frequency of BFU-E, CFU-E/ProE, Baso-E/Poly-E and OrthoE/Retic progenitors in PLAG1-S^{OE} and control cultures pushed through a 3-step erythroid differentiation culture from Figure 16B.

Data is presented as average +/- SEM unless otherwise indicated. Each point represents an individual CB unit. *** $p<0.005$, ** $p<0.01$, * $p<0.05$.

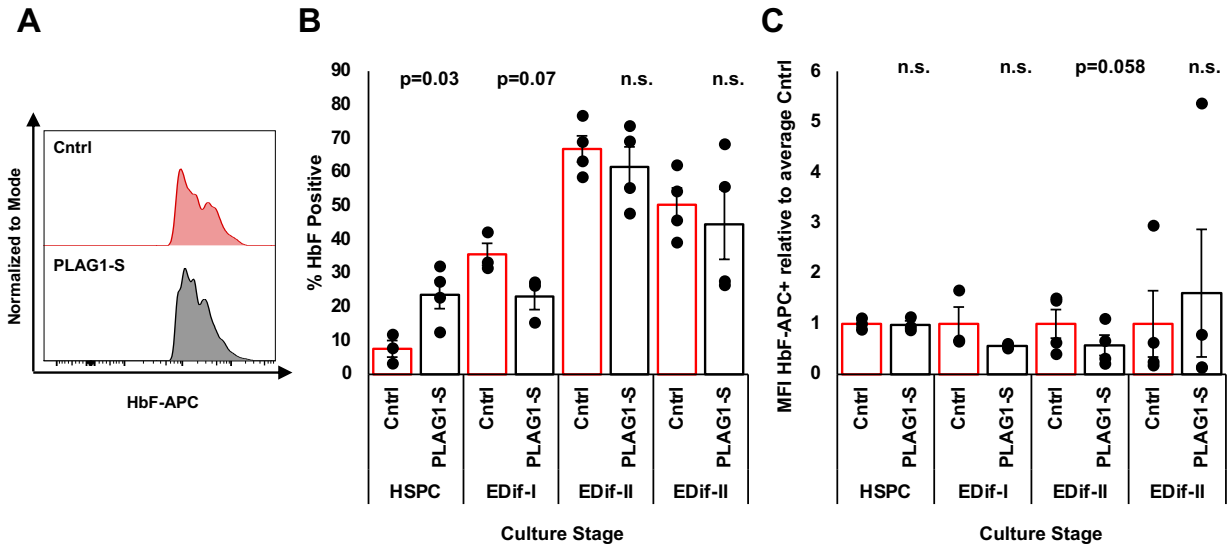
A
Cntrl
PLAG1-S
Normalized to Mode
HbF-APC
B
% HbF Positive
p=0.03
p=0.07
n.s.
n.s.
Cntrl
PLAG1-S
HSPC
EDif-I
EDif-II
EDif-II
Culture Stage
C
MFI HbF-APC+ relative to average Cntrl
n.s.
n.s.
p=0.058
n.s.
Culture Stage

Figure 18: PLAG1-S overexpression does not influence fetal hemoglobin expression. **(A)** Representative flow plots for fetal hemoglobin staining. **(B)** Percent of cells positive for fetal hemoglobin in HSPC-maintaining and erythroid-differentiating cultures. **(C)** Median fluorescence intensity of fetal hemoglobin staining in positive cells.

Data is presented as average +/- SEM unless otherwise indicated. Each point represents an individual CB unit. *** $p<0.005$, ** $p<0.01$, * $p<0.05$.

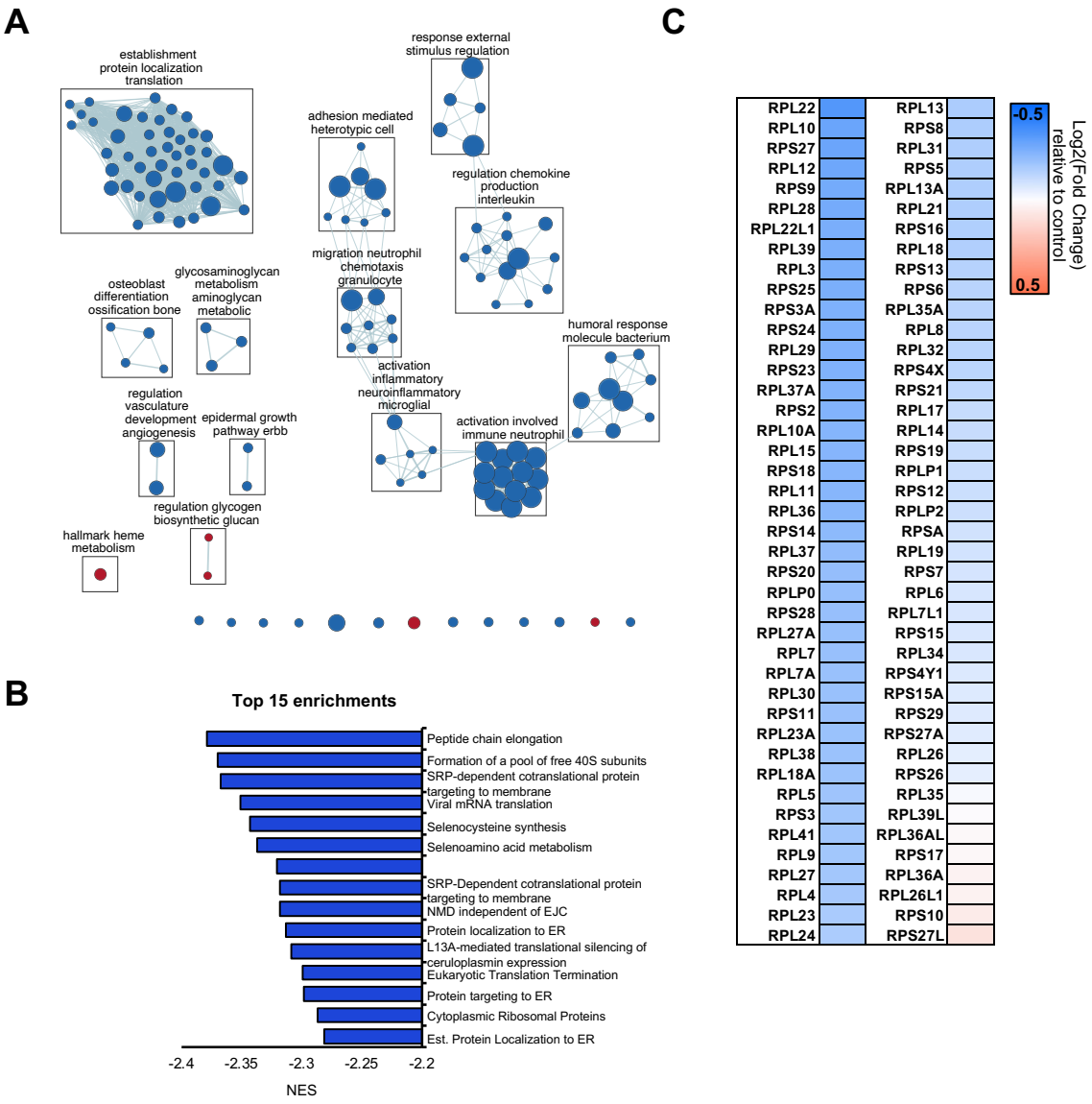
A
establishment protein localization translation
response external stimulus regulation
adhesion mediated heterotypic cell
regulation chemokine production interleukin
migration neutrophil chemotaxis granulocyte
osteoblast differentiation ossification bone
glycosaminoglycan metabolism aminoglycan metabolic
humoral response molecule bacterium
activation inflammatory neuroinflammatory microglial
regulation vasculature development angiogenesis
epidermal growth pathway erbb
activation involved immune neutrophil
regulation glycogen biosynthetic glucan
hallmark heme metabolism
B
Top 15 enrichments
Peptide chain elongation
Formation of a pool of free 40S subunits
SRP-dependent cotranslational protein targeting to membrane
Viral mRNA translation
Selenocysteine synthesis
Selenoamino acid metabolism
SRP-Dependent cotranslational protein targeting to membrane
NMD independent of EJC
Protein localization to ER
L13A-mediated translational silencing of ceruloplasmin expression
Eukaryotic Translation Termination
Protein targeting to ER
Cytoplasmic Ribosomal Proteins
Est. Protein Localization to ER
-2.4
-2.35
-2.3
-2.25
-2.2
NES
C
RPL22
RPL10
RPS27
RPL12
RPS9
RPL28
RPL22L1
RPL39
RPL3
RPS25
RPS3A
RPS24
RPL29
RPS23
RPL37A
RPS2
RPL10A
RPL15
RPS18
RPL11
RPL36
RPS14
RPL37
RPS20
RPLP0
RPS28
RPL27A
RPL7
RPL7A
RPL30
RPS11
RPL23A
RPL38
RPL18A
RPL5
RPS3
RPL41
RPL9
RPL27
RPL4
RPL23
RPL24
RPL13
RPS8
RPL31
RPS5
RPL13A
RPL21
RPS16
RPL18
RPS13
RPS6
RPL35A
RPL8
RPL32
RPS4X
RPS21
RPL17
RPL14
RPS19
RPLP1
RPS12
RPLP2
RPSA
RPL19
RPS7
RPL6
RPL7L1
RPS15
RPL34
RPS4Y1
RPS15A
RPS29
RPS27A
RPL26
RPS26
RPL35
RPL39L
RPL36AL
RPS17
RPL36A
RPL26L1
RPS10
RPS27L
-0.5
0.5
Log2(Fold Change) relative to control

Figure 19: PLAG1-S enforces a pro-HSC transcriptional state. (A) Enrichment map of significantly enriched gene sets (FDR<0.1) in PLAG1-S^{OE} Lin^-CD34^+ cells compared to control. **(B)** Normalized enrichment scores of the top 15 lowest-FDR gene sets in the PLAG1-S overexpression transcriptome. **(C)** Heatmap of Log2 expression fold change of ribosome protein coding genes in PLAG1-S^{OE} Lin^-CD34^+ cells relative to control, which are collectively reduced 9.7%+/-5.7% and the top twenty-five are reproducibly repressed ($p<0.05$) on average 15.7+/-1.8%.

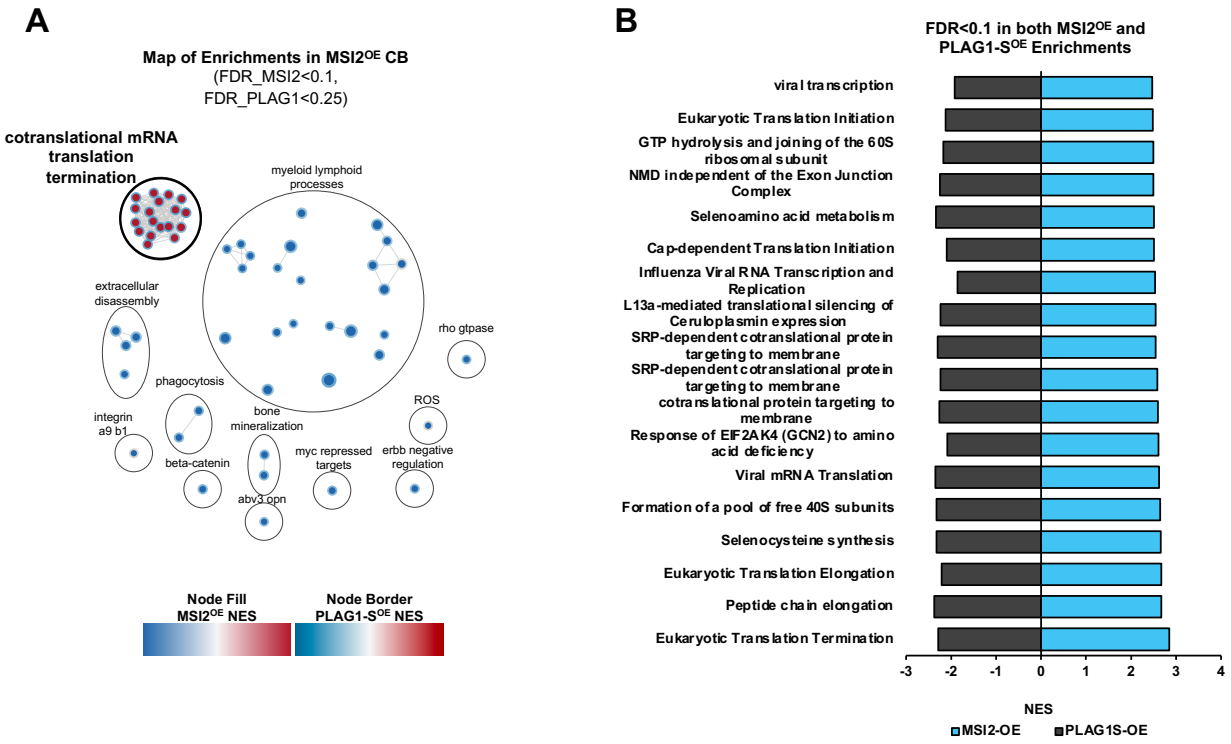
A
Map of Enrichments in MSI2OE CB
(FDR_MSI2<0.1,
FDR_PLAG1<0.25)
cotranslational mRNA translation termination
myeloid lymphoid processes
extracellular disassembly
rho gtpase
phagocytosis
bone mineralization
ROS
integrin a9 b1
beta-catenin
myc repressed targets
erbb negative regulation
abv3 opn
Node Fill MSI2OE NES
Node Border PLAG1-SOE NES
B
FDR<0.1 in both MSI2OE and PLAG1-SOE Enrichments
viral transcription
Eukaryotic Translation Initiation
GTP hydrolysis and joining of the 60S ribosomal subunit
NMD independent of the Exon Junction Complex
Selenoamino acid metabolism
Cap-dependent Translation Initiation
Influenza Viral RNA Transcription and Replication
L13a-mediated translational silencing of Ceruloplasmin expression
SRP-dependent cotranslational protein targeting to membrane
SRP-dependent cotranslational protein targeting to membrane
cotranslational protein targeting to membrane
Response of EIF2AK4 (GCN2) to amino acid deficiency
Viral mRNA Translation
Formation of a pool of free 40S subunits
Selenocysteine synthesis
Eukaryotic Translation Elongation
Peptide chain elongation
Eukaryotic Translation Termination
-3
-2
-1
0
1
2
3
4
NES
MSI2-OE
PLAG1S-OE

Figure 20: Dichotomous regulation of protein biosynthetic processes by PLAG1-S and MSI2 in human HSPCs. (A) Gene set enrichment mapping for $MSI2^{OE}$ CB HSPCs (FDR<0.1) with borders corresponding to normalized enrichment score (NES) from $PLAG1^{OE}$ CB HSPCs. **(B)** Normalized enrichment scores for significantly (FDR<0.1) enriched gene sets in both PLAG1-S^{OE} and $MSI2^{OE}$ HSPCs, showing signatures of translation regulation specifically is discordantly regulated.

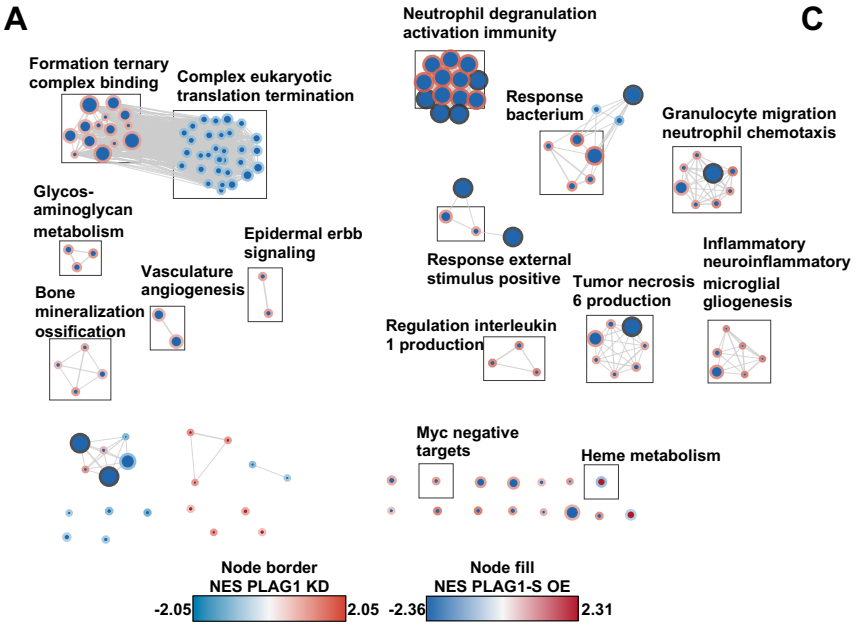

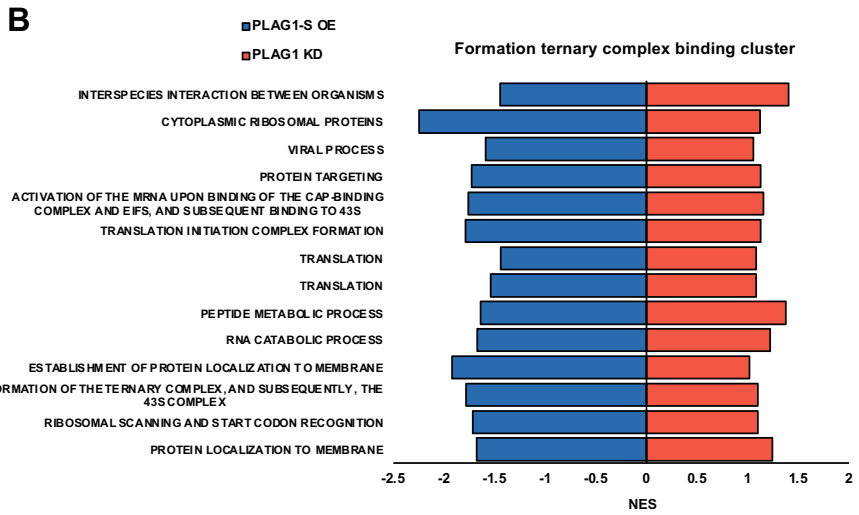

C

Formation ternary complex binding cluster

Shared leading edge		
AGRN	GFI1	**RPL10**
ANPEP	GGA2	**RPL10A**
AP1B1	GPX1	**RPL13**
AP1S3	GSDMD	**RPL13A**
AP2A2	GSTP1	**RPL15**
AP3D1	HCK	**RPL18**
ARF1	HMGA1	**RPL18A**
ARFRP1	HOMER3	**RPL27A**
ATG16L2	IDH1	**RPL28**
AZU1	INSR	**RPL29**
BACE2	IRF7	**RPL3**
BAG6	ITGAL	**RPL36**
BCS1L	ITGB2	**RPL4**
CAT	ITGB7	**RPL7**
CBL	LAPTM5	**RPL7A**
CCL2	LIN7A	**RPL8**
CCL3	LRSAM1	**RPLP0**
CD24	LYZ	**RPS11**
CD4	MPEG1	**RPS16**
CD81	MVB12A	**RPS19**
CPD	MVB12B	**RPS2**
CPM	NAALADL1	**RPS20**
CPSF4	NCF1	**RPS23**
CTDP1	NCSTN	**RPS28**
CTSG	NKD2	**RPS3**
CXCR4	NOA1	**RPS5**
DCPS	NPC1	**RPS6KA1**
DDOST	NUDT16L1	**RPS9**
DHRS4	NUP210	RRBP1
EDEM1	**PABPC1**	S100A9
EEF1A1	PC	SCARB1
EEF1B2	PCSK5	SEC16A
EEF2	PHB2	SEC61A1
EEFSEC	PIGR	SSR2
EIF3D	PPIB	SSR4
EIF3F	PRAM1	TARS2
EIF3G	RAB11B	TNFRSF1A
EIF4B	RAB31	TPP1
ELANE	RAB32	TTC7A
EMC1	RAB3D	UBA52
EMC10	RNASE2	USF2
ERAP1	RNASE3	VAMP5
FLOT1	RNASET2	YIF1B
		ZDHHC24

Figure 21: Dichotomous regulation of protein biosynthetic processes in PLAG1-S overexpressing and knockdown human HSPCs. (A) Gene set enrichment mapping for PLAG1-S^{OE} CB HSPCs (FDR<0.1) with borders corresponding to normalized enrichment score (NES) from PLAG1^{KD} CB HSPCs. **(B)** NES of discordantly regulated gene sets from "Formation ternary complex binding" cluster. **(C)** Leading edge genes belonging to "Formation ternary complex binding" cluster shared between both PLAG1-S OE and KD datasets.

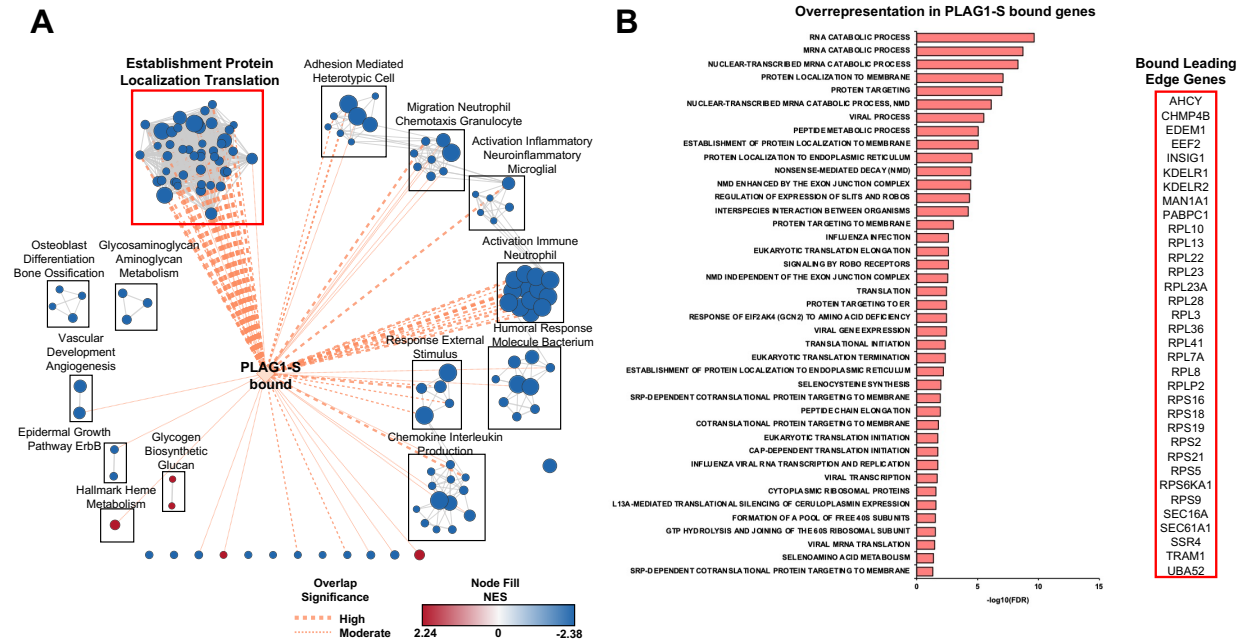
A
Establishment Protein Localization Translation
Adhesion Mediated Heterotypic Cell
Migration Neutrophil Chemotaxis Granulocyte
Activation Inflammatory Neuroinflammatory Microglial
Activation Immune Neutrophil
Humoral Response Molecule Bacterium
Response External Stimulus
Chemokine Interleukin Production
Osteoblast Differentiation Bone Ossification
Glycosaminoglycan Aminoglycan Metabolism
Vascular Development Angiogenesis
Epidermal Growth Pathway ErbB
Glycogen Biosynthetic Glucan
Hallmark Heme Metabolism
PLAG1-S bound
Overlap Significance
High
Moderate
Node Fill NES
2.24
0
-2.38
B
Overrepresentation in PLAG1-S bound genes
RNA CATABOLIC PROCESS
MRNA CATABOLIC PROCESS
NUCLEAR-TRANSCRIBED MRNA CATABOLIC PROCESS
PROTEIN LOCALIZATION TO MEMBRANE
PROTEIN TARGETING
NUCLEAR-TRANSCRIBED MRNA CATABOLIC PROCESS, NMD
VIRAL PROCESS
PEPTIDE METABOLIC PROCESS
ESTABLISHMENT OF PROTEIN LOCALIZATION TO MEMBRANE
PROTEIN LOCALIZATION TO ENDOPLASMIC RETICULUM
NONSENSE-MEDIATED DECAY (NMD)
NMD ENHANCED BY THE EXON JUNCTION COMPLEX
REGULATION OF EXPRESSION OF SLITS AND ROBOS
INTERSPECIES INTERACTION BETWEEN ORGANISMS
PROTEIN TARGETING TO MEMBRANE
INFLUENZA INFECTION
EUKARYOTIC TRANSLATION ELONGATION
SIGNALING BY ROBO RECEPTORS
NMD INDEPENDENT OF THE EXON JUNCTION COMPLEX
TRANSLATION
PROTEIN TARGETING TO ER
RESPONSE OF EIF2AK4 (GCN2) TO AMINO ACID DEFICIENCY
VIRAL GENE EXPRESSION
TRANSLATIONAL INITIATION
EUKARYOTIC TRANSLATION TERMINATION
ESTABLISHMENT OF PROTEIN LOCALIZATION TO ENDOPLASMIC RETICULUM
SELENOCYSTEINE SYNTHESIS
SRP-DEPENDENT COTRANSLATIONAL PROTEIN TARGETING TO MEMBRANE
PEPTIDE CHAIN ELONGATION
COTRANSLATIONAL PROTEIN TARGETING TO MEMBRANE
EUKARYOTIC TRANSLATION INITIATION
CAP-DEPENDENT TRANSLATION INITIATION
INFLUENZA VIRAL RNA TRANSCRIPTION AND REPLICATION
VIRAL TRANSCRIPTION
CYTOPLASMIC RIBOSOMAL PROTEINS
L13A-MEDIATED TRANSLATIONAL SILENCING OF CERULOPLASMIN EXPRESSION
FORMATION OF A POOL OF FREE 40S SUBUNITS
GTP HYDROLYSIS AND JOINING OF THE 60S RIBOSOMAL SUBUNIT
VIRAL MRNA TRANSLATION
SELENOAMINO ACID METABOLISM
SRP-DEPENDENT COTRANSLATIONAL PROTEIN TARGETING TO MEMBRANE
0
5
10
15
-log10(FDR)
Bound Leading Edge Genes
AHCY
CHMP4B
EDEM1
EEF2
INSIG1
KDELR1
KDELR2
MAN1A1
PABPC1
RPL10
RPL13
RPL22
RPL23
RPL23A
RPL28
RPL3
RPL36
RPL41
RPL7A
RPL8
RPLP2
RPS16
RPS18
RPS19
RPS2
RPS21
RPS5
RPS6KA1
RPS9
SEC16A
SEC61A1
SSR4
TRAM1
UBA52

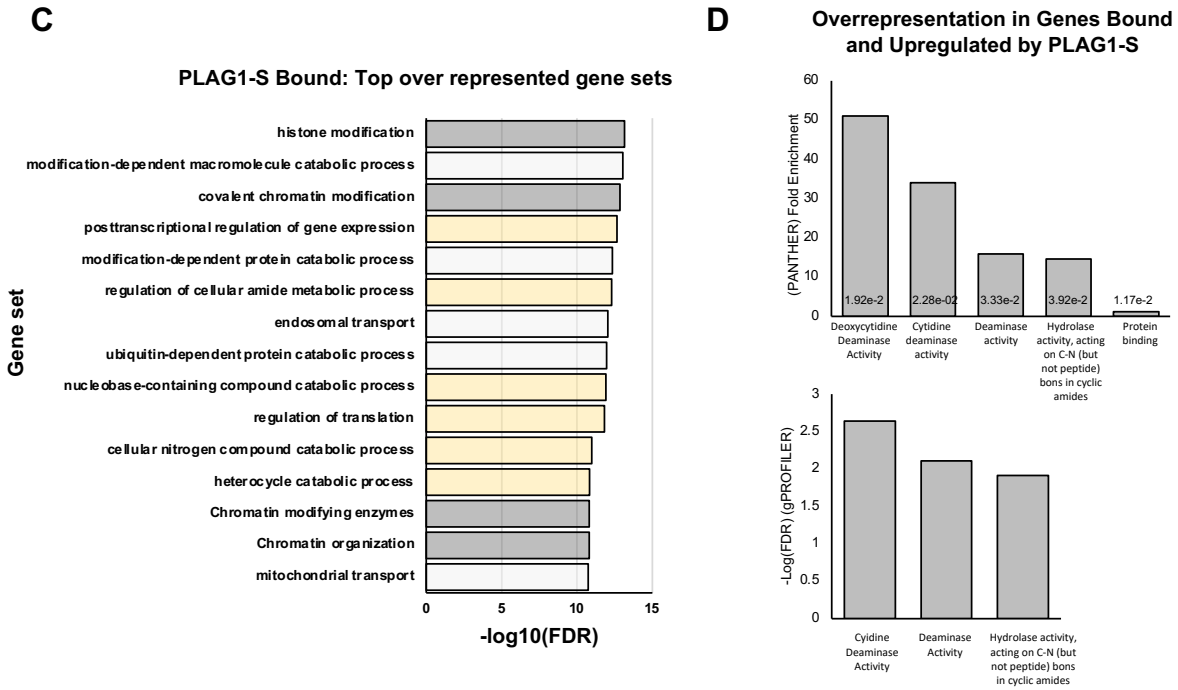
C
PLAG1-S Bound: Top over represented gene sets
Gene set
histone modification
modification-dependent macromolecule catabolic process
covalent chromatin modification
posttranscriptional regulation of gene expression
modification-dependent protein catabolic process
regulation of cellular amide metabolic process
endosomal transport
ubiquitin-dependent protein catabolic process
nucleobase-containing compound catabolic process
regulation of translation
cellular nitrogen compound catabolic process
heterocycle catabolic process
Chromatin modifying enzymes
Chromatin organization
mitochondrial transport
0
5
10
15
-log10(FDR)
D
Overrepresentation in Genes Bound and Upregulated by PLAG1-S
(PANTHER) Fold Enrichment
60
50
40
30
20
10
0
1.92e-2
2.28e-02
3.33e-2
3.92e-2
1.17e-2
Deoxycytidine Deaminase Activity
Cytidine deaminase activity
Deaminase activity
Hydrolase activity, acting on C-N (but not peptide) bons in cyclic amides
Protein binding
-Log(FDR) (gPROFILER)
3
2.5
2
1.5
1
0.5
0
Cyidine Deaminase Activity
Deaminase Activity
Hydrolase activity, acting on C-N (but not peptide) bons in cyclic amides

Figure 22: PLAG1-S enforces a pro-HSC transcriptional state. (A) Enrichment map of significantly enriched gene sets (FDR<0.1) in PLAG1-S^{OE} Lin$^-$CD34$^+$ cells compared to control. Genes bound by PLAG1-S in Lin$^-$CD34$^+$ cells (CUT&RUN q-value cutoff of 0.05) are intersected to gene sets by Mann-Whitney U test ($p<0.05$) and the width of orange edges correlates with increasing statistical significance of the overlap. Node size reflects the number of genes in the gene set. **(B)** 41 out of 46 gene sets from the "Establishment Protein Localization Translation" cluster that are over-represented among PLAG1-S genomic binding sites (g:Profiler FDR <0.1), and the list of bound leading-edge genes driving negative enrichments in this cluster. **(C)** Top ranking pathways based on over-representation FDR of genes proximally bound by PLAG1-S. Grey marks gene sets related to DNA binding/modification, yellow marks gene sets related to translation and white is other. **(D)** Pathway over-representation analysis for the subset of genes bound and activated by overexpressed PLAG1-S.

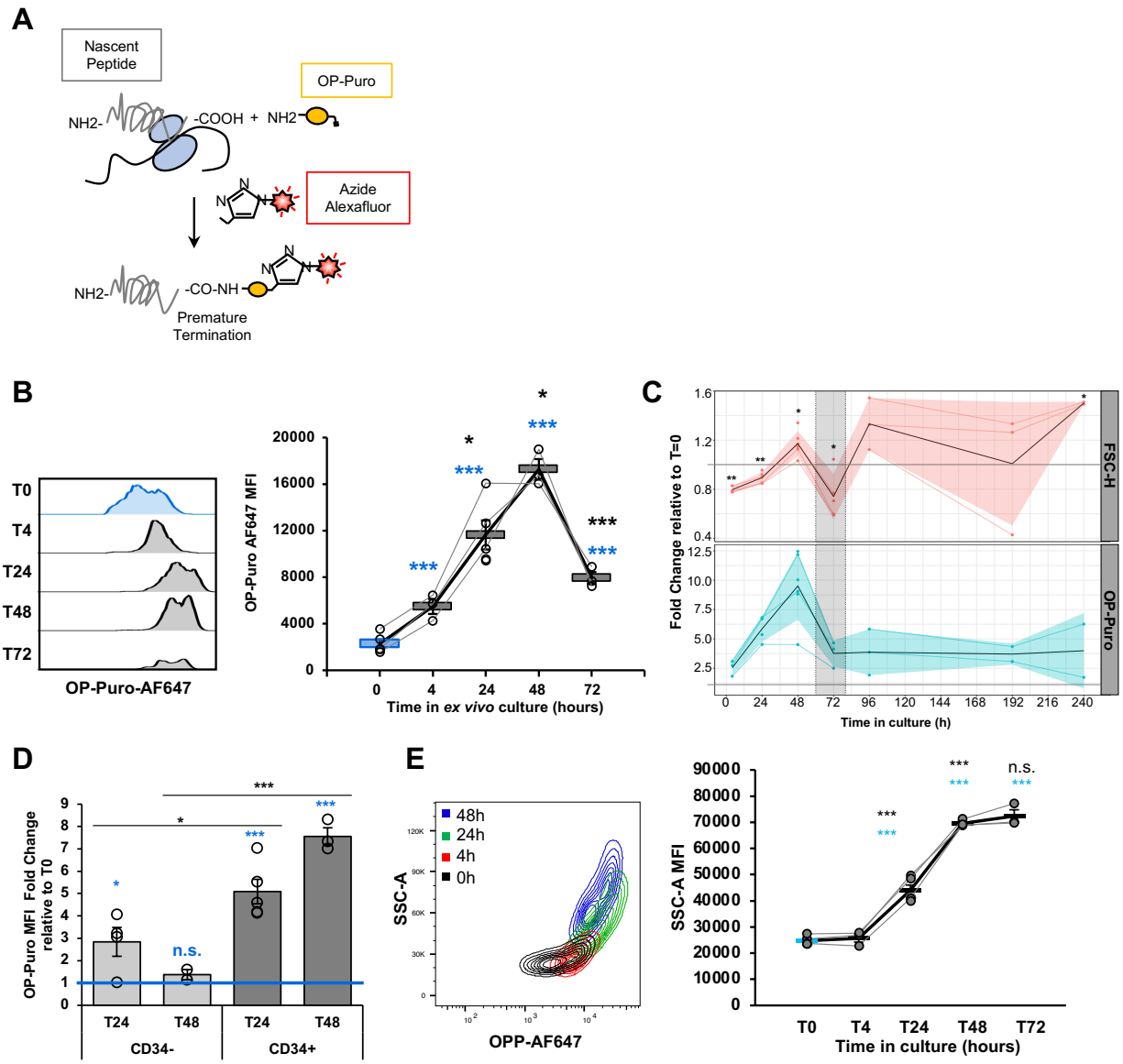
A
Nascent Peptide
OP-Puro
NH2-
-COOH + NH2
Azide Alexafluor
-CO-NH
Premature Termination
B
T0
T4
T24
T48
T72
OP-Puro-AF647
OP-Puro AF647 MFI
Time in ex vivo culture (hours)
C
Fold Change relative to T=0
FSC-H
OP-Puro
Time in culture (h)
D
OP-Puro MFI Fold Change relative to T0
n.s.
CD34-
CD34+
E
48h
24h
4h
0h
SSC-A
OPP-AF647
SSC-A MFI
Time in culture (hours)

Figure 23: Human HSPCs selectively, rapidly and transiently hyperactivate translation in response to culture stimulation. **(A)** Schematic of the OP-Puro incorporation assay to measure global translation rates in single cells by flow cytometry. **(B)** OP-Puro incorporation dynamics measured as median fluorescence intensity (MFI) in cultured $Lin^{-}CD34^{+}$ cells with representative flow cytometry plots (n=5 for 0h and 24h; n=3 for 4h, 48h and 72h). Black and blue asterisks denote statistical significance relative to previous timepoint or T0, respectively. **(C)** Dynamics of OP-Puro incorporation and flow cytometric median fluorescent intensities of FSC-H profiles of cultured $Lin^{-}CD34^{+}$ CB cells relative to when freshly isolated. Time interval shaded in grey denotes the expected timing of first cell division for long-term and short-term HSCs[139]. For FSC-H n= 3, 4, 6, 3, 3, 2, 2 for each timepoint respectively. OP-Puro is showing the same 3-5 CB units used in Figure 24A with additional n=3 for 48 and 96 hours, and n=2 for 192 and 240 hours. **(D)** Fold difference of OP-Puro MFI relative to T0 in cultured $Lin^{-}CD34^{+}$ compared to $Lin^{-}CD34^{-}$ CB fractions (n=4 for 24 hours, n=2 for 48 hours). Blue statistics are relative to 1x levels at T0 and black statistics are between cell types at matched time points. **(E)** Side scatter intensity profiles of Lin-CD34+ cells cultured for 72hours.

Data is presented as average +/- SEM unless otherwise indicated. Each point represents an individual CB unit. *** $p<0.005$, ** $p<0.01$, * $p<0.05$.

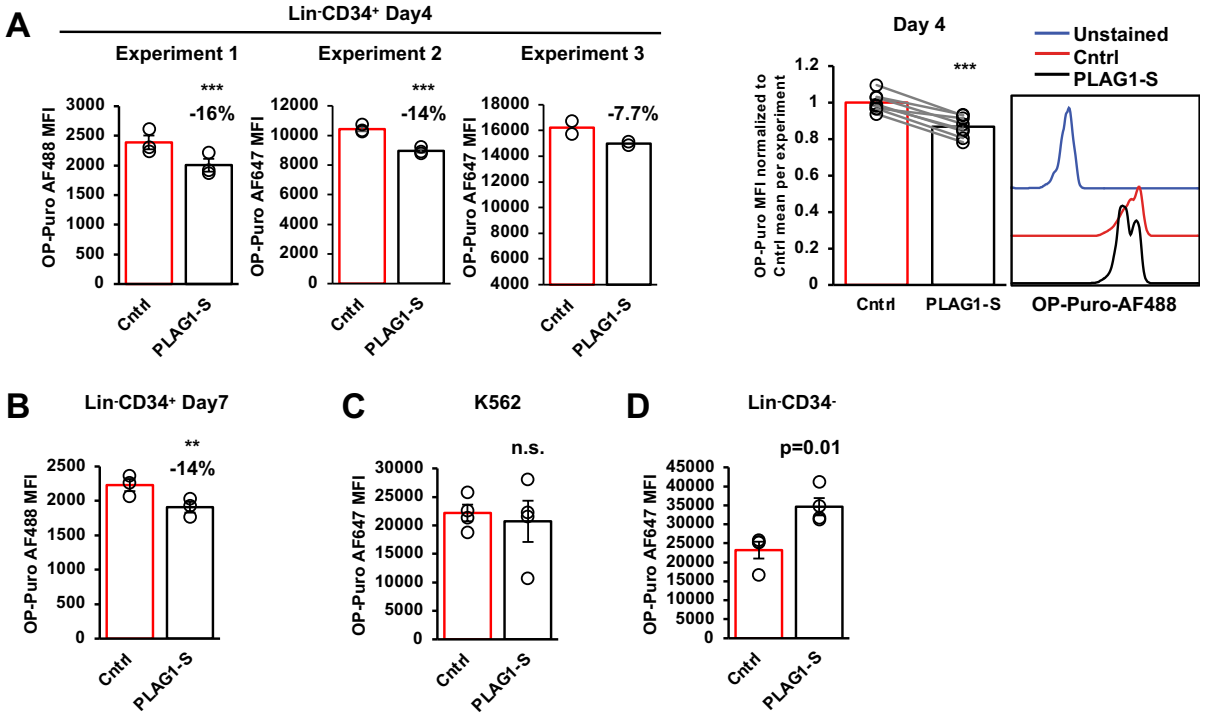
A
Lin-CD34+ Day4
Experiment 1
Experiment 2
Experiment 3
OP-Puro AF488 MFI
OP-Puro AF647 MFI
***
-16%
-14%
-7.7%
Cntrl
PLAG1-S
Day 4
OP-Puro MFI normalized to Cntrl mean per experiment
Unstained
Cntrl
PLAG1-S
OP-Puro-AF488
B
Lin-CD34+ Day7
**
-14%
C
K562
n.s.
D
Lin-CD34-
p=0.01

Figure 24: PLAG1-S overexpression selectively dampens protein synthesis in stimulated human HSPCs. (A) Left: Three independent measures of OP-Puro incorporation by PLAG1-S^{OE} and control Lin-$CD34^+$ cells on day 4 of *ex vivo* culture that were amalgamated and normalized for Figure 5B. (n= 3, 3, 2 for Experiment 1, 2 and 3, respectively). Right: Amalgamated date from three independent experiments of OP-Puro incorporation by PLAG1-S^{OE} and control Lin^-CD34^+ cells on day 4 of *ex vivo* culture (n=8) normalized to the average MFI in control cells per experiment. **(B)** OP-Puro incorporation by PLAG1-S^{OE} and control Lin^-CD34^+ cells on day 7 of *ex vivo* culture (n=3). **(C)** OP-Puro incorporation by K562 and **(D)** Lin^-CD34^- cells overexpressing either PLAG1-S or control (n=4).

Data is presented as average +/- SEM unless otherwise indicated. Each point represents an individual CB unit. *** $p<0.005$, ** $p<0.01$, * $p<0.05$.

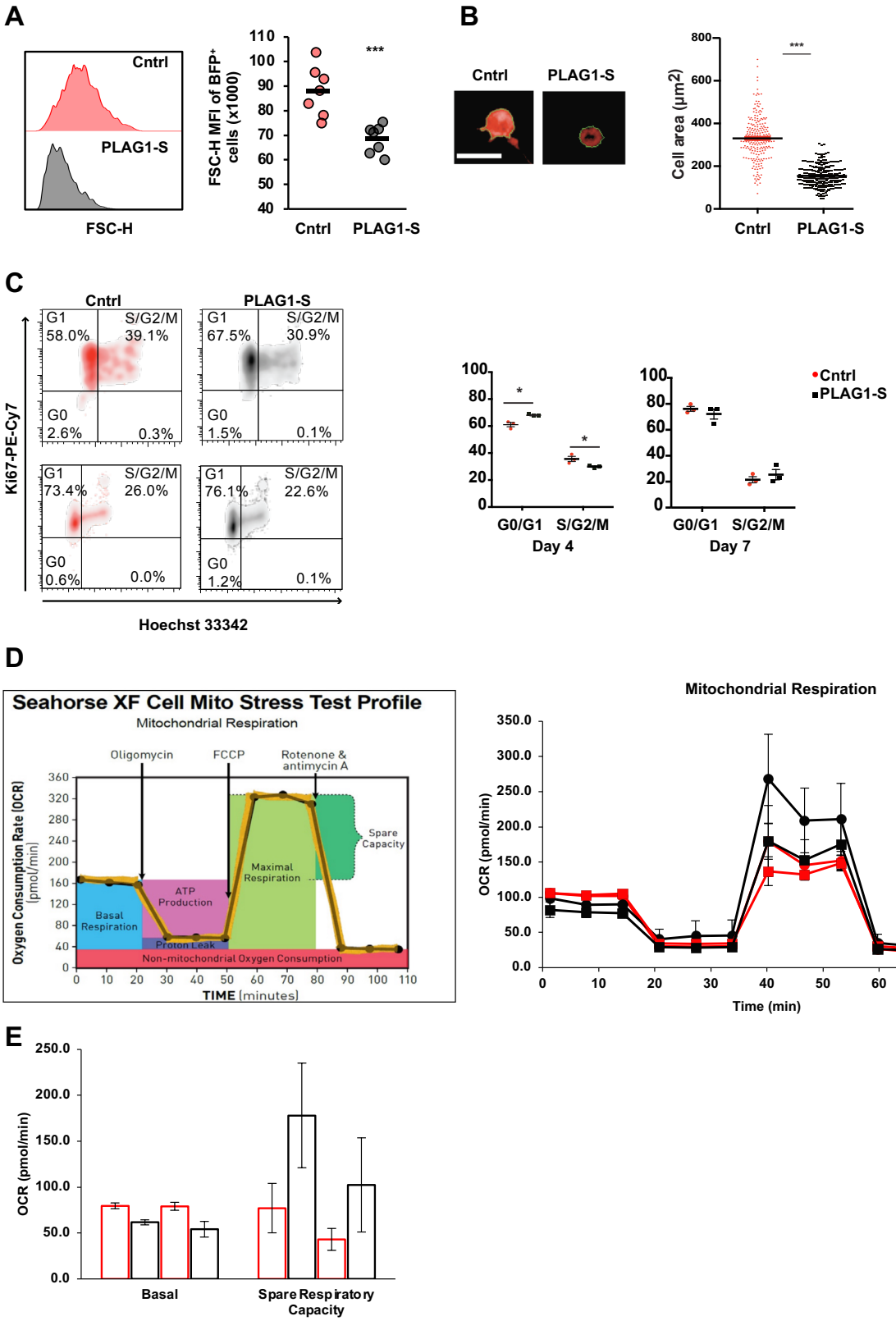
A
Cntrl
PLAG1-S
FSC-H
FSC-H MFI of BFP+ cells (x1000)
***
Cntrl
PLAG1-S
B
Cntrl
PLAG1-S
Cell area (µm2)
***
Cntrl
PLAG1-S
C
Cntrl
PLAG1-S
G1 58.0%
S/G2/M 39.1%
G0 2.6%
0.3%
G1 67.5%
S/G2/M 30.9%
G0 1.5%
0.1%
G1 73.4%
S/G2/M 26.0%
G0 0.6%
0.0%
G1 76.1%
S/G2/M 22.6%
G0 1.2%
0.1%
Ki67-PE-Cy7
Hoechst 33342
G0/G1
S/G2/M
Day 4
Day 7
Cntrl
PLAG1-S
D
Seahorse XF Cell Mito Stress Test Profile
Mitochondrial Respiration
Oligomycin
FCCP
Rotenone & antimycin A
Oxygen Consumption Rate (OCR) (pmol/min)
Basal Respiration
ATP Production
Proton Leak
Maximal Respiration
Spare Capacity
Non-mitochondrial Oxygen Consumption
TIME (minutes)
Mitochondrial Respiration
OCR (pmol/min)
Time (min)
E
OCR (pmol/min)
Basal
Spare Respiratory Capacity

Figure 25: PLAG1-S dampens protein synthesis and promotes dormancy in stimulated human HSPC. (A) Reduced size of PLAG1-S^{OE} Lin^-CD34^+ cells on day 4 of *ex vivo* culture determined by flow cytometric MFI of FSC-H profiles (n=7, top) and **(B)** immunofluorescence microscopy (bottom, each point is a single cell; Scale bar = 25um). **(C)** Representative flow plots and analysis of cell cycle by Hoechst and Ki67 staining of PLAG1-S^{OE} and control Lin^-CD34^+ cells on days 4 and 7 of *ex vivo* culture (n=3). **(D)** Seahorse Mito stress test output and interpretation of plot (left). **(E)** Basal respiration and spare respiratory capacity determined by seahorse Mito stress test (n=2).

Data is presented as average +/- SEM unless otherwise indicated. Each point represents an individual CB unit. *** $p<0.005$, ** $p<0.01$, * $p<0.05$.

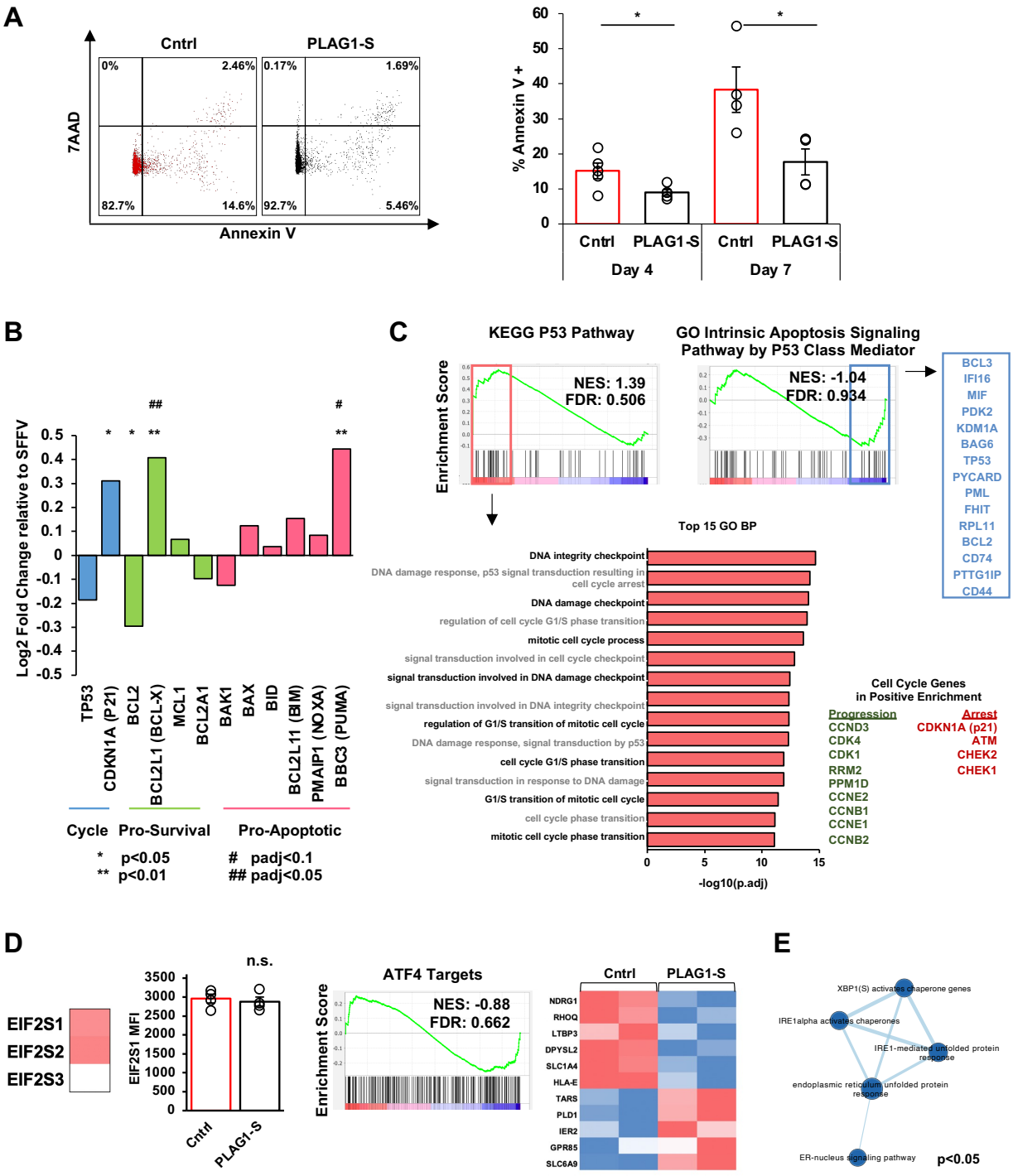
A
Cntrl
PLAG1-S
0%
2.46%
0.17%
1.69%
82.7%
14.6%
92.7%
5.46%
7AAD
Annexin V
% Annexin V +
Cntrl
PLAG1-S
Day 4
Day 7
B
Log2 Fold Change relative to SFFV
TP53
CDKN1A (P21)
BCL2
BCL2L1 (BCL-X)
MCL1
BCL2A1
BAK1
BAX
BID
BCL2L11 (BIM)
PMAIP1 (NOXA)
BBC3 (PUMA)
Cycle
Pro-Survival
Pro-Apoptotic
* p<0.05
** p<0.01
# padj<0.1
padj<0.05
C
KEGG P53 Pathway
NES: 1.39
FDR: 0.506
GO Intrinsic Apoptosis Signaling Pathway by P53 Class Mediator
NES: -1.04
FDR: 0.934
Enrichment Score
BCL3
IFI16
MIF
PDK2
KDM1A
BAG6
TP53
PYCARD
PML
FHIT
RPL11
BCL2
CD74
PTTG1IP
CD44
Top 15 GO BP
DNA integrity checkpoint
DNA damage response, p53 signal transduction resulting in cell cycle arrest
DNA damage checkpoint
regulation of cell cycle G1/S phase transition
mitotic cell cycle process
signal transduction involved in cell cycle checkpoint
signal transduction involved in DNA damage checkpoint
signal transduction involved in DNA integrity checkpoint
regulation of G1/S transition of mitotic cell cycle
DNA damage response, signal transduction by p53
cell cycle G1/S phase transition
signal transduction in response to DNA damage
G1/S transition of mitotic cell cycle
cell cycle phase transition
mitotic cell cycle phase transition
-log10(p.adj)
Cell Cycle Genes in Positive Enrichment
Progression
CCND3
CDK4
CDK1
RRM2
PPM1D
CCNE2
CCNB1
CCNE1
CCNB2
Arrest
CDKN1A (p21)
ATM
CHEK2
CHEK1
D
EIF2S1
EIF2S2
EIF2S3
EIF2S1 MFI
n.s.
Cntrl
PLAG1-S
ATF4 Targets
NES: -0.88
FDR: 0.662
Enrichment Score
Cntrl
PLAG1-S
NDRG1
RHOQ
LTBP3
DPYSL2
SLC1A4
HLA-E
TARS
PLD1
IER2
GPR85
SLC6A9
E
XBP1(S) activates chaperone genes
IRE1alpha activates chaperones
IRE1-mediated unfolded protein response
endoplasmic reticulum unfolded protein response
ER-nucleus signaling pathway
p<0.05

Figure 26: PLAG1-S dampens protein synthesis and promotes dormancy and survival in stimulated human HSPC. (A) Representative flow plots for PLAG1-S^{OE} and control $Lin^{-}CD34^{+}$ cells stained for 7-AAD and Annexin V with apoptosis measurements of surface positivity of Annexin V on day 4 (n=5) and day 7 (n=4) of *ex vivo* culture. **(B)** Expression of p53 targets in the transcriptome of PLAG1-S^{OE} HSPCs. **(C)** GSEA of p53 targets in the transcriptome of PLAG1-S^{OE} HSPCs showing overall nonsignificant changes where positively expressed transcripts are involved in mixed regulation of cell cycle and negatively expressed genes are involved in apoptosis. **(D)** Heatmap of log2FC of transcripts coding EIF2 subunits (left) and intracellular flow cytometric measures of EIF2S1 protein expression (n=4) in PLAG1-S^{OE} relative to control $Lin^{-}CD34^{+}$ cells on day 4 of *ex vivo* culture (right). **(E)** GSEA of the PLAG1-S^{OE} transcriptome to curated targets of ATF4 generated by Han et al. (2012)[274] and used by Van Galen et al. (2018)[171] and FPKM heatmap of ATF4 targets differentially expressed in PLAG1-S^{OE} HSPC (p.adj<0.1). **(F)** Negative enrichment of gene sets related to unfolded protein response (p<0.05).

Data is presented as average +/- SEM unless otherwise indicated. Each point represents an individual CB unit. *** p<0.005, ** p<0.01, * p<0.05.

CHAPTER 5

Molecular mechanisms downstream of PLAG1 in human HSPCs

5.1 MYC-induced translation impairs PLAG1-S-mediated stemness in human HSPC.

MYC is one of the best-known master regulators of mammalian protein synthesis. As a potent tissue non-specific regulator of protein production, MYC promotes multiple steps of ribosome biogenesis, including transactivation of ribosome protein gene expression, ribosomal RNA expression, and expression of many auxiliary factors involved in nuclear and cytosolic ribosome assembly[295]. In the murine context Myc deletion impairs hematopoietic differentiation[296-298], and Myc expression is concomitantly activated with translation machinery when murine HSC exit dormancy[148]. Recent findings in cultured human HSPCs also establish that MYC drives their *ex vivo* activation via promotion of anabolic programs[152]. Interestingly however, the direct link between MYC-induced activation of translation and HSC activation and impaired long-term function has yet to be demonstrated. Therefore, we next investigated firstly whether PLAG1-S acts through repression of MYC, and secondly whether MYC-mediated activation of translation could influence the ability of PLAG1-S to promote stemness.

In PLAG1-S^{OE} HSPCs MYC transcripts are modestly repressed (**Figure 27A**) however protein levels determined by ICF are not significantly reduced (**Figure 27B**). c-MYC activity is also tightly governed by post-translational modifications including phospho-dependent repression at Ser62, which primes for phosphorylation on Thr58 by the AKT substrate GSK3 and promotes MYC turnover[299,300]. However, we do not observe changes in total or phosphorylated GSKB levels, nor in MYC phosphorylation at Ser62 or Thr58 (**Figure 27C**). As expected with no changes in protein regulation the expression of MYC target genes are also not significantly reduced in PLAG1-S^{OE} HSPCs (**Figure 27D**)[296,301]. In fact, in contrast to repression of components of cytosolic ribosomes the class of MYC targets involved in nuclear ribosome assembly trend upwards in their regulation in PLAG1-S^{OE} HSPCs (**Figure 27E**). Therefore, negative RP gene regulation upon PLAG1-S overexpression appears autonomously of a PLAG1-S-MYC repressive signaling axis.

Given that MYC does not appear to be a negative target of PLAG1-S, modulation of its expression could serve as a molecular tool to independently activate translation rates as a means to query the dependency of PLAG1-S-enforced pro-stemness on its attenuation of protein synthesis. In principle if PLAG1-S can rescue HSC activation and differentiation imparted by c-MYC it could be attributed to its negative targeting of the cytosolic ribosome components and not the other anabolism-promoting axes stimulated by c-MYC since PLAG1 does not appear to directly target those programs nor does it directly inhibit c-MYC activity.

Modest overexpression of c-MYC via the PGK promoter endows a 25% increase in OP-Puro incorporation by Lin$^-$CD34$^+$ cells (**Figure 28A,B**). In order to test double PLAG1-S and c-MYC transduced cells we first tested the best experimental approach for double infection of CB. The first experimental approach involves dividing the culture into two infection conditions where one is transduced with both control vectors while the other is transduced with both gene of interest (**GOI**)-expressing vectors and GFP$^+$, BFP$^+$ and GFP$^+$BFP$^+$ cells are isolated for assessment (**Figure 28C,D**). We found that single control vector-transduced GFP$^+$ cells outcompete double transduced BFP$^+$GFP$^+$ cells from the same initial culture with regards to maintenance of CD34 positivity, total nucleated cell output and total CD34$^+$ cell output, and a similar but less pronounced trend was seen for single BFP$^+$ cells (**Figure 28E**). This outcome indicated that cross-comparison of single vs. double transduced cells (e.g. PLAG1-S vs. PLAG1-S + c-MYC) could be confounded by inherent differences in functional capacities of cells. Therefore, we concluded a second more standardized experimental approach should be used. For this methodology the culture is divided into four infection conditions of the following vector combinations: MA1-control + pSMALB-PLAG1-S;

MA1-c-MYC + pSMALB-control; MA1-c-MYC + pSMALB-PLAG1-S; MA1-control + pSMALB-control, and double BFP^+GFP^+ cells would be isolated from each for assessment and direct comparison of primitive cell maintenance *ex vivo* (**Figure 29A,B**). Consistent with other reports[152,296-298], ectopic c-MYC promotes hematopoietic differentiation, as measured by loss of $CD34^+$ and gain of $CD33^+$ cells (**Figure 29C, D**, blue vs. red bars). Consistent with elevated translation imparted by ectopic c-MYC, over 7 days of culture c-MYC^{OE} cells become significantly enlarged relative to control (**Figure 29E**) and display the highest rates of active translation (**Figure 29F**). PLAG1-S^{OE} significantly reduced protein production rates in c-MYC^{OE} cells (**Figure 29F**), and concomitantly countered c-MYC-induced cellular enlargement and pro-differentiative phenotypes (**Figure 29C, D**, top panel, blue vs. green bars). Finally, after 7 days cells co-overexpressing PLAG1-S and MYC have significantly reduced primitive cell output relative to cells solely overexpressing PLAG1-S (**Figure 29C, D**, bottom panel, green vs. grey bars), indicating that over the course of culture MYC expression and its accompanied activation of translation impairs the full capacity of PLAG1-S to maintain primitive hematopoietic cells *in vitro*. Together these findings provide an important proof of principle that dampened translation is key to the HSC-supportive programming imparted by PLAG1-S.

5.2 PLAG1-S activates imprinted loci to support human HSPCs.

A notable finding of the HSPC-specific PLAG1-S gene regulatory network is its direct binding and robust activation of DLK1/MEG3 and IGF2/H19 (**Figure 30A, B**), affirming that as in mouse tissues[203], these imprinted loci are direct targets of PLAG1-S in primitive human hematopoietic cells. PLAG1-induced activation of IGF2 can stimulate mitogenic and PI3K-AKT-mTOR signaling to promote tumorigenic growth and division[203,204,210,302]. However, H19 and MEG3 act in opposition to PI3K-AKT-mTOR signaling in support of fetal murine HSC quiescence and function[213,214]. When activated, this pleiotropic pathway can stimulate protein synthesis dually through phospho-dependent activation of ribosomal protein S6 kinase (RPS6K) and inhibition of translation initiation-regulating 4EBPs (**Figure 30C**)[303]. At the transcript level PI3K-AKT-mTOR signaling signatures are both up- and down-regulated in PLAG1-S^{OE} HSPC (**Figure 30D**). Definitive characterization of the pathway flux by ICF reveals subtle reductions in AKT and 4EBP1 phosphorylation, while RPS6 phospho-status was unchanged (**Figure 30E**), suggesting selective repression of 4EBP1-regulated translation initiation could partially contribute to reduced protein synthesis in PLAG1-S^{OE} HSPC. Human HSPC fitness can be enhanced by pharmacological inhibition of AKT (AKTi) which promotes quiescence[230] or by the addition of the mTOR inhibitor, rapamycin[231]. Given the pleiotropism of these signaling factors we investigated whether combining PLAG1-S^{OE} with AKTi or rapamycin could produce additive or synergistic effects on human HSPC output. As demonstrated previously in human Lin^-CD34^+ cells treated with AKTi[230] and murine Lin^-Sca^+ cells treated with rapamycin[304], addition of either inhibitor reduced total cells in both control and PLAG1-S^{OE} cultures (**Figure 30F**) while significantly enhancing the proportion of primitive $CD34^+$ cells (**Figure 30G**) resulting in maintenance of similar total $CD34^+$ cell outputs in culture (**Figure 30F**). In the case of rapamycin these growth dynamics were associated with a significant reduction in translation rates in PLAG1-S^{OE} cells, while AKTi treatment did not further reduce translation rates (**Figure 30H**); and neither treatment significantly altered apoptosis rates in control or PLAG1-S^{OE} cultures (**Figure 30I**).

The DLK1/MEG3 locus also encodes the largest miRNA mega-cluster in the mammalian genome, with possible roles transcending PI3K-AKT-mTOR regulation[305,306] (**Figure 31A**). Examining read counts derived from our bulk RNA-seq we identified 4 microRNAs (miR-770,

miR-433, miR-127 and miR-370) from within this locus that were reproducibly over-represented in PLAG1-S^{OE} Lin-CD34+ cells (**Figure 31B**). Comparison of experimentally-supported miRNA targets to transcripts down-regulated in PLAG1-S^{OE} HSPC found the highest overlap for miR-127 (**Figure 31C**)[307,308]. In support of PI3K-independent regulation, miR-127 targets specifically include genes involved in complex cap-dependent translation and RNA and peptide metabolic processing that are also down-regulated in PLAG1-SOE HSPCs (**Figure 31D**), providing impetus to test its role downstream of PLAG1-S. We performed two functional assays employing a miR-127 inhibitor or miR-127 overexpression. Simultaneous ectopic expression of PLAG1-S and an inhibitory miR-127-5p sponge consisting of multiple bulged 26-mer target sequences (miR127TB) [228,229] netted significantly reduced CD34$^+$ output and in the two CBs where sample amounts supported testing OP-Puro incorporation, this was associated with an increase in protein synthesis (**Figure 31E**). Finally, overexpression of miR-127 enhanced CD34$^+$ output while imparting reduced levels of protein synthesis (**Figure 31F**). Together these results suggest that miR-127 partially contributes to the effects of PLAG1-S in promoting a specific translational state and primitive cell maintenance.

5.3 Pharmacological inhibition of translation in Lin$^-$CD34$^+$ cells.

Altogether our investigation of the role of PLAG1-S in promoting human HSC function supports two emerging paradigms: 1) that dysregulation of protein synthesis is a key clinical demand on human HSCs and 2) that its modulation could be leveraged for therapeutic benefit. Therefore, we next explored whether pharmacological inhibition of translation in Lin$^-$CD34$^+$ cells could enhance CB HSPC output. Omacetaxine mepesuccinate (**OMA**, a.k.a. Homoharringtonine) is an FDA-approved drug for the treatment of CML that acts via inhibiting translation elongation. Treatment of CB Lin$^-$CD34$^+$ cells with 200nM OMA improved cellular viability in one report [167], however the effect on CD34$^+$ or HSC expansion was not measured. Lin$^-$CD34$^+$ cells were FACS isolated and cultured for 24 hours in the presence of 0, 1, 10, 50, 100, and 400nM OMA and the sustained impact was measured after 4 and 7 days in culture (**Figure 32A**). Protein synthesis is attenuated in OMA-treated cells dose-dependently, with levels comparable to PLAG1-S^{OE} achieved by 1nM OMA (**Figure 32B**). Low doses of OMA do not affect CD34 frequencies but do dose-dependently reduce total cell numbers (**Figure 32C, D**). One possible contributor to the reduction in total CD34$^+$ cells is reduced cellular viability, as there is an apparent dose-responsive increase in 7-AAD-positive cells in OMA-treated cultures (**Figure 31E**), in contrast to the findings of Stevens *et al*. (2018)[167]. Data is not shown for doses above 50nM, as cultures were almost entirely non-viable.

5.4 Summary.

Herein we present 3 key findings:

1. PLAG1-S enacts multifaceted and combinatorial programs to limit the expression of protein biosynthetic machinery including direct association with RP gene promoters, modulation of 4EBP1 and the translation-targeting miR-127, but does not attenuate c-MYC.
2. Toggling c-MYC-driven protein production as a molecular tool we provide proof of principal that diminished translation is an essential modality by which PLAG1-S enhances human HSPC output.
3. Future research into the application of translation regulation in regenerative therapies is warranted.

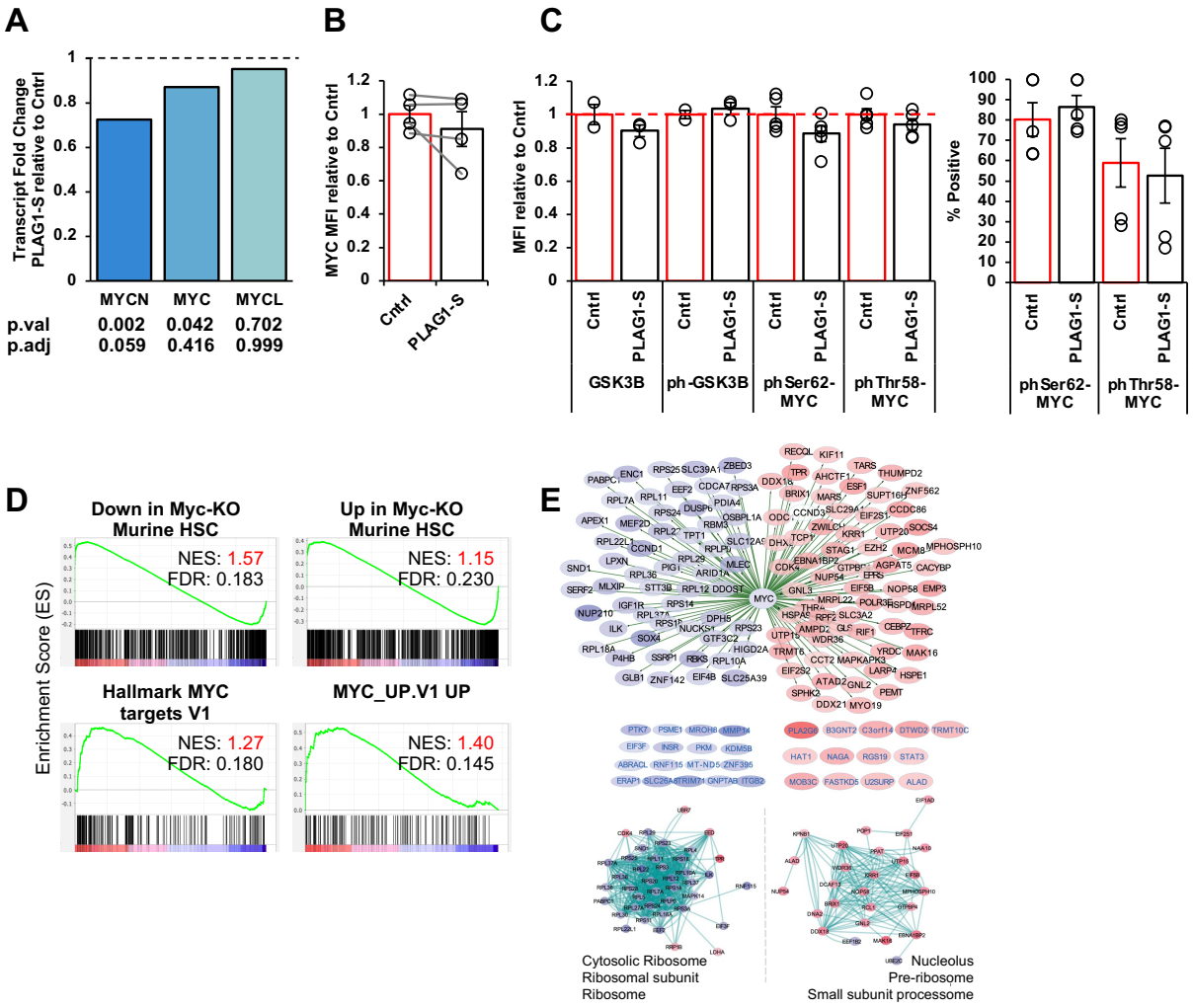
A
Transcript Fold Change PLAG1-S relative to Cntrl
MYCN MYC MYCL
p.val 0.002 0.042 0.702
p.adj 0.059 0.416 0.999
B
MYC MFI relative to Cntrl
Cntrl
PLAG1-S
C
MFI relative to Cntrl
% Positive
GSK3B
ph-GSK3B
ph Ser62-MYC
ph Thr58-MYC
D
Down in Myc-KO Murine HSC
NES: 1.57
FDR: 0.183
Up in Myc-KO Murine HSC
NES: 1.15
FDR: 0.230
Hallmark MYC targets V1
NES: 1.27
FDR: 0.180
MYC_UP.V1 UP
NES: 1.40
FDR: 0.145
Enrichment Score (ES)
E
Cytosolic Ribosome
Ribosomal subunit
Ribosome
Nucleolus
Pre-ribosome
Small subunit processome

Figure 27: PLAG1-S does not inhibit MYC to regulate protein synthesis in human HSPCs. **(A)** Log2 expression fold change of N-, C- and L- MYC transcripts from RNA-seq of PLAG1-S^{OE} HSPC relative to control. **(B)** Intracellular flow cytometric measurements of MYC protein expression in PLAG1-S^{OE} $Lin^{-}CD34^{+}$ cells (n=4). **(C)** Intracellular flow cytometric measures of total and phospho-Ser9 GSK3β (n=2 for Cntrl, n=3 for PLAG1-S^{OE}) and phospho-Ser62 or Thr58 c-MYC (n=5). **(D)** GSEA of the PLAG1-S transcriptome to signatures of MYC target genes[296,301] (E) Up- (red) or down- (blue) regulation of MYC ribosome biogenesis targets in PLAG1-S^{OE} HSPC.

Data is presented as average +/- SEM unless otherwise indicated. Each point represents an individual CB unit. *** $p<0.005$, ** $p<0.01$, * $p<0.05$.

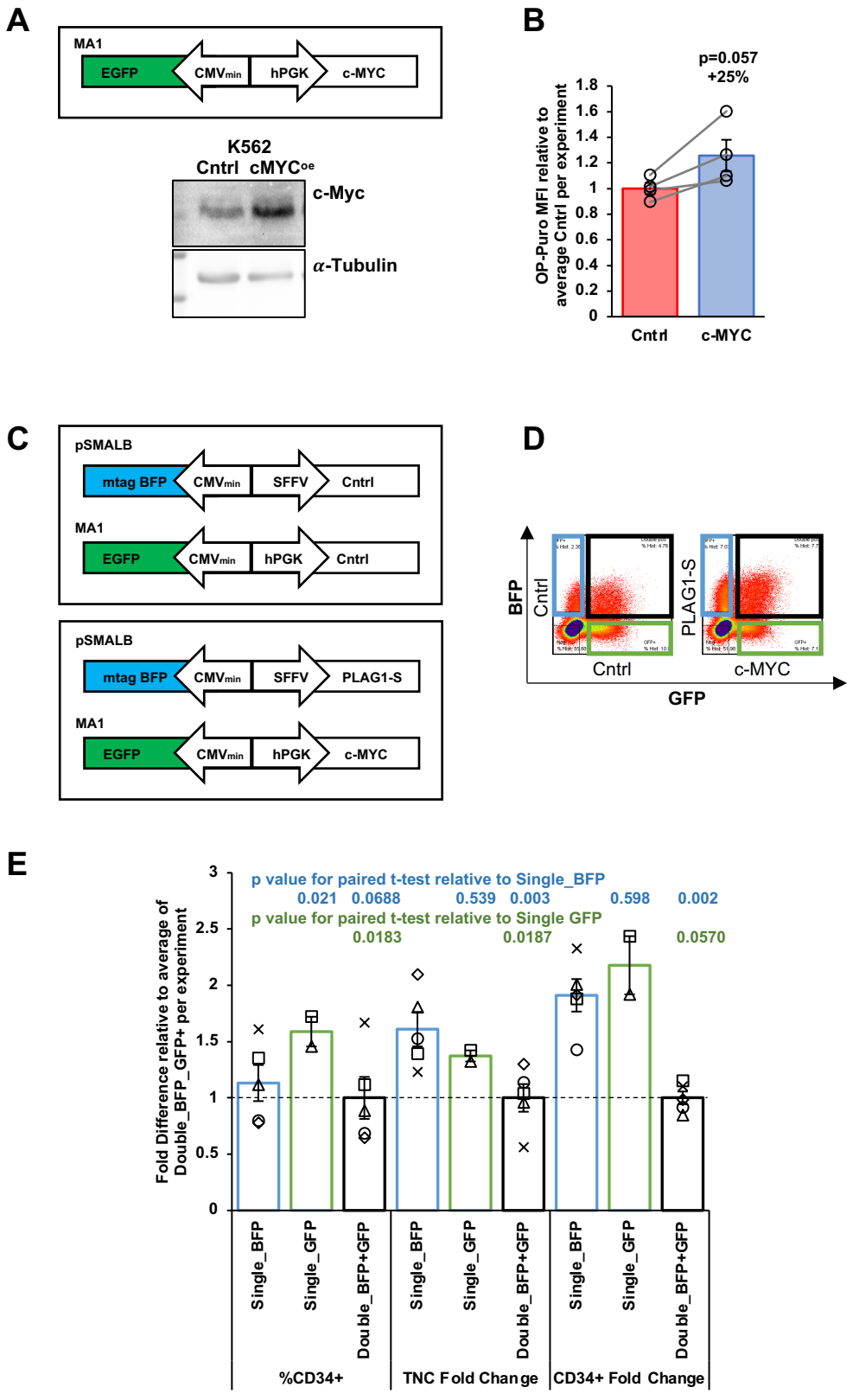
A
MA1
EGFP
CMVmin
hPGK
c-MYC
K562
Cntrl cMYCoe
c-Myc
α-Tubulin
B
p=0.057
+25%
OP-Puro MFI relative to average Cntrl per experiment
Cntrl
c-MYC
C
pSMALB
mtag BFP
CMVmin
SFFV
Cntrl
MA1
EGFP
hPGK
pSMALB
PLAG1-S
D
BFP
Cntrl
PLAG1-S
GFP
E
p value for paired t-test relative to Single_BFP
0.021 0.0688 0.539 0.003 0.598 0.002
p value for paired t-test relative to Single GFP
0.0183 0.0187 0.0570
Fold Difference relative to average of Double_BFP_GFP+ per experiment
Single_BFP
Single_GFP
Double_BFP+GFP
%CD34+
TNC Fold Change
CD34+ Fold Change

Figure 28: Development of c-MYC overexpression as a molecular tool to activate translation. **(A)** Schematic of MA1-PGK-c-MYC overexpression lentivector and western blot validation of MYC overexpression in K562 cells. **(B)** OP-Puro incorporation in $Lin^{-}CD34^{+}$ cells overexpressing c-MYC or control (n=4). **(C)** Schematic of control vs. gene of interest overexpression lentivectors with either BFP or GFP reporters of transduction. **(D)** Representative sorting gates to compare single vs. double transduced cells in an experimental design where half the culture receives only control vectors and the other half receives only gene of interest overexpressing vectors. **(E)** Significant difference in maintenance of the proportion of CD34+ cells, total cells and total CD34+ cells in cultures receiving a single virus vs. double viruses.

Data is presented as average +/- SEM unless otherwise indicated. Each point represents an individual CB unit. *** $p<0.005$, ** $p<0.01$, * $p<0.05$.

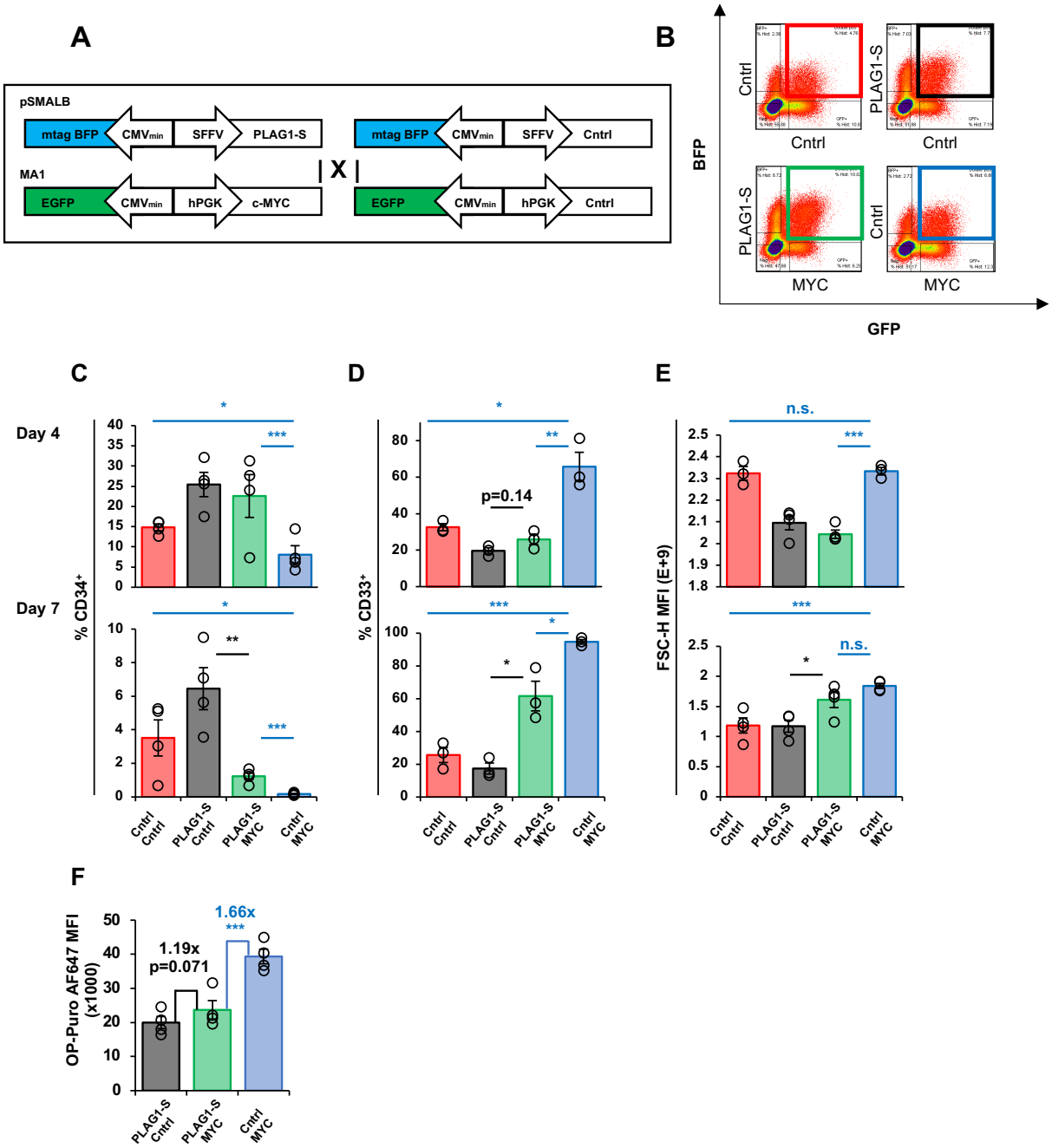
A
pSMALB
mtag BFP
CMVmin
SFFV
PLAG1-S
MA1
EGFP
hPGK
c-MYC
X
Cntrl
B
BFP
GFP
PLAG1-S
MYC
C
Day 4
Day 7
% CD34+
D
% CD33+
p=0.14
E
FSC-H MFI (E+9)
n.s.
Cntrl Cntrl
PLAG1-S Cntrl
PLAG1-S MYC
Cntrl MYC
F
OP-Puro AF647 MFI (x1000)
1.19x
p=0.071
1.66x

Figure 29: MYC-induced translation impairs PLAG1-S-mediated stemness in human HSPC. **(A)** Schematic of PLAG1-S, c-MYC and control overexpression lentivectors. **(B)** Representative sorting gates for dual-overexpression of PLAG1-S and c-MYC or controls in 4 distinct combinations. **(C)** CD34 (n=4) and **(D)** CD33 (n=3) positivity over 4 and 7 days of *ex vivo* culture. **(E)** Cell size determined by flow cytometric MFI of FSC-H (n=3-4) on day 4 and 7 of *ex vivo* culture. **(F)** OP-Puro incorporation on day 4 of *ex vivo* culture (n=4).

Data is presented as average +/- SEM unless otherwise indicated. Each point represents one mouse or an individual CB unit. Blue line is t-test relative to MYC alone, Black line is t-test relative to PLAG1-S alone *** $p<0.005$, ** $p<0.01$, * $p<0.05$.

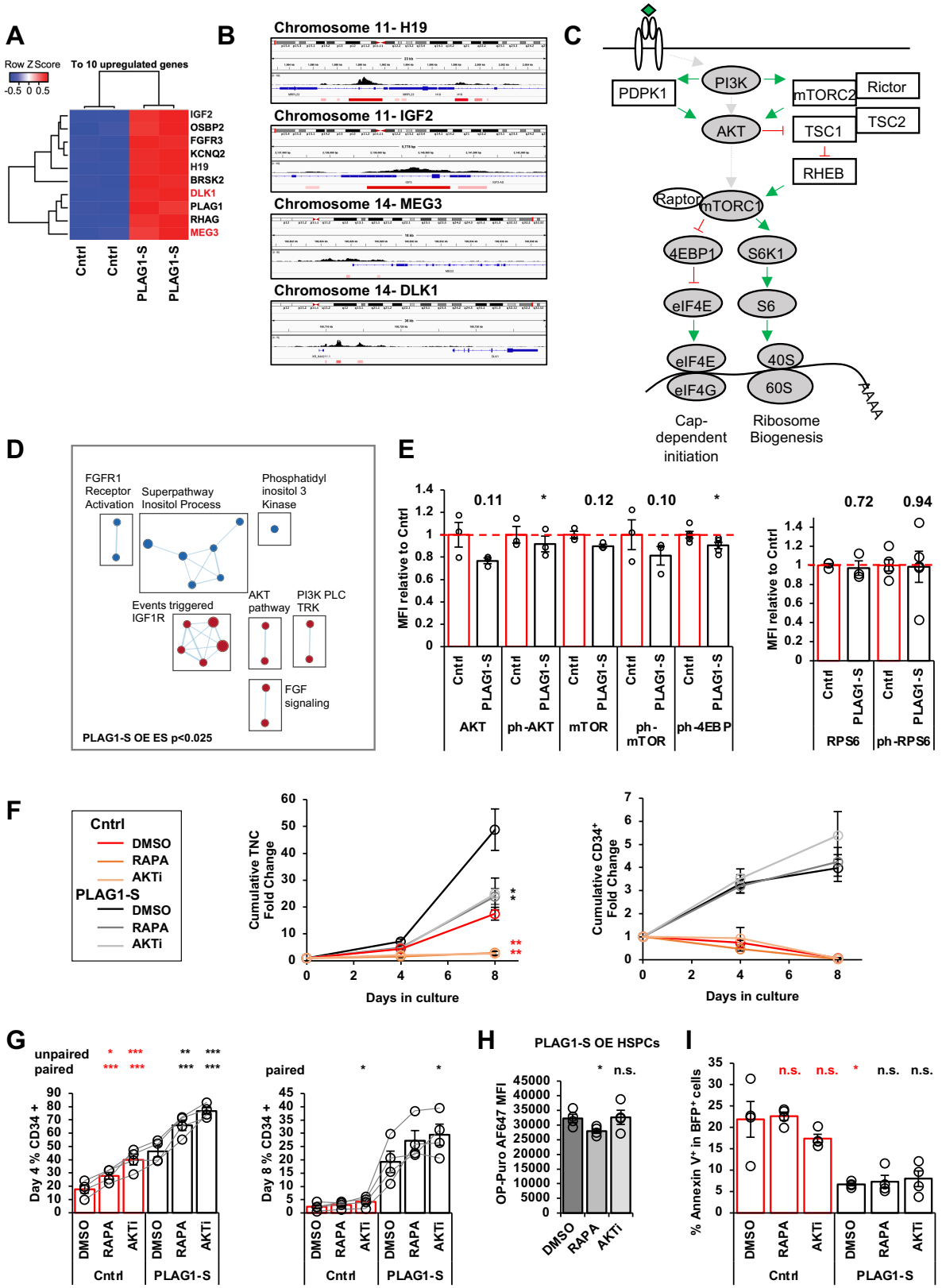
A
Row Z Score
-0.5 0 0.5
To 10 upregulated genes
IGF2
OSBP2
FGFR3
KCNQ2
H19
BRSK2
DLK1
PLAG1
RHAG
MEG3
Cntrl
Cntrl
PLAG1-S
PLAG1-S
B
Chromosome 11- H19
Chromosome 11- IGF2
Chromosome 14- MEG3
Chromosome 14- DLK1
C
PDPK1
PI3K
mTORC2
Rictor
AKT
TSC1
TSC2
RHEB
Raptor
mTORC1
4EBP1
S6K1
eIF4E
S6
eIF4E
40S
eIF4G
60S
AAAA
Cap-dependent initiation
Ribosome Biogenesis
D
FGFR1 Receptor Activation
Superpathway Inositol Process
Phosphatidyl inositol 3 Kinase
Events triggered IGF1R
AKT pathway
PI3K PLC TRK
FGF signaling
PLAG1-S OE ES p<0.025
E
MFI relative to Cntrl
0.11
*
0.12
0.10
*
AKT
ph-AKT
mTOR
ph-mTOR
ph-4EBP
0.72
0.94
RPS6
ph-RPS6
F
Cntrl
DMSO
RAPA
AKTi
PLAG1-S
DMSO
RAPA
AKTi
Cumulative TNC Fold Change
Days in culture
Cumulative CD34+ Fold Change
Days in culture
G
unpaired
paired
Day 4 % CD34 +
Day 8 % CD34 +
DMSO
RAPA
AKTi
Cntrl
PLAG1-S
H
PLAG1-S OE HSPCs
OP-Puro AF647 MFI
n.s.
I
% Annexin V+ in BFP+ cells
n.s.

Figure 30: PLAG1-S activates imprinted loci to support human HSPCs. (A) Heatmap of top 10 differentially expressed transcripts in the transcriptome of PLAG1-S^{OE} $Lin^{-}CD34^{+}$ HSPC. **(B)** CUT&RUN Peak tracks of PLAG1-S bound to IGF2/H19 and DLK1/MEG3 loci in $Lin^{-}CD34^{+}$ cells. **(C)** Simplified summary of PI3K-AKT-mTOR signaling to positively regulate protein biosynthesis. **(D)** Subset of the PLAG1-S overexpression enrichment map ($p<0.05$) showing nodes related to the PI3K signaling pathway. **(E)** Intracellular flow cytometry of components of the PI3K signaling pathway, including phospho-S473 AKT, phospho-S2448 mTOR, phospho-Thr37/46 4EBP1, and phospho- S240/244 RPS6 in PLAG1-S^{OE} $Lin^{-}CD34^{+}$ cells on day 4 of culture. Numbers above PLAG1-S^{OE} bars show the paired Student's t-test p value relative to control (n=3, ph-4EBP1 n=5, ph-RPS6 n=5). **(F)** Total nucleated cell and $CD34^{+}$ cell fold change in $Lin^{-}CD34^{+}BFP^{+}$ cultures overexpressing either PLAG1-S or Luciferase control and treated with 50nM rapamycin (RAPA), 1uM AKT inhibitor (AKTi) or vehicle (DMSO) (n=4). Student's t-test p values in red are relative to Cntrl-DMSO and in black are relative to PLAG1-S^{OE}-DMSO. **(G)** CD34 positivity in PLAG1-S^{OE} or control cells following 4 and 8 days of ex vivo culture with RAPA, AKTi or vehicle (n=4). Student's t-test p values in red are relative to Cntrl-DMSO and in black are relative to PLAG1-S^{OE}-DMSO. **(H)** OP-Puro incorporation by PLAG1-S^{OE} cells cultured in the presence of RAPA, AKTi or vehicle on day 4 of culture (n=4). **(I)** Annexin V positivity in PLAG1-S^{OE} or control cells following 8 days of ex vivo culture with RAPA, AKTi or vehicle (n=4). Student's t-test p values in red are relative to Cntrl-DMSO and in black are relative to PLAG1-S^{OE}-DMSO.

Data is presented as average +/- SEM unless otherwise indicated. Each point represents an individual CB unit. *** $p<0.005$, ** $p<0.01$, * $p<0.05$.

A

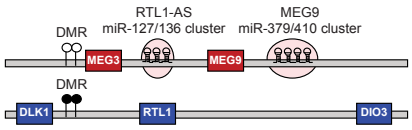

B

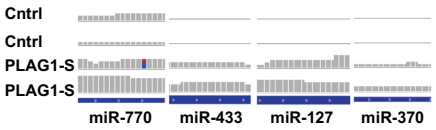

C

miRNA name	# total targets from Diana tools tarBase v7.0	# targets on EM (p<0.05)	# targets with DEseq p<0.05	# targets with p<0.05 and down
miR-370-5p	0	0	0	0
miR-370-3p	112	60	20	9
miR-127-5p	172	99	30	7
miR-127-3p	43	27	8	5
miR-770-5p	38	18	3	3
miR-770-3p	0	0	0	0
miR-433-5p	0	0	0	0
miR-433-3p	1	0	0	0

D

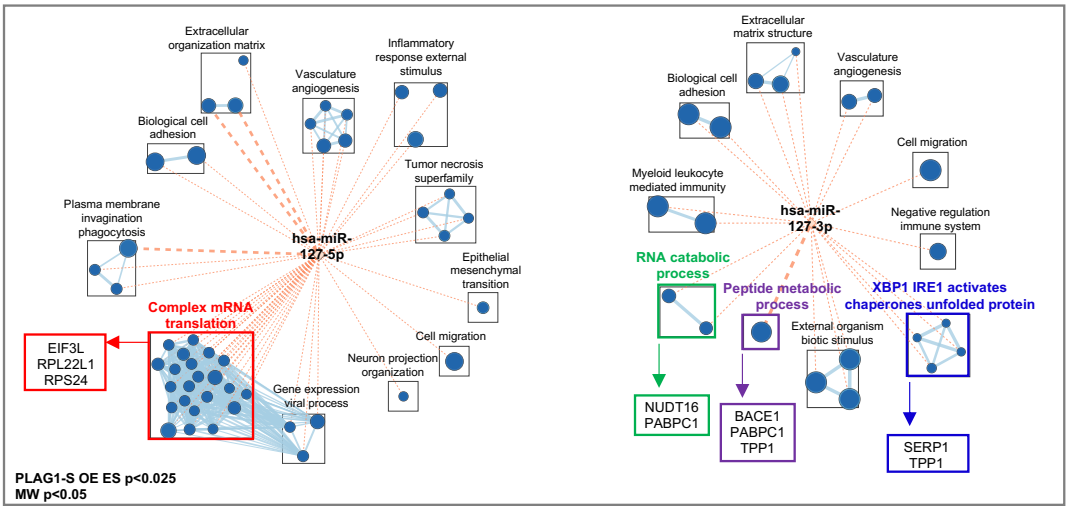

E

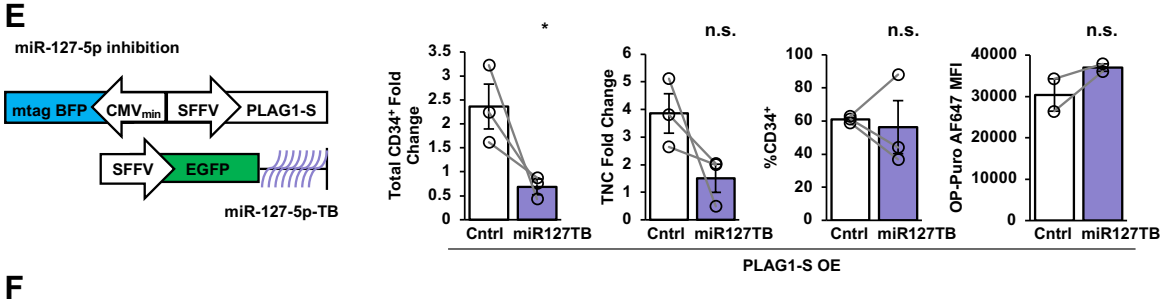

F

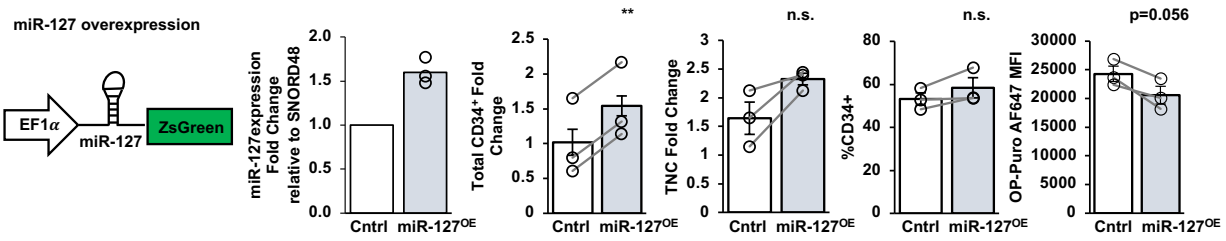

Figure 31: PLAG1-S activates imprinted miR-127 to support human HSPCs. (A) Schematic of the imprinted human DLK1/MEG3 locus which encodes miRNA mega-clusters miR127/136 (7 miRNAs) and miR-379/410 (39 miRNAs). **(B)** RNA-seq read tracks for microRNA transcripts from this locus detected in PLAG1-S^{OE} HSPC. **(C)** Summary of overlap between genes downregulated in the PLAG1-S^{OE} transcriptome and microRNA target genes. **(D)** Overlap of the PLAG1-S overexpression gene set enrichment map ($p<0.025$) to signatures of miR-127-5p and miR-127-3p validated targets (Mann-Whitney U test, $p<0.05$). **(E)** Schematic of lentivectors used for dual PLAG1-S overexpression and miR127-5p via a sponge consisting of multiple bulged 26-mer target sequences (miR127TB); and measures of total $CD34^+$ cell fold change, total cell fold change, $CD34^+$ frequencies and OP-Puro incorporation. **(F)** Schematic of lentivectors used for miR127 overexpression, qPCR measurements of miR127-5p expression in cells transduced with the EF1alpha-miR-127 overexpression relative to control lentivector; and measures of total $CD34^+$ cell fold change, total cell fold change, $CD34^+$ frequencies and OP-Puro incorporation.

Data is presented as average +/- SEM unless otherwise indicated. Each point represents an individual CB unit. *** $p<0.005$, ** $p<0.01$, * $p<0.05$.

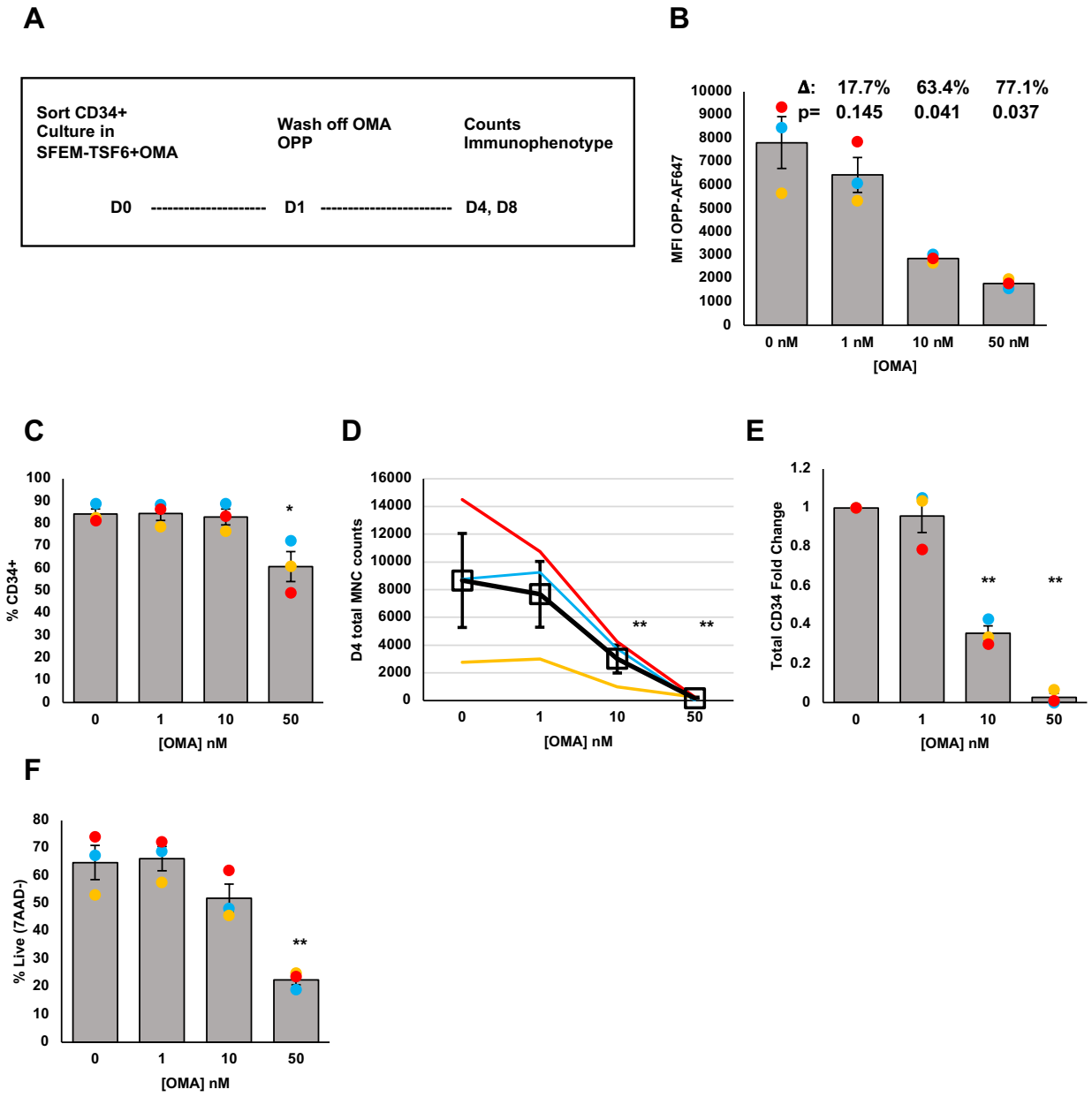
A
Sort CD34+
Culture in
SFEM-TSF6+OMA
Wash off OMA
OPP
Counts
Immunophenotype
D0
D1
D4, D8
B
Δ: 17.7% 63.4% 77.1%
p= 0.145 0.041 0.037
MFI OPP-AF647
0 nM
1 nM
10 nM
50 nM
[OMA]
C
% CD34+
[OMA] nM
D
D4 total MNC counts
[OMA] nM
E
Total CD34 Fold Change
[OMA] nM
F
% Live (7AAD-)
[OMA] nM

Figure 32: OMA treatment of Lin$^-$CD34$^+$ HSPC. **(A)** Experimental schematic. **(B)** OP-Puro incorporation in Lin$^-$CD34$^+$ cells following OMA treatment. **(C)** CD34 frequency **(D)** total cell counts and **(E)** total CD34$^+$ fold change in OMA treated Lin$^-$CD34$^+$ cells after 4 days of culture. **(F)** Cell viability in OMA treated Lin$^-$CD34$^+$ cells after 4 days of culture.

Data is presented as average +/- SEM unless otherwise indicated. Each point represents an individual CB unit. *** $p<0.005$, ** $p<0.01$, * $p<0.05$.

CHAPTER 6

Discussion

6.1 Highlights.

1. We have identified a novel molecular factor involved in human HSC biology, PLAG1
2. PLAG1 is enriched in dormant human HSCs and is essential for long-term hematopoietic repopulation
3. Ectopic PLAG1-S enhances human HSC fitness and promotes their early 15-fold expansion ex vivo, via MSI2- and AhR- independent mechanisms.
4. PLAG1 enforces stemness by dampening expression of translation machinery that is activated in HSC-stimulatory conditions, and promoting dormancy features.
5. Mechanistically PLAG1-S is directly associated with ribosome gene promoters, modulates regulation of 4EBP1 and the translation-targeting miR-127, but does not attenuate c-MYC, which was used as a molecular tool to validate the connection between PLAG1-S-mediated dampened translation and HSC maintenance.
6. Our findings highlight the potential clinical importance of continued research into translation control in stem cell-based therapies.

6.2 Discovery of a novel factor regulating human HSC.

We identify the novel ability of the transcription factor PLAG1-S to positively promote human HSC self-renewal. While initially in search of an upstream regulators of MSI2 to gain greater molecular insights into hematopoietic homeostasis, transplantation and possibly transformation from an MSI2-centric perspective[194], we surprisingly uncovered a critical role for PLAG1-S in human HSC with implications for clinical transplantation that are operational via MSI2- and AhR- independent mechanisms.

Consistent with the absence of MSI2 activation, the composition of primary CFUs generated by overexpression of PLAG1 proteins differs from that of $MSI2^{OE}$, where enhanced total colonies was significantly attributed to heightened CFU-M and CFU-GEMM. Moreover, 72-hours following transduction when transgene expression is maximized $MSI2^{OE}$ did not amplify the absolute number of HSC, in fact their frequencies appear reduced relative to control, and instead over the course of an additional 7 days in culture LT-HSC frequencies increased 6-fold and a net 23-fold via further *in vivo* expansion, which was associated with an enrichment in the $CD34^+$ compartment[234]. By contrast, we find the quantitative HSC advantage imparted by PLAG1-S can be achieved immediately following its ectopic expression, the $CD34^+$ compartment does not expand *in vivo*, and $PLAG1\text{-}S^{OE}$ HSC numbers remain stable over the course of serial *in vivo* repopulation. Not only do these notable distinctions point to discrete modes of action for these two factors, they also highlight a putative difference in the capacity of MSI2 vs. PLAG1-S to enforce leukemic or pre-leukemic traits in HSCs. Indeed, while PLAG1 levels appear relatively restricted to the most primitive healthy compartment and low in AML as well as MDS (**Figure 32**), MSI2 levels are elevated and associated with poor prognosis in a range of leukemias (**Figure 32C**)[184,190,191,193,309]. Loss-of-function experiments also confirm that MSI2 is essential for maintaining MDS SCs[183], leukemic blasts or cell lines and LSCs[185,187,189], and pharmacological inhibition of MSI1/2 reduced leukemic burden in a murine AML model[310]. These reports highlight many MSI2 effectors in leukemia including c-MYC[189,310], IL-6 signaling[311], SYNCRIP[312], HOXA9, IKZF2[189] and TGF-B signaling[186]. In addition, the AhR signaling effector CYP1B1, whose antagonism by MSI2 or SR-1 promotes healthy human HSC expansion, is concordantly diminished in human AML LSCs highlighting the activation of AhR as a potential therapeutic strategy for targeting these cells[313]. As such, by-passing MSI2 to enforce HSC stemness poses not only an opportunity for acquiring enhanced fundamental biological insights but also for identifying

important regulatory mechanisms that could lower manufacturing barriers while rendering safer *ex vivo* manipulated cell products for clinical applications. Given that the functional gains endowed by elevated PLAG1 are achieved rapidly *ex vivo*, and mechanistically distinct from existing HSC self-renewal agonists (i.e. SR-1 and UM171), it would be very interesting to test whether PLAG1 or its effectors could augment $CD34^+$ expansion by these compounds that require lengthy (>7days) culture regimes (See sections **6.7 Two sides of one coin: Stem cell expansion and Cancer stem cells** and **6.8 Translation control in cell therapy** for more discussion). Moreover, these findings emphasize key unexplored biological questions regarding additional mechanisms controlling MSI2 gene expression, the specific endogenous contexts where the PLAG1-S-MSI2 axis is active, and whether dysregulation of this axis contributes to certain backgrounds of MSI2-driven leukemia.

6.3 PLAG1-S regulation of human hematopoietic fate and erythropoiesis.

Overall PLAG1-S^{OE} did not appear to significantly skew or impair lineage output *in vivo*, which importantly points to healthy/balanced hematopoiesis. However, we did note elevated BFU-Es in primary *in vitro* CFU assay and suspension culture and enhanced expression of erythroid signatures *in vitro* by RNA-seq. While *in vitro* culture systems are exclusively myeloid-promoting, the NSG mouse niche is significantly more supportive of the lymphoid branch[314]. This interestingly suggests that the capacity of PLAG1-S to influence fate outcomes can be swayed by extrinsic signals, is consistent with the model of early hematopoietic differentiation existing on a continuum with considerable plasticity[73,75,307,315], and mirrors the findings of Weinreb *et al*. (2020) that fate outcomes are challenging to predict[81]. Given that NSG mice are not highly supportive of human erythropoiesis[314] we explored the role of PLAG1-S in influencing the later stages of erythroid specification via *in vitro* models[294]. Consistent with its role in promoting stemness there appeared to be a delayed loss of primitive immunophenotype, which seems to modestly influence the proportion of erythroid progenitors at each differentiation stage, but in general these differences do not seem to occur at the expense of a differentiation block.

In addition to erythroid signatures, we noted from our CB bulk-RNA-seq data a 4-fold activation of the fetal hemoglobin (HbF) gene *HBG2*. Although PLAG1-S was not detected by CUT&RUN as directly interacting with *HBG2* regulatory regions in HSPCs our ChIP-seq results showed that in the K562 context, and therefore possibly other contexts, PLAG1-S could bind to the *HBG2* promoter. In humans HbF is expressed in the developing fetus and up to approximately 1 year of age at which point there is a switch in the expression of gamma-globins (encoded by *HBG1/2*) to adult beta-globins (encoded by *HBB*), which is directed by BCL11A and results in the expression of adult hemoglobin (HbA)[293,316]. Defective production of the beta-globins underlies beta-thalassemia and sickle cell disease resulting in severe anemia. By contrast genetic mutations can also promote asymptomatic hereditary persistence of HbF, which when present in patients with SCD ameliorates the disease symptoms[259]. Therefore, in addition to strategies aimed at restoring functional beta-globin variants there is ongoing interest in reinstating/inducing chimeric HbF expression through approaches that include erythroid-specific BCL11A inhibition[317] or overexpression of gamma-globin via lenti vectors[318], as a means to treat beta-thalassemia and SCD[258,259]. Thus, our observations were promising in that they suggested that we may have uncovered a novel inducer of HbF. Although since we were investigating this effect in CB-derived HSPCs it was unlikely that PLAG1-S, like BCL11A, acts as a developmental switch. When investigated on a per-cell basis however it became apparent that PLAG1-S^{OE} was not significantly elevating HbF levels in the cells where it is expressed. The observation that a spike in the

proportion of cells expressing HbF occurs coincident with an elevation of more mature erythroid cell types in the second stage of erythroid-differentiation-promoting culture suggests, but was not confirmed, that HbF expression is tracking with cell identities. It is therefore possible that the elevation of HBG2 observed in bulk RNA-seq is a partial reflection of differences in the composition of cell identities in PLAG1-S^{OE} and control cultures.

6.4 HSPC-specific molecular circuitry downstream of PLAG1-S.

Our integrated omics analysis revealed an intriguing profile that indicates PLAG1-S orchestrates protein production rates in HSPCs by negatively regulating the expression of translation machinery, most notably cytosolic ribosome proteins. CUT&RUN evidence that PLAG1-S is directly associated to translation-regulating genes (and their promoters, data not shown), and that it is associated with a significant proportion of repressed genes, strongly suggests that in part PLAG1-S is acting directly as a negative regulator of gene expression, a previously unappreciated functionality[202]. However, the molecular mechanism of this action remains an open question, for example does PLAG1-S have unrecognized transcription repression function and/or has it influenced the recruitment of transcription activators/repressors and/or epigenetic modifiers to insulate gene expression? The latter point would be of significant interest to investigate given PLAG1-S's intriguing function in regulating gene expression from a number of imprinted loci[202,203], and the enrichment of epigenetic regulators and DNA-binding factors whose transcripts are bound and activated by ectopic PLAG1-S in HSPCs (**Table 7**). Follow up experiments, such as ATAC-seq or histone mark-specific CUT&TAG, both of which can be performed in single cells[319,320], would be interesting to explore the extent to which PLAG1-S reshapes the genomic landscape to promote its pro-stemness and or diminished translation functions. This presumed direct regulation over translation-regulating genes should also be experimentally validated via functional reporter assays, such as commonly used bioluminescence-based luciferase reporter assays, or our conceived fluorescence-based reporter assay (**Figure 34**), which offers a few advantages. Given that this reporter format can be assessed by flow cytometry not only do we circumvent the need for FACS-isolation of multi-transduced cell populations that can be limiting, we can also gain single cell insights correlated to proxy levels of PLAG1 via BFP intensity. Additionally, cells from early timepoints can be simultaneously analyzed and harvested by FACS to enable serial measurements over multiple culture timepoints.

6.5 PLAG1-S dampens protein synthesis and promotes dormancy in stimulated human HSPC

Through elucidation of its human HSPC-specific regulon, we demonstrate that PLAG1-S enacts multifaceted and combinatorial programs to limit the expression of protein biosynthetic machinery. In enforcing this mechanism, PLAG1-S endows an *in situ*-like rate of protein production and simultaneously restrains growth, mitochondrial metabolism, proliferation, differentiation and death to ultimately enhance human HSC preservation and function in stimulatory culture and transplantation settings (**Figure 35**). Thus, we have identified a novel positive regulator of human HSC dormancy and self-renewal.

It is intriguing that coordinated attenuation of ribosome and translation machinery is a dominant feature of the PLAG1-S enforced transcriptional state in human HSPC, given that strictly controlled rates of protein synthesis is a hallmark of stem cell biology [165,260-263] and influences stem cell activation [148,152,173], division, differentiation [165,261], and proteome integrity [162,168,172,321]. Activation of protein production in HSCs can therefore be thought of as a double-edged sword serving to

drive regenerative stem cell activation[322] but doing so at the expense of proteotoxic stress[168] that has the potential to ultimately compromise HSC integrity and function[170]. Maintaining HSCs that retain long-term functionality has thus been a significant challenge for realizing the full clinical potential of HSC-based therapies. Kruta *et al*. (2020) were the first to demonstrate that murine HSCs rapidly hyperactivate protein biosynthetic processes when exposed to *ex vivo* culture[172] and we now address this phenomena from a human perspective, adding activation of protein synthesis as a selective and robust feature of the molecular summary of compromised human HSC function upon culture-induced stimulation. However, whether the translation peak itself is maladaptive and/or the effective restoration of low translation rates is necessary remains up for debate. Moreover, by preceding cell division kinetics the proteostatic response likely also acts as an early determinant of cell fate[323], and is thus an important but underappreciated checkpoint for therapeutic procedures.

The intersection of translation, dormancy and stemness being elucidated in model stem cells is mirrored in PLAG1-S^{OE} human HSPC where concurrent with diminished translation we observe reduced differentiation, enlargement, division, death and enhanced self-renewal. While some of these features could be under translation-independent control it is also possible these phenotypes are enforced secondary to diminished translation. For example, the observation of depressed UPR signals could be secondary to the fact these cells have a diminished proteome in need of folding and this reduced proteostatic shock under activating culture conditions could be promoting their survival[170]. Stimulation of translation machinery and protein production precedes HSC division[139,148] and mitosis is one mode by which a cell dilutes toxic components, such as misfolded proteins[168]. Therefore, a conceivable hypothesis is that the accumulation of misfolded proteins during culture-induced hyperactivation of translation rates (as well as ROS-generating metabolism that can further damage proteome quality) may be inherited asymmetrically when HSPCs divide and that this could have consequences for daughter cell fates (i.e. differentiation-priming or senescence-priming induced secondary to context-dependent translation hyperactivation). Loeffler *et al*. (2019) demonstrated that asymmetric segregation of a number of cellular components including lysosomes, autophagosomes and mitophagosomes occurs during murine HSC cell divisions, and their inheritance imparts lower metabolism, translation, differentiation and unique LT fate outcomes in daughter cells [324]. In yeast cells unequal segregation of misfolded proteins supports the viability of the daughter cell, and therefore maintenance of the colony, at the expense of the viability of the mother cell [325]. The concept of asymmetric inheritance of misfolded proteins has also been shown in human embryonic stem cells, but to my knowledge there is no investigation of this in HSCs or its impact on long-term fates of the progeny cells [326]. As such, this presents a very interesting gap in our understanding of the contribution of proteome integrity to HSPC fate outcomes and whether micromanagement of translation rates plays an intervening role.

MYC is a potent tissue non-specific regulator of protein production through promotion of multiple steps of nuclear and cytosolic ribosome assembly[295]. As such, the observation that PLAG1-S is not apparently acting through direct inhibition of MYC very interestingly speaks to the likely capacity of PLAG1-S to independently coordinate the expression of protein synthesis machinery in CB HSPCs, and highlights it as a novel context-specific regulator of these genes. By toggling c-MYC-driven protein production as a molecular tool we provide proof of principal that diminished translation is an essential modality by which PLAG1-S enhances human HSPC output.

Altogether our results forward the notion that the physiological importance of low translation rates in homeostatic niche-associated HSCs can be harnessed for therapeutic benefit.

To this point, rebalancing proteostasis in murine satellite cells and HSCs by enacting stress-responsive effectors can improve their long-term regenerative capacities[172,174,262]. Importantly however, the role of ectopic PLAG1-S appears independent of stress effectors, as we do not see activation of the ISR, and instead observe depressed UPR signatures which suggest that by directly tuning the translation machinery PLAG1-S pre-empts and averts pro-apoptotic branches of stress signaling[170]. To my knowledge this is the first example of stress-signaling-independent means to promote HSPC proteostatic integrity and thereby HSC function; and suggests that direct modulation of translation is a putatively effective but untapped strategy to enhance HSC-based therapies.

In sum we have identified PLAG1-S as an enforcer of HSC stemness and a highly context-dependent regulator of protein synthesis. Notably such molecular insights into the function of PLAG1 in healthy adult stem cells are lacking given the long-held misconception that PLAG1 is not expressed in adult tissues[197,327], a concept that is beginning to shift in light of advancements in the sensitivity of global gene expression measurements at the single cell level. As such, our findings also provide impetus for future investigations of PLAG1 in regulation of stemness and/or translation in other primitive cell settings where its expression also appears enriched[305,327-329].

6.6. Context-specific biology: Regulators of translation downstream of PLAG1-S in HSPCs.

The role of PLAG1 in supporting healthy HSC self-renewal is strikingly at odds with its reported functions in oncogenic contexts. In a murine cbfß-translocated AML model ectopic PLAG1 promotes proliferation[330] and its elevation via lentiviral insertions was one of several co-occurring molecular abnormalities associated with the onset and progression of primate myelodysplastic clonal hematopoiesis[331], phenotypes notably absent upon PLAG1-S overexpression in the background of healthy human HSPC. (See section **6.7 Two sides of one coin: Stem cell expansion and Cancer stem cells** below for more discussion) Additionally, effectors downstream of PLAG1-IGF2 reported to support solid tumors[202-204,302] appear inert or repressed in PLAG1-S^{OE} HSPCs, implicating context-specific counter-acting mechanisms. It is particularly interesting that 4EBP1 displayed reduced activation in this setting, given that phospho-4EBP1/2 is currently the most predictive indicator of translation levels in murine HSC[332], and similarly selectively regulates renewal in neural stem cells[333]. At the same time it is clear that 4EBP1 phosphorylation does not fully account for the dampened translation observed in PLAG1-S^{OE} HSPC, where together with multiple functional nodes, including binding and modulation of RP genes and miR-127, PLAG1-S consolidates the restraint of translation to enhance HSC function. Interestingly, rapamycin treatment of PLAG1-S^{OE} HSPC appears to have an additive effect on diminished protein production, possibly due to the preferential inhibition of mTOR-RPS6K1 over mTOR-4EBP1[334]. While it cannot be ruled out that the effect of rapamycin in PLAG1-S^{OE} HSCPs could be attributed to this further reduction in translation, rapamycin treatment also enabled murine HSCs to resist culture-induced senescence by upregulating Bmi1 and downregulating p16[304], and its target, mTOR, coordinates several signals to mediate HSC dormancy and activation[303]. Notably, AKTi[230] imparted similar changes to CD34$^+$ cell growth dynamics without further reduction in translation rates, suggesting the contribution of other dormancy-promoting processes, which may in the context of AKT/mTOR inhibition be dominant over their translation influence[335]. Although neither AKTi nor rapamycin treatments significantly enhanced the total CD34$^+$ cell output in PLAG1-S^{OE} cultures, the elevated proportion of CD34$^+$ cells from these cultures could suggest the functional nature of these populations differs from vehicle-treated cells. As such an interesting question for future investigation is whether

pharmacological inhibition of AKT, mTOR or other pathways (e.g. via SR-1 or UM171) in PLAG1-S^{OE} HSPCs could further enhance their *in vivo* repopulating fitness, as has been shown for untransduced CB[51,105,230,231].

6.7 Two sides of one coin: Stem cell expansion and Cancer stem cells.

It is intriguing to speculate that ectopic PLAG1-S could be leveraged as a therapeutic tool to promote the *ex vivo* maintenance of HSPCs. Given that the advantage imparted by PLAG1-S can be largely achieved transiently it would be a compelling candidate to test using mRNA delivery platforms, which offer the advantages of realizing the full pro-stem effect of PLAG1-S without leaving behind permanent genetic changes. One can envision the addition of PLAG1-S might synergize or cooperate with existing HSC-promoting small molecules to potentially enhance functional HSPC output more rapidly and with reduced LT-HSC attrition. This was a fundamental paradigm driving the discovery and characterization of UM171 as a self-renewal agonist that acts independently of AhR signaling, however dual SR-1 and UM171 did not enhance human HSC fitness[51].

Unfortunately, because of many shared features between healthy hematopoietic and leukemic stem cells it is a common phenomenon that loss or gain of genes or dysregulation of processes that expand healthy HSC are similarly responsible for maintenance, progression or transformation to leukemia[336]. Indeed, stem cell expansion is a hallmark of pre-leukemic conditions such as clonal hematopoiesis of indeterminant potential (CHIP) and MDS[337]. Illustrative examples are the previously discussed case of MSI2 as well as the repression of components of the cohesin complex, responsible for genome organization and integrity. In the latter scenario cohesin complex disruption results in impaired hematopoietic differentiation and the expansion of primitive HSC[338] which also serve as a primed reservoir for co-operative secondary hits that then promote myeloid malignancies[339,340]. In addition, INKA1, which was in fact identified as an LSC-maintaining gene by screening in healthy CB HSPCs[341], supports both LSC and HSC maintenance via promoting their quiescence to promote their slow expansions[161,341] and there are many more examples from mouse models (i.e. Hoxa9 and Hoxb6[342,343]). In the case of PLAG1-S^{OE} HSPCs, no pre-leukemic or clonal hematopoietic phenotypes such as lineage bias, enhancement of the CD34^{+} compartment or *in vivo* HSC expansion, are evident. These results would indicate that despite significantly defending HSC integrity in activating conditions to impart *ex vivo* expansion, PLAG1-S^{OE} is insufficient to transform these cells or initiate leukemia. This however does not assure the safety of constitutive PLAG1-S^{OE} because as noted, neither ectopic expression of MSI2, INKA1 nor knockdown of STAG2/SMC3 cohesion molecules was sufficient to transform CB HSPCs but are all also supportive of leukemic contexts. It is also well understood that the development of cancer involves the progressive gain in genetic and molecular lesions, a fact obvious in the blood system where there exists a high incidence of leukemia development secondary to CHIP or MDS[344-346]. Moreover, it has proven extremely challenging to generate one-hit leukemia models in human HSPCs, whereas such models have been generated from murine cells, likely owing to different unresolved molecular and cellular mechanisms governing genome and cellular integrity from each species[38,347]. Looking at molecular targets we certainly find activation of genes implicated in pre-leukemia in PLAG1-S^{OE} HSPCs, such as IGF2[348],FGFR3[349], ZNF521[285], DLK1[350] and MEG3[351,352] to name just a few. These factors may be operating "in check" under context-dependent control but in the presence of secondary changes in these cells could sway the balance to enforce leukemia. Lastly to this point, abnormal expression of PLAG1 in

combination with 8 more genes, including the cytokine Stem Cell Factor (SCF), was associated with a fatal case of aberrant clonal hematopoiesis induced in non-human primate model[331].

Thus, there are a number of factors to consider in the PLAG1-S-centric discussion of stem cell gene therapy. First there is the obvious matter of context-dependent functions of PLAG1-S. Despite expression and prognosis data that implies endogenous PLAG1 may not significantly contribute to disease burden, direct measurements of the role of PLAG1 in leukemia and specifically LSC maintenance have yet to be performed and would be of value. Possibly more important is the reality that even if endogenous PLAG1 is not frequently dysregulated in clinical manifestations of aberrant hematopoiesis or hematopoietic cancers, this does not preclude the possibility that exogenously introduced PLAG1 could exacerbate cellular characteristics in a pre-leukemic cell[353].

We have already demonstrated evidence that when elevated with a co-factor, in this case USF2, PLAG1 can differentially regulate CB $CD34^+$ growth profiles *ex vivo* and activate MSI2 expression[194], presumably imparting a new set of self-renewal characteristics in those cells (e.g. a different global translation program) compared to when elevated in isolation. Thus, determining leukemia-specific targets of either endogenous or exogenous PLAG1 would be essential for anticipating the spectrum of possible negative outcomes of activating PLAG1 in HSPCs with uncertain genetic backgrounds or pre-existing attrition. For example, leukemic cells are dependent on higher biosynthetic activity than healthy HSC[167], and we did not observe reductions in K562 translation when PLAG1-S was overexpressed, suggesting that this program may somehow be overridden in a PLAG1-driven cancer context. Second, there is the general matter of safety in viral vectors and more cutting-edge gene therapy platforms. Gene delivery by viral (gammaretrovirus, lentivirus, adeno-associated virus) vectors or electroporation of protein, DNA and/or mRNA can all activate innate immune pathways in HSPCs that ultimately impair engraftment potential[354]. A clinical trial to treat SCID-X1 by correcting IL2RG in HSPCs via gammaretrovirus led to a number of cases of insertional oncogenesis[355]. As such, new generations of lentiviruses were developed with the aim of improving the safety and efficacy of viral based gene delivery[356]. To date lentiviruses are the most commonly used delivery system owing to their capacity to transduce non-cycling cell populations, and relatively lower induction of insertional oncogenesis and intracellular immune responses[354]. However, the case study presented by Espinoza *et al*. (2019) that random lentiviral insertions can lead to aberrant and fatal clonal hematopoiesis in a primate highlights a key safety concern even for transient or conditional transgene introductions via lentiviral vectors[331]. To this point, recently clinical trials of lentiviral-based beta-globin correction to treat SCD have been paused because of the onset of several cases of genetic lesions or acute myeloid leukemia. The development of these adverse outcomes spans long time periods (for example one patient was >5 years post-transplant) and the underlying pathophysiology is sometimes poorly understood with both direct or in some cases no traceable connection to the lentivirus[357]. Thus, the potential hazards of transgene introduction transcend even the molecular capacities of that individual target. Recent advances in effectively and safely delivering mRNA in the form of COVID-19 vaccines herald a new era of exciting opportunities for stem cell gene therapy and to translate our discoveries[359,360].

6.8 Translation control in cell therapy.

Altogether our investigation of the role of PLAG1-S in promoting human HSC function supports two emerging paradigms: 1) that dysregulation of protein synthesis is a key clinical demand on human HSC and 2) that its modulation could be leveraged for therapeutic benefit. In

contrast to approaches that ameliorate protein stress, the strategy of targeting translation rates directly might offer the advantage of preventing the cells from experiencing the protein stress. Notably, however, translation regulation requires plasticity and balance to ensure HSC function, thus low levels of translation without achieving this appropriate harmony also underlies hemopoietic defects. For example, heterozygous *Rpl24* mutant murine HSCs show reduced protein synthesis and impaired *in vivo* regeneration while *Pten* deletion activated translation but led to HSC depletion[165]. In human diseases, del(5q) MDS, characterized mainly by macrocytic anemia and megakaryocyte dysplasia with relatively low rates of secondary AML, is associated with haploinsufficiency of *RPS14*. Single allele *Rps14* knockout mouse HSCs recapitulated the erythroid block and displayed age-related expansion of a myeloid-skewed HSC compartment with reduced renewal capacity and induction of p53. Notably while *Rps14* haploinsufficiency reduced translation in all bone marrow factions tested, this effect was most pronounced in erythroid progenitors, possibly explaining pronounced anemia[361]. Similarly, diminished translation due to heterozygous loss of function mutations in a variety of RP genes underlies ribosomopathies such as Schwachman-Diamond syndrome and Diamond-Blackfan anemia[362], where impairment in the selection of translation targets impedes erythroid linage specification[175,363]. Additionally, in mouse HSCs deletion of the *Runx1* TF, which is commonly rendered defective as a result of mutations in MDS and AML, leads to differentiation defects and minor (LSK) HSPC expansion associated with reduced ribosome biogenesis. These cells also have increased resistance to tunicamycin-induced ER stress, which in preliminary experiments we notably did not observe for PLAG1-S^{OE} HSPCs (data not shown). The lack of hematopoietic defects and differences in stress resistance associated with PLAG1-S^{OE} HSPCs and the above examples may be attributed to unresolved and nuanced differences in molecular combinations in these various settings, the most obvious example being differential contribution of p53 signaling.

In general, inhibition of protein biosynthesis has had limited clinical utility due to its high multi-organ toxicity[364,365]. The requirement of handling HSC *ex vivo* for expansion, gene therapy or elimination of cancer stem cells from autologous samples may actually offer a suitable scenario for making the most of targeting translation. Relatively low levels of protein production distinguishes healthy HSCs from LSCs or pre-leukemia MDS stem cells (MDS-SCs)[167,366]. In contrast to the effect of PLAG1-S in promoting HSC function while diminishing translation rates, translation inhibition is a proposed therapeutic target in leukemia as both a single and sensitizing agent[367-371]. Omacetaxine mepesuccinate (OMA) is an FDA-approved drug for the treatment of CML, acts via inhibiting translation elongation[372] and is effective against AML[373]. OMA treatment of primary MDS cells significantly impaired primitive cell viability and engraftment in xenotransplantation while sparing healthy HSC and possibly improving their viability[167]. Treatment of human AML with rocaglamide or silverstrol also selectively eliminated disease-initiating LSC while sparing functional HSC, in part through repressing translation[367]. Neither study demonstrated a functional advantage of treating healthy HSPCs with these translation-targeting compounds, but they do allow for the possibility that there may be an optimized window of timing and dosing of these compounds to enhance HSC preservation in the context of *ex vivo* expansion or gene therapy objectives. With this in mind we attempted pulse treatment of CD34$^+$ cells with omacetaxine mepesuccinate to ameliorate their pro-translation response to *ex vivo* culture. While these experiments did not point to improved hematopoietic cell output there are several considerations for future evaluation:

First, while total CD34$^+$ cells has been a general benchmark to predict HSC content in clinical samples[87,374,375], we have not confirmed (by LDA xenotransplantation) the true HSC

content in the OMA-treated cultures. Of note, Goncalves *et al*. (2016)[174] showed that short-term treatment of angiogenin, an RNase that promotes a state of stress-associated low translation, increases the frequency of HSC in cultured Lin$^-$CD34$^+$ CB cells while decreasing total CD34$^+$ cells in culture, and similar culture profiles were seen with pharmacological inhibition of AKT or mTOR, which also enhanced engraftment in xenotransplantation[230,231,304]. Callahan *et al*. (2014)[367] also demonstrated that treatment of healthy human bone marrow HSCs with rocaglamide can have a subtle negative effect on viability *ex vivo* at high doses but does not impair long-term engraftment, indicating preservation of HSC. A likely explanation for these apparent paradoxes is that the preservation of HSCs in these contexts is the result of restraining their activation to restrict culture-induced differentiation[148,322]. Therefore, *in vivo* xenotransplantation assays may be necessary to properly assess the effect of translation inhibition via OMA on HSC preservation. This also spotlights an interesting contrast in PLAG1-S^{OE} HSPCs, which did not exhibit *in vitro* restraint and displayed elevated absolute hematopoietic engraftment in the injected femur 4 weeks following xenotransplantation. Although we did not assess short-term repopulating units by LDA these findings suggest PLAG1-S could also partially promote short-term progenitors. An intriguing point for future exploration is whether PLAG1-S utilizes dichotomous modes of action in stem vs progenitor cells, as was shown for angiopoietin in murine HSCs[174]. Secondly, Lin$^-$CD34$^+$ cells are highly heterogeneous with a large proportion of lineage-restricted progenitors. Therefore, responses in those cells can largely dilute or confound measurements of the more primitive compartment. Linage-restricted progenitors endogenously rely on higher translation rates[165] and do not amplify their translation rates as drastically as HSCs when cultured[172]. It is therefore possible those abundant cell types may have heightened sensitivity to the toxicity of translation inhibition factors, influencing total cell numbers in these cultures. Starting with a more pure primitive cell population and employing assays with superior capacities to measure self-renewal (namely xenotransplant, but also serial colony assays) may provide greater insights into the efficacy of OMA treatment on preservation or *in vitro* renewal of HSCs. Third, the timing of OMA treatment, similarly to dosage, may require optimization. Extended inhibition of protein synthesis is expected to be cytotoxic in all mammalian cells and we have not tested whether a 24-hour duration exceeds the tolerance of CB HSPC. Stevens *et al*. (2018)[167] treated HSPCs for 3 hours with OMA, which may explain differences in viability seen in our experiment. Another speculation is that the culture-induced translation response may not be completely maladaptive as HSPCs do exhibit some tolerance to manage protein stress[171] and some activation of translation is required to promote hematopoietic regeneration *ex vivo*[165,322]. In this case there may be an advantage to providing the cells with an acclimation phase and subsequently either attenuating the translation peak and/or promoting the restoration of a "dormant" (or *ex vivo*-optimized) translation rate. And lastly, there are many other drugs that interfere with different steps of translation. Endogenously the step of translation under the most regulatory control is translation initiation[376]. To this point, it may be warranted to explore the use of other pharmaceutical agents such as 4EGI-1 which mechanistically blocks eIF4E and eIF4G and encourages the association between 4E-BP1 and eIF4E to inhibit cap-dependent translation initiation[377,378]. Like OMA, rocaglamide and silverstrol, 4EGI-1 is also effective at killing cancer stem cells[379-382], and targeting 4E-BP, a key endogenous regulator of HSC translation rates[332], may therefore have a competitive edge over the use of inhibitors of translation elongation.

In sum, targeting exquisitely regulated protein synthesis and proteostasis in stem cells is far from a trivial endeavour. It continues to be a very compelling and potentially clinically important line of inquiry whether regulated translation control, independently of PLAG1-S

oversight, could improve HSC maintenance or expansion *ex vivo* and in transplantation to help fully realize the potential of HSC-based therapies. Forwarding these goals will benefit from greater fundamental biological insights into the interplay of protein production and stem cell biology.

6.9 Closing remarks:

Decades of work have culminated in our understanding of hematopoiesis as a stem cell-driven regenerative system and highlighted the incredible future potential of HSC to be effectively harnessed for lifesaving treatments of a host of devastating malignancies and immune disorders. The work presented in this thesis provides novel insights into molecular and cellular control mechanisms that govern HSC fitness and integrity. We provide a greater molecular understanding of human HSC biology through identification of PLAG1 as bona fide regulator of HSC long term function, dormancy and self-renewal. Through elucidation of its human HSPC-specific regulon, we demonstrate that PLAG1-S enacts multifaceted and combinatorial programs to limit the expression of protein biosynthetic machinery. In enforcing this mechanism, PLAG1-S endows an *in situ*-like rate of protein production and simultaneously restrains growth, metabolism, proliferation, differentiation and death to ultimately enhance human HSC preservation and function in stimulatory culture and transplantation settings. Our findings support the paradigm and continued research of translation control as a mode of enhancing *ex vivo* stem cell-based therapies. Lastly, our findings underscore that addressing the current deficit in our understanding of translation dynamics and its regulators in human HSCs *in vivo* when subject to demands of disease or injury could substantively inform future HSC-focused regenerative therapies. Altogether, the insights provided in this work are germane to the appreciation of translation control in determining human HSC fate and function but also highlight the promise of exploiting regulators of this fundamental feature of stem cell physiology to enhance regenerative therapies.

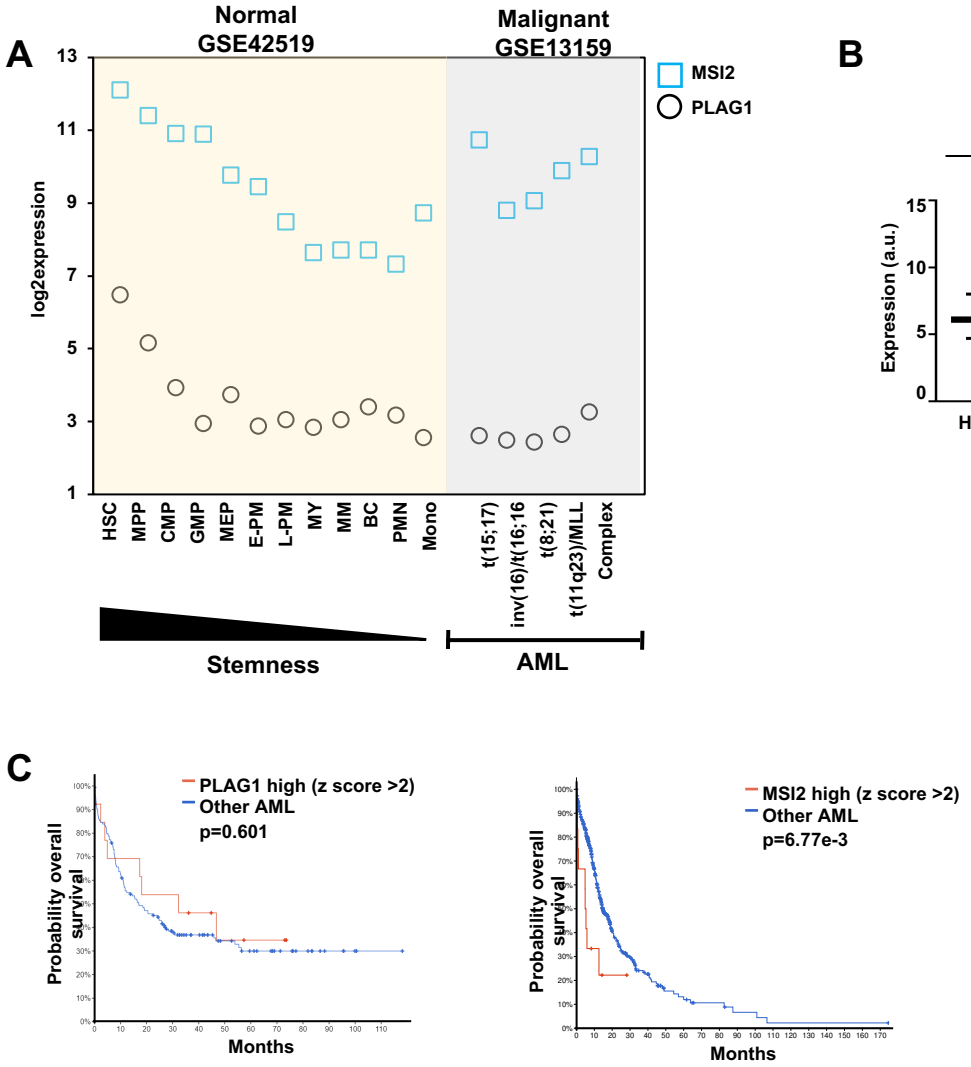
A
Normal
GSE42519
Malignant
GSE13159
MSI2
PLAG1
log2expression
13
11
9
7
5
3
1
HSC
MPP
CMP
GMP
MEP
E-PM
L-PM
MY
MM
BC
PMN
Mono
t(15;17)
inv(16)/t(16;16
t(8;21)
t(11q23)/MLL
Complex
Stemness
AML
B
PLAG1
GSE58831
Expression (a.u.)
15
10
5
0
Healthy
MDS
C
PLAG1 high (z score >2)
Other AML
p=0.601
Probability overall survival
Months
MSI2 high (z score >2)
Other AML
p=6.77e-3
Probability overall survival
Months

Figure 33: PLAG1 and MSI2 expression in leukemia. (A) PLAG1 and MSI2 transcript expression in the normal human hematopoietic hierarchy[383] and patient samples of diverse types of leukemia[309,384]. **(B)** PLAG1 transcript expression in MDS patient samples[385]. **(C)** Survival curves for AML patients stratified by PLAG1 or MSI2 expression[386-388].

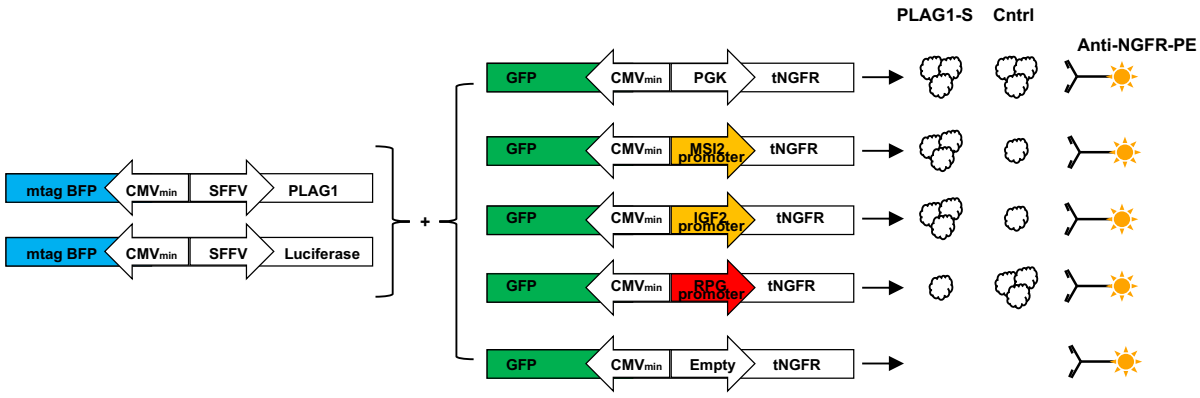
PLAG1-S
Cntrl
Anti-NGFR-PE
mtag BFP
CMVmin
SFFV
PLAG1
mtag BFP
CMVmin
SFFV
Luciferase
+
GFP
CMVmin
PGK
tNGFR
GFP
CMVmin
MSI2 promoter
tNGFR
GFP
CMVmin
IGF2 promoter
tNGFR
GFP
CMVmin
RPG promoter
tNGFR
GFP
CMVmin
Empty
tNGFR

Figure 34: Fluorescence-based reporter assay. Schematic summary of a fluorescence-based reporter assay to validate direct gene expression regulation. Cells will be double transduced to overexpress either PLAG1 or Luciferase along with one of the GFP-expressing reporter constructs. GFP will serve as an internal control of the level of reporter construct introduced into the cell, analogous to renilla in a bioluminescence-based assay. Activation of truncated NGFR which can be detected by flow cytometry using a fluorescent tagged antibody serves as a read out of promoter activation. White and yellow promoter represent built-in controls. The PGK promoter is a positive control independent of PLAG1 or Luciferase. The MSI2 promoter can be used as a positive control in K562[194]. The IGF2 promoter is a likely positive control for PLAG1-S in HSPCs. An empty or unbound and non-activating genomic region can be used as a negative control. Various ribosome gene promoters (red) can be tested for putative direct repression of gene expression.

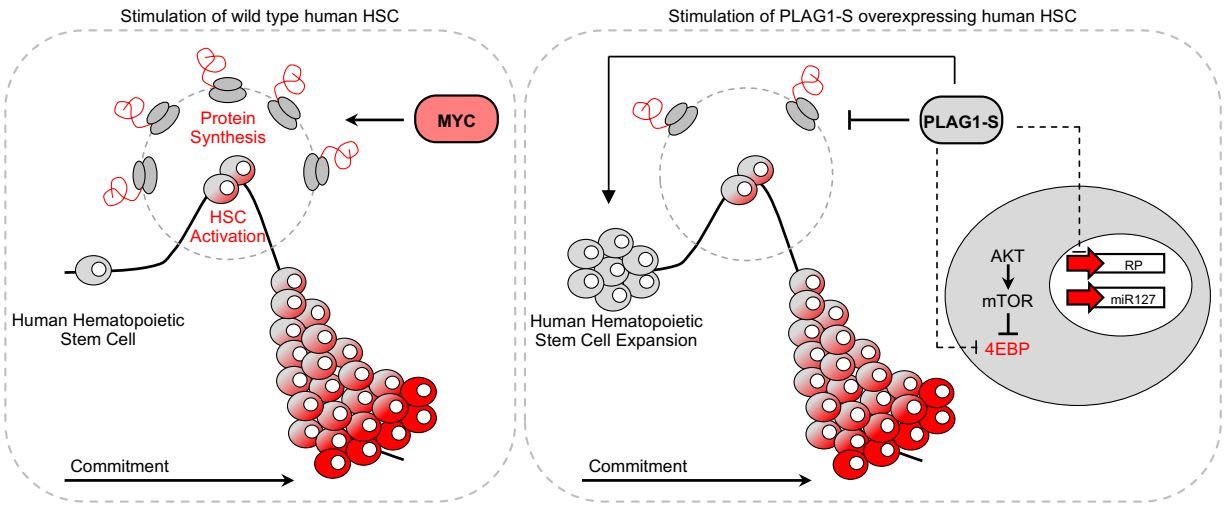
Stimulation of wild type human HSC
Protein Synthesis
MYC
HSC Activation
Human Hematopoietic Stem Cell
Commitment
Stimulation of PLAG1-S overexpressing human HSC
PLAG1-S
AKT
mTOR
4EBP
RP
miR127
Human Hematopoietic Stem Cell Expansion
Commitment

Figure 35: Visual Abstract. Stimulation of CB CD34^{+} HSPC activates protein synthesis promoting loss of dormancy and stemness. Overexpression of PLAG1-S defends HSPC dormancy and HSC stemness by directly modulating the translation machinery via a combination of functional nodes.

BIBLIOGRAPHY

1. Doulatov S, Notta F, Laurenti E, Dick JE. Hematopoiesis: a human perspective. *Cell Stem Cell*. 2012;10(2):120-136.
2. Sykes SM, Scadden DT. Modeling human hematopoietic stem cell biology in the mouse. *Semin Hematol*. 2013;50(2):92-100.
3. Copley MR, Eaves CJ. Developmental changes in hematopoietic stem cell properties. *Exp Mol Med*. 2013;45:e55.
4. Wagner JE. Umbilical cord blood stem cell transplantation. *Am J Pediatr Hematol Oncol*. 1993;15(2):169-174.
5. Eaves CJ. Hematopoietic stem cells: concepts, definitions, and the new reality. *Blood*. 2015;125(17):2605-2613.
6. Weissman IL, Shizuru JA. The origins of the identification and isolation of hematopoietic stem cells, and their capability to induce donor-specific transplantation tolerance and treat autoimmune diseases. *Blood*. 2008;112(9):3543-3553.
7. Appelbaum FR. Hematopoietic-cell transplantation at 50. *N Engl J Med*. 2007;357(15):1472-1475.
8. OSGOOD EE, RIDDLE MC, MATHEWS TJ. APLASTIC ANEMIA TREATED WITH DAILY TRANSFUSIONS AND INTRAVENOUS MARROW; CASE REPORT. Vol. 13: Ann Intern Med; 1939:357-367.
9. Granot N, Storb R. History of hematopoietic cell transplantation: challenges and progress. *Haematologica*. 2020;105(12):2716-2729.
10. JACOBSON LO, MARKS EK. The role of the spleen in radiation injury. *Proc Soc Exp Biol Med*. 1949;70(4):740-742.
11. JACOBSON LO, SIMMONS EL, MARKS EK, ROBSON MJ, BETHARD WF, GASTON EO. The role of the spleen in radiation injury and recovery. *J Lab Clin Med*. 1950;35(5):746-770.
12. LORENZ E, CONGDON C, UPHOFF D. Modification of acute irradiation injury in mice and guinea-pigs by bone marrow injections. *Radiology*. 1952;58(6):863-877.
13. LORENZ E, UPHOFF D, REID TR, SHELTON E. Modification of irradiation injury in mice and guinea pigs by bone marrow injections. *J Natl Cancer Inst*. 1951;12(1):197-201.
14. REKERS PE, COULTER MP, WARREN SL. EFFECT OF TRANSPLANTATION OF BONE MARROW INTO IRRADIATED ANIMALS. Vol. 60: *Arch Surg.*; 1950:635–667.
15. TALBOT JM, GERSTNER HB. Bone Marrow Implants in the Treatment of Radiation Sickness. Vol. Project 21-47-001: USAF School of Aviation Medicine; 1951.
16. NOWELL PC, COLE LJ, HABERMEYER JG, ROAN PL. Growth and continued function of rat marrow cells in x-radiated mice. *Cancer Res*. 1956;16(3):258-261.
17. THOMAS ED, LOCHTE HL, LU WC, FERREBEE JW. Intravenous infusion of bone marrow in patients receiving radiation and chemotherapy. *N Engl J Med*. 1957;257(11):491-496.
18. BARNES DW, CORP MJ, LOUTIT JF, NEAL FE. Treatment of murine leukaemia with X rays and homologous bone marrow; preliminary communication. *Br Med J*. 1956;2(4993):626-627.
19. BARNES DW, LOUTIT JF. Treatment of murine leukaemia with x-rays and homologous bone marrow. II. *Br J Haematol*. 1957;3(3):241-252.
20. Chabannon C, Kuball J, Bondanza A, et al. Hematopoietic stem cell transplantation in its 60s: A platform for cellular therapies. *Sci Transl Med*. 2018;10(436).

21. Ramalho-Santos M, Willenbring H. On the origin of the term "stem cell". *Cell Stem Cell*. 2007;1(1):35-38.
22. Baserga A, Zavagli G. Ferrata's stem cells: an historical review on hemocytoblasts and hemohistioblasts. *Blood Cells*. 1981;7(3):537-545.
23. MCCULLOCH EA, TILL JE. The radiation sensitivity of normal mouse bone marrow cells, determined by quantitative marrow transplantation into irradiated mice. *Radiat Res*. 1960;13:115-125.
24. TILL JE, McCULLOCH EA. A direct measurement of the radiation sensitivity of normal mouse bone marrow cells. *Radiat Res*. 1961;14:213-222.
25. BECKER AJ, McCULLOCH EA, TILL JE. Cytological demonstration of the clonal nature of spleen colonies derived from transplanted mouse marrow cells. *Nature*. 1963;197:452-454.
26. SIMINOVITCH L, MCCULLOCH EA, TILL JE. THE DISTRIBUTION OF COLONY-FORMING CELLS AMONG SPLEEN COLONIES. *J Cell Comp Physiol*. 1963;62:327-336.
27. Wu AM, Till JE, Siminovitch L, McCulloch EA. Cytological evidence for a relationship between normal hemotopoietic colony-forming cells and cells of the lymphoid system. *J Exp Med*. 1968;127(3):455-464.
28. Wu AM, Till JE, Siminovitch L, McCulloch EA. A cytological study of the capacity for differentiation of normal hemopoietic colony-forming cells. *J Cell Physiol*. 1967;69(2):177-184.
29. Worton RG, McCulloch EA, Till JE. Physical separation of hemopoietic stem cells differing in their capacity for self-renewal. *J Exp Med*. 1969;130(1):91-103.
30. Wolf NS, Trentin JJ. Differential proliferation of erythroid and granuloid spleen colonies following sublethal irradiation of the bone marrow donor. *J Cell Physiol*. 1970;75(2):225-229.
31. Magli MC, Iscove NN, Odartchenko N. Transient nature of early haematopoietic spleen colonies. *Nature*. 1982;295(5849):527-529.
32. Zijlmans JM, Visser JW, Laterveer L, et al. The early phase of engraftment after murine blood cell transplantation is mediated by hematopoietic stem cells. *Proc Natl Acad Sci U S A*. 1998;95(2):725-729.
33. Jones RJ, Celano P, Sharkis SJ, Sensenbrenner LL. Two phases of engraftment established by serial bone marrow transplantation in mice. *Blood*. 1989;73(2):397-401.
34. Shen FW, Tung JS, Boyse EA. Further definition of the Ly-5 system. *Immunogenetics*. 1986;24(3):146-149.
35. Spangrude GJ, Weissman IL. Mature T cells generated from single thymic clones are phenotypically and functionally heterogeneous. *J Immunol*. 1988;141(6):1877-1890.
36. Spangrude GJ, Heimfeld S, Weissman IL. Purification and characterization of mouse hematopoietic stem cells. *Science*. 1988;241(4861):58-62.
37. Trevisan M, Iscove NN. Phenotypic analysis of murine long-term hemopoietic reconstituting cells quantitated competitively in vivo and comparison with more advanced colony-forming progeny. *J Exp Med*. 1995;181(1):93-103.
38. Beer PA, Eaves CJ. Modeling Normal and Disordered Human Hematopoiesis. *Trends Cancer*. 2015;1(3):199-210.
39. Muller-Sieburg CE, Whitlock CA, Weissman IL. Isolation of two early B lymphocyte progenitors from mouse marrow: a committed pre-pre-B cell and a clonogenic Thy-1-lo hematopoietic stem cell. *Cell*. 1986;44(4):653-662.

40. Morrison SJ, Lagasse E, Weissman IL. Demonstration that Thy(lo) subsets of mouse bone marrow that express high levels of lineage markers are not significant hematopoietic progenitors. *Blood*. 1994;83(12):3480-3490.
41. Osawa M, Hanada K, Hamada H, Nakauchi H. Long-term lymphohematopoietic reconstitution by a single CD34-low/negative hematopoietic stem cell. *Science*. 1996;273(5272):242-245.
42. Oguro H, Ding L, Morrison SJ. SLAM family markers resolve functionally distinct subpopulations of hematopoietic stem cells and multipotent progenitors. *Cell Stem Cell*. 2013;13(1):102-116.
43. Kiel MJ, Yilmaz OH, Iwashita T, Terhorst C, Morrison SJ. SLAM family receptors distinguish hematopoietic stem and progenitor cells and reveal endothelial niches for stem cells. *Cell*. 2005;121(7):1109-1121.
44. Benveniste P, Frelin C, Janmohamed S, et al. Intermediate-term hematopoietic stem cells with extended but time-limited reconstitution potential. *Cell Stem Cell*. 2010;6(1):48-58.
45. Kamel-Reid S, Dick JE. Engraftment of immune-deficient mice with human hematopoietic stem cells. *Science*. 1988;242(4886):1706-1709.
46. Shultz LD, Schweitzer PA, Christianson SW, et al. Multiple defects in innate and adaptive immunologic function in NOD/LtSz-scid mice. *J Immunol*. 1995;154(1):180-191.
47. Shultz LD, Lyons BL, Burzenski LM, et al. Human lymphoid and myeloid cell development in NOD/LtSz-scid IL2R gamma null mice engrafted with mobilized human hemopoietic stem cells. *J Immunol*. 2005;174(10):6477-6489.
48. Ito M, Hiramatsu H, Kobayashi K, et al. NOD/SCID/gamma(c)(null) mouse: an excellent recipient mouse model for engraftment of human cells. *Blood*. 2002;100(9):3175-3182.
49. Hogan CJ, Shpall EJ, McNulty O, et al. Engraftment and development of human CD34(+)-enriched cells from umbilical cord blood in NOD/LtSz-scid/scid mice. *Blood*. 1997;90(1):85-96.
50. Civin CI, Strauss LC, Brovall C, Fackler MJ, Schwartz JF, Shaper JH. Antigenic analysis of hematopoiesis. III. A hematopoietic progenitor cell surface antigen defined by a monoclonal antibody raised against KG-1a cells. *J Immunol*. 1984;133(1):157-165.
51. Fares I, Chagraoui J, Gareau Y, et al. Cord blood expansion. Pyrimidoindole derivatives are agonists of human hematopoietic stem cell self-renewal. *Science*. 2014;345(6203):1509-1512.
52. Wagner JE, Brunstein CG, Boitano AE, et al. Phase I/II Trial of StemRegenin-1 Expanded Umbilical Cord Blood Hematopoietic Stem Cells Supports Testing as a Stand-Alone Graft. *Cell Stem Cell*. 2016;18(1):144-155.
53. Baum CM, Weissman IL, Tsukamoto AS, Buckle AM, Peault B. Isolation of a candidate human hematopoietic stem-cell population. *Proc Natl Acad Sci U S A*. 1992;89(7):2804-2808.
54. Bhatia M, Wang JC, Kapp U, Bonnet D, Dick JE. Purification of primitive human hematopoietic cells capable of repopulating immune-deficient mice. *Proc Natl Acad Sci U S A*. 1997;94(10):5320-5325.
55. Conneally E, Cashman J, Petzer A, Eaves C. Expansion in vitro of transplantable human cord blood stem cells demonstrated using a quantitative assay of their lympho-myeloid repopulating activity in nonobese diabetic-scid/scid mice. *Proc Natl Acad Sci U S A*. 1997;94(18):9836-9841.

56. Lansdorp PM, Sutherland HJ, Eaves CJ. Selective expression of CD45 isoforms on functional subpopulations of CD34+ hemopoietic cells from human bone marrow. *J Exp Med*. 1990;172(1):363-366.
57. Notta F, Doulatov S, Laurenti E, Poeppl A, Jurisica I, Dick JE. Isolation of single human hematopoietic stem cells capable of long-term multilineage engraftment. *Science*. 2011;333(6039):218-221.
58. Cheng H, Zheng Z, Cheng T. New paradigms on hematopoietic stem cell differentiation. *Protein Cell*. 2020;11(1):34-44.
59. Morrison SJ, Wandycz AM, Hemmati HD, Wright DE, Weissman IL. Identification of a lineage of multipotent hematopoietic progenitors. *Development*. 1997;124(10):1929-1939.
60. Adolfsson J, Borge OJ, Bryder D, et al. Upregulation of Flt3 expression within the bone marrow Lin(-)Sca1(+)c-kit(+) stem cell compartment is accompanied by loss of self-renewal capacity. *Immunity*. 2001;15(4):659-669.
61. Akashi K, Traver D, Miyamoto T, Weissman IL. A clonogenic common myeloid progenitor that gives rise to all myeloid lineages. *Nature*. 2000;404(6774):193-197.
62. Manz MG, Miyamoto T, Akashi K, Weissman IL. Prospective isolation of human clonogenic common myeloid progenitors. *Proc Natl Acad Sci U S A*. 2002;99(18):11872-11877.
63. Kondo M, Weissman IL, Akashi K. Identification of clonogenic common lymphoid progenitors in mouse bone marrow. *Cell*. 1997;91(5):661-672.
64. Kawamoto H, Ohmura K, Fujimoto S, Katsura Y. Emergence of T cell progenitors without B cell or myeloid differentiation potential at the earliest stage of hematopoiesis in the murine fetal liver. *J Immunol*. 1999;162(5):2725-2731.
65. Adolfsson J, Månsson R, Buza-Vidas N, et al. Identification of Flt3+ lympho-myeloid stem cells lacking erythro-megakaryocytic potential a revised road map for adult blood lineage commitment. *Cell*. 2005;121(2):295-306.
66. Månsson R, Hultquist A, Luc S, et al. Molecular evidence for hierarchical transcriptional lineage priming in fetal and adult stem cells and multipotent progenitors. *Immunity*. 2007;26(4):407-419.
67. Welner RS, Pelayo R, Kincade PW. Evolving views on the genealogy of B cells. *Nat Rev Immunol*. 2008;8(2):95-106.
68. Wilson A, Laurenti E, Oser G, et al. Hematopoietic stem cells reversibly switch from dormancy to self-renewal during homeostasis and repair. *Cell*. 2008;135(6):1118-1129.
69. Pietras EM, Reynaud D, Kang YA, et al. Functionally Distinct Subsets of Lineage-Biased Multipotent Progenitors Control Blood Production in Normal and Regenerative Conditions. *Cell Stem Cell*. 2015;17(1):35-46.
70. Sommerkamp P, Romero-Mulero MC, Narr A, et al. Mouse multipotent progenitor 5 cells are located at the interphase between hematopoietic stem and progenitor cells. *Blood*. 2021;137(23):3218-3224.
71. Goardon N, Marchi E, Atzberger A, et al. Coexistence of LMPP-like and GMP-like leukemia stem cells in acute myeloid leukemia. *Cancer Cell*. 2011;19(1):138-152.
72. Doulatov S, Notta F, Eppert K, Nguyen LT, Ohashi PS, Dick JE. Revised map of the human progenitor hierarchy shows the origin of macrophages and dendritic cells in early lymphoid development. *Nat Immunol*. 2010;11(7):585-593.
73. Laurenti E, Doulatov S, Zandi S, et al. The transcriptional architecture of early human hematopoiesis identifies multilevel control of lymphoid commitment. *Nat Immunol*. 2013;14(7):756-763.

74. Notta F, Zandi S, Takayama N, et al. Distinct routes of lineage development reshape the human blood hierarchy across ontogeny. *Science*. 2016;351(6269):aab2116.
75. Velten L, Haas SF, Raffel S, et al. Human haematopoietic stem cell lineage commitment is a continuous process. *Nat Cell Biol*. 2017;19(4):271-281.
76. Karamitros D, Stoilova B, Aboukhalil Z, et al. Single-cell analysis reveals the continuum of human lympho-myeloid progenitor cells. *Nat Immunol*. 2018;19(1):85-97.
77. Keyvani Chahi A, Hope KJ. Hematopoiesis in High Definition: Combining State and Fate Mapping. *Cell Stem Cell*. 2020;27(3):354-355.
78. Ganuza M, Hall T, Obeng EA, McKinney-Freeman S. Clones assemble! The clonal complexity of blood during ontogeny and disease. *Exp Hematol*. 2020;83:35-47.
79. Kester L, van Oudenaarden A. Single-Cell Transcriptomics Meets Lineage Tracing. *Cell Stem Cell*. 2018;23(2):166-179.
80. Wagner DE, Klein AM. Lineage tracing meets single-cell omics: opportunities and challenges. *Nat Rev Genet*. 2020;21(7):410-427.
81. Weinreb C, Rodriguez-Fraticelli A, Camargo FD, Klein AM. Lineage tracing on transcriptional landscapes links state to fate during differentiation. *Science*. 2020;367(6479).
82. Pei W, Shang F, Wang X, et al. Resolving Fates and Single-Cell Transcriptomes of Hematopoietic Stem Cell Clones by PolyloxExpress Barcoding. *Cell Stem Cell*. 2020;27(3):383-395.e388.
83. Lu R, Neff NF, Quake SR, Weissman IL. Tracking single hematopoietic stem cells in vivo using high-throughput sequencing in conjunction with viral genetic barcoding. *Nat Biotechnol*. 2011;29(10):928-933.
84. Weinreb C, Wolock S, Tusi BK, Socolovsky M, Klein AM. Fundamental limits on dynamic inference from single-cell snapshots. *Proc Natl Acad Sci U S A*. 2018;115(10):E2467-E2476.
85. Bowling S, Sritharan D, Osorio FG, et al. An Engineered CRISPR-Cas9 Mouse Line for Simultaneous Readout of Lineage Histories and Gene Expression Profiles in Single Cells. *Cell*. 2020;181(7):1693-1694.
86. Massey JC, Sutton IJ, Ma DDF, Moore JJ. Regenerating Immunotolerance in Multiple Sclerosis with Autologous Hematopoietic Stem Cell Transplant. *Front Immunol*. 2018;9:410.
87. Norkin M, Lazarus HM, Wingard JR. Umbilical cord blood graft enhancement strategies: has the time come to move these into the clinic? *Bone Marrow Transplant*. 2013;48(7):884-889.
88. Broxmeyer HE. Enhancing the efficacy of engraftment of cord blood for hematopoietic cell transplantation. *Transfus Apher Sci*. 2016;54(3):364-372.
89. Danby R, Rocha V. Improving engraftment and immune reconstitution in umbilical cord blood transplantation. *Front Immunol*. 2014;5:68.
90. El-Badawy A, El-Badri N. Clinical Efficacy of Stem Cell Therapy for Diabetes Mellitus: A Meta-Analysis. *PLoS One*. 2016;11(4):e0151938.
91. Lotfy A, Elgamal A, Burdzinska A, et al. Stem cell therapies for autoimmune hepatitis. *Stem Cell Res Ther*. 2021;12(1):386.
92. Talib S, Shepard KA. Unleashing the cure: Overcoming persistent obstacles in the translation and expanded use of hematopoietic stem cell-based therapies. *Stem Cells Transl Med*. 2020;9(4):420-426.
93. Müller AM, Kohrt HE, Cha S, et al. Long-term outcome of patients with metastatic breast cancer treated with high-dose chemotherapy and transplantation of purified autologous hematopoietic stem cells. *Biol Blood Marrow Transplant*. 2012;18(1):125-133.

94. Gragert L, Eapen M, Williams E, et al. HLA match likelihoods for hematopoietic stem-cell grafts in the U.S. registry. *N Engl J Med*. 2014;371(4):339-348.
95. Ballen KK. Is there a best graft source of transplantation in acute myeloid leukemia? *Best Pract Res Clin Haematol*. 2015;28(2-3):147-154.
96. Zhu X, Tang B, Sun Z. Umbilical cord blood transplantation: Still growing and improving. *Stem Cells Transl Med*. 2021;10 Suppl 2:S62-S74.
97. Pineault N, Abu-Khader A. Advances in umbilical cord blood stem cell expansion and clinical translation. *Exp Hematol*. 2015;43(7):498-513.
98. Smith AR, Wagner JE. Alternative haematopoietic stem cell sources for transplantation: place of umbilical cord blood. *Br J Haematol*. 2009;147(2):246-261.
99. Gluckman E, Devergié A, Bourdeau-Esperou H, et al. Transplantation of umbilical cord blood in Fanconi's anemia. *Nouv Rev Fr Hematol*. 1990;32(6):423-425.
100. Gupta AO, Wagner JE. Umbilical Cord Blood Transplants: Current Status and Evolving Therapies. *Front Pediatr*. 2020;8:570282.
101. Miller PH, Knapp DJ, Eaves CJ. Heterogeneity in hematopoietic stem cell populations: implications for transplantation. *Curr Opin Hematol*. 2013;20(4):257-264.
102. Holyoake TL, Nicolini FE, Eaves CJ. Functional differences between transplantable human hematopoietic stem cells from fetal liver, cord blood, and adult marrow. *Exp Hematol*. 1999;27(9):1418-1427.
103. Barker JN, Fei M, Karanes C, et al. Results of a prospective multicentre myeloablative double-unit cord blood transplantation trial in adult patients with acute leukaemia and myelodysplasia. *Br J Haematol*. 2015;168(3):405-412.
104. Barker JN, Weisdorf DJ, DeFor TE, et al. Transplantation of 2 partially HLA-matched umbilical cord blood units to enhance engraftment in adults with hematologic malignancy. *Blood*. 2005;105(3):1343-1347.
105. Boitano AE, Wang J, Romeo R, et al. Aryl hydrocarbon receptor antagonists promote the expansion of human hematopoietic stem cells. *Science*. 2010;329(5997):1345-1348.
106. Mehta RS, Rezvani K, Shpall EJ. Cord Blood Expansion: A Clinical Advance. *J Clin Oncol*. 2019;37(5):363-366.
107. Shpall EJ, Quinones R, Giller R, et al. Transplantation of ex vivo expanded cord blood. *Biol Blood Marrow Transplant*. 2002;8(7):368-376.
108. Delaney C, Varnum-Finney B, Aoyama K, Brashem-Stein C, Bernstein ID. Dose-dependent effects of the Notch ligand Delta1 on ex vivo differentiation and in vivo marrow repopulating ability of cord blood cells. *Blood*. 2005;106(8):2693-2699.
109. Delaney C, Heimfeld S, Brashem-Stein C, Voorhies H, Manger RL, Bernstein ID. Notch-mediated expansion of human cord blood progenitor cells capable of rapid myeloid reconstitution. *Nat Med*. 2010;16(2):232-236.
110. McNiece I, Harrington J, Turney J, Kellner J, Shpall EJ. Ex vivo expansion of cord blood mononuclear cells on mesenchymal stem cells. *Cytotherapy*. 2004;6(4):311-317.
111. de Lima M, McNiece I, Robinson SN, et al. Cord-blood engraftment with ex vivo mesenchymal-cell coculture. *N Engl J Med*. 2012;367(24):2305-2315.
112. Gutman JA, Turtle CJ, Manley TJ, et al. Single-unit dominance after double-unit umbilical cord blood transplantation coincides with a specific CD8+ T-cell response against the nonengrafted unit. *Blood*. 2010;115(4):757-765.

113. de Lima M, McMannis J, Gee A, et al. Transplantation of ex vivo expanded cord blood cells using the copper chelator tetraethylenepentamine: a phase I/II clinical trial. *Bone Marrow Transplant*. 2008;41(9):771-778.
114. Horwitz ME, Chao NJ, Rizzieri DA, et al. Umbilical cord blood expansion with nicotinamide provides long-term multilineage engraftment. *J Clin Invest*. 2014;124(7):3121-3128.
115. Horwitz ME, Wease S, Blackwell B, et al. Phase I/II Study of Stem-Cell Transplantation Using a Single Cord Blood Unit Expanded Ex Vivo With Nicotinamide. *J Clin Oncol*. 2019;37(5):367-374.
116. Goessling W, Allen RS, Guan X, et al. Prostaglandin E2 enhances human cord blood stem cell xenotransplants and shows long-term safety in preclinical nonhuman primate transplant models. *Cell Stem Cell*. 2011;8(4):445-458.
117. Holst J, Watson S, Lord MS, et al. Substrate elasticity provides mechanical signals for the expansion of hemopoietic stem and progenitor cells. *Nat Biotechnol*. 2010;28(10):1123-1128.
118. Bai T, Li J, Sinclair A, et al. Expansion of primitive human hematopoietic stem cells by culture in a zwitterionic hydrogel. *Nat Med*. 2019;25(10):1566-1575.
119. Chaurasia P, Gajzer DC, Schaniel C, D'Souza S, Hoffman R. Epigenetic reprogramming induces the expansion of cord blood stem cells. *J Clin Invest*. 2014;124(6):2378-2395.
120. Schaniel C, Papa L, Meseck ML, et al. Evaluation of a clinical-grade, cryopreserved, ex vivo-expanded stem cell product from cryopreserved primary umbilical cord blood demonstrates multilineage hematopoietic engraftment in mouse xenografts. *Cytotherapy*. 2021;23(9):841-851.
121. Bug G, Gül H, Schwarz K, et al. Valproic acid stimulates proliferation and self-renewal of hematopoietic stem cells. *Cancer Res*. 2005;65(7):2537-2541.
122. De Felice L, Tatarelli C, Mascolo MG, et al. Histone deacetylase inhibitor valproic acid enhances the cytokine-induced expansion of human hematopoietic stem cells. *Cancer Res*. 2005;65(4):1505-1513.
123. Cohen S, Roy J, Lachance S, et al. Hematopoietic stem cell transplantation using single UM171-expanded cord blood: a single-arm, phase 1-2 safety and feasibility study. *Lancet Haematol*. 2020;7(2):e134-e145.
124. Orkin SH, Zon LI. Hematopoiesis: an evolving paradigm for stem cell biology. *Cell*. 2008;132(4):631-644.
125. Kondo M, Wagers AJ, Manz MG, et al. Biology of hematopoietic stem cells and progenitors: implications for clinical application. *Annu Rev Immunol*. 2003;21:759-806.
126. Morrison SJ, Hemmati HD, Wandycz AM, Weissman IL. The purification and characterization of fetal liver hematopoietic stem cells. *Proc Natl Acad Sci U S A*. 1995;92(22):10302-10306.
127. Fleming WH, Alpern EJ, Uchida N, Ikuta K, Spangrude GJ, Weissman IL. Functional heterogeneity is associated with the cell cycle status of murine hematopoietic stem cells. *J Cell Biol*. 1993;122(4):897-902.
128. Bowie MB, McKnight KD, Kent DG, McCaffrey L, Hoodless PA, Eaves CJ. Hematopoietic stem cells proliferate until after birth and show a reversible phase-specific engraftment defect. *J Clin Invest*. 2006;116(10):2808-2816.
129. da Silva CL, Gonçalves R, Porada CD, et al. Differences amid bone marrow and cord blood hematopoietic stem/progenitor cell division kinetics. *J Cell Physiol*. 2009;220(1):102-111.
130. Nakamura-Ishizu A, Takizawa H, Suda T. The analysis, roles and regulation of quiescence in hematopoietic stem cells. *Development*. 2014;141(24):4656-4666.

131. Singh S, Jakubison B, Keller JR. Protection of hematopoietic stem cells from stress-induced exhaustion and aging. *Curr Opin Hematol*. 2020;27(4):225-231.
132. Trumpp A, Essers M, Wilson A. Awakening dormant haematopoietic stem cells. *Nat Rev Immunol*. 2010;10(3):201-209.
133. Cheshier SH, Morrison SJ, Liao X, Weissman IL. In vivo proliferation and cell cycle kinetics of long-term self-renewing hematopoietic stem cells. *Proc Natl Acad Sci U S A*. 1999;96(6):3120-3125.
134. Passegué E, Wagers AJ, Giuriato S, Anderson WC, Weissman IL. Global analysis of proliferation and cell cycle gene expression in the regulation of hematopoietic stem and progenitor cell fates. *J Exp Med*. 2005;202(11):1599-1611.
135. Hodgson GS, Bradley TR, Radley JM. The organization of hemopoietic tissue as inferred from the effects of 5-fluorouracil. *Exp Hematol*. 1982;10(1):26-35.
136. Randall TD, Weissman IL. Phenotypic and functional changes induced at the clonal level in hematopoietic stem cells after 5-fluorouracil treatment. *Blood*. 1997;89(10):3596-3606.
137. Foudi A, Hochedlinger K, Van Buren D, et al. Analysis of histone 2B-GFP retention reveals slowly cycling hematopoietic stem cells. *Nat Biotechnol*. 2009;27(1):84-90.
138. Kiel MJ, He S, Ashkenazi R, et al. Haematopoietic stem cells do not asymmetrically segregate chromosomes or retain BrdU. *Nature*. 2007;449(7159):238-242.
139. Laurenti E, Frelin C, Xie S, et al. CDK6 levels regulate quiescence exit in human hematopoietic stem cells. *Cell Stem Cell*. 2015;16(3):302-313.
140. Catlin SN, Busque L, Gale RE, Guttorp P, Abkowitz JL. The replication rate of human hematopoietic stem cells in vivo. *Blood*. 2011;117(17):4460-4466.
141. Abkowitz JL, Catlin SN, McCallie MT, Guttorp P. Evidence that the number of hematopoietic stem cells per animal is conserved in mammals. *Blood*. 2002;100(7):2665-2667.
142. Mahmud N, Devine SM, Weller KP, et al. The relative quiescence of hematopoietic stem cells in nonhuman primates. *Blood*. 2001;97(10):3061-3068.
143. Mohrin M, Bourke E, Alexander D, et al. Hematopoietic stem cell quiescence promotes error-prone DNA repair and mutagenesis. *Cell Stem Cell*. 2010;7(2):174-185.
144. Milyavsky M, Gan OI, Trottier M, et al. A distinctive DNA damage response in human hematopoietic stem cells reveals an apoptosis-independent role for p53 in self-renewal. *Cell Stem Cell*. 2010;7(2):186-197.
145. Simsek T, Kocabas F, Zheng J, et al. The distinct metabolic profile of hematopoietic stem cells reflects their location in a hypoxic niche. *Cell Stem Cell*. 2010;7(3):380-390.
146. Takubo K, Nagamatsu G, Kobayashi CI, et al. Regulation of glycolysis by Pdk functions as a metabolic checkpoint for cell cycle quiescence in hematopoietic stem cells. *Cell Stem Cell*. 2013;12(1):49-61.
147. Kohli L, Passegué E. Surviving change: the metabolic journey of hematopoietic stem cells. *Trends Cell Biol*. 2014;24(8):479-487.
148. Cabezas-Wallscheid N, Buettner F, Sommerkamp P, et al. Vitamin A-Retinoic Acid Signaling Regulates Hematopoietic Stem Cell Dormancy. *Cell*. 2017;169(5):807-823.e819.
149. Umemoto T, Hashimoto M, Matsumura T, Nakamura-Ishizu A, Suda T. Ca. *J Exp Med*. 2018;215(8):2097-2113.
150. Liang R, Arif T, Kalmykova S, et al. Restraining Lysosomal Activity Preserves Hematopoietic Stem Cell Quiescence and Potency. *Cell Stem Cell*. 2020;26(3):359-376.e357.

151. Norddahl GL, Pronk CJ, Wahlestedt M, et al. Accumulating mitochondrial DNA mutations drive premature hematopoietic aging phenotypes distinct from physiological stem cell aging. *Cell Stem Cell*. 2011;8(5):499-510.
152. García-Prat L, Kaufmann KB, Schneiter F, et al. Dichotomous regulation of lysosomes by MYC and TFEB controls hematopoietic stem cell fate. *bioRxiv*. 2021:2021.2002.2024.432720.
153. Glimm H, Oh IH, Eaves CJ. Human hematopoietic stem cells stimulated to proliferate in vitro lose engraftment potential during their S/G(2)/M transit and do not reenter G(0). *Blood*. 2000;96(13):4185-4193.
154. Szilvassy SJ, Meyerrose TE, Grimes B. Effects of cell cycle activation on the short-term engraftment properties of ex vivo expanded murine hematopoietic cells. *Blood*. 2000;95(9):2829-2837.
155. Qiu J, Gjini J, Arif T, Moore K, Lin M, Ghaffari S. Using mitochondrial activity to select for potent human hematopoietic stem cells. *Blood Adv*. 2021;5(6):1605-1616.
156. Gan B, Hu J, Jiang S, et al. Lkb1 regulates quiescence and metabolic homeostasis of haematopoietic stem cells. *Nature*. 2010;468(7324):701-704.
157. Kocabas F, Zheng J, Thet S, et al. Meis1 regulates the metabolic phenotype and oxidant defense of hematopoietic stem cells. *Blood*. 2012;120(25):4963-4972.
158. Papa L, Djedaini M, Hoffman R. Ex vivo HSC expansion challenges the paradigm of unidirectional human hematopoiesis. *Ann N Y Acad Sci*. 2020;1466(1):39-50.
159. Oedekoven CA, Belmonte M, Bode D, et al. Hematopoietic stem cells retain functional potential and molecular identity in hibernation cultures. *Stem Cell Reports*. 2021;16(6):1614-1628.
160. Luchsinger LL, Strikoudis A, Danzl NM, et al. Harnessing Hematopoietic Stem Cell Low Intracellular Calcium Improves Their Maintenance In Vitro. *Cell Stem Cell*. 2019;25(2):225-240.e227.
161. Kaufmann KB, Zeng AGX, Coyaud E, et al. A latent subset of human hematopoietic stem cells resists regenerative stress to preserve stemness. *Nat Immunol*. 2021;22(6):723-734.
162. Xie SZ, Garcia-Prat L, Voisin V, et al. Sphingolipid Modulation Activates Proteostasis Programs to Govern Human Hematopoietic Stem Cell Self-Renewal. *Cell Stem Cell*. 2019;25(5):639-653.e637.
163. Lloyd AC. The regulation of cell size. *Cell*. 2013;154(6):1194-1205.
164. Polymenis M, Aramayo R. Translate to divide: control of the cell cycle by protein synthesis. *Microb Cell*. 2015;2(4):94-104.
165. Signer RA, Magee JA, Salic A, Morrison SJ. Haematopoietic stem cells require a highly regulated protein synthesis rate. *Nature*. 2014;509(7498):49-54.
166. Magee JA, Signer RAJ. Developmental Stage-Specific Changes in Protein Synthesis Differentially Sensitize Hematopoietic Stem Cells and Erythroid Progenitors to Impaired Ribosome Biogenesis. *Stem Cell Reports*. 2021;16(1):20-28.
167. Stevens BM, Khan N, D'Alessandro A, et al. Characterization and targeting of malignant stem cells in patients with advanced myelodysplastic syndromes. *Nat Commun*. 2018;9(1):3694.
168. Hidalgo San Jose L, Sunshine MJ, Dillingham CH, et al. Modest Declines in Proteome Quality Impair Hematopoietic Stem Cell Self-Renewal. *Cell Rep*. 2020;30(1):69-80.e66.
169. Miharada K, Sigurdsson V, Karlsson S. Dppa5 improves hematopoietic stem cell activity by reducing endoplasmic reticulum stress. *Cell Rep*. 2014;7(5):1381-1392.

170. van Galen P, Kreso A, Mbong N, et al. The unfolded protein response governs integrity of the haematopoietic stem-cell pool during stress. *Nature*. 2014;510(7504):268-272.
171. van Galen P, Mbong N, Kreso A, et al. Integrated Stress Response Activity Marks Stem Cells in Normal Hematopoiesis and Leukemia. *Cell Rep*. 2018;25(5):1109-1117.e1105.
172. Kruta M, Sunshine MJ, Chua BA, et al. Hsf1 promotes hematopoietic stem cell fitness and proteostasis in response to ex vivo culture stress and aging. *Cell Stem Cell*. 2021.
173. Llorens-Bobadilla E, Zhao S, Baser A, Saiz-Castro G, Zwadlo K, Martin-Villalba A. Single-Cell Transcriptomics Reveals a Population of Dormant Neural Stem Cells that Become Activated upon Brain Injury. *Cell Stem Cell*. 2015;17(3):329-340.
174. Goncalves KA, Silberstein L, Li S, et al. Angiogenin Promotes Hematopoietic Regeneration by Dichotomously Regulating Quiescence of Stem and Progenitor Cells. *Cell*. 2016;166(4):894-906.
175. Khajuria RK, Munschauer M, Ulirsch JC, et al. Ribosome Levels Selectively Regulate Translation and Lineage Commitment in Human Hematopoiesis. *Cell*. 2018;173(1):90-103.e119.
176. Raiser DM, Narla A, Ebert BL. The emerging importance of ribosomal dysfunction in the pathogenesis of hematologic disorders. *Leuk Lymphoma*. 2014;55(3):491-500.
177. Teng T, Thomas G, Mercer CA. Growth control and ribosomopathies. *Curr Opin Genet Dev*. 2013;23(1):63-71.
178. Antonchuk J, Sauvageau G, Humphries RK. HOXB4-induced expansion of adult hematopoietic stem cells ex vivo. *Cell*. 2002;109(1):39-45.
179. Buske C, Feuring-Buske M, Abramovich C, et al. Deregulated expression of HOXB4 enhances the primitive growth activity of human hematopoietic cells. *Blood*. 2002;100(3):862-868.
180. Amsellem S, Pflumio F, Bardinet D, et al. Ex vivo expansion of human hematopoietic stem cells by direct delivery of the HOXB4 homeoprotein. *Nat Med*. 2003;9(11):1423-1427.
181. Hope KJ, Cellot S, Ting SB, et al. An RNAi screen identifies Msi2 and Prox1 as having opposite roles in the regulation of hematopoietic stem cell activity. *Cell Stem Cell*. 2010;7(1):101-113.
182. Rentas S, Holzapfel N, Belew MS, et al. Musashi-2 attenuates AHR signalling to expand human haematopoietic stem cells. *Nature*. 2016;532(7600):508-511.
183. Taggart J, Ho TC, Amin E, et al. MSI2 is required for maintaining activated myelodysplastic syndrome stem cells. *Nat Commun*. 2016;7:10739.
184. Byers RJ, Currie T, Tholouli E, Rodig SJ, Kutok JL. MSI2 protein expression predicts unfavorable outcome in acute myeloid leukemia. *Blood*. 2011;118(10):2857-2867.
185. Palacios F, Yan XJ, Ferrer G, et al. Musashi 2 influences chronic lymphocytic leukemia cell survival and growth making it a potential therapeutic target. *Leukemia*. 2021;35(4):1037-1052.
186. Park SM, Deering RP, Lu Y, et al. Musashi-2 controls cell fate, lineage bias, and TGF-β signaling in HSCs. *J Exp Med*. 2014;211(1):71-87.
187. Kharas MG, Lengner CJ, Al-Shahrour F, et al. Musashi-2 regulates normal hematopoiesis and promotes aggressive myeloid leukemia. *Nat Med*. 2010;16(8):903-908.
188. Han Y, Ye A, Zhang Y, et al. Musashi-2 Silencing Exerts Potent Activity against Acute Myeloid Leukemia and Enhances Chemosensitivity to Daunorubicin. *PLoS One*. 2015;10(8):e0136484.
189. Park SM, Gönen M, Vu L, et al. Musashi2 sustains the mixed-lineage leukemia-driven stem cell regulatory program. *J Clin Invest*. 2015;125(3):1286-1298.

190. Aly RM, Ghazy HF. Prognostic significance of MSI2 predicts unfavorable outcome in adult B-acute lymphoblastic leukemia. *Int J Lab Hematol*. 2015;37(2):272-278.
191. Zhao HZ, Jia M, Luo ZB, et al. Prognostic significance of the Musashi-2 (MSI2) gene in childhood acute lymphoblastic leukemia. *Neoplasma*. 2016;63(1):150-157.
192. Hattori A, McSkimming D, Kannan N, Ito T. RNA binding protein MSI2 positively regulates FLT3 expression in myeloid leukemia. *Leuk Res*. 2017;54:47-54.
193. Kaeda J, Ringel F, Oberender C, et al. Up-regulated MSI2 is associated with more aggressive chronic myeloid leukemia. *Leuk Lymphoma*. 2015;56(7):2105-2113.
194. Belew MS, Bhatia S, Keyvani Chahi A, Rentas S, Draper JS, Hope KJ. PLAG1 and USF2 Co-regulate Expression of Musashi-2 in Human Hematopoietic Stem and Progenitor Cells. *Stem Cell Reports*. 2018;10(4):1384-1397.
195. Giannola DM, Shlomchik WD, Jegathesan M, et al. Hematopoietic expression of HOXB4 is regulated in normal and leukemic stem cells through transcriptional activation of the HOXB4 promoter by upstream stimulating factor (USF)-1 and USF-2. *J Exp Med*. 2000;192(10):1479-1490.
196. Zhu J, Giannola DM, Zhang Y, Rivera AJ, Emerson SG. NF-Y cooperates with USF1/2 to induce the hematopoietic expression of HOXB4. *Blood*. 2003;102(7):2420-2427.
197. Van Dyck F, Declercq J, Braem CV, Van de Ven WJ. PLAG1, the prototype of the PLAG gene family: versatility in tumour development (review). *Int J Oncol*. 2007;30(4):765-774.
198. Kas K, Voz ML, Röijer E, et al. Promoter swapping between the genes for a novel zinc finger protein and beta-catenin in pleiomorphic adenomas with t(3;8)(p21;q12) translocations. *Nat Genet*. 1997;15(2):170-174.
199. Voz ML, Aström AK, Kas K, Mark J, Stenman G, Van de Ven WJ. The recurrent translocation t(5;8)(p13;q12) in pleomorphic adenomas results in upregulation of PLAG1 gene expression under control of the LIFR promoter. *Oncogene*. 1998;16(11):1409-1416.
200. Aström AK, Voz ML, Kas K, et al. Conserved mechanism of PLAG1 activation in salivary gland tumors with and without chromosome 8q12 abnormalities: identification of SII as a new fusion partner gene. *Cancer Res*. 1999;59(4):918-923.
201. Juma AR, Damdimopoulou PE, Grommen SV, Van de Ven WJ, De Groef B. Emerging role of PLAG1 as a regulator of growth and reproduction. *J Endocrinol*. 2016;228(2):R45-56.
202. Voz ML, Mathys J, Hensen K, et al. Microarray screening for target genes of the proto-oncogene PLAG1. *Oncogene*. 2004;23(1):179-191.
203. Declercq J, Van Dyck F, Braem CV, et al. Salivary gland tumors in transgenic mice with targeted PLAG1 proto-oncogene overexpression. *Cancer Res*. 2005;65(11):4544-4553.
204. Declercq J, Van Dyck F, Van Damme B, Van de Ven WJ. Upregulation of Igf and Wnt signalling associated genes in pleomorphic adenomas of the salivary glands in PLAG1 transgenic mice. *Int J Oncol*. 2008;32(5):1041-1047.
205. Voz ML, Agten NS, Van de Ven WJ, Kas K. PLAG1, the main translocation target in pleomorphic adenoma of the salivary glands, is a positive regulator of IGF-II. *Cancer Res*. 2000;60(1):106-113.
206. Zatkova A, Rouillard JM, Hartmann W, et al. Amplification and overexpression of the IGF2 regulator PLAG1 in hepatoblastoma. *Genes Chromosomes Cancer*. 2004;39(2):126-137.
207. Hensen K, Van Valckenborgh IC, Kas K, Van de Ven WJ, Voz ML. The tumorigenic diversity of the three PLAG family members is associated with different DNA binding capacities. *Cancer Res*. 2002;62(5):1510-1517.

208. Samani AA, Yakar S, LeRoith D, Brodt P. The role of the IGF system in cancer growth and metastasis: overview and recent insights. *Endocr Rev*. 2007;28(1):20-47.
209. Hensen K, Braem C, Declercq J, et al. Targeted disruption of the murine Plag1 proto-oncogene causes growth retardation and reduced fertility. *Dev Growth Differ*. 2004;46(5):459-470.
210. Abi Habib W, Brioude F, Edouard T, et al. Genetic disruption of the oncogenic HMGA2-PLAG1-IGF2 pathway causes fetal growth restriction. *Genet Med*. 2018;20(2):250-258.
211. Matsumoto A, Takeishi S, Kanie T, et al. p57 is required for quiescence and maintenance of adult hematopoietic stem cells. *Cell Stem Cell*. 2011;9(3):262-271.
212. Zou P, Yoshihara H, Hosokawa K, et al. p57(Kip2) and p27(Kip1) cooperate to maintain hematopoietic stem cell quiescence through interactions with Hsc70. *Cell Stem Cell*. 2011;9(3):247-261.
213. Venkatraman A, He XC, Thorvaldsen JL, et al. Maternal imprinting at the H19-Igf2 locus maintains adult haematopoietic stem cell quiescence. *Nature*. 2013;500(7462):345-349.
214. Qian P, He XC, Paulson A, et al. The Dlk1-Gtl2 Locus Preserves LT-HSC Function by Inhibiting the PI3K-mTOR Pathway to Restrict Mitochondrial Metabolism. *Cell Stem Cell*. 2016;18(2):214-228.
215. Cheng NC, van de Vrugt HJ, van der Valk MA, et al. Mice with a targeted disruption of the Fanconi anemia homolog Fanca. *Hum Mol Genet*. 2000;9(12):1805-1811.
216. Bakker ST, de Winter JP, te Riele H. Learning from a paradox: recent insights into Fanconi anaemia through studying mouse models. *Dis Model Mech*. 2013;6(1):40-47.
217. Walne AJ, Dokal I. Advances in the understanding of dyskeratosis congenita. *Br J Haematol*. 2009;145(2):164-172.
218. Alexander WS, Roberts AW, Nicola NA, Li R, Metcalf D. Deficiencies in progenitor cells of multiple hematopoietic lineages and defective megakaryocytopoiesis in mice lacking the thrombopoietic receptor c-Mpl. *Blood*. 1996;87(6):2162-2170.
219. Kimura S, Roberts AW, Metcalf D, Alexander WS. Hematopoietic stem cell deficiencies in mice lacking c-Mpl, the receptor for thrombopoietin. *Proc Natl Acad Sci U S A*. 1998;95(3):1195-1200.
220. King S, Germeshausen M, Strauss G, Welte K, Ballmaier M. Congenital amegakaryocytic thrombocytopenia: a retrospective clinical analysis of 20 patients. *Br J Haematol*. 2005;131(5):636-644.
221. McGowan KA, Li JZ, Park CY, et al. Ribosomal mutations cause p53-mediated dark skin and pleiotropic effects. *Nat Genet*. 2008;40(8):963-970.
222. Devlin EE, Dacosta L, Mohandas N, Elliott G, Bodine DM. A transgenic mouse model demonstrates a dominant negative effect of a point mutation in the RPS19 gene associated with Diamond-Blackfan anemia. *Blood*. 2010;116(15):2826-2835.
223. Grenda DS, Johnson SE, Mayer JR, et al. Mice expressing a neutrophil elastase mutation derived from patients with severe congenital neutropenia have normal granulopoiesis. *Blood*. 2002;100(9):3221-3228.
224. Peckl-Schmid D, Wolkerstorfer S, Königsberger S, et al. HAX1 deficiency: impact on lymphopoiesis and B-cell development. *Eur J Immunol*. 2010;40(11):3161-3172.
225. Conley ME, Rohrer J, Rapalus L, Boylin EC, Minegishi Y. Defects in early B-cell development: comparing the consequences of abnormalities in pre-BCR signaling in the human and the mouse. *Immunol Rev*. 2000;178:75-90.

226. Fellmann C, Hoffmann T, Sridhar V, et al. An optimized microRNA backbone for effective single-copy RNAi. *Cell Rep*. 2013;5(6):1704-1713.
227. Moffat J, Grueneberg DA, Yang X, et al. A lentiviral RNAi library for human and mouse genes applied to an arrayed viral high-content screen. *Cell*. 2006;124(6):1283-1298.
228. Gentner B, Schira G, Giustacchini A, et al. Stable knockdown of microRNA in vivo by lentiviral vectors. *Nat Methods*. 2009;6(1):63-66.
229. Lechman ER, Gentner B, van Galen P, et al. Attenuation of miR-126 activity expands HSC in vivo without exhaustion. *Cell Stem Cell*. 2012;11(6):799-811.
230. Chen S, Gao R, Kobayashi M, et al. Pharmacological inhibition of AKT activity in human CD34. *Exp Hematol*. 2017;45:74-84.
231. Rohrabaugh SL, Campbell TB, Hangoc G, Broxmeyer HE. Ex vivo rapamycin treatment of human cord blood CD34+ cells enhances their engraftment of NSG mice. *Blood Cells Mol Dis*. 2011;46(4):318-320.
232. Hu Y, Smyth GK. ELDA: extreme limiting dilution analysis for comparing depleted and enriched populations in stem cell and other assays. *J Immunol Methods*. 2009;347(1-2):70-78.
233. Colvin GA, Lambert JF, Abedi M, et al. Murine marrow cellularity and the concept of stem cell competition: geographic and quantitative determinants in stem cell biology. *Leukemia*. 2004;18(3):575-583.
234. Rentas S, Holzapfel NT, Belew MS, et al. Musashi-2 attenuates AHR signalling to expand human haematopoietic stem cells. *Nature*. 2016;532(7600):508-511.
235. Kim D, Langmead B, Salzberg SL. HISAT: a fast spliced aligner with low memory requirements. *Nat Methods*. 2015;12(4):357-360.
236. Li H, Handsaker B, Wysoker A, et al. The Sequence Alignment/Map format and SAMtools. *Bioinformatics*. 2009;25(16):2078-2079.
237. Ramírez F, Ryan DP, Grüning B, et al. deepTools2: a next generation web server for deep-sequencing data analysis. *Nucleic Acids Res*. 2016;44(W1):W160-165.
238. Feng J, Liu T, Zhang Y. Using MACS to identify peaks from ChIP-Seq data. *Curr Protoc Bioinformatics*. 2011;Chapter 2:Unit 2.14.
239. Quinlan AR, Hall IM. BEDTools: a flexible suite of utilities for comparing genomic features. *Bioinformatics*. 2010;26(6):841-842.
240. Heinz S, Benner C, Spann N, et al. Simple combinations of lineage-determining transcription factors prime cis-regulatory elements required for macrophage and B cell identities. *Mol Cell*. 2010;38(4):576-589.
241. Yu G, Wang LG, He QY. ChIPseeker: an R/Bioconductor package for ChIP peak annotation, comparison and visualization. *Bioinformatics*. 2015;31(14):2382-2383.
242. Yu G, Wang LG, Han Y, He QY. clusterProfiler: an R package for comparing biological themes among gene clusters. *OMICS*. 2012;16(5):284-287.
243. Skene PJ, Henikoff JG, Henikoff S. Targeted in situ genome-wide profiling with high efficiency for low cell numbers. *Nat Protoc*. 2018;13(5):1006-1019.
244. Chen S, Zhou Y, Chen Y, Gu J. fastp: an ultra-fast all-in-one FASTQ preprocessor. *Bioinformatics*. 2018;34(17):i884-i890.
245. Langmead B, Salzberg SL. Fast gapped-read alignment with Bowtie 2. *Nat Methods*. 2012;9(4):357-359.
246. Zhang Y, Liu T, Meyer CA, et al. Model-based analysis of ChIP-Seq (MACS). *Genome Biol*. 2008;9(9):R137.

247. Raudvere U, Kolberg L, Kuzmin I, et al. g:Profiler: a web server for functional enrichment analysis and conversions of gene lists (2019 update). *Nucleic Acids Res*. 2019;47(W1):W191-W198.
248. Novershtern N, Subramanian A, Lawton LN, et al. Densely interconnected transcriptional circuits control cell states in human hematopoiesis. *Cell*. 2011;144(2):296-309.
249. Amon S, Meier-Abt F, Gillet LC, et al. Sensitive Quantitative Proteomics of Human Hematopoietic Stem and Progenitor Cells by Data-independent Acquisition Mass Spectrometry. *Mol Cell Proteomics*. 2019;18(7):1454-1467.
250. Cabezas-Wallscheid N, Klimmeck D, Hansson J, et al. Identification of regulatory networks in HSCs and their immediate progeny via integrated proteome, transcriptome, and DNA methylome analysis. *Cell Stem Cell*. 2014;15(4):507-522.
251. Pellin D, Loperfido M, Baricordi C, et al. A comprehensive single cell transcriptional landscape of human hematopoietic progenitors. *Nat Commun*. 2019;10(1):2395.
252. Hay SB, Ferchen K, Chetal K, Grimes HL, Salomonis N. The Human Cell Atlas bone marrow single-cell interactive web portal. *Exp Hematol*. 2018;68:51-61.
253. Dircio-Maldonado R, Flores-Guzman P, Corral-Navarro J, et al. Functional Integrity and Gene Expression Profiles of Human Cord Blood-Derived Hematopoietic Stem and Progenitor Cells Generated In Vitro. *Stem Cells Transl Med*. 2018;7(8):602-614.
254. Amendola M, Venneri MA, Biffi A, Vigna E, Naldini L. Coordinate dual-gene transgenesis by lentiviral vectors carrying synthetic bidirectional promoters. *Nat Biotechnol*. 2005;23(1):108-116.
255. Kas K, Voz ML, Hensen K, Meyen E, Van de Ven WJ. Transcriptional activation capacity of the novel PLAG family of zinc finger proteins. *J Biol Chem*. 1998;273(36):23026-23032.
256. Skene PJ, Henikoff S. An efficient targeted nuclease strategy for high-resolution mapping of DNA binding sites. *Elife*. 2017;6.
257. Wong J, Damdimopoulos A, Damdimopoulou P, et al. Transcriptome analysis of the epididymis from Plag1 deficient mice suggests dysregulation of sperm maturation and extracellular matrix genes. *Dev Dyn*. 2020;249(12):1500-1513.
258. Musallam KM, Taher AT, Cappellini MD, Sankaran VG. Clinical experience with fetal hemoglobin induction therapy in patients with β-thalassemia. *Blood*. 2013;121(12):2199-2212; quiz 2372.
259. Abraham AA, Tisdale JF. Gene therapy for sickle cell disease: moving from the bench to the bedside. *Blood*. 2021;138(11):932-941.
260. Blanco S, Bandiera R, Popis M, et al. Stem cell function and stress response are controlled by protein synthesis. *Nature*. 2016;534(7607):335-340.
261. Sampath P, Pritchard DK, Pabon L, et al. A hierarchical network controls protein translation during murine embryonic stem cell self-renewal and differentiation. *Cell Stem Cell*. 2008;2(5):448-460.
262. Zismanov V, Chichkov V, Colangelo V, et al. Phosphorylation of eIF2α Is a Translational Control Mechanism Regulating Muscle Stem Cell Quiescence and Self-Renewal. *Cell Stem Cell*. 2016;18(1):79-90.
263. Sanchez CG, Teixeira FK, Czech B, et al. Regulation of Ribosome Biogenesis and Protein Synthesis Controls Germline Stem Cell Differentiation. *Cell Stem Cell*. 2016;18(2):276-290.

264. Hidalgo San Jose L, Signer RAJ. Cell-type-specific quantification of protein synthesis in vivo. *Nat Protoc*. 2019;14(2):441-460.
265. Liu J, Xu Y, Stoleru D, Salic A. Imaging protein synthesis in cells and tissues with an alkyne analog of puromycin. *Proc Natl Acad Sci U S A*. 2012;109(2):413-418.
266. Cook M, Tyers M. Size control goes global. *Curr Opin Biotechnol*. 2007;18(4):341-350.
267. Schmoller KM, Skotheim JM. The Biosynthetic Basis of Cell Size Control. *Trends Cell Biol*. 2015;25(12):793-802.
268. Yamamoto K, Mak TW. Mechanistic aspects of mammalian cell size control. *Dev Growth Differ*. 2017;59(1):33-40.
269. Donati G, Montanaro L, Derenzini M. Ribosome biogenesis and control of cell proliferation: p53 is not alone. *Cancer Res*. 2012;72(7):1602-1607.
270. Lengefeld J, Cheng C-W, Maretich P, et al. Cell size is a determinant of stem cell potential during aging. *bioRxiv*. 2020:2020.2010.2027.355388.
271. Sriskanthadevan S, Jeyaraju DV, Chung TE, et al. AML cells have low spare reserve capacity in their respiratory chain that renders them susceptible to oxidative metabolic stress. *Blood*. 2015;125(13):2120-2130.
272. Golomb L, Volarevic S, Oren M. p53 and ribosome biogenesis stress: the essentials. *FEBS Lett*. 2014;588(16):2571-2579.
273. Nii T, Marumoto T, Tani K. Roles of p53 in various biological aspects of hematopoietic stem cells. *J Biomed Biotechnol*. 2012;2012:903435.
274. Han J, Back SH, Hur J, et al. ER-stress-induced transcriptional regulation increases protein synthesis leading to cell death. *Nat Cell Biol*. 2013;15(5):481-490.
275. Thoren LA, Fog CK, Jensen KT, et al. PRDM11 is dispensable for the maintenance and function of hematopoietic stem and progenitor cells. *Stem Cell Res*. 2013;11(3):1129-1136.
276. Fog CK, Asmar F, Côme C, et al. Loss of PRDM11 promotes MYC-driven lymphomagenesis. *Blood*. 2015;125(8):1272-1281.
277. Zheng Y, Zhang H, Wang Y, et al. Loss of Dnmt3b accelerates MLL-AF9 leukemia progression. *Leukemia*. 2016;30(12):2373-2384.
278. Zhang TJ, Zhang LC, Xu ZJ, Zhou JD. Expression and prognosis analysis of. *Aging (Albany NY)*. 2020;12(14):14677-14690.
279. Schulze I, Rohde C, Scheller-Wendorff M, et al. Increased DNA methylation of Dnmt3b targets impairs leukemogenesis. *Blood*. 2016;127(12):1575-1586.
280. Azagra A, Román-González L, Collazo O, et al. In vivo conditional deletion of HDAC7 reveals its requirement to establish proper B lymphocyte identity and development. *J Exp Med*. 2016;213(12):2591-2601.
281. Barneda-Zahonero B, Collazo O, Azagra A, et al. The transcriptional repressor HDAC7 promotes apoptosis and c-Myc downregulation in particular types of leukemia and lymphoma. *Cell Death Dis*. 2015;6:e1635.
282. de Barrios O, Galaras A, Trincado JL, et al. HDAC7 is a major contributor in the pathogenesis of infant t(4;11) proB acute lymphoblastic leukemia. *Leukemia*. 2021;35(7):2086-2091.
283. Conserva MR, Anelli L, Zagaria A, Specchia G, Albano F. The Pleiotropic Role of Retinoic Acid/Retinoic Acid Receptors Signaling: From Vitamin A Metabolism to Gene Rearrangements in Acute Promyelocytic Leukemia. *Int J Mol Sci*. 2019;20(12).

284. Garrison BS, Rybak AP, Beerman I, et al. ZFP521 regulates murine hematopoietic stem cell function and facilitates MLL-AF9 leukemogenesis in mouse and human cells. *Blood*. 2017;130(5):619-624.
285. Germano G, Morello G, Aveic S, et al. ZNF521 sustains the differentiation block in MLL-rearranged acute myeloid leukemia. *Oncotarget*. 2017;8(16):26129-26141.
286. Chiarella E, Aloisio A, Scicchitano S, et al. ZNF521 Enhances MLL-AF9-Dependent Hematopoietic Stem Cell Transformation in Acute Myeloid Leukemias by Altering the Gene Expression Landscape. *Int J Mol Sci*. 2021;22(19).
287. Kang YJ, Shin JW, Yoon JH, et al. Inhibition of erythropoiesis by Smad6 in human cord blood hematopoietic stem cells. *Biochem Biophys Res Commun*. 2012;423(4):750-756.
288. Pimanda JE, Donaldson IJ, de Bruijn MF, et al. The SCL transcriptional network and BMP signaling pathway interact to regulate RUNX1 activity. *Proc Natl Acad Sci U S A*. 2007;104(3):840-845.
289. Narvaiza I, Landry S, Weitzman MD. APOBEC3 proteins and genomic stability: the high cost of a good defense. *Cell Cycle*. 2012;11(1):33-38.
290. Knisbacher BA, Gerber D, Levanon EY. DNA Editing by APOBECs: A Genomic Preserver and Transformer. *Trends Genet*. 2016;32(1):16-28.
291. Talluri S, Samur MK, Buon L, et al. Dysregulated APOBEC3G causes DNA damage and promotes genomic instability in multiple myeloma. *Blood Cancer J*. 2021;11(10):166.
292. Wells M, Steiner L. Epigenetic and Transcriptional Control of Erythropoiesis. *Front Genet*. 2022;13:805265.
293. Nandakumar SK, Ulirsch JC, Sankaran VG. Advances in understanding erythropoiesis: evolving perspectives. *Br J Haematol*. 2016;173(2):206-218.
294. Doulatov S, Vo LT, Macari ER, et al. Drug discovery for Diamond-Blackfan anemia using reprogrammed hematopoietic progenitors. *Sci Transl Med*. 2017;9(376).
295. van Riggelen J, Yetil A, Felsher DW. MYC as a regulator of ribosome biogenesis and protein synthesis. *Nat Rev Cancer*. 2010;10(4):301-309.
296. Laurenti E, Varnum-Finney B, Wilson A, et al. Hematopoietic stem cell function and survival depend on c-Myc and N-Myc activity. *Cell Stem Cell*. 2008;3(6):611-624.
297. Poortinga G, Wall M, Sanij E, et al. c-MYC coordinately regulates ribosomal gene chromatin remodeling and Pol I availability during granulocyte differentiation. *Nucleic Acids Res*. 2011;39(8):3267-3281.
298. Wilson A, Murphy MJ, Oskarsson T, et al. c-Myc controls the balance between hematopoietic stem cell self-renewal and differentiation. *Genes Dev*. 2004;18(22):2747-2763.
299. Vervoorts J, Lüscher-Firzlaff J, Lüscher B. The ins and outs of MYC regulation by posttranslational mechanisms. *J Biol Chem*. 2006;281(46):34725-34729.
300. Hermida MA, Dinesh Kumar J, Leslie NR. GSK3 and its interactions with the PI3K/AKT/mTOR signalling network. *Adv Biol Regul*. 2017;65:5-15.
301. Bild AH, Yao G, Chang JT, et al. Oncogenic pathway signatures in human cancers as a guide to targeted therapies. *Nature*. 2006;439(7074):353-357.
302. Huang W, Li BR, Feng H. PLAG1 silencing promotes cell chemosensitivity in ovarian cancer via the IGF2 signaling pathway. *Int J Mol Med*. 2020;45(3):703-714.
303. Fernandes H, Moura J, Carvalho E. mTOR Signaling as a Regulator of Hematopoietic Stem Cell Fate. *Stem Cell Rev Rep*. 2021.

304. Luo Y, Li L, Zou P, et al. Rapamycin enhances long-term hematopoietic reconstitution of ex vivo expanded mouse hematopoietic stem cells by inhibiting senescence. *Transplantation*. 2014;97(1):20-29.
305. Berg JS, Lin KK, Sonnet C, et al. Imprinted genes that regulate early mammalian growth are coexpressed in somatic stem cells. *PLoS One*. 2011;6(10):e26410.
306. Kircher M, Bock C, Paulsen M. Structural conservation versus functional divergence of maternally expressed microRNAs in the Dlk1/Gtl2 imprinting region. *BMC Genomics*. 2008;9:346.
307. Karagkouni D, Paraskevopoulou MD, Chatzopoulos S, et al. DIANA-TarBase v8: a decade-long collection of experimentally supported miRNA-gene interactions. *Nucleic Acids Res*. 2018;46(D1):D239-D245.
308. Vlachos IS, Paraskevopoulou MD, Karagkouni D, et al. DIANA-TarBase v7.0: indexing more than half a million experimentally supported miRNA:mRNA interactions. *Nucleic Acids Res*. 2015;43(Database issue):D153-159.
309. Bagger FO, Kinalis S, Rapin N. BloodSpot: a database of healthy and malignant haematopoiesis updated with purified and single cell mRNA sequencing profiles. *Nucleic Acids Res*. 2019;47(D1):D881-D885.
310. Minuesa G, Albanese SK, Xie W, et al. Small-molecule targeting of MUSASHI RNA-binding activity in acute myeloid leukemia. *Nat Commun*. 2019;10(1):2691.
311. Duggimpudi S, Kloetgen A, Maney SK, et al. Transcriptome-wide analysis uncovers the targets of the RNA-binding protein MSI2 and effects of MSI2's RNA-binding activity on IL-6 signaling. *J Biol Chem*. 2018;293(40):15359-15369.
312. Vu LP, Prieto C, Amin EM, et al. Functional screen of MSI2 interactors identifies an essential role for SYNCRIP in myeloid leukemia stem cells. *Nat Genet*. 2017;49(6):866-875.
313. Ly M, Rentas S, Vujovic A, et al. Diminished AHR Signaling Drives Human Acute Myeloid Leukemia Stem Cell Maintenance. *Cancer Res*. 2019;79(22):5799-5811.
314. Wunderlich M, Chou FS, Sexton C, et al. Improved multilineage human hematopoietic reconstitution and function in NSGS mice. *PLoS One*. 2018;13(12):e0209034.
315. Macaulay IC, Svensson V, Labalette C, et al. Single-Cell RNA-Sequencing Reveals a Continuous Spectrum of Differentiation in Hematopoietic Cells. *Cell Rep*. 2016;14(4):966-977.
316. Bauer DE, Kamran SC, Orkin SH. Reawakening fetal hemoglobin: prospects for new therapies for the β-globin disorders. *Blood*. 2012;120(15):2945-2953.
317. Esrick EB, Lehmann LE, Biffi A, et al. Post-Transcriptional Genetic Silencing of. *N Engl J Med*. 2021;384(3):205-215.
318. - Gene Therapy for Sickle Cell Anemia Using a Modified Gamma Globin Lentivirus Vector and Reduced Intensity Conditioning Transplant Shows Promising Correction of the Disease Phenotype.- 1021.
319. Ranzoni AM, Tangherloni A, Berest I, et al. Integrative Single-Cell RNA-Seq and ATAC-Seq Analysis of Human Developmental Hematopoiesis. *Cell Stem Cell*. 2021;28(3):472-487.e477.
320. Kaya-Okur HS, Wu SJ, Codomo CA, et al. CUT&Tag for efficient epigenomic profiling of small samples and single cells. *Nat Commun*. 2019;10(1):1930.
321. Vilchez D, Simic MS, Dillin A. Proteostasis and aging of stem cells. *Trends Cell Biol*. 2014;24(3):161-170.

322. Lv K, Gong C, Antony C, et al. HectD1 controls hematopoietic stem cell regeneration by coordinating ribosome assembly and protein synthesis. *Cell Stem Cell*. 2021;28(7):1275-1290.e1279.
323. Grinenko T, Eugster A, Thielecke L, et al. Hematopoietic stem cells can differentiate into restricted myeloid progenitors before cell division in mice. *Nat Commun*. 2018;9(1):1898.
324. Loeffler D, Wehling A, Schneiter F, et al. Asymmetric lysosome inheritance predicts activation of haematopoietic stem cells. *Nature*. 2019;573(7774):426-429.
325. Neumüller RA, Knoblich JA. Dividing cellular asymmetry: asymmetric cell division and its implications for stem cells and cancer. *Genes Dev*. 2009;23(23):2675-2699.
326. Fuentealba LC, Eivers E, Geissert D, Taelman V, De Robertis EM. Asymmetric mitosis: Unequal segregation of proteins destined for degradation. *Proc Natl Acad Sci U S A*. 2008;105(22):7732-7737.
327. Juma AR, Grommen SVH, O'Bryan MK, et al. PLAG1 deficiency impairs spermatogenesis and sperm motility in mice. *Sci Rep*. 2017;7(1):5317.
328. Kim E, Kim M, Hwang SU, et al. Neural induction of porcine-induced pluripotent stem cells and further differentiation using glioblastoma-cultured medium. *J Cell Mol Med*. 2019;23(3):2052-2063.
329. Goto Y, Ibi M, Sato H, et al. PLAG1 enhances the stemness profiles of acinar cells in normal human salivary glands in a cell type-specific manner. *J Oral Biosci*. 2020;62(1):99-106.
330. Landrette SF, Kuo YH, Hensen K, et al. Plag1 and Plagl2 are oncogenes that induce acute myeloid leukemia in cooperation with Cbfb-MYH11. *Blood*. 2005;105(7):2900-2907.
331. Espinoza DA, Fan X, Yang D, et al. Aberrant Clonal Hematopoiesis following Lentiviral Vector Transduction of HSPCs in a Rhesus Macaque. *Mol Ther*. 2019;27(6):1074-1086.
332. Signer RA, Qi L, Zhao Z, et al. The rate of protein synthesis in hematopoietic stem cells is limited partly by 4E-BPs. *Genes Dev*. 2016;30(15):1698-1703.
333. Hartman NW, Lin TV, Zhang L, Paquelet GE, Feliciano DM, Bordey A. mTORC1 targets the translational repressor 4E-BP2, but not S6 kinase 1/2, to regulate neural stem cell self-renewal in vivo. *Cell Rep*. 2013;5(2):433-444.
334. Choo AY, Yoon SO, Kim SG, Roux PP, Blenis J. Rapamycin differentially inhibits S6Ks and 4E-BP1 to mediate cell-type-specific repression of mRNA translation. *Proc Natl Acad Sci U S A*. 2008;105(45):17414-17419.
335. Wu F, Chen Z, Liu J, Hou Y. The Akt-mTOR network at the interface of hematopoietic stem cell homeostasis. *Exp Hematol*. 2021;103:15-23.
336. Yamashita M, Dellorusso PV, Olson OC, Passegué E. Dysregulated haematopoietic stem cell behaviour in myeloid leukaemogenesis. *Nat Rev Cancer*. 2020;20(7):365-382.
337. Woll PS, Jacobsen SEW. Stem cell concepts in myelodysplastic syndromes: lessons and challenges. *J Intern Med*. 2021;289(5):650-661.
338. Galeev R, Baudet A, Kumar P, et al. Genome-wide RNAi Screen Identifies Cohesin Genes as Modifiers of Renewal and Differentiation in Human HSCs. *Cell Rep*. 2016;14(12):2988-3000.
339. Galeev R, Larsson J. Cohesin in haematopoiesis and leukaemia. *Curr Opin Hematol*. 2018;25(4):259-265.
340. Jann JC, Tothova Z. Cohesin mutations in myeloid malignancies. *Blood*. 2021;138(8):649-661.
341. Kaufmann KB, Garcia-Prat L, Liu Q, et al. A stemness screen reveals. *Blood*. 2019;133(20):2198-2211.

342. Fischbach NA, Rozenfeld S, Shen W, et al. HOXB6 overexpression in murine bone marrow immortalizes a myelomonocytic precursor in vitro and causes hematopoietic stem cell expansion and acute myeloid leukemia in vivo. *Blood*. 2005;105(4):1456-1466.
343. Thorsteinsdottir U, Mamo A, Kroon E, et al. Overexpression of the myeloid leukemia-associated Hoxa9 gene in bone marrow cells induces stem cell expansion. *Blood*. 2002;99(1):121-129.
344. Bowman RL, Busque L, Levine RL. Clonal Hematopoiesis and Evolution to Hematopoietic Malignancies. *Cell Stem Cell*. 2018;22(2):157-170.
345. Welch JS, Ley TJ, Link DC, et al. The origin and evolution of mutations in acute myeloid leukemia. *Cell*. 2012;150(2):264-278.
346. Magee JA, Piskounova E, Morrison SJ. Cancer stem cells: impact, heterogeneity, and uncertainty. *Cancer Cell*. 2012;21(3):283-296.
347. Bulaeva E, Pellacani D, Nakamichi N, et al. MYC-induced human acute myeloid leukemia requires a continuing IL-3/GM-CSF costimulus. *Blood*. 2020;136(24):2764-2773.
348. Xu DD, Wang Y, Zhou PJ, et al. The IGF2/IGF1R/Nanog Signaling Pathway Regulates the Proliferation of Acute Myeloid Leukemia Stem Cells. *Front Pharmacol*. 2018;9:687.
349. Guo C, Ran Q, Sun C, et al. Loss of FGFR3 Delays Acute Myeloid Leukemogenesis by Programming Weakly Pathogenic CD117-Positive Leukemia Stem-Like Cells. *Front Pharmacol*. 2020;11:632809.
350. Zhang W, Shao Z, Fu R, Wang H, Li L, Yue L. Effect of DLK1 on tumorigenesis in CD34. *Oncol Lett*. 2013;6(1):203-206.
351. Sellers ZP, Bolkun L, Kloczko J, et al. Increased methylation upstream of the MEG3 promotor is observed in acute myeloid leukemia patients with better overall survival. *Clin Epigenetics*. 2019;11(1):50.
352. Yu Y, Kou D, Liu B, et al. LncRNA MEG3 contributes to drug resistance in acute myeloid leukemia by positively regulating ALG9 through sponging miR-155. *Int J Lab Hematol*. 2020;42(4):464-472.
353. Prelich G. Gene overexpression: uses, mechanisms, and interpretation. *Genetics*. 2012;190(3):841-854.
354. Charlesworth CT, Hsu I, Wilkinson AC, Nakauchi H. Immunological barriers to haematopoietic stem cell gene therapy. *Nat Rev Immunol*. 2022.
355. Hacein-Bey-Abina S, Garrigue A, Wang GP, et al. Insertional oncogenesis in 4 patients after retrovirus-mediated gene therapy of SCID-X1. *J Clin Invest*. 2008;118(9):3132-3142.
356. Milone MC, O'Doherty U. Clinical use of lentiviral vectors. *Leukemia*. 2018;32(7):1529-1541.
357. Leonard A, Tisdale JF. A pause in gene therapy: Reflecting on the unique challenges of sickle cell disease. *Mol Ther*. 2021;29(4):1355-1356.
358. Frangoul H, Ho TW, Corbacioglu S. CRISPR-Cas9 Gene Editing for Sickle Cell Disease and β-Thalassemia. Reply. *N Engl J Med*. 2021;384(23):e91.
359. Chabanovska O, Galow AM, David R, Lemcke H. mRNA - A game changer in regenerative medicine, cell-based therapy and reprogramming strategies. *Adv Drug Deliv Rev*. 2021;179:114002.
360. Yakubov E, Rechavi G, Rozenblatt S, Givol D. Reprogramming of human fibroblasts to pluripotent stem cells using mRNA of four transcription factors. *Biochem Biophys Res Commun*. 2010;394(1):189-193.

361. Schneider RK, Schenone M, Ferreira MV, et al. Rps14 haploinsufficiency causes a block in erythroid differentiation mediated by S100A8 and S100A9. *Nat Med*. 2016;22(3):288-297.
362. Narla A, Ebert BL. Ribosomopathies: human disorders of ribosome dysfunction. *Blood*. 2010;115(16):3196-3205.
363. Horos R, Ijspeert H, Pospisilova D, et al. Ribosomal deficiencies in Diamond-Blackfan anemia impair translation of transcripts essential for differentiation of murine and human erythroblasts. *Blood*. 2012;119(1):262-272.
364. Bhat M, Robichaud N, Hulea L, Sonenberg N, Pelletier J, Topisirovic I. Targeting the translation machinery in cancer. *Nat Rev Drug Discov*. 2015;14(4):261-278.
365. Malina A, Mills JR, Pelletier J. Emerging therapeutics targeting mRNA translation. *Cold Spring Harb Perspect Biol*. 2012;4(4):a012377.
366. Ruggero D, Pandolfi PP. Does the ribosome translate cancer? *Nat Rev Cancer*. 2003;3(3):179-192.
367. Callahan KP, Minhajuddin M, Corbett C, et al. Flavaglines target primitive leukemia cells and enhance anti-leukemia drug activity. *Leukemia*. 2014;28(10):1960-1968.
368. Tamburini J, Green AS, Bardet V, et al. Protein synthesis is resistant to rapamycin and constitutes a promising therapeutic target in acute myeloid leukemia. *Blood*. 2009;114(8):1618-1627.
369. Tamburini J, Green AS, Chapuis N, et al. Targeting translation in acute myeloid leukemia: a new paradigm for therapy? *Cell Cycle*. 2009;8(23):3893-3899.
370. Emmrich S, Engeland F, El-Khatib M, et al. miR-139-5p controls translation in myeloid leukemia through EIF4G2. *Oncogene*. 2016;35(14):1822-1831.
371. Herzog LO, Walters B, Buono R, et al. Targeting eIF4F translation initiation complex with SBI-756 sensitises B lymphoma cells to venetoclax. *Br J Cancer*. 2021;124(6):1098-1109.
372. Narayanan V, Gutman JA, Pollyea DA, Jimeno A. Omacetaxine mepesuccinate for the treatment of chronic myeloid leukemia. *Drugs Today (Barc)*. 2013;49(7):447-456.
373. Lam SS, Ho ES, He BL, et al. Homoharringtonine (omacetaxine mepesuccinate) as an adjunct for FLT3-ITD acute myeloid leukemia. *Sci Transl Med*. 2016;8(359):359ra129.
374. Horwitz ME. Ex Vivo Expansion or Manipulation of Stem Cells to Improve Outcome of Umbilical Cord Blood Transplantation. *Curr Hematol Malig Rep*. 2016;11(1):12-18.
375. Wilkinson AC, Igarashi KJ, Nakauchi H. Haematopoietic stem cell self-renewal in vivo and ex vivo. *Nat Rev Genet*. 2020;21(9):541-554.
376. Sonenberg N, Hinnebusch AG. Regulation of translation initiation in eukaryotes: mechanisms and biological targets. *Cell*. 2009;136(4):731-745.
377. Moerke NJ, Aktas H, Chen H, et al. Small-molecule inhibition of the interaction between the translation initiation factors eIF4E and eIF4G. *Cell*. 2007;128(2):257-267.
378. Papadopoulos E, Jenni S, Kabha E, et al. Structure of the eukaryotic translation initiation factor eIF4E in complex with 4EGI-1 reveals an allosteric mechanism for dissociating eIF4G. *Proc Natl Acad Sci U S A*. 2014;111(31):E3187-3195.
379. De A, Jacobson BA, Peterson MS, et al. 4EGI-1 represses cap-dependent translation and regulates genome-wide translation in malignant pleural mesothelioma. *Invest New Drugs*. 2018;36(2):217-229.
380. Yi T, Kabha E, Papadopoulos E, Wagner G. 4EGI-1 targets breast cancer stem cells by selective inhibition of translation that persists in CSC maintenance, proliferation and metastasis. *Oncotarget*. 2014;5(15):6028-6037.

381. Descamps G, Gomez-Bougie P, Tamburini J, et al. The cap-translation inhibitor 4EGI-1 induces apoptosis in multiple myeloma through Noxa induction. *Br J Cancer*. 2012;106(10):1660-1667.
382. Willimott S, Beck D, Ahearne MJ, Adams VC, Wagner SD. Cap-translation inhibitor, 4EGI-1, restores sensitivity to ABT-737 apoptosis through cap-dependent and -independent mechanisms in chronic lymphocytic leukemia. *Clin Cancer Res*. 2013;19(12):3212-3223.
383. Rapin N, Bagger FO, Jendholm J, et al. Comparing cancer vs normal gene expression profiles identifies new disease entities and common transcriptional programs in AML patients. *Blood*. 2014;123(6):894-904.
384. Kohlmann A, Kipps TJ, Rassenti LZ, et al. An international standardization programme towards the application of gene expression profiling in routine leukaemia diagnostics: the Microarray Innovations in LEukemia study prephase. *Br J Haematol*. 2008;142(5):802-807.
385. Gerstung M, Pellagatti A, Malcovati L, et al. Combining gene mutation with gene expression data improves outcome prediction in myelodysplastic syndromes. *Nat Commun*. 2015;6:5901.
386. Cerami E, Gao J, Dogrusoz U, et al. The cBio cancer genomics portal: an open platform for exploring multidimensional cancer genomics data. *Cancer Discov*. 2012;2(5):401-404.
387. Gao J, Aksoy BA, Dogrusoz U, et al. Integrative analysis of complex cancer genomics and clinical profiles using the cBioPortal. *Sci Signal*. 2013;6(269):pl1.
388. Tyner JW, Tognon CE, Bottomly D, et al. Functional genomic landscape of acute myeloid leukaemia. *Nature*. 2018;562(7728):526-531.
389. Wu R, Pai A, Liu L, Xing S, Lu Y. NanoTPOT: Enhanced Sample Preparation for Quantitative Nanoproteomic Analysis. *Anal Chem*. 2020;92(9):6235-6240.

APPENDIX 1

Exploring changes in the proteome of PLAG1-S^{OE} HSPCs

Exploring changes in the proteome of PLAG1-S^{OE} HSPCs.

The ability of PLAG1-S to repress translation machinery in Lin$^-$CD34$^+$ cells prompted the question of its impact on the PLAG1-S^{OE} proteome landscape. To address this question, we performed proteome profiling in Lin$^-$CD34$^+$BFP$^+$ cells transduced with either PLAG1-S overexpression or control (**Appendix Figure 1A**). We employed a previously published a protocol for low cell input proteomics which required a minimum of 1ug total protein to detect ~7000 unique peptides[389]. We first determined by sorting, lysing and BCA assay that 50,000 and 75,000 Lin$^-$CD34$^+$ cells yield 1.5ug and 1.99ug total protein, respectively (data not shown). For proteome profiling ~80,000 transduced PLAG1-S^{OE} and control Lin$^-$CD34$^+$ cells were collected for 3 biological replicates and TMT-labelled total protein extracts were measured on 2D LC- MS/MS according to methods published in Wu *et al*. (2020)[389]. Only 3447 unique peptides were detected, which was approximately half of the expected outcome. By referencing to the transcriptome, it is apparent that proteins detected were primarily translated from abundant mRNA species (**Appendix Figure 1B**), therefore likely to be high copy number proteins. Cursory analysis of the proteomics data revealed 236 significantly differentially expressed proteins (**Appendix Figure 1C**). Of the 543 significantly ($p.adj<0.05$) differentially expressed transcripts only 143 were detected in the proteome, with only 15 also significantly changed at the protein level (**Appendix Figure 1D**; Red: Concordantly up, Dark Blue: Concordantly down, Black: Discordant). GSEA of detected proteins resulted in relatively few significant enrichments, which can be explained by the low protein counts, but did uncover repression of adhesion proteins (**Appendix Figure 1E**). The leading-edge proteins driving negative enrichment of cell adhesion in the PLAG1-S^{OE} proteome are significantly overlapped (Mann-Whitney two-sided $p<0.05$) to negative expression of signatures of mature immune processes in the PLAG1-S^{OE} transcriptome (**Appendix Figure 1F**). Therefore, though any conclusions from this data set is associated with significant technical caveat, it appears that the molecular state of reduced mature hematopoietic processes are measurable in both the PLAG1-S^{OE} transcriptome and proteome.

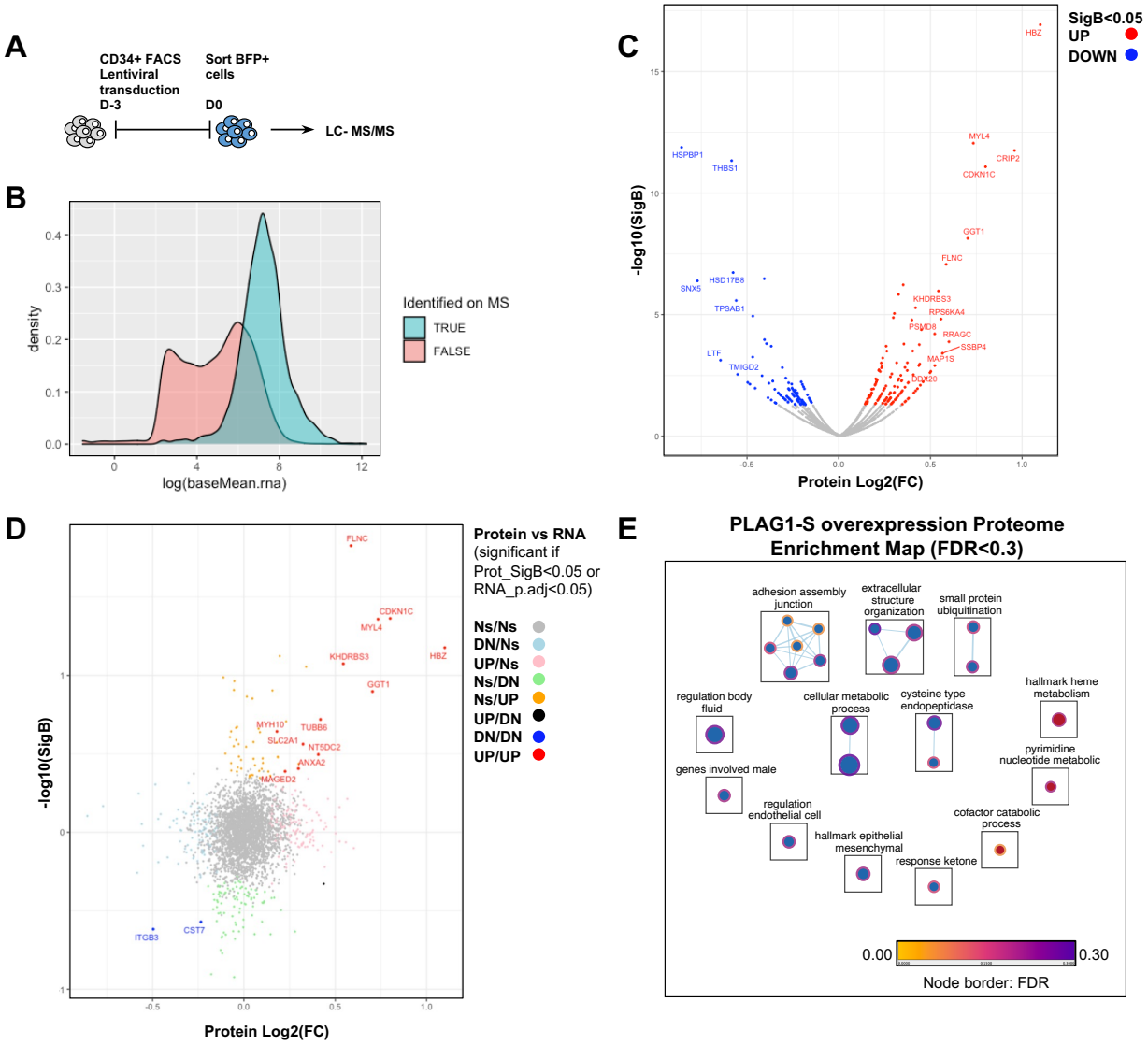
A
CD34+ FACS
Lentiviral
transduction
D-3
Sort BFP+
cells
D0
LC- MS/MS
B
density
log(baseMean.rna)
Identified on MS
TRUE
FALSE
C
SigB<0.05
UP
DOWN
-log10(SigB)
Protein Log2(FC)
D
Protein vs RNA
(significant if
Prot_SigB<0.05 or
RNA_p.adj<0.05)
Ns/Ns
DN/Ns
UP/Ns
Ns/DN
Ns/UP
UP/DN
DN/DN
UP/UP
-log10(SigB)
Protein Log2(FC)
E
PLAG1-S overexpression Proteome
Enrichment Map (FDR<0.3)
adhesion assembly junction
extracellular structure organization
small protein ubiquitination
regulation body fluid
cellular metabolic process
cysteine type endopeptidase
hallmark heme metabolism
pyrimidine nucleotide metabolic
genes involved male
regulation endothelial cell
cofactor catabolic process
hallmark epithelial mesenchymal
response ketone
0.00
0.30
Node border: FDR
F
PLAG1-S overexpression Transcriptome
Enrichment Map (FDR<0.1)
establishment protein localization translation
response external stimulus regulation
adhesion mediated heterotypic cell
regulation chemokine production interleukin
migration neutrophil chemotaxis granulocyte
osteoblast differentiation ossification bone
glycosaminoglycan metabolism aminoglycan metabolic
humoral response molecule bacterium
activation inflammatory neuroinflammatory microglial
regulation vasculature development angiogenesis
epidermal growth pathway erbb
activation involved immune neutrophil
regulation glycogen biosynthetic glucan
hallmark heme metabolism
Down
Adhesion
proteins

Appendix Figure 1: Proteome of PLAG1-S overexpressing Lin$^-$CD34$^+$ CB HSPCs. (A) Schematic of Lin-CD34+ isolation and transduction for mass spectrometry analysis. **(B)** Distribution of genes detected in RNAseq and proteome profiling based on the average normalized RNA read counts. **(C)** Volcano plot of protein differential expression with significantly (SigB<0.05) changed proteins coloured and labeled if the magnitude of change is log2FC>0.5. **(D)** Correlation of differential expression in the transcriptome and proteome with gene names identified for the 14 genes concordantly significantly changed in both datasets. **(E)** PLAG1-S overexpression proteome enrichment map (FDR<0.3). **(H)** Intersection of the enriched adhesion proteins to the PLAG1-S overexpression transcriptome enrichment map.